Final Report

Version 1.1: Final

Design Synthesis Exercise: The Hybrid Electric Mini-Feeder Case

Group 17

4449444	-	Patrick Brill	4487249	-	Thomas De Jonghe
4298772	-	Myron Beukelman	4453182	-	Paul van Kessel
4276191	-	Lukas Flenner	4217446	-	Josse Lubberink
4436857	-	Flores Germonpré	4465121	-	Kaat Pareyns
4346912	-	Roemer Hendrikx	4359895	-	Kilian Swannet

TU Delft

This page is intentionally left blank.

Preface

The following report entails the design process of the E-COmmuter. For the Design Synthesis Exercise of the Faculty of Aerospace Engineering at the Delft University of Technology, we, Group 17, designed a hybrid electric commuter aircraft. The goal of the E-COmmuter is to carry 14 passengers from small, local airfields to commercial airports and back while minimizing travel time, cost and exhaust emissions.

We would like to express our gratitude towards our tutor, Dr. Fabrizio Oliviero, for his excellent guidance and advice throughout this project. Furthermore, we would like to thank our coaches Salil Luesutthiviboon and Vinh Ho-Huu, for steering us in the right direction and providing valuable tools regarding noise calculations. Finally, our gratitude goes out to the Faculty of Aerospace Engineering, for organizing the Design Synthesis Exercise. It has been a truly educational assignment: it gave us the opportunity to apply all our acquired knowledge throughout the Bachelor program and it taught us how to work in a team.

DSE Group 17 - E-COmmuter
July 3, 2018
Delft, The Netherlands

Executive Overview

Market Analysis

Passengers who live far away from commercial airports experience large travel times. While, smaller/local airfields are incapable of providing national or international flights. However, they do have the potential to provide commuter services using small feeder aircraft. Using these aircraft, the accessibility of commercial airports can be improved and the travel time of the passengers is reduced. Furthermore, ground transportation often involves high costs (traffic congestion, fuel costs, parking costs, etc.) and this is unfavorable for the environment. Therefore, an opportunity for an environmentally friendly, mini-feeder aircraft with limited passenger capacity arises [1].

Mission Need Statement:
Due to the introduction of innovative and more efficient power systems based on alternative energy sources, a properly designed novel and sustainable commuter aircraft can help to reduce the emissions (such as noise and CO_2-emissions) around airports as well as the amount of private transportation from/to commercial airports, decreasing both the ground infrastructure congestion and the transportation costs for the potential users.

For this project, a propeller-driven hybrid electric aircraft is considered, as hybrid aircraft are seen as a sustainable alternative to the classic fuel consuming aircraft [2]. To be competitive with ground transportation, the aircraft should be able to operate on local airfields, providing short travel times and a one-way range of 370 km using the hub-and-spoke model. Thus, the Project Objective Statement becomes [1]:

Project Objective Statement:
Design a short range hybrid electric aircraft capable of carrying 14 passengers from local (grass) airfields to major/commercial airports, by 10 students in 10 weeks time.

In this project the aircraft that is designed for this project objective is the E-COmmuter.

Functional Analysis and Requirements

Following from the market analysis, a functional analysis of the E-COmmuter is performed to analyze the mission need. From the analysis, it was quickly found that the operational functions of the aircraft have to include the capability to take-off and land on different types of runway, possibly grass strips or asphalt. Moreover, the propulsion system needs the ability to perform a fully electric takeoff and landing to make the aircraft sustainable.

In order to satisfy the functions as found in the functional analysis, stakeholder requirements as well as mission and subsystem requirements are defined. Requirements that do not follow the V.A.L.I.D. (Verifiable, Achievable, Logical, Integral and Definitive)[3] criteria are left out of consideration. This is required because the mission has changed compared to the conceptual design [4] and some requirements are assessed to not be relevant anymore to the detailed design.

Mission Profile

The requirements found are used as a starting point to come up with a mission profile for the E-COmmuter. The design range requirement (**HEF-OPR-03**) of 370 km, the emission requirement (**HEF-MAN-02**) of no more than 118.5 g km^{-1} CO_2 per seat and the zero emission takeoff and landing requirement (**HEF-PROP-02**) are the driving design requirements.

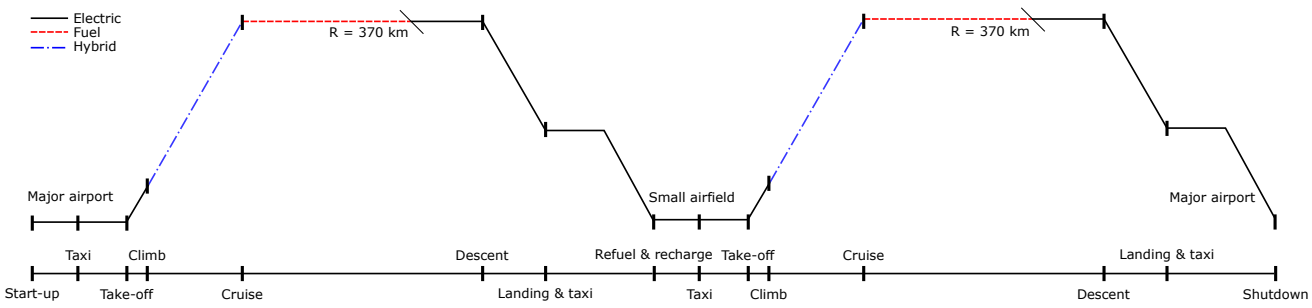

Figure 1: Mission profile for the E-COmmuter.

This results in a mission profile which connects small airfields with big airports and vice versa, with battery charging at both the airfield and airport as shown in Figure 1. A hybrid climb is used after which during cruise, 80% of the time the

flight is powered purely by the internal combustion engines (ICEs) and the other 20% by the batteries. All other flight phases including ground operations are done fully electrically.

Sustainability Strategy
Sustainability is highly important in the current aerospace industry. Therefore, after the mission profile is created, a sustainability strategy is set up to account for sustainability during the more detailed subsystem design. More specifically, metrics are set up to represent numerous stakeholder wishes and needs. The metrics that are identified are: accessibility, safety, ecosystem health, resource use, noise and affordability.

The aforementioned metrics will already be partially implemented into the subsystem designs via the found requirements and the mission profile. However, a second manner to implement sustainability is by making decisions based on an understanding of sustainability. This includes choices that decrease the aircraft weight to reduce emissions or redundancies to make the aircraft even safer than regulations. These two methods are continuously incorporated into design of the E-COmmuter.

Trade-off Summary
A trade-off is performed using all the gathered requirements, the mission profile and the sustainability strategy. During the midterm report phase [4], this trade-off has already resulted in the most suitable concept to perform the mission. This was done using an aircraft configuration trade-off as well as a propulsion system trade-off. Both trade-offs were performed separately and a final concept was chosen using a weighting representing the numerous requirements and the desired mission profile. The trade-off results are summarized in Table 1.

Table 1: Trade-off summary.

Trade-off	**Result**
Fuselage shape	Rectangular cross-section, conventional longitudinal shape
Wing-tail layout	High-wing conventional wing with a T-tail
Powertrain configuration	Series hybrid system
Power cell	Battery
Propulsion layout	Distributed electric propulsion plus two larger propellers
Electric motor	Compact Dynamics motors
Internal combustion engine	ICE running on Avgas

Design Approach and Budgets
For the selected concept from the trade-off, a Class I and Class II weight estimation has been performed to come up with a maximum takeoff weight (MTOW). After a Class I weight estimation based on reference aircraft, the MTOW came out to be 5415 kg. Using this MTOW, wing loading diagrams are constructed to obtain a sizing for the preliminary wing, tail, and high-lift devices. These geometric parameters are then used in the Class II weight estimation to come up with subsystem weights which are used to update the MTOW. However, the MTOW after both weight estimation came out to be different. Therefore, iterations were performed between both weight estimations to obtain a MTOW estimate of 6589 kg. After the detailed design in this report, this MTOW has been brought down to a final MTOW of 5835 kg.

Using the Class II weight estimation, maximum values for the most important technical parameters are determined such as the maximum total energy consumption of the E-COmmuter. This budgeting is done to prevent the tendency of these parameters to grow in an undesired direction throughout the design process.

Fuselage Design
To start off the detailed design, the fuselage is discussed first. The fuselage is designed to fit 14 passengers and has a luggage compartment to account for the 280 kg of luggage that passengers can take with them. Behind the luggage compartment, the ICEs are stored in a separate compartment with space provided for the necessary protection structure and cabling. The fuselage has a total length of 14.4 m [4]. Additionally, the weight of the fuselage is estimated. This results in a total fuselage weight of 669 kg.

To finalize the fuselage design, the environmental control system (ECS) is elaborated upon to ensure a comfortable flight experience. A standalone ECS is necessary because the ICEs do not run during electric flight phases. It is found that an ECS equipped with a ram air intake, fan and electric heater is sufficient to cycle the air and heat the cabin and cockpit of the E-COmmuter.

Wing Design
The next component to be designed is the wing. The wing planform is obtained by making multiple power loading to wing loading diagrams. By doing so, a design region constrained by a power-off stall and takeoff is obtained. The wing loading is then maximized for the E-COmmuter design requirements, which results in a wing surface area of 36.5 m^2. Furthermore, an aspect ratio of 12 is chosen as a high aspect ratio is highly important to have enough space for a blown wing design. This results in a span of 20.9 m. In order to achieve a finite maximum lift coefficient of 1.6, the general

aviation NASA/LANGLEY LS(1)-0417 (GA(W)-1) airfoil is chosen as it offers good lift-to-drag capabilities and a high maximum lift coefficient.
Using the newly found wing geometry and the selected airfoil, the loads acting on the wing for the ultimate loading case are determined using XFLR5[1]. However, corrections on the lift and drag have to be included due to the presence of the large and blown wing propellers that increase the dynamic pressure over the wing. Using the obtained forces, shear force and moment diagrams are obtained that are used during the wingbox design.

While designing the wingbox, GLARE 3 is chosen as material due to its high strength and favourable fatigue resistance. Using the identified loads and the mechanical properties of GLARE, the sizing of the wing box is performed. While doing a boom bending and shear stress analysis, the amount of stringers as well as the thickness of different components was iterated to make optimum use of the properties of GLARE and to meet the maximum buckling stresses. Additionally, the thicknesses of stringers, skin, spars and ribs are varied, which is possible when using a composite material such as GLARE. Finally, the design settled on two corner stringers as well as 14 additional stringers on the upper and lower skin of the wingbox. The final wing weight is then found to be 596 kg, which is 7% lighter than the Class II weight estimation.

Performance Analysis
As performance is crucial for the commercial success of an aircraft, a performance analysis is carried out now more is known about the fuselage and especially the wing. The different flight phases that are analyzed consist of takeoff, climb, cruise, descent and landing. For each of these phases, the E-COmmuter is designed in accordance with the requirements. Some of the most important requirements for the performance of the E-COmmuter consist of the 370 km design range and the short takeoff and landing (STOL) performance on a 700 m runway. From the performance analysis, the aircraft is found to perform well on both requirements as it has a takeoff distance of 503 m, a landing distance of 566 m and is capable of a design range of 370 km. The good takeoff and landing performance is for a large part possible due to the blown wing of the E-COmmuter.

Next to the nominal mission, a payload range diagram is constructed to analyze different missions with less payload and additional fuel or batteries. It is found that extra batteries in the cargo compartment (up to 280 kg) can be added to increase the range while 100 kg of extra fuel can be added in the wingbox to also increase the range. In this way, a maximum range of 989 km can be achieved. The different possibilities corresponding range, payload and emissions are summarized in Table 2.

Table 2: Range, payload options and CO_2 emissions for different missions. The payload options are only indicative of the possibilities and are not the only options available.

Missions	**Range**	**Payload option 1**	**Payload option 2**	**CO_2 Emissions**
Nominal mission	389 km	14 pax. with 20 kg lug. p.p.	-	112.7 g km^{-1} seat^{-1}
100 kg Extra fuel mission	590 km	14 pax. with 12 kg lug. p.p.	12 pax. with 28 kg lug. p.p.	159.0 g km^{-1} seat^{-1}
280 kg Extra battery pack mission	565 km	14 pax. with 0 kg lug. p.p.	11 pax. with 20 kg lug. p.p.	98.8 g km^{-1} seat^{-1}
100 kg Extra fuel and 280 kg extra battery pack mission	766 km	12 pax. with 4.5 kg lug. p.p.	10 pax. with 20 kg lug. p.p.	80.2 g km^{-1} seat^{-1}

Propulsion System Design
Using the performance analysis, the architecture and layout of the propulsion system can be determined. It is chosen to go with a series hybrid electric propulsion system with a distributed electric propulsion layout. A combination of power generation by ICEs and batteries powers the electric motors. Fourteen small blown wing propellers are used for propulsion as well as two large propellers which are chosen for cruise performance.

Another part of the design is to select the batteries used by the E-COmmuter. Lithium-Sulfur type batteries were selected for this use. These batteries are considered to have a battery specific energy of 750 W h kg^{-1} and an estimated life cycle of 1500 cycles.

Stability & Control and Tail & Landing Gear Design
Using the results from the wing design and the weights from all other components, the stability and control of the E-COmmuter can be assessed and the landing gear can be designed. The wing placement is the determining factor for the stability and control of the aircraft. This location is determined using a scissor plot and loading diagram. The center of gravity range is found to be between 19% and 51% of the mean aerodynamic chord (MAC). This results in a position of the MAC measured from the nose of 6.9 m. The position of the main gear is determined from the combined scissor and potato plot to be at 8.4 m measured from the nose. From the static stability analysis, the horizontal tail surface is required to be 8.5 m^2 and the vertical tail surface 6.0 m^2.

[1] URL: `http://www.xflr5.com/xflr5.htm` [cited 2 July 2018]

The last part of the stability of the E-COmmuter consists of the dynamic response of the E-COmmuter. For this, the stability and control derivatives are determined using DATCOM methods and are used to evaluate the aperiodic roll, spiral, dutch roll, phugoid, and the short period response. From the analysis it is clear that all eigenmotions are stable with the exception of the spiral. However, according to CS-23 regulations, the spiral instability is within the limits for certification and is not considered an issue.

System Integration

Combining all detailed designed parts, the final configuration of the E-COmmuter is obtained as visualized in Figure 2.

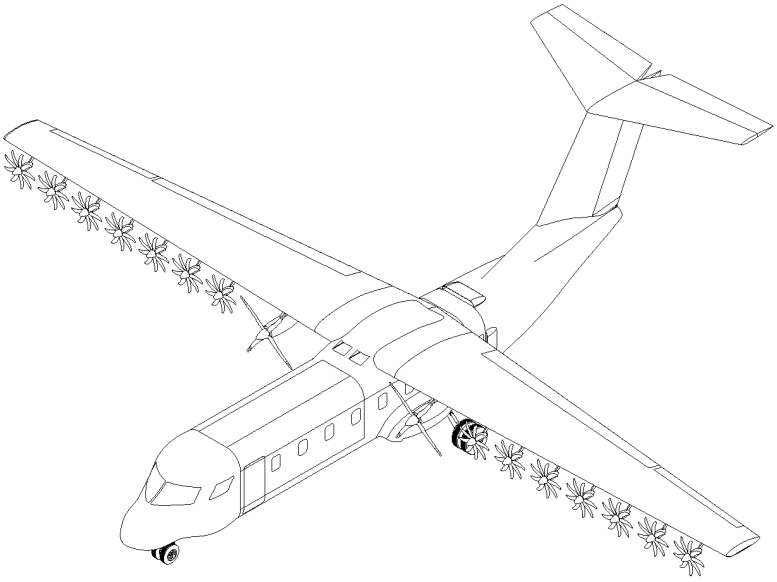

Figure 2: System integrated isometric view of the E-COmmuter.

To assess the sensitivity of the design due to factors like a change in battery specific energy, a sensitivity analysis is performed on the E-COmmuter. The variables that are studied consist of the battery specific energy, payload weight, range and ICE specific fuel consumption. From the analysis, all variables have a reasonable small effect on the MTOW, energy consumption, operating cost and aircraft span. Mainly a change in payload weight affects the aforementioned parameters significantly.

A remarkable result is the effect on the emission output. In the analysis, the emissions change with an unexpected magnitude and direction for different variable changes. For example, decreasing the payload weight resulted in an increase in emissions, which is not expected. This should be investigated in a later project stage by checking if this is intended behaviour or a cause of erroneous implementation or reasoning.

Operations and Logistics

As now the detailed design and system integration is complete, attention can be given to the operations and logistics concerning the E-COmmuter. In order to minimize operating cost and turnaround time, an operations concept must be established. The ground handling activities (consisting of aircraft and passenger handling) are assessed to be the most critical for the turnaround time of the E-COmmuter. In order to have efficient ground handling, different support systems are necessary to quickly serve passengers and the E-COmmuter at airfields. Most importantly, a fuel facility, charging facility, runway lights, metal detector, and a building with passenger facilities is to be provided. In addition to this, the presence of personnel will be necessary to ensure the fast ground handling of the E-COmmuter.

To check compliance with **HEF-PAX-02** (the door-to-door travel time for passengers shall be at least 20% lower than the corresponding ground transport time), the total travelling time is analyzed using three different cases for airfield to airport and airport to airfield transportation. From this analysis it was found that in the worst case the E-COmmuter passenger experiences 79% of the total travel time as experienced by a similar trip using a car. Hence, **HEF-PAX-02** is met.

RAMS Characteristics

To ensure the reliability, availability, maintainability and safety (RAMS) of the E-COmmuter, a RAMS analysis is performed. A qualitative reliability analysis is performed first and is based on aircraft reliability data from the US. It is clear from this analysis that the landing gear and propulsion system are the most critical parts of the E-COmmuter. Based on the reliability analysis, a maintenance strategy is constructed especially for the E-COmmuter. The maintenance is divided into scheduled and unscheduled maintenance that both determine the availability of the E-COmmuter for the

operator. Evaluating this availability, a scheduled availability of 93.7% is obtained. This availability will be slightly lower for airliners actually operating the E-COmmuter due to unscheduled maintenance that is not taken into account in this availability evaluation. Finally, a safety analysis is done where all safety factors and redundancies are checked and organized. These are necessary to account for uncertainties that can not be estimated during the detailed design phase or are required due to CS-23 regulations.

Technical Risk Assessment
Besides the RAMS analysis, a technical risk assessment is performed to evaluate the risks in the design of the E-COmmuter. Many different risk mitigation strategies from Brill et al. [4] are already performed during the detailed design by the application of safety factors in the structural design. Furthermore, battery cooling is integrated in the wing and the blown wing usage for controllability is checked as redundancy to the rudder. Finally, a computer system defines the division of energy between ICEs and batteries automatically to mitigate human error.
However, some risks are still present or newly identified during the detailed design. These have to be taken into account in further operations or design. For example, deep stall risk is still present due to the T-tail but can be mitigated by the application of a stick pusher. Moreover, flutter and stress concentrations around cutouts require further research to mitigate the risks they pose on the structure of the aircraft. Finally, an effective implementation and testing of the fireproof wall and temperature control for the batteries is required to mitigate critical electrical power source risks.

Sustainability Assessment
As all the detailed design is now performed, the sustainability of the E-COmmuter can be assessed using the metrics from the sustainability strategy. As the metrics are continuously evaluated during the design process, sustainability has been a driver for the E-COmmuter design. Hence, it is no suprise that the E-COmmuter complies with all but one sustainability requirement, which is the operational cost requirement (**HEF-OPR-05**).

The noise of the E-COmmuter is assessed in more detail as this is a strength of the E-COmmuter blown wing design and is a key requirement. The airframe noise is assessed using the aircraft noise prediction program method [5], while the propeller noise is evaluated by a simple model based on empirical data. The total maximum noise values are found to not exceed the regulations and requirements.

Further Project Development
For further development of the E-COmmuter, the battery capacity needs to be adapted to current available technologies. Also, the aircraft can not be launched in 2035 but has to launch earlier as a release in 2035 would increase the risk of competitors entering the market. This is especially true considering that the demand for aircraft such as the E-COmmuter is significant. The team is convinced that the E-COmmuter is still sustainable if adapted to currently available battery technologies and an early launch is therefore considered a good strategy.

Manufacturing Approach
As the design project stops before the aircraft is actually build and tested, multiple plans are set up for activities after the project has finished. These plans consist of a manufacturing, assembly, and integration plan and an end-of-life strategy.

The manufacturing of the wingbox composites (GLARE) is mostly done by lay-up, as highly adaptable shapes can be constructed with varying thickness using the ply drop-off of the composite. Moreover, manufacturing of the aluminum fuselage can be done using stretch forming of the skins as well as deep drawing of the fuselage stringers. Manufacturing analysis of the tail, batteries and motors is still to be performed as a more detailed design is required for this. Assembly is mostly done using riveting as this is recommended for GLARE as well as aluminum. The integration of the components is done in a logical order where first the fuselage is manufactured, after which plumbing and electronics are added. This continues with the wing and tail and, finally, the landing gear and motors are assembled. The aircraft is finished by furnishing the fuselage.

An end-of-life strategy for the E-COmmuter is developed including decommissioning, disassembly, dismantling and recycling. Recycling is the most critical step for the GLARE as well as the lithium-sulfur (Li-S) batteries as it has a direct impact on the sustainability of the E-COmmuter. It is analyzed that the aluminum has a recycling rate of 90% and that GLARE recyclability is higher than 85% using a thermal heating process which meets the material recyclability requirement (**HEF-STR-03**). The Li-S batteries are the most critical with a recycling rate of 60%. Future developments in battery recycling are expected to grow this percentage, allowing a higher recyclability. The total recycling rate of all E-COmmuter components totals to 71%.

Cost Analysis
One of the most important information for the operators of the E-COmmuter Re the costs. Hence, a cost analysis is performed to evaluate the operational and purchase cost of the E-COmmuter. An aircraft minimum sales price of €3.100.000 is obtained taking into account manufacturing, certification and component cost. This meets the requirement of €3.900.000 sales price from **HEF-MAN-01**.

The direct operating costs of the E-COmmuter are €2.690.000 and is obtained on a yearly basis. Dividing this by the flight cycles and amount of passengers, a direct operating cost of €91 per passenger per flight is obtained. When

including a margin for the operator and taking into account a 80% occupancy rate, the ticket price is estimated at €120. This result does not meet requirement **HEF-PAX-01**, but the obtained ticket price is still competitive when compared to ground transport.

Project Revision
Using new data from the detailed design and comparing the data to preliminary estimations and Class II weight estimations, an updated budget breakdown is obtained. It is clear that the required power is similar to the preliminary design phase. However, the propulsion mass decreased tremendously due to the addition of a hybrid climb and cruise, which was not taken into account during the early design phases. Next to the power decrease, the operating empty weight dropped sharply. This is a direct result of the decreased propulsion system mass causing a reverse snowball effect. Lastly, the E-COmmuter cost decreased significantly. However, it is expected that this rises towards later development stages, as the novelty features of the E-COmmuter are expected to cause delays.

Recommendations
In general, the major recommendations for the E-COmmuter design consist of doing further research on different subsystems that could not be done due to time constraints. For example, the fuselage design needs to move from an estimation to a calculation. One could also consider to use Finite Element Methods to analyze the wing for flutter and optimal stringer usage. For the propulsion system, a design study on the electronic control system is considered crucial as well as a kinematic study of the folding propeller mechanism. Also, the battery specific energy used in the current design seems large and while some research shows it is attainable, extensive analysis is required to either prove or disprove this.

Conclusion
The E-COmmuter is a hybrid electric commuter aircraft that is able to carry 14 passengers from rural airfields to commercial airports. Its travel time is approximately 35% less compared with driving to the airport by car. In addition, 5% less CO_2 emissions are expelled when compared to an equivalent amount of cars. However, the ticket price is 33% higher than the total cost associated with driving, refueling and parking a car. Even though the costs are higher than the corresponding ground transportation, it is still a competitive aircraft due to its good range flexibility and STOL performance. Hence, the post-DSE activities for the E-COmmuter are planned such so that the aircraft can be in the market earlier than 2035 and meet its high demand.

Contents

1 Introduction

This report details the design process and results of the hybrid electric aircraft named E-COmmuter. Building on the project plan, baseline report and midterm report of Brill et al. [1][4][6], detailed subsystem design are performed. In addition to this, it is of great importance that a solid post-DSE process is established for the production and operation of the E-COmmuter. It should be noted that throughout the design phases, sustainability is highly valued and applied continuously in the decision making process.

The aim of this report is to describe the final design of the E-COmmuter as performed by DSE Group 17. Methods as well as results are discussed for the different subsystems to clarify the design process. In particular, the unique design features of the blown wing design is elaborated upon. Furthermore, the operational characteristics of the novel mission profile are analyzed, as well as the costs related to manufacturing and operations. Technical risks and reliability estimates of the E-COmmuter are included in the analysis as well. Also, the post-DSE activities are discussed including production process, sales and further development of the design.

First, a market analysis for a hybrid electric mini-feeder is performed in chapter 2. The current situation is analyzed and a business strategy is constructed to fit the mission needs and to formulate a project objective. After this, the functional analysis in chapter 3 describes all functions the E-COmmuter shall perform in order to fulfill the prescribed mission. Based on the functional flow diagram (FFD) and the functional breakdown structure (FBS), a requirement list is constructed in chapter 4 for the stakeholders, mission and subsystems.

Using the requirement list, a mission profile is defined in chapter 5. This mission profile defines the electric, fuel and hybrid mission flight phases that are to be considered in the upcoming design process. After this, a sustainability strategy is setup in chapter 6 which is used in chapter 7 to trade-off different aircraft configurations and propulsion system options. The outcome of this trade-off is used during the subsystem design following chapter 7.

Once the best concept for the E-COmmuter is chosen, a design approach and budget is constructed in chapter 8. This explains the processes of the midterm report of Brill et al. [4] concerning the Class I and Class II weight estimations. After the design approach, the design of subsystems can start. After each subsystem is designed, a verification, validation and results section is present to conclude the subsystem and verify its correctness. As a first subsystem, the fuselage is designed in limited detail in chapter 9 resulting in a more detailed cabin layout, weight estimation and environmental control system. Moreover, the wing geometry and load carrying structure is designed in chapter 10, including an analysis on the material choice and wing box layout. A performance analysis is done to analyze different flight phases and to come up with alternative missions in chapter 11. Using the performance characteristics and the fuselage and wing designs, the propulsion system layout and architecture is explained in chapter 12. Using the knowledge of the propulsion system layout, the stability & control of the E-COmmuter is considered in chapter 13 including stability derivatives and static and dynamic control. Directly following from this is the placement of the tail and landing gear in chapter 14. Finally, the system integration in chapter 15 links together all subsystem designs and elaborates on the final design result.

As after chapter 15 the technical design of the E-COmmuter is finished, its operations are discussed. This starts with the operations and logistics concept as explained in chapter 16. After this, the RAMS characteristics in chapter 17 evaluate the reliability, availability, maintainability and safety of the E-COmmuter. Technical risks are identified, assessed and mitigated in chapter 18 to decrease the probability of severe consequences. In addition, the sustainability of the design focusing on noise is assessed in chapter 19.

Finally, further developments of the projects in chapter 20 show the future work to be done. This directly flows into a manufacturing approach for the E-COmmuter in chapter 21. Using chapter 20 and chapter 21, a cost is done to find manufacturing as well as operating costs in chapter 22. To conclude the design, the requirements and budgets set beforehand are evaluated in chapter 23 after which recommendations for future designs are made in chapter 24. The report is concluded in chapter 25.

2

Market Analysis

In order to find the needs, opportunities and possible niches in the market, a market analysis is performed. This analysis investigates the needs of the customer such that the new product can compete with other transportation modes to and from the airport. This chapter first provides the current problem in the market along with the determination of the mission range. Afterwards the users and competitors are discussed and a preliminary business plan and SWOT analysis is given. Finally, the problem assessment by means of case studies is summarized and a study on the market size is provided.

2.1. Current Problem

Current European travel times to airports differ largely between regions. Due to a large airport density, the average time to a major airport is relatively small in western European countries like the Netherlands, Germany and Belgium. This becomes much larger, however, in more rural regions and in regions with a much lower airport density. A visualization of this is shown in Figure 2.1. Regions in France, Spain, Scandinavia and Eastern Europe show areas where travel times can be as large as three hours. Apart from the airport density, many regions with bad infrastructure (for instance, in the Alps) show similar travel times. Large travel times can be costly, considering fuel costs, toll fees and possible parking costs. Also, environmental pollution should not be underestimated.

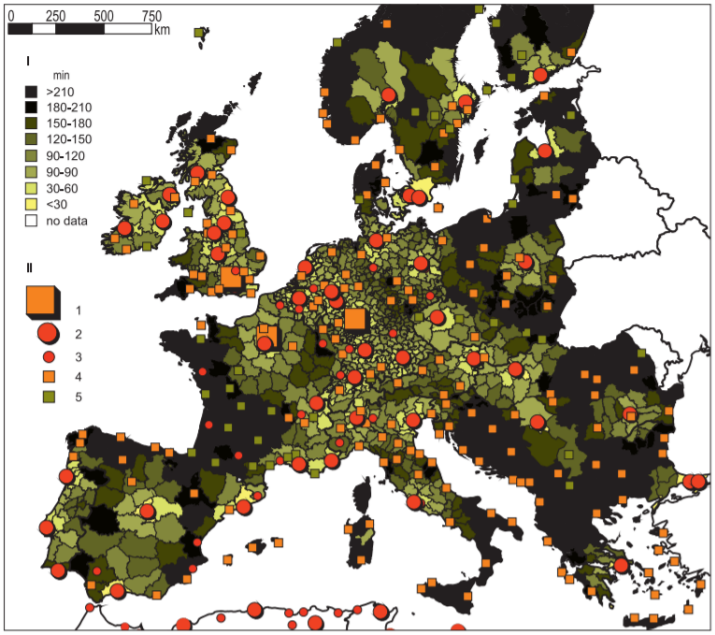

Figure 2.1: Average travel times from European municipalities to the nearest intercontinental airport and airport locations. Explanation: I – time needed to reach the closest intercontinental airport by car, II – categories of international airports, consisting of: 1 – global, 2 – long-haul intercontinental, 3 – short-haul intercontinental, 4 – interregional [7].

The costs for travel (in terms of time and money) will grow significantly in the future due to increasing road congestion and increasing fuel prices [8]. Also, with more societal awareness regarding environmental impact and more effort towards sustainability, new solutions have to be found. Next to updating the current solutions (i.e. better road system, electric cars), new alternatives can be found as well.

The problem described shows that both time and costs are relevant parameters to any possible solution. They are, however, two measures which are not directly linked to each other. To quantify accessibility, Kouwenhoven [9] provides

a measure known as the LogSum method. Using this method, the accessibility of different places can be quantified for comparison, taking into account the speed and cost of the available transportation modes. The method is however very complex, thus considered out of the scope of this project. However, the project will keep in mind both time and cost as a measure of accessibility during the analysis.

2.2. Range Determination

As a starting point, the range required to successfully respond to the market is determined. The range requirement given by the operator is analyzed (**HEF-OPR-03**). It can be fulfilled in two ways; a one-way range of 370 km can be considered, or a return trip of 370 km. In order to discover which range responds best to the market, a graphical analysis is performed. Circles are drawn around the 40 largest European airports in terms of passenger numbers, as well as the European airports of the countries with no airport in the top 40. In Figure 2.2(a) circles with a radius of 185 km are drawn, in Figure 2.2(b) circles with a radius of 370 km. By comparing these two, it becomes clear that with a range of 185 km, many areas are not reached. With a range of 370 km, almost all regions are reached and there even is a lot of overlap. Thus, it can be concluded that a range of 370 km is needed in order to reach almost every location in Europe, especially the rural regions.

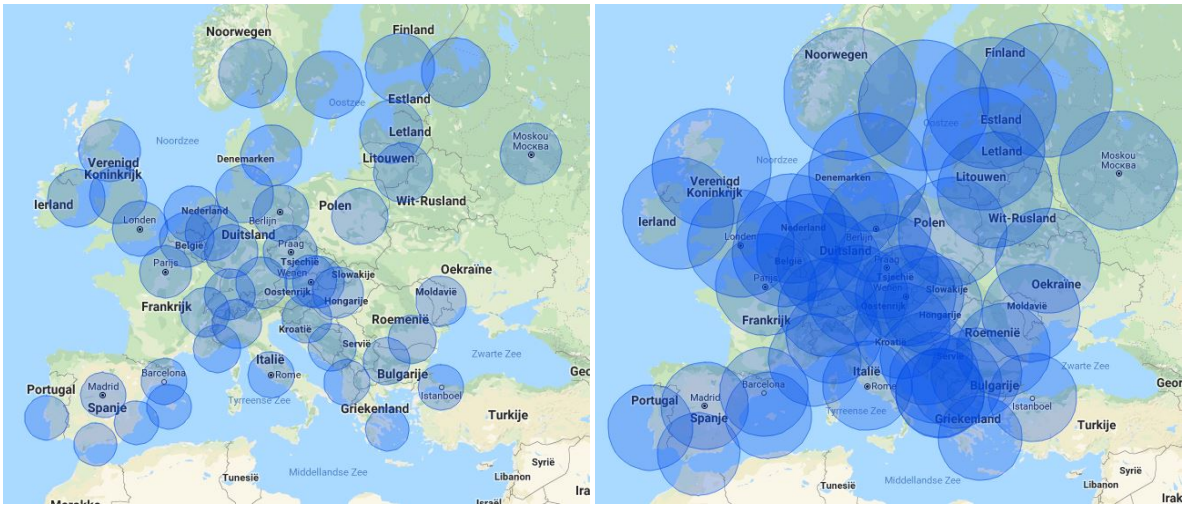

(a) One-way range of 185 km.

(b) One-way range of 370 km.

Figure 2.2: Maps of Europe showing ranges around the 40 largest European airports in terms of passenger numbers..

2.3. Users and Competitors

This section elaborates on the determination of possible users and competitors of the E-COmmuter. The users are divided into two categories in order to find their individual requirements. The first category, the end user, is defined as the passengers using the aircraft as a travel mode to and from the airport. The second category consists of the economic buyers, also called the operators.

The main interest of the end user is the improvement of accessibility to commercial airports by the product. Therefore, time and cost requirements are of great importance to them. With the travel time expected to decrease more than the cost, business passengers are expected to be the main users of the product. This is because time has a greater value for business travellers than for holiday and leisure passengers.

Zooming in on the European market, it can be seen that there are different operators with different strategies. If freighter carriers are excluded for now, three types can be identified (derived from Reichmuth et al. [10]): low cost carriers including holiday carriers (LCCs), full service network carriers (FSNCs), and regional carriers (RCs).

LCCs (e.g. Easyjet, Ryanair, Norwegian) in general provide point-to-point flights with no connection possibilities [10], so LCCs are not expected to operate commuter type aircraft. The other two can be discussed together, as many RCs are feeders for FSNCs [10]. The overall strategy for these two is based on the hub-and-spoke model. In this model, the RCs feed passengers to the airline hub. Connections are key in this model and therefore these airlines are considered the main possible users.

Other possible users can be identified for enlargement of the market. For example, regional airlines and airlines providing services to islands, such as Win Air, can be addressed. Key properties for these operators are low operating costs, short takeoff and landing capabilities, thin-haul services and low passenger numbers. Other users are (previously excluded) freighter services flying to or in rural areas.

The competition is mostly from other aircraft manufacturers, if looking purely at the direct customers (operators) of the E-COmmuter. The competition arises from price (e.g. cheaper unit price or operating cost) and performance.

When looking at passenger level, competition rises from LCCs flying point to point from and towards airports in regions serviced by the E-COmmuter. If the LCCs can provide flights at lower cost or faster than the connection by the E-COmmuter, the profitability of servicing a region will drop. Furthermore, very important competitors of the E-COmmuter are other means of (ground) transportation to the airport. If the passengers choose to travel by car or train, for instance, the E-COmmuter loses profitability.

2.4. Business Strategy and SWOT Analysis

Considering the previously determined users together with the hybrid electric propulsion system, a business model for the aircraft is determined. Rural areas of the world (concentrated on the European market) are connected by the aircraft to major airports by means of a hub-and-spoke model. In this way, the aircraft feeds FSNCs and their RCs with passengers from rural areas. The aircraft can then provide a faster and cheaper way to airports. The CO_2 emission can also be reduced with respect to similar aircraft by use of hybrid electric propulsion.

From the analysis above, a mission statement can be defined. It addresses the combination of sustainability, congestion problems and costs related to travelling to major airports.

Mission Need Statement:
Due to the introduction of innovative and more efficient power systems based on alternative energy sources, a properly designed novel and sustainable commuter aircraft can help to reduce the emissions (such as noise and CO_2-emissions) around airports as well as the amount of private transportation from/to commercial airports, decreasing both the ground infrastructure congestion and the transportation costs for the potential users.

For this mission, a propeller-driven hybrid electric aircraft can be considered, as there are currently major innovations in this domain. In order to compete with ground transportation, the aircraft should be able to operate on cheap, local airfields. Consequently, a project objective can be set up.

Project Objective Statement:
Design a short range hybrid electric aircraft capable of carrying 14 passengers from local (grass) airfields to major/commercial airports, by 10 students in 10 weeks time.

Now, a SWOT analysis is carried out. It focuses on the market in which the aircraft will be operating which is the aviation market for short range and low passenger count transport. As explained before, Europe is considered the main market for the implementation of the business model. The SWOT analysis is tabulated in Table 2.1.

Table 2.1: SWOT analysis diagram for the aircraft's main market segment.

	Helpful	Harmful
Internal	**Strengths**	**Weaknesses**
	Sustainable design	Non-conventional, new design
	Low emissions, green flying	Limited range
	Improvement of accessibility	Limited infrastructure at airfields
	Possible implementation in other markets	
External	**Opportunities**	**Threats**
	New electric propulsion technologies	Alternative transportation modes
	Rising interest in flying as travel mode	Alternative commuter aircraft
	New beneficial emission regulations	Improvement of ground infrastructure near airports
	Rising fuel costs	Seasonal interest of tourist sector

2.5. Case Study

Four case studies are conducted for a more in-depth investigation of the opportunities. All of them consider a European country, namely France, Spain, Poland and the Netherlands. The choice of these countries is based on the accessibility of airports in terms of travel time [7]. If accessibility to an airport is high, people are more willing to consider flying [9]. A higher demand leads to more traffic around an airport, possibly causing congestion, thus more capacity is required. On the other hand, if the accessibility is low, people have less incentives to fly from this airport which can be improved by providing new transportation modes.

The results of the case studies are summarized in Table 2.2. The summary shows the large differences in travel times and cost. This means also different needs can be defined depending on region. In order to assess the CO_2 emissions in a comparable way, the 2017 European Union targets are used. This target corresponds to an average emission of

118.5 g km^{-1} seat^{-1}[1]. The parking cost is calculated for five days, from Monday to Friday.

Table 2.2: Summary of the conducted case studies.

	CS 1: France	**CS 2: Spain**	**CS 3: Poland**	**CS 4: Netherlands**
Travel time	3h30	3h22	3h53	2h
Distance	318 km	352 km	267 km	194 km
CO_2 emission	75.4 kg	83.4 kg	63.3 kg	46.0 kg
Fuel cost	€48.92	€44.64	€31.04	€32.00
Toll cost	€15.00	€25.00	€0.00	€0.00
Parking cost	€53.00	€39.00	€46.80	€80.00
Total cost	€116.92	€108.64	€77.84	€112.00
Cost per km	€0.37 km^{-1}	€0.31 km^{-1}	€0.29 km^{-1}	€0.57 km^{-1}

From these results it is clear that the needs are not the same for whole Europe. For France, Spain and Poland there is the need to reduce the travel time. In the Netherlands the travel time is already quite low because of the high accessibility in this region of Europe. The costs can be greatly reduced for France, Spain and the Netherlands. Furthermore, the largest portion of the costs is the parking cost in France and the Netherlands.

As it is not possible at this stage to address all of these needs, some choices are made. It is decided to focus on the reduction in travel time. This corresponds to requirement **HEF-PAX-02** ("The door-to-door travel time for passengers shall be at least 20% lower than the corresponding ground transport time."). Cost is aimed to remain competitive with the car. This agrees with requirement **HEF-PAX-01** ("The ticket price per passenger shall be equal to or lower than 125% of the corresponding ground transportation and parking costs."). Consequently, the target area consists of France, Spain, Central- and Eastern-Europe. This addresses rural areas with poor airport connections. Extra effort is dedicated to sustainability and environmental impact. CO_2 emissions are limited to the corresponding car emissions for the set range of 370 km.

Some remarks should be made regarding this analysis. Firstly, only the car is considered as transportation mode. However, some major airports have good railway connections or other services are available. Secondly, only single travellers (e.g. business people) for a short time period are considered. The case for a family or couple going on an extended vacation could vary in terms of costs. They also have different needs; for business people fast travel is more important than cheap travel, whereas for families the opposite is usually true. Thirdly, only major airports are considered now. Depending on the travel destination, some local airports may provide flights. In that case, the travel time and cost will be lower. Fourthly, environmental impact is only addressed in terms of CO_2 emissions of the car. Other influencing aspects, such as manufacturing and other green house gases, are not taken into account yet. Finally, only Europe is examined. The market in other parts of the world may be different and require a separate analysis.

2.6. Market Size And Value

In 2016 the total European aviation market was nearly 973 million passengers[2]. It includes all passengers with connecting flights through airports. For instance, Schiphol saw 36.7% of their passengers transferring to another flight. Furthermore, not all passengers travel by car to airports: car usage is estimated to be 45% of the transportation modes to airports [9]. Lastly, considering the target end users of the product, an estimated 30% of all passengers is travelling for business purposes [11].

The distance passengers travel to an airport should be investigated for a more in-depth analysis of the European market. This shows how many passengers (thus possible users) can be interested in using the product. However, no actual data on this is available, as car travel is hard to estimate [10]. Thus, the market size estimation is something considered out of the scope of the project from here on. However, it is highly advised to perform a detailed analysis by specialized experts for further development of the aircraft.

2.7. Conclusion

From this market analysis, it is decided to design an aircraft with a range of 370 km. The target area consists of South- and East-European countries, such as France, Spain and Poland. Furthermore, it is chosen to focus on a reduction in travel time and remaining cost competitive with the car. It is also decided to reduce emissions with respect to similar aircraft and to be in the same range as . The end users are expected to be mainly business people. The operating airlines are RCs and FSNCs airlines. The main competitors are aircraft manufacturers producing similar aircraft and the car.

[1] URL: `https://ec.europa.eu/clima/policies/transport/vehicles/cars_en` [cited 9 May 2018]

[2] URL: `http://ec.europa.eu/eurostat/documents/2995521/8306203/7-11102017-BP-EN.pdf/88f3089c-20d7-4bbe-8012-68addd95cee9` [cited 14 May 2018]

3
Functional Analysis

To translate the results from chapter 2 into a tangible aircraft, a functional analysis is performed. The functional analysis results from two separate analyses: the functional flow diagram and the functional breakdown structure. The functional flow diagram shows the order of the functions which the product has to perform and the functional breakdown shows the hierarchy between said functions.

3.1. Functional Flow Diagram

The functional flow diagram (FFD) (given in Appendix A in Figure A.1) is split up in the following five sections: design, production, distribution, operation and retirement. These five sections represent the phases through which a product should pass. The most determining part for the design of the E-COmmuter consists of its operation and hence the emphasis in the FFD is on the operational part. A more detailed breakdown of each section is carried out in the functional breakdown structure in section 3.2.

In Figure A.1 there is a unique identifier for each function. Furthermore, there is a unique color for each level in the diagram. Levels 1, 2, 3, 4 and 5 are indicated in red, orange, blue, grey and yellow, respectively. The following abbreviations are used: SOC stands for State Of Charge and ICE stands for Internal Combustion Engine.

3.2. Functional Breakdown Structure

The functional breakdown structure (FBS) (given in Appendix A in Figure A.2) of the aircraft system is a derivative from the functional flow diagram shown in section 3.1. The aircraft system is again split in the five phases. From this diagram one can derive the functions that the different subsystems of the aircraft will have to perform during certain phases. Following from the market analysis, it is apparent that the aircraft has to be able to takeoff from and land on different types of runway, possibly on grass strips or asphalt. Furthermore, it is clearly visible in the FBS that the propulsion system adopted will have to perform its takeoff and landing using only electrical propulsion.

Functions that are split up in subfunctions in the FFD are not displayed in the FBS since all the sub-functions are already given in there. The identified functions in the FFD and FBS will serve as a guide to figure out technical requirements and design options in chapter 4 and chapter 7 respectively.

The color scheme displaying the levels for the FBS in Figure A.2 is adopted from the FFD explained in section 3.1. The numbering in the FFD and the FBS are consistent with each other.

4

Requirements

This chapter gives an overview of all the requirements set up for this project and indicates whether they are met. The requirements are divided into three categories: stakeholder, mission and subsystem requirements. Subsystem requirements are divided in: structural, propulsion, stability & control, performance and operations requirements. The stakeholder and mission requirements follow from the market analysis. The subsystem requirements follow from the functional flow diagram and breakdown structure. Additionally, a preliminary technical risk assessment is done resulting in additional subsystem requirements. This technical risk assessment is revised in chapter 18. Subsystem requirements which follow from regulations made by the European Aviation Safety Agency (EASA) are indicated with a CS-23 code.

Table 4.1 is the compliance matrix of the design. The abbreviations in the compliance matrix are the following:: Hybrid-Electric-Mini-Feeder (HEF), Operator (OPR), Passenger (PAX), Airport (APR), Manufacturer (MAN), Regulator (REG), Mission (MIS), Structural (STR), Propulsion (PROP), Stability & Control (SC), Performance (PERF), Operational (OPS), International Civil Aviation Organization (ICAO), and Short TakeOff and Landing (STOL). The table contains all the requirements that are set up for this project and gives an overview if they are met or not. An explanation is given for each of the requirements. Furthermore, for each requirement the section is given containing the elaborate explanation or designing process to meet the requirement. If one of the requirements is not met, recommendations need to be given for feasible modifications to the design in order to meet the requirements. This is done in chapter 23.

All the requirements must comply with the V.A.L.I.D. criteria [3]: Verifiable, Achievable, Logical, Integral, and Definitive. For some of the requirements it became clear that this is not the case and these requirements are crossed out in the table. All the requirements that are checked off with a ✓ are requirements that are met. The requirements with an x are not met, requirements which could not be checked at this stage of the design are marked with ⁘.

Table 4.1: Requirement compliance matrix.

Identifier	Requirement		Comment
	STAKEHOLDER		
	Operator		
HEF-OPR-01	The total ground handling time shall not be any longer than 40 min.	✓	$t_{\text{ground handling}} = 40\,\text{min}$. (*subsection 16.2.1*)
HEF-OPR-02	The aircraft shall be able to transport 14 passengers carrying 20 kg each.	✓	$n_{\text{seats}} = 14$ and $W_{\text{cargo}} = 280\,\text{kg}$. (*section 9.1*)
HEF-OPR-03	The design range R_D of the aircraft shall be at least 370 km one-way.	✓	$R_D = 389.12\,\text{km}$. (*section 11.4*)
HEF-OPR-04	The aircraft shall be made from renewable materials that have a recycling rate of at least 85%.	✓	GLARE wing structure, aluminum alloy fuselage, titanium alloy landing gear. (*subsection 21.2.4*)
HEF-OPR-05	The direct operating costs (DOC) shall be lower than €545 h^{-1}.	x	DOC = €640 h^{-1}. (*subsection 22.3.2*)
	Passenger		
HEF-PAX-01	The ticket price per passenger shall be equal to or lower than 125% of the corresponding ground transportation and parking costs.	x	Ticket price = € 120, which is 133% of ground transportation cost. (*subsection 22.3.2*)
HEF-PAX-02	The door-to-door travel time for passengers shall be at least 20% lower than the corresponding ground transport time.	✓	Difference in time with ground transportation 35% less. (*subsection 16.2.2*)
	Airport		
HEF-ARP-01	The maximum noise level emitted shall be at least 10 dB lower than the ICAO standards.	✓	Noise levels are at least 15dB below standards. (*subsection 19.2.1*)

~~HEF-ARP-02~~	~~The aircraft shall be capable of flying at least 300 km h^{-1} during the approach of the runway.~~		Different means of approach for commuter category aircraft compared to airliners.
HEF-ARP-03	The aircraft shall have STOL capabilities such that it can takeoff and land on a local airfield with a minimum runway length of 700 m.	✓	$s_{\text{takeoff}} = 503$ m, $s_{\text{landing}} = 566$ m. (*subsection 11.3.2, subsection 11.3.7*)
HEF-ARP-04	The aircraft wing shall have a maximum span of 24 m.	✓	$b = 20.92$ m. (*section 10.10*)
	Manufacturer		
HEF-MAN-01	The aircraft shall have a unit price of equal to or less than €3.9 million.	✓	Minimum sales price per unit is €3.1 million. (*subsection 22.3.1*)
HEF-MAN-02	The average CO_2 emissions for a nominal mission shall be less than 118.5 g km^{-1} seat^{-1}.	✓	For the nominal mission 112.7 g km^{-1} seat^{-1} of CO_2 emission is emitted. (*subsection 11.4.1*)
~~HEF-MAN-03~~	~~The failure rate shall be less than 10^{-6} per flight hour.~~		Failure rate only applicable to the propulsion system.
	Regulator		
HEF-REG-01	The aircraft shall comply with all requirements stated in the CS-23 regulations.	⁛	Is designed for, can only be fully checked at later design stage.
	MISSION		
HEF-MIS-01	The aircraft shall have a cruise speed V_c higher than 180 km h^{-1} at an altitude of 3000 m above sea level.	✓	$V_c = 250$ km h^{-1} at 3048 m above sea level. (*section 10.4, section 13.3*)
HEF-MIS-02	The aircraft shall have a design range of up to 370 km.	✓	$R_D = 389.12$ km. (*section 11.4*)
HEF-MIS-03	The aircraft shall be able to carry at least 14 passengers and their luggage with an average weight of 77 kg and 20 kg respectively.	✓	$n_{\text{seats}} = 14$ and $W_{\text{cargo compartment}} = 280$ kg. (*section 9.1*)
~~HEF-MIS-04~~	~~The aircraft shall be able to arrive at an airfield with at least 60% battery charge left.~~		Change in mission, refueling and recharging at airfield.
	STRUCTURAL		
HEF-STR-01	The aircraft structure shall be able to support limit loads without detrimental, permanent deformation. *(CS-23.305)*	⁛	Wing structure is designed for limit loads, other structures still need to be designed in detail. (*subsection 9.3.1, section 10.6*)
HEF-STR-02	The aircraft structure shall be able to support ultimate loading without failure for at least three seconds. *(CS-23.305)*	⁛	Same as HEF-STR-01.
HEF-STR-03	The aircraft shall be made from renewable materials with a recycling rate of at least 85%.	✓	GLARE, aluminum alloy, titanium alloy. (*subsection 21.2.4*)
HEF-STR-04	The structure of the aircraft shall be designed such that each occupant is protected during emergency landing conditions.	⁛	Not designed for yet.
HEF-STR-05	The aircraft fuselage shall not be pressurized.	✓	The aircraft has a squared unpressurized fuselage. (*section 9.1*)
HEF-STR-06	The aircraft fuselage and wing structures shall be made from lightweight materials.	✓	GLARE, aluminum alloy. (*section 9.2, section 10.6*)
HEF-STR-07	The strength requirements for the aircraft structure shall be met at any combination of airspeed and load factor within the boundaries of the aircraft its flight envelope.	⁛	Structure is designed for limit loads, needs further analysis and testing to meet the requirement. (*subsection 9.3.1, section 10.6*)
	Technical Risk		
HEF-STR-08	A factor of safety of 1.5 shall be used for limit loading. *(CS-23.303)*	✓	$n_{\text{ult}} = 1.5 \cdot n_{\text{limit}}$. (*subsection 9.3.1, section 10.6*)
HEF-STR-09	The passengers shall be protected against propulsion system failure during normal operation.	⁛	Not designed for yet.
	PROPULSION		
~~HEF-PROP-01~~	~~The propulsion system shall have the ability to recharge its batteries up to at least 60%.~~		Change in mission, refueling and recharging at airfield.

HEF-PROP-02	The propulsion system shall not produce any exhaust gasses or particulate matter during takeoff and landing.	✓	Takeoff and landing, batteries provide power to the propulsion system. (*chapter 6*)
~~HEF-PROP-03~~	~~The mean maximum noise level emitted during zero-emission mode shall be equal to or lower than 55 dB measured from the ground at an airport.~~		Wrong interpretation of information, decibel level of 55 dB is not realistic.
HEF-PROP-04	The propulsion system shall be able to be operated until at least the maximum operating altitude.	✓	Cruise altitude is 3048 m. (*section 12.7*)
HEF-PROP-05	The propulsion system shall have a failure rate of less than 10^{-6}.	✓	Failure rate = 10^{-6}. (*section 17.2*)
HEF-PROP-06	The propulsion system shall emit a maximum of $118.5\,g\,km^{-1}\,seat^{-1}$ in CO_2 emissions averaged over a nominal mission.	✓	For the nominal mission $112.7\,g\,km^{-1}\,seat^{-1}$ CO_2 is emitted. (*section 11.4*)
	Technical Risk		
HEF-PROP-07	The propulsion system shall be equipped with an overcurrent protection for all electric motors.	✓	Equipped with Electric Control Unit (ECU). (*section 12.1*)
HEF-PROP-08	The propulsion system shall be equipped with an overcharge protection for all electric batteries.	✓	Equipped with ECU. (*section 12.1*)
HEF-PROP-09	The propulsion system shall be equipped with an overdischarge protection for all electric batteries.	✓	Equipped with ECU. (*section 12.1*)
HEF-PROP-10	The propulsion system shall be equipped with a protection system to avoid over-discharge rates for all electric batteries.	✓	Equipped with ECU. (*section 12.1*)
HEF-PROP-11	The propulsion system shall be equipped with a protection system to avoid over-charge rates for all electric batteries.	✓	Equipped with ECU. (*section 12.1*)
HEF-PROP-12	All electrical motors for thrust generation shall be equipped with a minimum of two speed controllers.	✓	More than two inverters with speed controller integration. (*section 12.1*)
HEF-PROP-13	If the aircraft uses a generator, a minimum number of two generators shall be required.	✓	Two generators are used. (*section 12.1*)
HEF-PROP-14	All internal combustion engines shall be equipped with an over-speed protection system.	✓	Equipped with ECU. (*section 12.1*)
HEF-PROP-15	The propulsion system shall be equipped with a cooling system.	✓	Cooling system integrated in the propulsion system. (*section 12.1*)
	STABILITY & CONTROL		
HEF-SC-01	The aircraft shall be safely controllable and manoeuvrable during all flight phases. *(CS-23.143a)*	⁛	Will be checked as soon as HEF-SC-07 is met.
HEF-SC-02	The aircraft shall be able to acquire a state of trim longitudinally, laterally and directionally, without any movement or pressure upon the controls. *(CS-23.161)*	✓	Inherently and control stable, with trim tabs it can thus acquire a state of trim. (*section 13.2, section 13.5*)
HEF-SC-03	The aircraft shall be statically stable longitudinally, directionally, and laterally. *(CS-23.171)*	✓	Wing placement, tail sizing, and blown wing control applications entirely based on stability and controllability. (*section 13.2, section 13.5*)
HEF-SC-04	All aircraft's dynamic eigenmotions shall be stable. *(CS-23.181)*	✓	Eigenmotions described in CS-23 are stable, with required damping. (*section 13.4*)
HEF-SC-05	The aircraft shall always be able to recover from any stall condition. *(CS-23.201)*	✓	Longitudinally stable, tail is sized and placed to prevent deep stall. (*section 13.2*)
HEF-SC-06	The aircraft shall have a clear and distinctive stall warning. *(CS-23.207a)*	✓	Added to the flight deck. (*section 13.6*)
HEF-SC-07	The aircraft shall be able to recover from a one-turn/three second spin, whichever longer, in not more than one additional turn after initiation of control forces for recovery. *(CS-23.221a)*	⁛	Not yet checked due to scope of the project at this stage. Analysis left for more detailed design phase.

HEF-SC-08	The aircraft shall have longitudinal and directional ground stability and control during taxi, takeoff and landing operations, also on unpaved surfaces. *(CS-23.231, CS-23.233c)*	✓	Landing gear sizing. (*section 14.2*)
	Technical Risk		
HEF-SC-09	The aircraft stability & control system shall actively deter pilots from causing upset conditions.	✓	Stability requirements are met. (*section 13.6*)
HEF-SC-10	When an upset condition occurs, the stability & control system shall automatically or inherently recover the aircraft from that state.	✓	Follows from HEF-SC-05. (*section 13.2, section 13.6*)
HEF-SC-11	The stability & control system shall warn the pilot of ground proximity.	✓	Ground Proximity Warning System added. (*section 13.6*)
HEF-SC-12	The aircraft shall have a flight interface that allows the pilot to safely operate the aircraft during all operations.	✓	Flight interface which is to be chosen in a later design stage. (*section 13.6*)
HEF-SC-13	The aircraft shall still be stable and controllable after all primary control surfaces have failed.	✓	Blown wing control applications, engine failure analyses. (*section 13.5*)
HEF-SC-14	The aircraft shall be safe and fully functional for the whole range of c.g. positions possible.	✓	Achieved by placement of the wing and tail sizing. (*section 13.2*)
HEF-SC-15	The landing gear shall be positioned such that it allows any combination of pitch and roll that might occur during operation.	✓	Landing gear sizing is based on these requirements. (*section 14.2*)
HEF-SC-16	The landing gear shall be positioned such that the nose gear load is in between 8% and 15% of maximum takeoff weight.	*x*	Nose landing gear load is between 8% and 17% maximum takeoff weight. (*section 14.2*)
HEF-SC-17	The aircraft shall be able to rotate during takeoff.	✓	Landing gear sizing is based on these requirements. (*section 14.2*)
	PERFORMANCE		
HEF-PERF-01	The aircraft shall be equipped with high lift devices.	✓	Flaps + distributed electrical propulsion system with high lift propellers. (*section 13.5*)
~~HEF-PERF-02~~	~~The aircraft shall have a runway approach velocity $V_{approach}$ of at least 300 km h^{-1}.~~		Different means of approach for commuter category aircraft compared to airlines.
HEF-PERF-04	The aircraft shall have a maximum takeoff weight of no more than 8618 kg. *(CS-23.1)*	✓	Maximum takeoff weight is 5835 kg. (*chapter 15*)
HEF-PERF-06	The aircraft shall have an operating altitude of at least 3048 m above main sea level.	✓	Cruise altitude is 3048 m above main sea level. (*section 13.3*)
HEF-PERF-08	The aircraft shall be able to takeoff from an unpaved runway of no more than 700 m in length.	✓	$s_{\text{takeoff}} = 503$ m. (*subsection 11.3.2*)
HEF-PERF-09	The aircraft shall be able to land on an unpaved runway of no more than 700 m in length.	✓	$s_{\text{landing}} = 566$ m. (*subsection 11.3.7*)
HEF-PERF-10	The aircraft shall be able to achieve a climb gradient after takeoff of at least 4% at sea level with engine and wings in takeoff positions and landing gear extended. *(CS-23.65)*	✓	Climb gradient = 7.58%. (*subsection 11.3.3*)
	OPERATIONAL		
HEF-OPS-01	All destinations of the aircraft shall have the ability to fully refuel and recharge the aircraft.	✓	Refueling and recharging possible at all destinations. (*subsection 16.2.1*)
HEF-OPS-02	The ground handling time shall not be longer than 40 min, including recharging, refueling, safety checks, loading and unloading.	✓	The ground handling lasts 40 min. (*subsection 16.2.1*)
HEF-OPS-03	The security level of every aircraft destination shall comply with European Commission Aviation Security Regulation.	⁘	Not yet checked due to scope of the project. (*section 16.1*)

5
Mission Profile

One of the most important and determining factors for the E-COmmuter is its mission profile. The mission profile determines how competitive the aircraft aims to be and what it is designed for. To construct the mission profile, the requirements from chapter 4 are taken as a starting point. The most important requirement for the mission is **HEF-OPR-03**, which sets the range of the aircraft at 370 km. This range is specifically designed to allow rural areas and the people who live there to connect with the major cities and their airports, enabling their participation in the global economy. Next to this requirement and in accordance with **HEF-MAN-02**, the aircraft cannot emit more than 118.5 g km^{-1} seat^{-1} of CO_2 and has to have the ability to do a zero emission takeoff and landing. Based on these (and other requirements), the mission profile is constructed which is displayed in Figure 5.1.

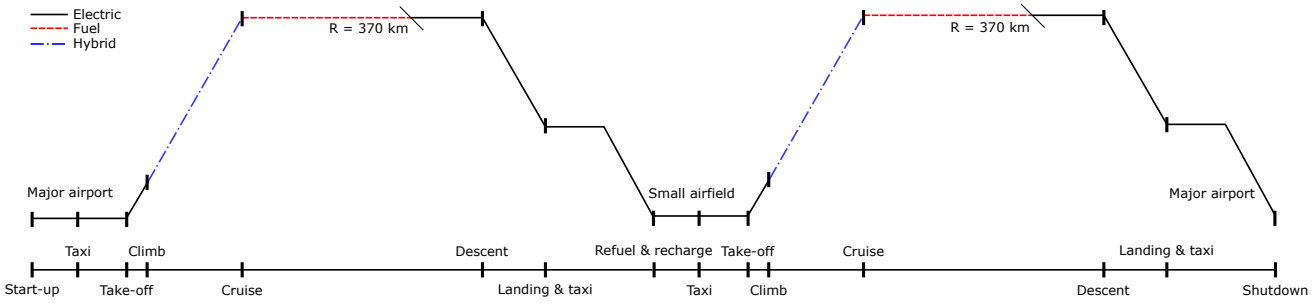

Figure 5.1: Mission profile for the E-COmmuter.

An important characteristic for the mission profile of the E-COmmuter is the fact that it includes both a landing and an approach at a small airfield. The mission profile follows from section 2.2 and the requirement to connect big airfields to small airports and vice versa. Next to this, Figure 5.1 shows the measures taken to reduce the emissions of the aircraft. All flight phases, except climb and cruise, are done in a pure electric power mode with zero emissions. To enable this mode, the aircraft carries batteries on board which are recharged at both the large airport and the small airfield with sustainable energy sources. During climb, the aircraft fires up its internal combustion engines (ICEs) to extend the range of the batteries. Using the ICEs in tandem with the batteries allows for a smaller ICE and generator size, which saves on the weight and therefore fuel costs of the aircraft. For the cruise phase, the aircraft runs for 80% on its ICEs only and for 20% on its batteries. With this division, the E-COmmuter first gets rid of its fuel to make the aircraft lighter, after which the rest of the cruise is fulfilled by travelling on batteries.

The amount of fuel the E-COmmuter can take on board is the maximum amount of fuel as allowed by requirement **HEF-MAN-02**. chapter 11 goes into further detail about the mission profile and its construction.

6

Sustainability Strategy

The aim of this chapter is to elaborate on the strategy on how sustainability is implemented into the design of the E-COmmuter. First, the background of the concept of sustainability for this project will be discussed in section 6.1. This includes an argumentation as to why sustainability is of such importance to the E-COmmuter. Next in section 6.2, it is discussed how the E-COmmuter system takes into account sustainability in its requirements, mission definition and how the subsystems take into account sustainability on a more detailed level.

6.1. Background

Transport sustainability is one of the most important and growing concerns in the aviation industry. It affects the environment, society and economy. Due to such a wide and often powerful impact, sustainability is also a subject that numerous groups, organizations or institutions are involved in. Therefore, it is even more important that the aircraft complies with as many of the wishes and needs of those groups as possible.

In order to be able to effectively implement these wishes and needs, they are categorized into five sustainability metrics groups which have been elaborately developed in the previous reports of this project [1][4][6]. These metrics are based on the sustainability criteria for sustainable mobility, as defined by the EU Council of Sustainable Transport and INFRAS, which does research on sustainable development [12]. As the focus area for development of the E-COmmuter is Europe, and it also has to comply with European regulations, these metrics are most applicable to the E-COmmuter.

These metrics have been actively incorporated into the design of the aircraft, which are listed below. They are described here to give the reader an insight into the reasoning why sustainability is important for the E-COmmuter design.

Accessibility

Accessibility describes how the the basic access and development needs of individuals, societies, and companies are met. This metric is important to the societal aspect of sustainability. In practice it means that the developed mode of transport should be accessible to anyone who might want to use it, and should be able to provide a platform needed for the user to develop itself in a positive way. This primarily includes the disclosure of rural areas and their people, empowering them to take part in global development and connect with the global network.

Safety

Safety is, especially in aviation, one of the most important drivers for any design or any new concept. The strict constraints for this metric are mainly provided by regulatory bodies, such as the European Aviation Safety Agency (EASA) and regulations that they develop. Furthermore, governments, stakeholders, but also users might have additional safety requirements, or will otherwise waive their interest for acceptance, investment or use of the aircraft. Therefore, a unsafe design will always be short-lived, making safety one of the most important metrics.

Ecosystem Health

In recent years, the awareness of the effect of emission of exhaust gases and particulate matters has substantially grown, and so have the emission themselves. These type of emissions have by far the widest negative impact of all aviation emission types. It affects human health, wildlife, ecological systems, the climate, and more. By far the largest contributors to these effects are the global emissions due to CO_2, and local emissions due to NO_x. The former has a detrimental effect for global warming and the latter on local air quality. CO_2 pollution due to aviation is expected to grow with a factor of 2.0-3.6 by the year 2050, and NO_x by a factor of 1.2-2.7 [13]. Therefore, CO_2 and NO_x emission reduction are very important in the E-COmmuter project.

Resource Use

In order to assure the availability of finite resources for future generations, it is essential to use those existing resources efficiently today. Resource usage can generally be split into four key categories: materials, energy, water and land use [14]. As this project focuses on the production of an aircraft, the categories most relevant are materials and energy usage. Sustainable material usage can be measured by the usage of recycled and recyclable raw materials. But also by

the achievable recycling rate after usage. Also the waste during production and the shipping distance of the materials should be minimized. As energy usage is directly linked to greenhouse gases emitted, it can easily be quantified by the amount of energy used during production.

Noise
The noise impact of aircraft is one of the most important and most publicly debated issues. This is mainly due to the very high number of affected people that live in the vicinity of airports and because the results of noise nuisance can be very substantial. Very serious negative effects have been investigated including that, from Stansfeld et al. [15]: "Our findings indicate that a chronic environmental stressor—aircraft noise—could impair cognitive development in children, specifically reading comprehension. Schools exposed to high levels of aircraft noise are not healthy educational environments," or even that, from Huss et al. [16]: "Aircraft noise was associated with mortality from myocardial infarction, with a dose-response relationship for level and duration of exposure." These very serious results ask for serious noise reduction efforts. Therefore, noise reduction is a very important driver for the E-COmmuter project.

Affordability
Sustainability applies to affordability, as it is socially and economically desirable to have an affordable means of transport. Socially it means that the transport mode shall be able to provide mobility to users, even if they might not be able to afford other means of transport. Economically it means that it should be cheap and profitable to operators of the aircraft. Both are desirable aspects and therefore they are incorporated into the design.

6.2. Application of Sustainability to System and Subsystems

The application of sustainability to the E-COmmuter design is mainly done via two ways. First, there are a significant number of requirements and the mission profile, which set goals for the design regarding sustainability. These requirements are powerful tools, as these are factors the subsystems need to actually be designed for.

For the requirements, a number of important stakeholder requirements are listed together with the subsystem that they have a large influence on.

- **HEF-OPR-04:** Setting the recyclability of the aircraft to a minimum of 85% will greatly influence the resource use in a positive way, and will take away the need to harvest new natural resources for future aircraft. *Influences structures.*
- **HEF-PAX-01 & HEF-MAN-01:** A low ticket and unit cost will increase the affordability of the aircraft, opening up the transport mode to new communities of people and increasing profitability for the operator. *Influences cost of operations.*
- **HEF-PAX-02:** Travel time increases the accessibility of the aircraft, optimizing the use of the E-COmmuter as a platform suitable to support development. *Influences performance.*
- **HEF-ARP-01:** This is the most important requirement for reduction of the noise. Meeting the ICAO noise restrictions is an important sustainable requirement. *Influences propulsion.*
- **HEF-MAN-02:** This is the most important emission requirement which states the maximum amount of CO_2 that may be emitted. This will lower the global emissions of the aircraft significantly. Furthermore, requirement **HEF-PROP-02** states zero emission takeoff and landing, which causes the aircraft to have no local emissions at all. *Influences propulsion and performance.*
- **HEF-REG-01:** CS-23 are the most important safety regulations that should be adhered to. Designing the subsystems according to regulations will guarantee the safety of the aircraft. *Influences all subsystems.*

Next to this list, the mission profile for the E-COmmuter is developed entirely to disclose rural areas with the incorporation of hybrid systems to perform zero-emission takeoff and landing. Therefore, the mission itself is one of the most sustainable features of the E-COmmuter design. This together with the list containing the most important sustainable stakeholder requirements, will thus have a direct sustainable effect on the aircraft. Furthermore, all the subsystems themselves have additional, more detailed sustainable requirements.

The second manner of implementation is not by requirements, but by making design decisions based on an understanding of sustainability. For these there are no explicit design targets, but they can make a substantial difference if sustainability is prioritized over other factors. This may include, for example, design choices in order to make the aircraft lighter and reduce emissions even further, or redundancies to make the aircraft even safer than the regulations prescribe.

These two methods described above apply directly to the technical design of the aircraft and explanation on how these are met are therefore present throughout all chapters on the design of the aircraft.

7

Trade-off Summary

Several different technologies and configurations were looked into in order to make the aircraft perform as desired. This chapter summarizes the trade-off process for the aircraft configuration and propulsion system concepts. First, the trade-off methodology is defined. Next, the trade-off for the aircraft configuration is covered. Finally, the propulsion configuration trade-off is performed. The results are summarized at the end in section 7.4 [4].

7.1. Trade-off Methodology

Every trade-off has a couple of criteria specific for the system being evaluated. The trade-offs are performed in matrix form. The criteria occupy the top row and the weighting of the criteria is indicated by the respective width of the columns. The weights range from 1/4 for the least important ones to 4/4 for the highest priority criteria. The different configurations/options, placed in the rows of the matrix, are then graded for each criteria and compared. To aid in the visualization of the trade-off, every cell of the matrix is color coded. The color would indicate whether a concept meets the criteria or not, if it exceeds the requirement or if results are unacceptable.

Two major trade-offs are performed: one for the aircraft configuration (section 7.2) and one for the propulsion system (section 7.3). Both of these are subdivided in smaller trade-offs [4]:

- **Aircraft configuration trade-off:**
  - Fuselage trade-off
  - Wing-tail trade-off
  - Final aircraft configuration trade-off
- **Propulsion system trade-off:**
  - Powertrain configuration trade-off
  - Power cell trade-off
  - Propulsion layout trade-off
  - Electric motor trade-off

A sensitivity analysis is performed on each trade-off to ensure the robustness of the chosen concept and to ensure that the decision making was unbiased. This is done by varying the weights of the criteria, adjusting the assumptions for when a criterion is met and leaving out a criterion. After this the definitive outcome of the trade-off is determined. Two criteria that return for every trade-off are cost and development risk. Cost is generally weighted low as there is no driving requirement concerning a budget. The development risk accounts for possible deviations in final product outcome due to required research on new technologies. This is also weighted low as the project is to take shape by 2035, which means there is plenty of time for technology to mature.

7.2. Aircraft Configuration Trade-off

The aircraft configuration is determined by combining different kinds of wings with different kinds of tails. The combinations are assessed on cruise and low speed (takeoff and landing) performance to meet runway length and travel time requirements, stability and controllability to assure safe flight and passenger comfort, and structural weight. The fuselage shape is also determined here. The highest weighted criteria are takeoff and landing performance (STOL) and structural weight, followed by stability, controllability and cruise performance.

7.2.1. Wing-Tail Trade-off

Table 7.1: Considered wing-tail trade-offs.

Conventional high-wing	Prandtl box wing	Canard high-wing
T-tail	T-tail	T-tail
Conventional tail	Conventional tail	Twin tail
V-tail	V-tail	No tail
Cruciform tail	Cruciform tail	

The options which came out of a design option tree are a conventional or Prandtl wing, combined with either a conventional tail, a V-tail, a T-tail or a cruciform tail. Another option is a canard high wing configuration, either without a tail or with a T- or twin tail. The combinations are shown in Table 7.1.

After performing the trade-off using the criteria mentioned above, it is concluded that a conventional high-wing configuration with a T-tail is the most suitable option for this project. Compared to the Prandtl wing and canard configuration, the conventional wing configuration offers lower structural weight and better stability. Furthermore, combined with a T-tail, this option shows significant advantages in cruise performance and even more improved stability due to the horizontal stabilizer being located outside the wing wake. It has better spin recovery and STOL characteristics and increases controllability thanks to a longer tail arm. The only drawback of the conventional high-wing with a T-tail compared to the other two concepts is a weakness to deep stall. However, the deep stall risk associated to this is mitigated by adding a stall warning. This concept is worked out further in the next design stages.

7.2.2. Fuselage Selection

In addition to the wing-tail configuration, the fuselage shape should be defined. The aircraft has no need for pressurization since the cruise altitude is kept below 3048 m. This means that the fuselage does not necessarily need to be circular, as a circular fuselage is usually used to carry tensile pressurization loads. For internal geometry reasons, to allow for enough room for passengers, luggage, etc., a rectangular fuselage is preferable. This also results in a simpler and therefore, cheaper manufacturing process. Concluding, the conventional longitudinal fuselage shape with a rectangular cross-section is chosen, since this is a well-known configuration, which results in lower manufacturing cost.

7.3. Propulsion System Trade-off

This section discusses the design options for the hybrid electric propulsion system. Trade-offs are performed for the powertrain configuration (subsection 7.3.1), the power cell (subsection 7.3.2), the propulsion system layout (subsection 7.3.3) and the electric motor (subsection 7.3.4). The trade-off criteria are identified based on the mission definition and requirements. Weights are assigned based on their importance for the propulsion design. Here again, development risk and cost are considered for all options.

7.3.1. Powertrain Configuration Trade-off

For the powertrain configuration, four options are considered: series, parallel, series-parallel and complex hybrid configuration (HC) [17]. These configurations are visualized in Figure 7.1, where the electrical and mechanical links are bidirectional and the hydraulic link is unidirectional.

The highest weighted criteria used for the trade-off is the weight, based on components, which should be minimized. Next up are reliability and implementability or complexity, the ease of incorporating the system in the design.

The series HC is the lightest option, not requiring gearboxes or clutches. The engines can be placed anywhere in aircraft as they do not power the propellers directly. There is also more freedom in placement of the electric motors and thus the propeller locations. This is due to the electric motors being a lot smaller than an engine and they only require electric wire connections to operate. The main disadvantage is its limited redundancy; if a singly element in the chain fails, so will the whole propulsion system (see Figure 7.1). This is overcome, however, by implementing redundancy by doubling certain components. For example by using multiple converters, which regulate power to the motor, there will be no or only a partial power loss if one fails.

The parallel HC is promising, but it is more complex and thus more expensive, and is heavier since it needs a gearbox transmission system The parallel HC is also a good candidate, with a disadvantage of complexity in terms of the amount of mechanical couplings and power flow regulation. This is a drawback if a distributed propulsion system is used. It should be noted that an important advantage of the parallel HC is that the motor and engine can be scaled down, if always operating simultaneously. However, for this mission, with full electric takeoff and landing, this does not apply. The series-parallel HC and the complex HC are not well developed yet, are still costly and are difficult to implement in the aircraft. Concluding, the series hybrid configuration is the best choice as powertrain configuration.

7.3.2. Power Cell Trade-off

Three different electrical power cells are under consideration: batteries, fuel cells, and solar cells. The comparison is based on the following criteria: Emissions, safety and specific energy are weighted the highest. The used technology should at all times be safe and reliable. Emissions are an important factor in the design of the E-COmmuter and the specific energy should be high so that the cell does not take up too much space are is too heavy.
From the power cell trade-off, it is apparent that batteries offer the best characteristics for the mini-feeder. The use of solar cells is not an option since they become useless during bad weather or night operations. Additionally, they do not generate nearly as much power as is needed to power an aircraft.

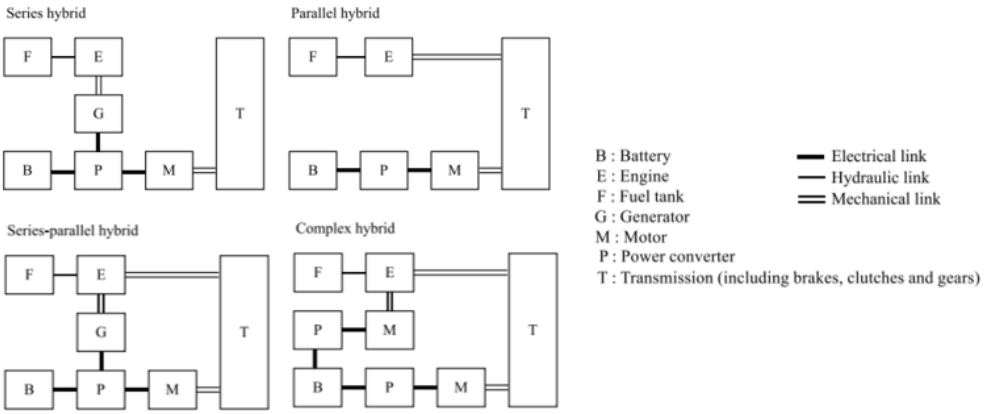

Figure 7.1: Series, parallel, series-parallel and complex hybrid powertrain configurations [17].

Batteries are being implemented more and more within the car industry. With hybrid electric and fully electric cars gaining popularity quickly, the aviation industry soon follows. Batteries are currently the most reliable power cell available. They are a long used, trusted technology even though their power densities are still relatively low. This is expected to chance in the coming years however. Compared to the fuel cell, battery use in aviation is already more regulated and fuels cells require for example hydrogen which is highly flammable and requires high pressure storage. It is also worth noting that fuel cells require specialized refueling stations. The biggest drawback for batteries is the fact that failure can have catastrophic consequences. With regulations, regular checks and protection systems, this can easily be overcome. Therefore, the battery is chosen as power cell.

7.3.3. Propulsion Layout Trade-off

Two possibilities are looked at concerning the layout of the propulsion system: a distributed electric propulsion system and a conventional propulsion configuration. The distributed electric propulsion system (DEP) provides high lift during takeoff and landing through a group of small propellers spread out across the the wing. It is paired with two additional larger motors to provide thrust during cruise. The conventional configuration consists out of multiple (2-4) main motors which provide thrust equally during all flight phases paired with high lift devices (HLD) for extra lift during takeoff and landing. The criteria used for the trade-off are noise, as it is part of the low emissions requirements close to airports, the capability to allow short takeoff and landing (STOL), and weight. A lower weighted criterion is cruise efficiency followed by maintainability. Therefore, the propulsion layout will consist of a distributed electric propulsion system.

Performing trade-off analysis on the propulsion system layout shows that the blown wing has some major benefits over the conventional motor configuration. The use of multiple small propellers with a high blade count, which results in lower tip speeds, greatly reduces the noise produced. This is important considering the noise requirements the hybrid electric feeder has to meet. Furthermore, with the wing designed purely for cruise instead of for takeoff and landing too, it can cruise much more efficiently which will further decrease fuel consumption and therefore make the design more sustainable. It has extraordinary STOL characteristics due to an increased dynamic pressure over the wing. The blown wing / distributed electric propulsion system works well with the series hybrid system since the latter allows much more freedom in motor and engine placement.

7.3.4. Electric Motor Trade-off

Several types of electric motors were looked at, of which three seemed to be commonly used in electric vehicles: DC brushless, AC synchronous and AC induction/asynchronous motors. However, no clear arguments were found which pushed the decision to one kind in particular. Instead, looking at the actual motor developments, three manufacturers that stand out: Siemens, Compact Dynamics and Emrax. A trade-off between the different designs by these manufacturers is performed, for which the criteria are: power-to-weight ratio, to get the highest amount of power out of the lightest package, the reliability, since these motors will provide thrust for the aircraft but also power the blown wing and thus replace high lift devices, and the peak and continuous power as this will determine the performance. The power-to-volume ratio is also considered to keep the frontal area as low as possible when mounting these on the wings, and finally the efficiency was looked at, but weighted very low since all the motors that were compared offered near identical efficiency values.

The manufacturers and respective motor designs which were compared are:

- **Siemens:** A 260kW brushless motor weighing about 50 kg giving it a power-to-weight ratio of 5.2 $kW\,kg^{-1}$ which has been used successfully to power a modified Extra330 and a hybrid-electric Pipistrel Panthera[1] [2].
- **Emrax:** Motors with peak power ratings ranging from 70 kW to 300 kW with power-to-weight ratios of around 8 $kW\,kg^{-1}$ [3]. For now, these motors are designed for and only used in motorized, self-launching gliders and thus have fairly low continuous power values [4].
- **Compact Dynamics:** Currently working on a motor, claiming it will have a 400 kW peak power rating, a continuous power rating of at least 260 kW and a power-to-weight ratio of 10.9 $kW\,kg^{-1}$ [5]. Power scaling is done by developing small, powerful motors which can be stacked to achieve the desired power. With a power-to-weight ratio of 10.9 $kW\,kg^{-1}$. These values are still estimations, but these motors should be ready in the coming years.

With the motors developed by Compact Dynamics having a clear power and weight advantage over the alternatives, the choice is easy. The advantage of electric motors in general is that they are scalable. This allows the designs to be increased in size to match any power requirement.

7.4. Trade-off Conclusion

In section 7.2 and section 7.3, trade-offs for the aircraft configuration and propulsion system are performed. The outcomes of those are displayed in Table 7.2. Additionally, as explained before, to assure the results are unbiased, a sensitivity analysis is conducted after every trade-off.

There is no trade-off performed on the internal combustion engines (ICEs). The choice merely depends on the required power and the available size in the aircraft. The selection of the ICE is performed in section 12.2, which discusses the propulsion layout. It is decided that the ICE will run on Avgas, since Avgas is available at practically all airfields. This allows the aircraft to be refueled at any destination without needing additional expensive refueling infrastructures.

Table 7.2: Trade-off summary.

Trade-off	**Result**
Fuselage shape	Rectangular cross-section, conventional longitudinal shape
Wing-tail layout	High-wing conventional wing with a T-tail
Powertrain configuration	Series hybrid system
Power cell	Battery
Propulsion	Distributed electric propulsion plus two larger propellers
Electric motor	Compact Dynamics motors
Internal combustion engine	ICE running on Avgas

[1] URL: `https://w3.siemens.com/topics/global/en/electromobility/pages/eair.aspx` [cited 9 May 2018]
[2] URL: `http://www.pipistrel.si/news/most-powerful-hybrid-electric-powertrain-powers-up` [cited 9 May 2018]
[3] URL: `http://emrax.com/products/` [cited 9 May 2018]
[4] URL: `http://emrax.com/references/aviation-aerospace/` [cited 9 May 2018]
[5] URL: `http://www.compact-dynamics.de/en/aviation/` [cited 9 May 2018]

8

Design Approach and Budgeting

This chapter explains the design approach of the project. First, the preliminary sizing is discussed, covering the Class I and II weight estimations. Then, the strategy for the detailed design phase is explained. Finally, the preliminary budget breakdown is covered, together with the contingency assessment.

8.1. Design Approach

The aim of this section is to give an insight into the the design approach of the E-COmmuter. This consists of two parts. First the preliminary sizing is performed. This part is based primarily on empirical relations from reference aircraft. Next, the detailed sizing is performed with values found in the sizing of the subsystems of the E-COmmuter. This results in a more accurate sizing of the aircraft.

Throughout the entire sizing and design described in this report, multiple different empty weight designations are used. Operational Empty Weight (OEW) always means the aircraft weight needed for operation, excluding fuel and payload (passengers and cargo). This is as given in Equation 13.2. In all situations where the empty weight (EW) is stated, this means the OEW minus the weight of the crew and trapped fuel and liquids. These are the wing group and fuselage group as described in section 13.1 and it thus also includes the battery weight. In situations where these two do not apply, it is explicitly stated (e.g. "empty weight without batteries" as in subsection 8.1.1).

8.1.1. Preliminary Sizing

In the preliminary sizing in the design process, Class I and Class II weight estimations are performed. For a more detailed explanation of these calculations, please consult Brill et al. [4].

For the Class I estimation, use is made of reference aircraft of similar class, size and configuration as the E-COmmuter. From these, an empirical empty weight without batteries of 3150 kg is found. Class I uses fuel fractions and the mission profile to calculate the maximum takeoff weight (MTOW) of initially 5415 kg.

After the Class I estimation the landing gear, cabin, fuselage and empennages are designed conceptually. Furthermore, wing loading diagrams are constructed to find a preliminary wing planform and to select an airfoil. The high lift devices and the tail are sized afterwards. Lastly, the flight envelope and the propulsion system architecture are designed.

All these calculations form a set of inputs to be used in the Class II weight estimation, which estimates the aircraft weight on subsystem level. Iterating the calculations provide more accurate data, as many inputs from Class I estimations are no longer obtained from reference data or initial guesses. The Class II provides updated input values for a new Class I estimation. After iteration of the two methods, the new MTOW estimate is 6589 kg. The EW without batteries is the value found after iteration 15 as indicated in Figure 8.2 with an empty weight of 4200 kg. An overview of the described iterative process can be found in Figure 8.1.

8.1.2. Detailed Design Phase

After convergence of the preliminary sizing enough system parameters are known to start the detailed sizing of the subsystems. An overview of all the steps of this phase is given in Figure 8.3. This figure should be used by the reader as a summary for all the methods extensively described in chapter 9 through chapter 14. Moreover, in these chapters a large number of programs is used to assist in calculations for the aircraft design. This same figure thus also acts as a code flow chart showing the most important inter dependencies of the programs.

The design starts at the outcome of the preliminary sizing. The values from this sizing are used in the wide-encompassing hybridization program described in chapter 11 and chapter 12. Then, the code flow branches into two flows. In the left branch the horizontal tail is sized and wing is placed along the fuselage, according to the methods in chapter 13. The right branch involves the design of the fuselage and main wing parameters, which are more detailed versions of the programs of the preliminary sizing described in Brill et al. [4]. A summary of these methods are given in chapter 9 and chapter 10.

Then, the two branches combine again and the landing gear and tail are sized according to chapter 14, which are updated versions of the preliminary sizing. Next, the wing-propeller interactions are investigated according to chap-

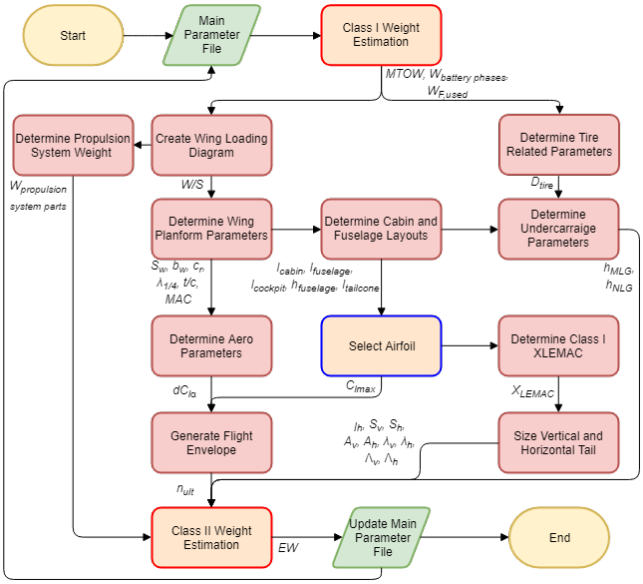

Figure 8.1: Flow chart of the weight estimation process [4].

ter 10, resulting in important propeller design parameters. Last, the Class II weight estimation from Brill et al. [4] is used to find a new, detailed empty weight. This empty weight is compared to the one from the hybridization program and the loop is iterated until the difference is less than 1%. The convergence of the programs lead to the EW without batteries of 3435 kg, as depicted at the last iteration in Figure 8.2. One can see there is a significant difference with the preliminary sizing, which is primarily due to the refined estimation used for hybridization in the detailed design phase as described in section 11.1. The corresponding final MTOW is 5835 kg.

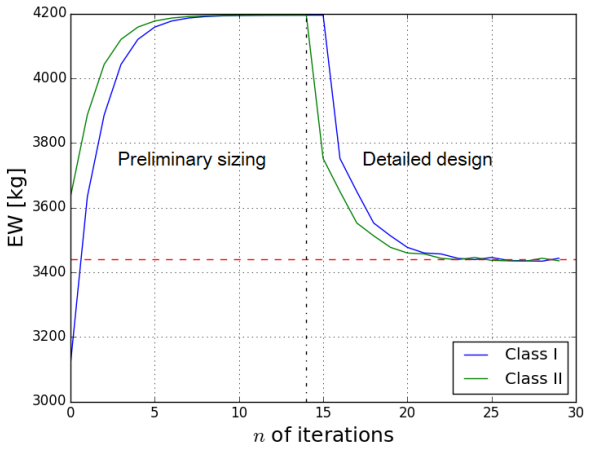

Figure 8.2: Development of the empty weight (excluding batteries) of the aircraft during the iterations of the midterm and final phase of the project.

After the convergence, a so-called "design freeze" was performed, in order to freeze the values for further design. In the flow chart of Figure 8.3, these are depicted by the four branches after the "Update Main Parameter File" box. These four rely on fixed values for the analyses performed in the design of their subsystems. The top branch is part of stability & control in chapter 13. The second branch is part of the structure subsystem, primarily from chapter 10. It comes after the design freeze because frozen values are needed for a number of calculations here. If the weight of e.g. the wing structure becomes higher than the overestimating Class II, the iteration will have to be done again in the future. If not, the structure is designed for higher loads, and thus slightly safer than required. The third branch is part of the performance subsystem from chapter 11. The last branch is part of the operations subsystem described in chapter 16 and chapter 22.

8.2. Budget Breakdown

Product costs are greatly influenced by technical resources. They tend to grow in an undesired direction throughout the design process. Therefore, maximum values, including appropriate contingencies, are defined in the initial phases

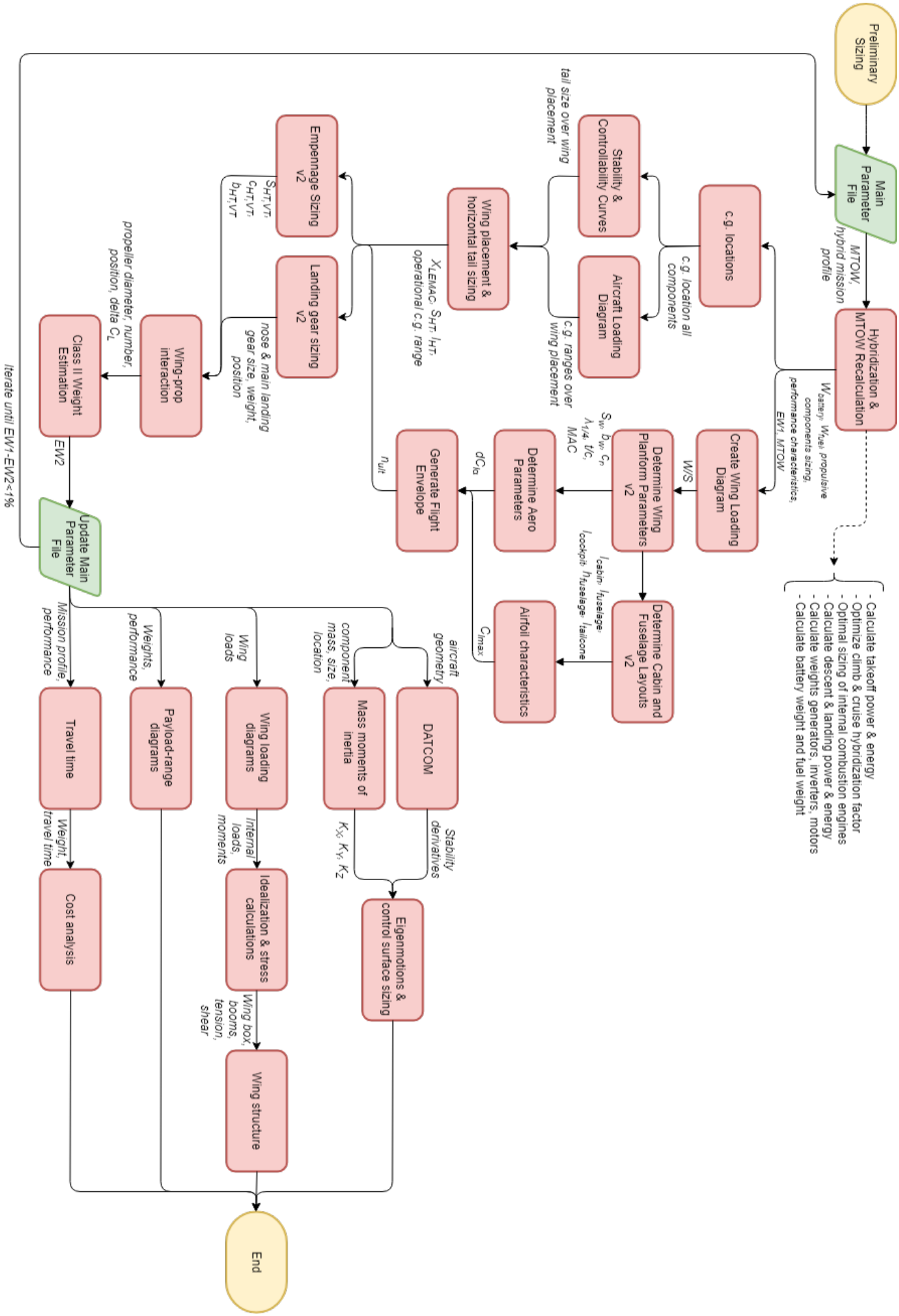

Figure 8.3: Flow chart of the detailed design phase.

of the project. In this chapter, the most important technical parameters are determined. Initially these were based on reference aircraft, but they have been carefully managed throughout the project. The final values determined are discussed in chapter 23. The parameters are: required power, total energy consumption, operational empty weight (OEW), propulsion system mass and unit cost.

8.2.1. Required Power

The required power is important for takeoff and landing performance and is therefore addressed in this budget breakdown.

Preliminary estimate: A first estimate was derived from the power-to-weight ratio and OEW, based on reference aircraft. This resulted in a preliminary estimate of 1000 kW.

After Class II: An updated required power budget is obtained after the Class II weight estimation. An iteration through Class I and Class II until convergence results in a required power of 780 kW. This value is derived from the W/S vs. P/W diagram of the aircraft: at the optimal design point, the required power is 780 kW. This is the updated power budget.

8.2.2. Total Energy Consumption

The total energy consumption is based on the mission profile and mission duration. Estimations for the required power of different mission phases are made : cruise, takeoff, landing, loiter.

Preliminary estimate: An initial mission definition was derived from the market analysis. A design range of 370 km was defined. Moreover, it was assumed that no charging facilities were present at the airfields, so a charge of at least 60% had to be left in the battery to have enough power for another takeoff and potential in-flight emergencies.

Power settings were assumed: 100% during takeoff, 50% during climb and cruise and 20% for descend, and mission phase durations were derived from the cruise speed and climb/descend rate, based on reference aircraft. This all resulted in a first estimate for the total energy consumption of 1000 kW h.

After Class II: During the conceptual design, a new mission profile is defined. To comply with **HEF-PROP-06** (a maximum CO_2 emission of 118.5 g km^{-1} seat^{-1}) and the sustainability requirements of the aircraft, it has to perform ground operations, takeoff and landing fully electric and hybrid during cruise. It is assumed that the specific energy of the batteries is 750 W h kg^{-1} (2035 technologies). From the Class I estimation, it became clear that the previous mission profile needed to be revised, since the required battery mass was too high to support two takeoffs and landings on one charge. Therefore, the mission profile is changed, such that the aircraft is charged both at the airport and airfield. Moreover, the batteries are sized such that they have 20% charge left after landing, in order to provide electric ground operations.

From the Class I estimation, values for the required battery mass and fuel are obtained: Due to the emission requirements the amount of fuel is limited to 201 kg. The fuel has a specific energy of 2930 W h kg^{-1}. From the class I & class II iteration the battery weight ended up at 1220 kg. By using the weights and specific energy for the batteries and fuel, a total required energy of 1320 kW h is obtained. This is rounded up to 1350 kW h.

8.2.3. Operating Empty Weight

The initial OEW was based on reference aircraft. Since no hybrid electric commuter aircraft is operational, high contingency values are assigned. The OEW has been updated throughout the design, resulting in a new budget.

Preliminary estimate: Reference aircraft, having similar passenger numbers and missions were considered. An OEW was estimated based on this, and an additional mass for the electrical energy storage was added, to account for the batteries. Assuming the OEW increases linearly with the number of passengers, the empty mass per passenger was obtained and multiplied by 14. This resulted in a mass of 3100 kg. From the initial mission definition, a charge of 60% had to remain in the battery at the airfields. A battery energy density of 500 W h kg^{-1} is estimated [18]. Furthermore, assuming an electric climb duration of 360 s at full power, an energy consumption of 100 kW h and 20% charge at the end of climb, the total battery capacity was estimated to be 250 kW h. Therefore, a battery mass budget of 500 kg is determined. This results in a total mass budget for the OEW of 3600 kg.

After Class II: With the newly defined mission profile, an iteration through Class I and Class II results in a new OEW budget. The battery mass is determined from the mission profile and is 1220 kg. Moreover, the Class II weight estimation outputs a more accurate OEW, based on the different components of the aircraft. The budget for the OEW is 4795 kg, this is rounded up to 4800 kg.

8.2.4. Propulsion System Mass

In this section, the propulsion system mass budget is determined. This parameter is considered important because the hybrid electric propulsion system plays a large role in the sustainability aspect of this project. Its influence on the rest of the design is considered to be very large.

Preliminary estimation: Initially, no propulsion system was selected yet, so the estimation was based on reference aircraft: only on electric aircraft engine was found: Hypstair from Siemens [19]. From this, masses for the electric motor,

converter and generator were derived. The delivered power of one motor is 200 kW, so to reach the required 1000 kW for takeoff (estimated in subsection 8.2.3), five motors are needed. An internal combustion engine (ICE) mass was based on reference aircraft. It was estimated that two ICE and four generators were needed. Combined, a propulsion system mass of 940 kg was obtained. This value was rounded up to 1000 kg, to take into account to mass of the wiring and for redundancy.

After Class II: The chosen propulsion system from the trade-off is worked out further. A blown wing is used together with two main electric motors to provide propulsion. Batteries are used as power source for takeoff and landing and internal combustion engines during cruise. It is expected that three engines are used: each of these has its own generator and inverter. The Class II weight estimation outputs the mass for each of these components, this can be seen in Table 8.1. It is based on specific power values for each of the components and the required power calculated in subsection 8.2.1. The budget for the propulsion system mass becomes, rounded up, 2000 kg.

Table 8.1: Estimated masses of propulsion subsystems after the Class II weight estimation.

	Wing motors	Inverters	ICE	Blown wing motors	Generators	Total
Mass	80 kg	109 kg	1046 kg	40 kg	159 kg	1961 kg

8.2.5. Cost Budget

Cost is a large aspect of any project, so budget resources need to be allocated to the different subsystems of the aircraft.

Preliminary estimation: Reference aircraft were analyzed, more specifically their unit prices. These aircraft were built during different time periods, so these values were corrected to inflation such that they represented the 2018 price in euros. The cost was based on the unit cost per passenger. With 14 passengers, the unit price of the aircraft was estimated to be €4,301,700. Note that this is the customer purchase price, including a profit margin. Therefore, the budgeted price needed to be reduced. Assuming a profit margin[1] of 10%,the budgeted development & production cost of the product was estimated to be €3,870,000.

This value was subdivided into budgets for each subsystem, to reduce the risk of exceeding the set budget. The cost break-down was derived from statistics based on historical data [20]. Because of the novelty of the propulsion system, a larger budget was assigned to this subsystem. This was expected to be compensated by the low development and manufacturing cost of the fuselage. This all results in Figure 8.4. It was assumed that 20-30% of the dedicated development budget is used for the design, as a general guidance. Exact values depend on the novelty of the subsystem design. These can be seen in Table 8.2.

The cost budget has been evaluated throughout the design process, but has not been updated. It is still difficult at this stage of the project to make a more detailed budget estimation.

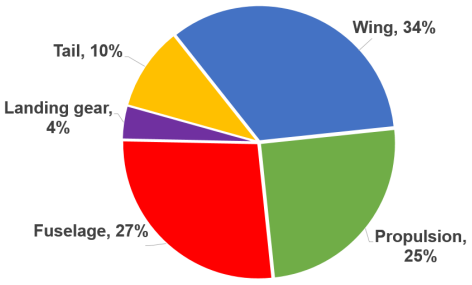

Figure 8.4: Unit cost budget breakdown per subsystem.

Table 8.2: Cost budget breakdown per subsystem for development and manufacturing [21]. All costs are in 2018 values.

	Wing	Propulsion	Fuselage	Landing gear	Tail
Percent budget for design	25%	30%	20%	25%	25%
Budget for development (thousand)	€329	€290	€209	€39	€97
Budget for manufacturing (thousand)	€987	€677	€836	€116	€290

8.2.6. Total Budget Breakdown

The budgets are summarized in Table 8.3. At the end of this design phase, the current values for these parameters are checked for compliance with these budgets. This can be found in chapter 23.

8.2.7. Contingency Assessment

The estimations and calculations above are still subject to change due to uncertainties in the design. Therefore, contingency values have to be determined for these budgets. The first, rough estimations are expected to be most uncertain, resulting in rather large contingency values. During the design process, the contingencies are expected to decrease to a zero contingency upon actual measurement. In Table 8.4, the contingency values throughout the entire process can

[1] URL: `https://www.textron.com/assets/FB/2017/aviation.html` [cited 14 May 2018]

Table 8.3: Summarized budgets throughout the the preliminary steps of the project.

Resource parameter	**Preliminary estimation**	**After Class II**
Required power	1000 kW	780 kW
Total energy consumption	1000 kW h	1350 kW h
Operating empty weight	3600 kg	4800 kg
Propulsion system mass	1000 kg	2000 kg
Development & production cost (thousand)	€3870	€3870

be seen. Currently, the values seen under "preliminary design" are considered. It should be noted that the contingencies are a qualitative estimation: they serve as an indication and are based on Verhagen [22]. The reasoning for the contingency ranges are listed below.

- **Required power:** The first estimate is very preliminary as it is only based on reference aircraft. Therefore, a sufficiently large contingency value is applied, namely 20-25%.
- **Total energy consumption:** The initial calculation is based on mission profile and the estimated required power. The uncertainty is high, as the required power estimation is rough (see above) and as mission profile can be altered during the design. This results in a contingency of 25-35%.
- **OEW:** The OEW is subject to many uncertainties: it depends on the subsystem masses, the propulsion system and the electronics. If the OEW increases, the propulsion system has to provide more power, making the system heavier, and increasing the OEW again. This is known as the snowball effect. Because of the novelty of the design, uncertainties increase even more, as conventional design methods have to be altered for the hybrid design. So, initially a large contingency value was selected: 20-25%.
- **Propulsion system mass:** This depends on the maximum power to be delivered and the system type. Furthermore, hybrid systems are rarely applied in aviation, introducing a lot of uncertainty. Therefore, large contingency values were initially selected: 25-35%.
- **Cost:** Because the cost budget is based on rather old, conventional aircraft, a large contingency value was applied initially. In this project, a novel aircraft is designed: novel propulsion systems, new materials, configurations etc. These are expected to be more expensive. So, an initial upper limit contingency of 25-35% was applied. Even in later stages of the development, problems can arise, resulting in an increased cost, especially if re-development of components is required. Therefore, the contingency value is kept relatively high, also in later stages.

Table 8.4: Resource contingency allowance table.

	Design Maturity					
Resource parameter	First estimate	Conceptual design	Preliminary design	Detailed design	Certification	Actual measurement
Required power	20-25%	10-15%	5-10%	3%	2%	0%
Total energy consumption	25-35%	10-20%	5-10%	3%	2%	0%
Operating empty weight	20-25%	10-15%	5-10%	2%	1%	0%
Propulsion system mass	25-35%	10-20%	5-10%	2%	1%	0%
Development & production cost	25-35%	15-25%	5-15%	5%	3%	0%

9
Fuselage Design

This chapter deals with the fuselage and cabin design. First the cabin is designed based on CS-23 regulations and reference aircraft. This leads to the fuselage design. Afterwards, a fuselage material is selected and a detailed weight estimation is provided. This design is preliminary, a detailed, structural fuselage design is out of the scope of this project.

9.1. Cabin and Fuselage Design

Requirement **HEF-OPR-02** states that the E-COmmuter shall carry 14 passengers with 20 kg each. It is decided to place the hold luggage in a compartment behind the cabin, whereas the hand luggage can be placed underneath the seats. A seat configuration with seven rows of two seats abreast is selected. Other arrangements, for example two rows of seven passengers facing each other, have been considered, but are discarded due to lack of passenger comfort and safety during turbulence. Furthermore, economy seats are chosen with a pitch of 81 cm [23]. Based on this, the cabin dimensions can be determined.

CS-23 regulations prescribe requirements regarding door dimensions, amount and clearance [24]. One passenger door with dimensions 1.22 m x 0.61 m and one emergency exit with dimensions 0.91 m x 0.51 m are installed opposite of each other. A clearance of 28 cm from the cockpit and of 31 cm from the first row of seats is provided. The stairs to board the aircraft are integrated into the passenger door. A free space of 0.5 m behind the last row is added for extra storage, fire extinguishers and first aid kits. This results in a total cabin length of 7.06 m.

The aisle width is set by CS-23 to be 51 cm. The seats have a total width of 52 cm, including two armrests of 5 cm each. A margin of 5 cm is added, resulting in a total cabin width of 1.6 m. The fuselage width consequently measures 1.714 m, taking into account a total wall thickness of 5.7 cm ($0.02 \cdot w_{cabin} + 2.5cm$) on each side [23].

The cabin height is based on the maximum height of a person sitting of 1.41 m [25]. A margin of 19 cm is added, resulting in a cabin height of 1.6 m. The floor is made of a fibre reinforced honeycomb structure with a thickness of 1 cm [26]. Underneath the floor there is 15 cm space left for cables and landing gear storage. The total height of the fuselage then equals 1.87 m.

The results of the calculations above are shown in Figure 9.1.

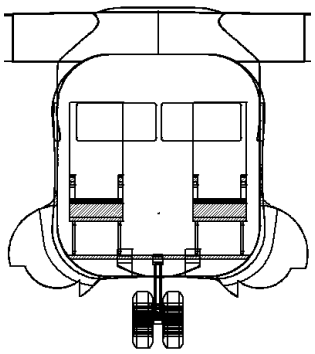

Figure 9.1: Cross-sectional view of the fuselage.

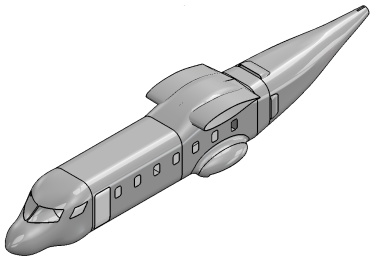

Figure 9.2: Rendering of the entire fuselage.

The total length of the fuselage is based on slenderness ratios of similar regional aircraft [27]. An apparent diameter of the fuselage is calculated to use this method, as the cross-section of the E-COmmuter is rectangular. The average between the width and height is taken as $d_f = \frac{1.714+1.874}{2} = 1.794$ m. For a slenderness ratio of 8.03, a total fuselage length of 14.4 m is obtained. This is compared with reference aircraft and seems a reasonable result for aircraft of this size.

The cockpit length is based on a typical flight deck length of 2.3 m [23]. The actual nose length is set to 30 cm for the storage of avionics. Consequently, the cockpit measures 2.6 m. The length of the tail depends on the root chord of the vertical stabilizer, which is discussed in subsection 14.1.2. A tail length of 2.42 m is obtained. A preliminary tailcone size is estimated at 4.75 m based on the dimensions calculated above. However, a more detailed calculations is performed in subsection 14.2.1. The complete fuselage layout can be seen in Figure 9.2 and Figure 9.3.

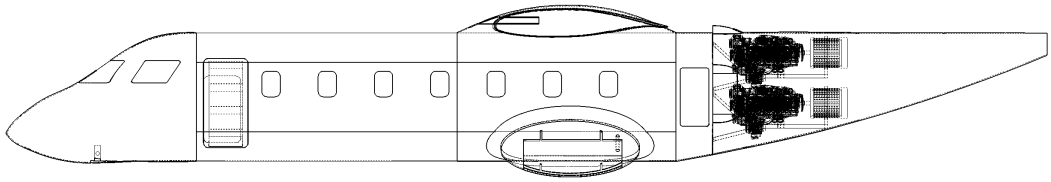

Figure 9.3: Technical drawing of the fuselage side view with the engines and generators in the tailcone.

As explained earlier, the hold luggage is placed behind the cabin. A compartment of 2.25 m^3 is provided (1.5 m x 1.5 m x 1 m). This is based on a luggage density of 170 $kg\,m^{-3}$, a packing density of 85% and some extra margin. Behind the luggage compartment, space is provided for the two engines and generators (section 12.2). The engine compartment has a length of 2.0 m. This provides sufficient space for cabling and protection structure.

9.2. Material Selection

For the fuselage, the selected material is Aluminum alloy 2024. This is a material commonly used in the aerospace industry. This means it is a material that is proven to work and reliable. Furthermore, as the E-COmmuter is a low subsonic aircraft, the fuselage material is less likely to heat up during flight, so the melting temperature of Aluminum will never be exceeded. Aluminum is a high strength, relatively lightweight material. It is easy to produce and can be fabricated in almost every shape. Moreover, regarding sustainability, there are many recyclability options, as discussed in section 21.2. Lastly, it is affordable compared to other material options such as composites or GLARE. Some important properties of Aluminum alloy 2024 can be seen below.

Table 9.1: Properties of Al2024-T3 [28].

Parameter	**Value**	**Parameter**	**Value**
Ultimate stress	496 MPa	Yield stress	393 MPa
Stiffness	73 GPa	Mass density	2700 $kg\,m^{-3}$

9.3. Fuselage Structural Weight

In this section, a detailed weight calculation on the fuselage is performed. It is based on the different structural components present in the fuselage.

9.3.1. Gross Shell Weight

The fuselage structural weight is estimated using the weight penalty method of Torenbeek [23]. First, the weight estimation of the load carrying fuselage shell is performed. This gross weight consists of the gross skin weight $W_{\text{fus, skin}}$, gross stringer weight $W_{\text{fus, stringer}}$ and gross frame weight $W_{\text{fus, frame}}$ as shown in Equation 9.1 [23].

$$W_{\text{fus, G}} = W_{\text{fus, skin}} + W_{\text{fus, stringer}} + W_{\text{fus, frame}} \tag{9.1}$$

The E-COmmuter is a non-pressurized aircraft, which means that the aircraft skin has no hoop stresses acting on it. Therefore, the gross skin weight can be calculated using Equation 9.2. The factor k_λ in this equation, which is obtained from Equation 9.3, takes the fuselage slenderness into account. Moreover, V_D is the diving speed obtained in section 10.4. S_G is the gross shell area arising from the Class II weight estimation, which gives the outer surface area of the fuselage [23]. l_t, b_f and h_f are the horizontal tail arm, width of the fuselage and height of the fuselage, respectively.

$$W_{\text{fus, skin}} = 0.5428 \cdot k_\lambda \cdot S_G^{1.07} \cdot V_D^{0.743} \tag{9.2}$$

$$k_\lambda = 0.56 \cdot \left(\frac{l_t}{b_f + h_f}\right)^{\frac{3}{4}} \tag{9.3}$$

In addition to the fuselage skin, stringers and longerons are present in order to transfer aerodynamic bending loads between skin and frame. The weight of those is estimated using Equation 9.4. In this equation, the ultimate load factor n_{ult}=4.75 is introduced in the fuselage design [23].
Finally, a fuselage frame weight estimation is performed using Equation 9.5. The fuselage frame is carrying the loads on the skin that are transferred via the stringers and longerons.

$$W_{\text{fus, stringer}} = 0.0117 \cdot k_\lambda \cdot S_G^{1.45} \cdot V_D^{0.39} \cdot n_{ult}^{0.316} \quad (9.4) \qquad W_{\text{fus, frame}} = 0.19 \cdot (W_{\text{fus, skin}} + W_{\text{fus, stringer}}) \quad (9.5)$$

All above mentioned shell parts of the fuselage structure total to a gross shell weight. This weight is the load carrying basis of the loads acting on the fuselage itself.

9.3.2. Gross Shell Modifications

On the fuselage gross shell weight, modifications have to be performed to account for the presence of cut-outs and other connections and attachments present in the fuselage. All calculations are performed using Torenbeek [23] for an unpressurized cabin. First, a percentage of the wetted area that is covered by cut-outs (W_{removed}) is removed from the fuselage weight (Equation 9.6). Afterwards, a filling weight W_{fill} and surrounding weight W_{sur} to strengthen the stress concentrations around those is added. The weight of fillings and surrounds is given per category in Table 9.2. Applying these relations, the modified gross weight of the fuselage ($W_{\text{fus, Gmod}}$) is obtained in Equation 9.7 [23].

$$W_{\text{removed}} = \frac{W_{\text{fus, G}}}{A_{\text{wetted}}} \cdot \sum A_{\text{cut-out}} \quad (9.6) \qquad W_{\text{fus, Gmod}} = W_{\text{fus, G}} - W_{\text{removed}} + \sum W_{\text{fill}} + \sum W_{\text{sur}} \quad (9.7)$$

Table 9.2: Modification weight of fillings and surroundings for cut-outs [23].

Weight Contribution	Fillings (Unpressurized)	Surrounds (Unpressurized)
Passenger and cargo doors	$9.765 \cdot A_{\text{cutout}}$	$14.9 \cdot \sqrt{A_{\text{cutout}}}$
Emergency doors	$9.765 \cdot A_{\text{cutout}}$	$14.9 \cdot \sqrt{A_{\text{cutout}}}$
Cockpit window	$(15.9 + 0.104 \cdot V_D) \cdot A_{\text{cutout}}$	$2.98 \cdot \sqrt{A_{\text{cutout}}}$
Cabin window	$12.2 \cdot A_{\text{cutout}}$	Frame included in filling

9.3.3. Floor

The passenger floor is a floor where the beams are directly built on the frames of the fuselage. This is the most convenient solution as a rectangular fuselage is adopted, meaning the lower fuselage part is straight. The weight estimation of the cabin floor is given by Equation 9.8, where the floor surface is the only input needed. On the other hand, the cargo floor weight is obtained using Equation 9.9. For the cargo floor, the volume of the cargo V_{cargo} is of importance, as well as the floor loading P_{floor} [23].

$$W_{\text{floor, cabin}} = 4.62 \cdot S_{\text{floor}}^{1.045} \quad (9.8) \qquad W_{\text{floor, cargo}} = V_{\text{cargo}}^{0.7} \cdot \sqrt{P_{\text{floor}}} \quad (9.9)$$

9.3.4. Subsystem Interference

Different subsystems are having an influence on the fuselage as well. The major components connected to the current aircraft fuselage are: nose landing gear, main landing gear, wing, tail and paint. A weight estimation for all of these is performed to make sure that enough weight budget is available to design dedicated fairings, bays etc.

The landing gear bay weight estimation is different for the nose (Equation 9.10) and main landing gear (Equation 9.11). These calculations are mainly based on the maximum takeoff weight of the aircraft (MTOW). It should be noted that these formulas are only the landing gear bays, which means that the structure itself belongs to the landing gear group weight [23].

$$W_{\text{bay, nose}} = 0.00026 \cdot n_{\text{ult}} \cdot W_{\text{MTOW}} \quad (9.10) \qquad W_{\text{bay, main}} = 0.003 \cdot n_{\text{ult}} \cdot W_{\text{MTOW}} \quad (9.11)$$

As the wing is the subsystem where most forces are acting upon, a significant load is to be transferred to the fuselage load carrying structure. This is done using the wing-fuselage connection, for which a weight estimation is carried out in Equation 9.12. This prediction is highly dependent on n_{ult}, which is obtained multiplying the limit load factor from the flight envelope in section 10.4 with 1.5. Also the the maximum takeoff weight is a variable that relates closely to the aerodynamic forces acting on the wing [23].

$$W_{\text{support, wf}} = \frac{2}{3} \cdot 0.0004 \cdot (n_{\text{ult}} \cdot W_{\text{MTOW}})^{1.185} \quad (9.12) \qquad W_{\text{support, tf}} = 0.1 \cdot W_{\text{tail}} \quad (9.13)$$

Similar to the wing-fuselage connection, a reinforcement is needed to mount the tail to the fuselage. This relationship is described Equation 9.13. In comparison to the other fuselage estimates, this relationship is dependent on the weight of the tail W_{tail}. The tail weight from the Class II weight estimation is used for this, as a detailed tail weight is not known [23].

Finally, the weight of the paint applied to the fuselage is a considerable factor. In order to account for this, a 1% value is taken of the fuselage gross weight [23].

9.3.5. Conclusion

Using the gross weight estimation from Equation 9.1, the modification of the gross weight in Table 9.2 and other miscellaneous contributions from subsection 9.3.4, a final weight of the fuselage of $W_{\text{fus, tot}} = 669.3\,\text{kg}$ is obtained using Equation 9.14. It should be noted that this value is higher than the Class II weight estimation. However, this increase can be explained by the main landing gear bays that are accounted for in the fuselage in comparison to the Raymer method adopted in the Class II weight estimation. Furthermore, the fuselage has been completely designed.

$$W_{\text{fus, tot}} = W_{\text{fus, Gmod}} + W_{\text{floor, cabin}} + W_{\text{floor, cargo}} + W_{\text{bay, nose}} + W_{\text{bay, main}} + W_{\text{support, nf}} + W_{\text{support, tf}} \tag{9.14}$$

9.4. Environmental Control System

Besides being structurally sound, the fuselage also needs to provide a comfortable flight experience to its occupants. This is especially crucial when it comes to temperature and cycling fresh air. The aircraft might not be pressurized but at the 3048 m cruising altitude of the E-COmmuter, the outside temperature is about –4.8 °C which is too uncomfortable to pump into the cabin directly. Besides the temperature, a certain air quality has to be guaranteed for the passengers and the crew.

Environmental Control System Sizing

As the E-COmmuter has no jet engines, hot bleed air is not an option. Alternatively, one could think to use the heat generated by the ICEs as a heating power source. However, the ICEs are not on during the electric flight phases and hence a separate, standalone environmental control system (ECS) has to be chosen that can service the cabin, cockpit and its passengers and crew. As the E-COmmuter is unpressurized, outside air can directly be taken into the cabin as ram air and heated to appropriate temperatures using an electric heater. On the ground, a small fan supplies the required airflow to cycle the air in the cabin and the cockpit. The following sections will size the ram air intake and the electric heater.

Ventilation

According to Martinez [29], a passenger requires a minimum of $5\,\text{L}\,\text{s}^{-1}$ of air. The E-COmmuter ECS has to guarantee this amount of fresh air per passenger. For 14 passengers and two crew, this comes down to about $80\,\text{L}\,\text{s}^{-1}$ or $0.08\,\text{m}^3\,\text{s}^{-1}$ of air. At a cruise speed of $250\,\text{km}\,\text{h}^{-1}$, this requires a ram air intake of $1152\,\text{mm}^2$. Considering a stall speed of $122\,\text{km}\,\text{h}^{-1}$ however (as calculated in chapter 11), a ram air intake of $2367\,\text{mm}^2$ would be required for the necessary airflow. However, since the ECS is equipped with a fan that can provide the necessary airflow on the ground at zero airspeed, a smaller ram air intake of $1200\,\text{mm}^2$ is sufficient. The fan can then also be used to increase the air intake at lower airspeeds than $250\,\text{km}\,\text{h}^{-1}$. Assuming an average airflow of $0.083\,\text{m}^3\,\text{s}^{-1}$ and an air volume of $22.86\,\text{m}^3$ (cockpit + cabin), the aircraft is air cycled in about 4.57 min.

Temperature

To keep passengers comfortable, a temperature of $22 \pm 2\,°\text{C}$ is preferred [29]. With an outside temperature of –4.8 °C at 3048 m cruising altitude, the ECS needs to heat the air to appropriate temperatures. However, colder average temperatures of –40 °C have been observed at Yakutsk airport. Using the specific heat of dry air of $1.006\,\text{J}\,\text{g}^{-1}\,\text{K}^{-1}$ and an air flow of $0.083\,\text{m}^3\,\text{s}^{-1}$, the required power to heat the air can be calculated. For a temperature difference of –40 °C to 20 °C, a maximum heating performance of 6.13 kW is required. Cooling of the E-COmmuter is not required, as the outside temperature quickly goes down when ascending. Also, an electric cooler is usually heavier than an electric heater due to additional components such as a compressor and cooling loop. The drawback of not including a cooler will be higher temperatures in the cabin during ground operations, which might make the E-COmmuter less attractive to operators in tropical countries.

Based on the above sections, the ECS of the E-COmmuter will be very simple in size and construction, consisting only of a ram air intake, fan and electric heater. A small ECS makes the aircraft more sustainable and also fits the short travel time the passengers will experience.

9.5. Verification and Validation

The verification and validation of the fuselage design is rather limited, as the calculations are merely based on logical thinking and statistics. As a verification, the calculations are performed by code and by hand for comparison, and are checked by non-involved team members. The results are validated with dimensions of reference aircraft from Torenbeek [23]. For the weight estimation, similar approaches are followed.

For the environmental control system, a calculation is performed to check whether the selected system can deliver the required power.

9.6. Results

The main results for the cabin and fuselage design are given in Table 9.3.

Table 9.3: The results obtained for the fuselage design.

Parameter	Symbol	Value	Unit	Parameter	Symbol	Value	Unit
Fuselage Weight							
Fuselage skin weight	$W_{\text{fus, skin}}$	287	kg	Fuselage stringer weight	$W_{\text{fus, stringer}}$	99.5	kg
Nose landing gear bay weight	$W_{\text{bay, nose}}$	7.2	kg	Main landing gear bay weight	$W_{\text{bay, main}}$	27.7	kg
Fuselage frame weight	$W_{\text{fus, frame}}$	73.5	kg	Wing support weight	$W_{\text{support, wf}}$	49.0	kg
Gross shell weight	$W_{\text{fus, G}}$	460	kg	Tail support	$W_{\text{support, tf}}$	9.9	kg
Shell modification weight	$W_{\text{fus, Gmod}}$	69.0	kg	Paint weight	$W_{\text{fus, paint}}$	4.6	kg
Cabin floor weight	$W_{\text{floor, cabin}}$	51.8	kg	Cargo floor weight	$W_{\text{floor, cargo}}$	24.1	kg
Total fuselage weight	$W_{\text{fus, tot}}$	669	kg				
Fuselage Dimensions							
Seat pitch	p_{seat}	0.81	m	Seat width	w_{seat}	0.42	m
Passenger door height	$h_{\text{pax, door}}$	1.22	m	Passenger door width	$w_{\text{pax, door}}$	0.61	m
Emergency door height	$h_{\text{em, door}}$	0.91	m	Emergency door width	$w_{\text{em, door}}$	0.51	m
Cabin length	l_{cabin}	7.06	m	Fuselage length	l_{fus}	14.4	m
Cabin width	w_{cabin}	1.60	m	Fuselage width	w_{fus}	1.71	m
Cabin height	h_{cabin}	1.60	m	Fuselage height	h_{fus}	1.87	m
Luggage compartment volume	$V_{\text{luggage, comp}}$	2.25	m^3	Engine compartment length	$l_{\text{engine, comp}}$	2.00	m
Cockpit length	l_{cockpit}	2.60	m	Tail length	l_{tail}	2.42	m
Environmental Control System							
Model	ECS-Y12F			Heating power	P_{heating}	19.7	kW
Weight	W_{ECS}	41.0	kg	Cooling power	P_{cooling}	7.0	kW
Maximum air flow	$\dot{m}_{\text{ECS}}$	1000	kg h^{-1}				

10
Wing Design

The following chapter concerns the wing design of the aircraft. First, the wing planform is designed. Then, an airfoil best suited for the wing and mission is selected and the flight envelope is constructed. Next, the forces acting on the wing are analyzed and broken down. Using these, a wing box design can be established by evaluating the direct and shear stresses acting on the load bearing structure. All the results are summarized at the end of the chapter and all assumptions are stated when relevant.

10.1. Wing Planform Design

This section deals with the design of the wing planform. First, the wing loading and power constraints resulting from a performance analysis are determined. From this, a design region is defined and an optimal design point can be selected. This serves as an input for the wing planform parameter calculation.

10.1.1. Wing and Power Loading Constraints

A power-to-weight (W/P) to wing loading (W/S) diagram is constructed. This results in a design range for the wing surface area. A performance analysis is done to find the loading constraints.

The wing loading constraints are shown as the vertical lines (wing loading for stall speed and landing speed) in Figure 10.1: the region left of these lines represents the design range. The wing loading equation reads:

$$\frac{W}{S} \leq \frac{1}{2} \cdot \rho \cdot V^2 \cdot C_L \tag{10.1}$$

CS-23 regulations dictate that at sea level conditions the stall requirement is 113 km h^{-1} and that no power is to be used [24]. Therefore, C_L is taken to be $C_{L_{\text{max,clean}}}$ with $V = V_{\text{stall}}$. This results in the first wing loading constraint.

Landing performance also poses a constraint on the wing loading. In Equation 10.1, C_L becomes $C_{L_{\text{max,land}}}$ and is based on estimations. To find the stall speed, use is made of the landing distance requirement of 700 m. Statistical equations are used:

$$S_{LG} = \frac{S_L}{1.938} \tag{10.2}$$

$$V_{S_{\text{land}}} = \sqrt{\frac{S_L}{0.5915}} \tag{10.3}$$

Here, S_L and S_{LG} are the total landing and ground run distance respectively. The density at the highest airport served by aircraft is used in Equation 10.1, to ensure that the aircraft is able to land at any airport. To determine this minimum density, the highest airport in Europe (Engadin airport in Samedan, Switzerland[1]) is used at an altitude of 1707 m.

Power constraints are based on the required power for cruise, takeoff and climb. The curves shown in Figure 10.1, define the design region: the requirements are met beneath the lines.

The minimum takeoff distance dictates the takeoff performance. Using statistical formulae [27], the takeoff parameter can be obtained (TOP_{23}). From this, the takeoff distance (the horizontal distance from start of the takeoff until an altitude of 15 m is reached) can be computed using Equation 10.4. Using all of this, the power loading constraint for takeoff can be obtained (Equation 10.5).

$$TOP_{23} = \frac{-8.134 + \sqrt{66.162 + 0.0596 \cdot S_{\text{TO}}}}{0.0298} \tag{10.4}$$

The climb gradient requirement is given by regulations and is set to be 4% at sea level [24]. The power loading constraint can be seen in Equation 10.6.

$$\left(\frac{W}{P}\right)_{\text{TO}} \leq \frac{\text{TOP}_{23} \cdot C_{L_{\text{max,TO}}} \cdot \rho}{\left(\frac{W}{S}\right)_{\text{TO}} \cdot \rho} \tag{10.5}$$

$$\left(\frac{W}{P}\right)_{\text{climb}} \leq \frac{\eta_p}{\sqrt{\frac{W}{S} \cdot \frac{2}{\rho_0} \cdot \frac{1}{C_L} \cdot \left(\frac{c}{V} + \frac{C_D}{C_L}\right)}} \tag{10.6}$$

[1] URL: `https://skyvector.com/airport/LSZS/Samedan-Airport` [cited 2 July 2018]

Lastly, cruise performance constraints have to be obtained. For this, the power setting during cruise (P_s) is needed. This is obtained from the drag polar. The cruise power loading constraint can be obtained by Equation 10.7. Here, W_{cr} represents the ratio of cruise weight to takeoff weight.

$$\left(\frac{W}{P}\right)_{\text{cruise}} \leq \frac{P_s}{W_{cr}} \cdot \eta_p \cdot \left(\frac{\rho}{\rho_0}\right)^{\frac{3}{4}} \cdot \left(\frac{C_{D_0} \cdot \rho \cdot V^3}{2 \cdot W_{cr} \cdot \frac{W}{S}} + \left(W_{cr} \cdot \frac{W}{S}\right) \cdot \left(\frac{2}{\pi \cdot A \cdot e \cdot \rho \cdot V}\right)\right)^{-1} \tag{10.7}$$

This all results in Figure 10.1. The red region indicates the entire design region that results in an aircraft fulfilling the wing- and power loading conditions during different flight phases. The optimal design point can be obtained: it is the most right and upper point in the design region. Thus, the design point here is the intersection point of the takeoff and stall performance.

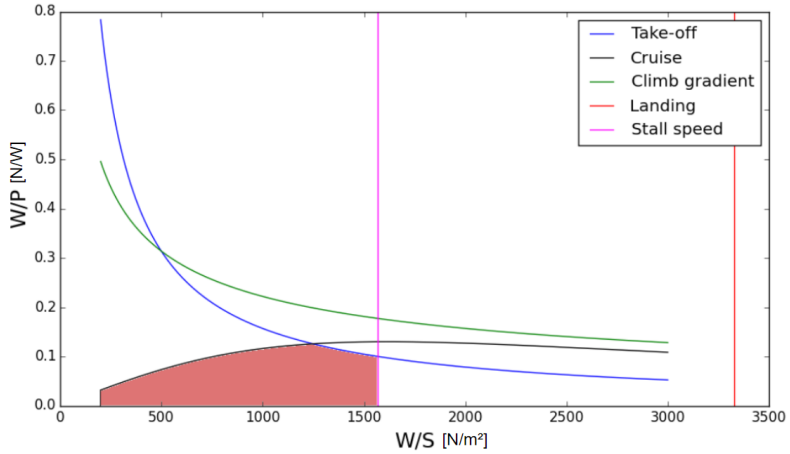

Figure 10.1: Wing loading diagram.

10.1.2. Wing Planform

Using the wing loading, the wing planform can be designed. The wing surface is obtained using Equation 10.8. Using this, the wing span b can be computed, based on the aspect ratio of the wing A (Equation 10.9).

$$S = \frac{\text{MTOW} \cdot g}{\left(\frac{W}{S}\right)_{\text{TO}}} \tag{10.8}$$

$$b = \sqrt{A \cdot S} \tag{10.9}$$

Since the Mach at cruise is smaller than 0.7, the sweep at the quarter chord $\Lambda_{\frac{c}{4}}$ is given to be zero. The taper ratio is chosen to be 0.4: this results in an almost elliptical lift distribution, leading to low induced drag and easy manufacturing. Using these, the root chord can be obtained (Equation 10.10). The tip chord is computed using $c_t = \lambda \cdot c_r$. The wing's dihedral angle is determined using Equation 10.11.

$$c_r = \frac{2 \cdot S}{(1+\lambda) \cdot b} \tag{10.10}$$

$$\Gamma = \left(3 - \frac{\Lambda_{\frac{c}{4}} \cdot \frac{180°}{\pi}}{10} - 2\right) \cdot \frac{\pi}{180°} \tag{10.11}$$

The mean aerodynamic chord can be obtained using Equation 10.12. Its lateral position, measured from the root chord can be computed as well with Equation 10.13.

$$\text{MAC} = \frac{2}{3} \cdot c_r \cdot \frac{1+\lambda+\lambda^2}{1+\lambda} \tag{10.12}$$

$$y_{\text{MAC}} = \frac{b}{2} \cdot \frac{1+2\cdot\lambda}{3\cdot(1+\lambda)} \tag{10.13}$$

Furthermore, the longitudinal position of the mean aerodynamic chord is a useful tool when considering the stability and control of the aircraft. A preliminary estimate is made using Equation 10.14. This estimation is refined in chapter 13, when evaluating the aircraft's static stability.

$$X_{\text{LEMAC}} = 0.5 \cdot l_{\text{cabin}} - 0.25 \cdot \text{MAC} + l_{\text{cockpit}} \tag{10.14}$$

10.2. Wing Airfoil Selection

In order to choose an airfoil for this design, a preliminary estimate for the maximum lift coefficient had to be made: $C_{L_{\text{max,clean}}} = 1.6$, which is obtained from the power-off stall speed in pink in Figure 10.1 together with a lift coefficient increment of the flaps. This can be translated to a maximum lift coefficient that need to be delivered by the airfoil, $C_{l_{\text{max}}}$. This is done using Equation 10.15. A factor of 1.08 is used to take into account the average tail down load, to trim the aircraft, depending on the ratio of the tail arm to mean aerodynamic chord.

$$C_{l_{\text{max}}} = 1.08 \frac{C_{L_{\text{max}}}}{\cos(\Lambda_{c/4})} \tag{10.15}$$

$$C_{l_{\text{des}}} = \frac{1.08}{2} \cdot \frac{\frac{\text{MTOW}}{S} - \frac{\text{MTOW} - W_{\text{fuel}}}{S}}{\frac{1}{2} \cdot \rho_{\text{cr}} \cdot V_{\text{cr}}^2} \tag{10.16}$$

This results in a maximum lift coefficient for the airfoil of 1.73. Using the Airfoil Investigation Database, coordinates of an airfoil with a thickness to chord ratio of around 17% are analyzed in XFLR5[2]. This ratio is chosen, because wings with a higher thickness to chord ratio show a significantly lower structural weight. Furthermore, higher thickness to chord ratios result in a higher $C_{L_{max}}$ at low speeds. The analysis for each airfoil is performed at the mean aerodynamic chord. The NASA/LANGLEY LS(1)-0417 (GA(W)-1) airfoil is selected (see Figure 10.5): it gives $C_{l_{max}} = 1.93$ at the lowest Reynolds number ($Re2$) of 3523618, resulting in the lowest $C_{l_{max}}$. Figure 10.2 shows the lift curve of the airfoil: it can be observed that there is a gradual transition to stall, which is desirable. In Figure 10.3, the $C_m - \alpha$ curve can be seen. At stall condition, $\alpha = \pm 20°$, it is obvious that the airfoil reacts in a stable way: for a negative α, C_m is increasing and the other way around. Furthermore, C_m is always negative: the aircraft naturally pitches down.

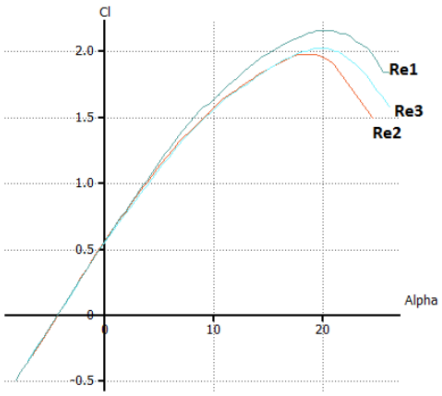

Figure 10.2: $C_l - \alpha$ curve for the selected airfoil.

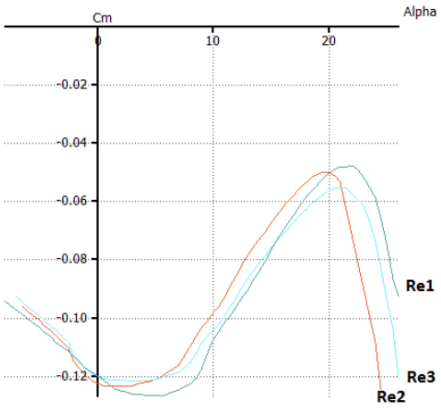

Figure 10.3: $C_m - \alpha$ curve for the selected airfoil.

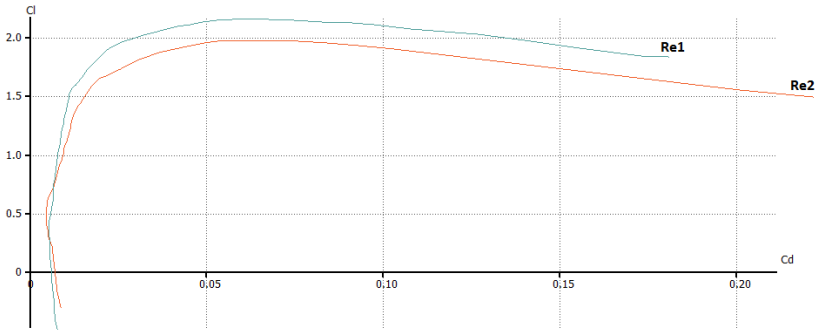

Figure 10.4: $C_l - C_d$ curve for the selected airfoil.

Finally, the design lift coefficient needs to be obtained (see Equation 10.16). This indicates the average lift coefficient required during cruise conditions with Reynolds number $Re1$. It is assumed that the weight at the beginning of cruise is equal to the maximum takeoff weight, as a result from the zero-emissions takeoff. With a $C_{l_{des}}$ of 0.78, the airfoil needs to be mounted to the fuselage at an incidence angle of 2.2°. This is the angle of attack for which $C_l = C_{l_{des}}$.

The airfoil and incidence angle are re-evaluated after the initial design phases. They are still consistent with the current aerodynamic parameters and requirements. A safety factor of 0.9 is used on the maximum lift coefficient $C_{l_{max}}$ to account for the overestimation problem of XFLR5 obtained by comparing $Re3$ in Figure 10.2 and Figure 10.3 to [30, Figure 12].

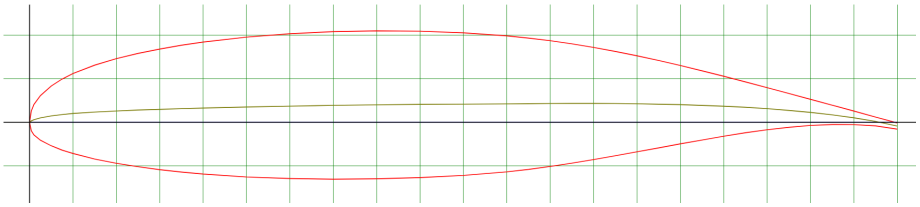

Figure 10.5: The NASA/LANGLEY LS(1)-0417 (GA(W)-1) airfoil.

[2] URL: `http://www.xflr5.com/xflr5.htm` [cited 2 July 2018]

10.3. Flap Sizing

In order to comply with CS-23 requirements to have a stall speed of 31.8 m s^{-1} in case of engine failure and to provide sufficient lift during landing high lift devices are required. Single slotted, hinged flaps are chosen as these provide just enough $\Delta C_{L_{\max}}$ while keeping complexity low. The flap sizing is done according to the DATCOM method. With the two equations in Equation 10.17 and Equation 10.18 shown below one can determine the wings flapped span and the flaps actual dimensions. Based on the stall speed requirement a $\Delta C_{L_{\text{flaps}}} = 1.0$ is designed for.

$$\Delta C_{l_{\max_{\text{flaps}}}} = k_1 \cdot k_2 \cdot k_3 \cdot \Delta C_{l_{\max_{\text{base}}}} \tag{10.17}$$

$$S_{w_{\text{flaps}}} = \frac{\Delta C_{L_{\max_{\text{flaps}}}} \cdot S_w}{\Delta C_{l_{\max_{\text{flaps}}}} \cdot K_\Lambda} \tag{10.18}$$

First $\Delta C_{l_{\max_{\text{flaps}}}}$, the maximum extra lift that the 2D airfoil can generate, is determined. In equation Equation 10.17 k_1, k_2 and k_3 are correction factors which can be read off of graphs in [31]. $\Delta C_{l_{\max_{\text{base}}}}$ is the maximum $C_{l_{\max_{\text{base}}}}$ theoretical possible for single slotted flaps with a length of 25% chord. The maximum desired $C_{L_{\max_{\text{flaps}}}}$ is an input to calculate the total flapped area of the wing $S_{w_{\text{flaps}}}$. K_Λ is empirical correction factor for sweep. From this the flaps spans and surface area can be computed. The final results can be seen in section 10.10.

10.4. Flight Envelope

In order to design the wing based on the ultimate loads acting on it, the flight envelope needs to be constructed to identify the ultimate load factor. The flight envelope is created based on the CS-23 regulations [24]: CS-23.333 Flight envelope, CS-23.335 Design airspeeds, CS-23.337 Limit maneuvering factors and CS-23-341 Gust load factors. The flight envelope can be seen in Figure 10.6.

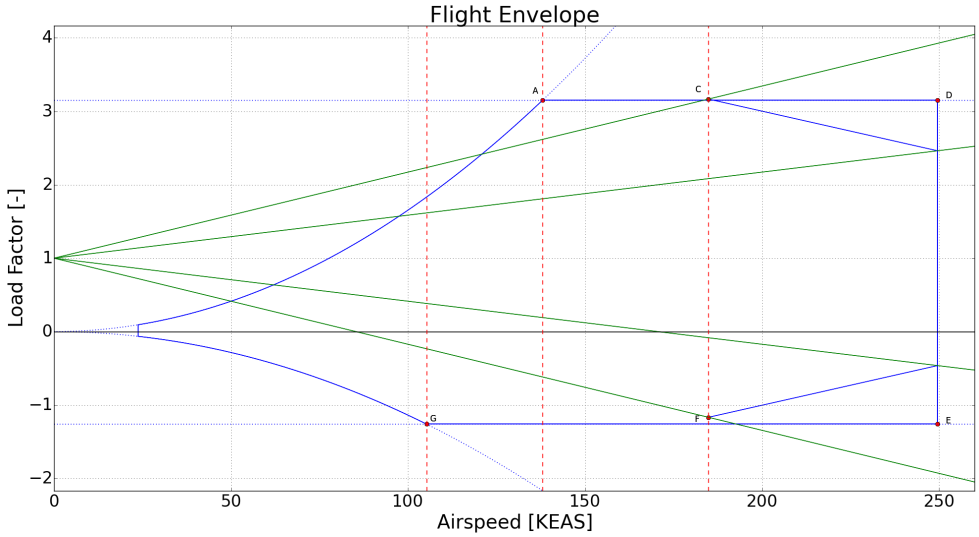

Figure 10.6: Flight envelope of the E-COmmuter.

From Figure 10.6 can be seen that the maximum load factor, so the limit load factor is 3.167. To obtain the ultimate load factor, a safety factor of 1.5 is applied [24]. This results in an ultimate load factor of 4.75. The flight envelope is extensively used throughout the next chapter, so that the wing is designed to sustain the ultimate loads acting on it.

10.5. Wing Loading Analysis

The wing is subjected to several forces during all flight and ground conditions. These need to be identified in order to design a wing box capable of carrying all loads acting on it. First, a reference frame has to be defined. Afterwards, all the forces and moments can be identified and reaction loads along the wing span can be obtained.

10.5.1. Reference Frame

Assumptions

AS-STR-01: The aerodynamic center is fixed and located in the quarter chord. This is justified if wing has a high aspect ratio and low sweep [32]. This is the case, so this assumption has a limited effect on the accuracy of the analysis.
AS-STR-02: Aerodynamic forces generated by the wing apply in the aerodynamic center. Limited effect [32].

A reference frame is defined on the wing for the structural analyses: it is fixed to the root of the wing in the quarter chord. This reference point is chosen based on **AS-STR-01**. This is justified, since the wing has a high aspect ratio and low sweep. Furthermore, the sweep on its quarter chord is equal to zero. It is also assumed that the aerodynamic

forces generated by the wing apply in the quarter chord along the wingspan (**AS-STR-02**). The x-direction is parallel to the chord and is defined positive towards the leading edge, the y-axis is defined positive towards the right wing (when looking at the leading edge) and the z-direction is defined positive downwards, perpendicular to the x-axis. This can be seen in Figure 10.7.

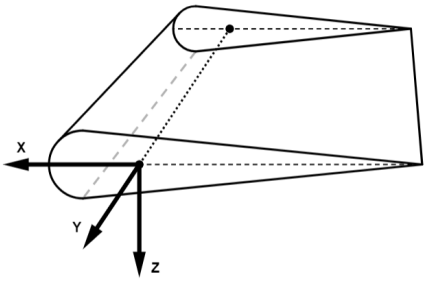

Figure 10.7: Reference frame used for the structural analysis of the wing.

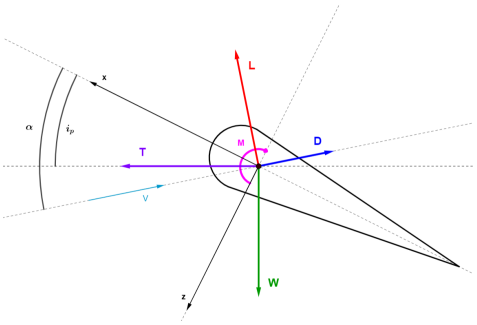

Figure 10.8: Representation of the forces acting on every section along the wingspan.

10.5.2. Forces Acting on the Wing

Performing a structural analysis of the wing requires the identification of forces acting on it. It is assumed that all the aerodynamic forces generated by the wing apply in the quarter chord (or aerodynamic center) of every section along the wing. Forces generated by the propulsion system or the flaps are translated to the quarter chord, resulting in a torsional moment about it. In Figure 10.8, a graphical representation of the forces and moment acting on every section along the wingspan can be observed. As can be seen, 4 main forces need to be identified: lift (L), drag (D), thrust (T) and weight (W), see Figure 10.8.

The torsional moment follows from the multiplication of the non-aerodynamic forces with the moment arm to the quarter chord. The forces need to be decomposed to be in the specified reference frame: α represents the angle of attack at which the aircraft flies and i_p is the incidence angle of the wing with respect to the fuselage center line.

To start off the loading analysis, forces generated by the wing itself are identified first, using a model of the wing in XFLR5. Afterwards, weights of the propulsion system and fuselage are specified. Next, the thrust generated by the propulsion system is added. Lastly, extra lift and drag generated by the wing-propeller interaction is computed.

Forces Generated by the Wing

The wing is modeled in XFLR5 for different flight phases. The lift- and drag coefficients along the wing span are calculated for a range of angles of attack. Using Equation 10.19, chords at every spanwise mesh point can be computed.

$$c_i = \frac{2 \cdot S}{(1+\lambda) \cdot b} \cdot \left(1 - \frac{1-\lambda}{b}\right) \cdot |2y_i| \tag{10.19}$$

Here, λ is the taper ratio, S and b are the wing surface and wing span respectively and y is the spanwise location from root to tip (left wing tip: y = negative, right wing tip: positive).

Using these, the lift and drag of the wing structure at every mesh point can be calculated. A loop is created that runs through every spanwise location i with a specific chord c_i, and multiplies this by the mesh spacing (Δy) to end up with a local surface area $S_i = c_i \cdot \Delta y$. The lift and drag can then be calculated using Equation 10.20 and Equation 10.21 respectively. The ultimate load factor n_{ult} is obtained from the flight envelope discussed in section 10.4.

$$L_i = \frac{1}{2} \cdot C_{L_i} \cdot \rho \cdot V^2 \cdot S_i \cdot n_{\text{ult}} \tag{10.20}$$

$$D_i = \frac{1}{2} \cdot C_{D_i} \cdot \rho \cdot V^2 \cdot S_i \tag{10.21}$$

Weight

Now that the lift and drag of the wing have been obtained, the weight of additional structural components needs to be added: the wing weight, fuselage weight and propulsion system weight. The wing weight is assumed to be a linearly varying distributed load along the span (larger weight at the root than at the tip). The fuselage weight, including passengers, crew, furnishing, payload etc. is distributed over the width of the fuselage. The propulsion system weight is more complicated: a number of small electrical motors with propellers are distributed along the span of the wing, and two bigger motors are located at the root. Furthermore, the inverters are also located in the wing. These masses, obtained from chapter 12, are considered as point masses along the span.

The weight of the batteries and fuel, which are both located inside the wing box, is adopted from the calculations performed in design of the propulsion system in chapter 12. It is assumed that the batteries have a density of $\rho_{\text{batteries}} = 1.333\,\text{kg}\,\text{m}^{-3}$ and the fuel has a density $\rho_{\text{fuel}} = 721\,\text{kg}\,\text{m}^{-3}$. The battery weight at each cross-section along the span are distributed using the declining volume towards the tip. For the batteries, the volume is multiplied by a factor of 2 to account for the necessary thermal control, firewall and puncture proof casing.

Thrust

Next, the thrust generated by the propellers has to be considered. A thrust estimate is obtained from chapter 12 and is implemented in the program.

10.5.3. Wing-Propeller Interaction

Assumptions

AS-STR-03: The influence of the swirl of the propellers is neglected [33].
AS-STR-04: The flow is assumed to be incompressible [33]. This has a limited effect on the accuracy of the analysis: the aircraft flies at relatively low speeds.
AS-STR-05: The wing airfoil is assumed to be symmetric [33].
AS-STR-06: The effect of a propeller on its adjacent ones is neglected [33].
AS-STR-07: The effect of the propellers on the wing is limited to their location on the wing [33].
AS-STR-08: The effect on the wing is considered uniform along the span [33].
AS-STR-09: The wing is fully immersed in the flow [33].
AS-STR-10: The wingspan is considered a rectangular flat plat with span b and constant chord c.

The assumptions summarized above result in limited accuracy of the analysis, but are assumed to be valid in this phase of the design.

Finally, the blown wing configuration induces additional lift and drag. This needs to be taken into consideration as well. Since this has proven to be a very complex analysis that is out of the scope of this project, a simplified model is used [33][34]. This model is based on actuator disc theory: the propeller is represented as an infinitely thin disc perpendicular to the thrust direction. The static pressure across the disc increases. A volume of flow travels across the disc. Realizing that the thrust is generated by the pressure difference across the actuator disc plane and using Bernoulli's equation, it can be concluded that the velocity at the propeller location is the average of the velocity downstream and the velocity upstream of the propeller [35]. Figure 10.9 gives a visual representation of actuator disc theory. Assumptions **AS-STR-03** to **AS-STR-10** are valid for this method.

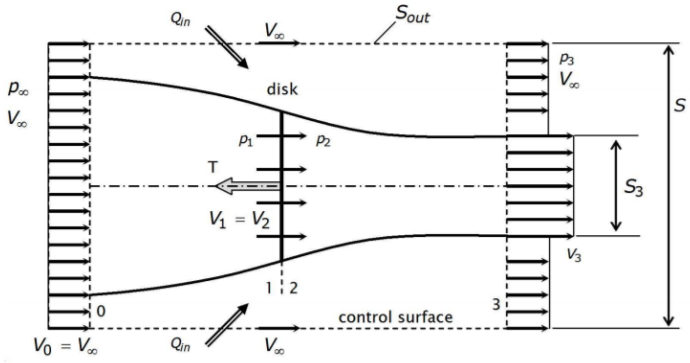

Figure 10.9: Actuator disc model [35].

A simplified geometry of the wing is presented: a rectangular flat plate with span b and constant chord c, equal to the mean aerodynamic chord. Looking at Figure 10.10, the simplified geometry can be seen: the propellers represented as actuator discs are located a distance $\frac{x_p}{c}$ in front of the wing's leading edge and they are distributed along a distance of $\bar{b}_{dp} \cdot \frac{b}{2}$. The number of discs is indicated by N (so $N/2$ for half the wing span). They have a diameter of D_p and a spacing between them of $\delta_y \cdot D_p$.

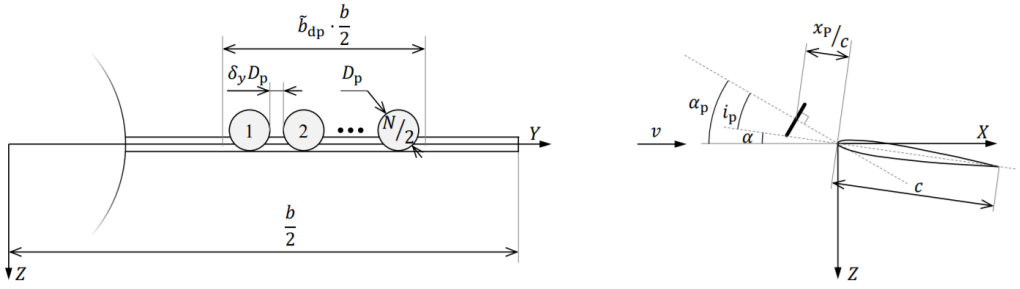

Figure 10.10: Simplified geometry used for the propeller-wing interaction analysis [33].

For a given number of propellers, for which an optimum value is found through iteration, and a region of the wingspan, the diameter can be computed using Equation 10.22 [33]. The thrust needed from a single propeller can be represented by the thrust coefficient T_c [33].

$$D_p = \frac{b \cdot \bar{b}_{\text{dp}} \cdot \frac{b}{2}}{N \cdot (1+\delta_y)} \tag{10.22}$$

$$T_c = \frac{1}{N} \cdot \frac{\frac{T}{W}}{\rho \cdot V \cdot \frac{D_p^2}{W}} \tag{10.23}$$

In Equation 10.23, T represents the thrust required from all the propellers combined and is derived from chapter 12. Finally, with this, the extra lift and drag resulting from the propeller-wing interaction can be calculated. First, the axial induction factor a is computed, where Δv is the velocity increase caused by the propeller [33].

$$a_p = \frac{\Delta v}{V} = \frac{1}{2} \cdot \left(-1 + \sqrt{1 + \frac{8}{\pi} \cdot T_c} \right) \tag{10.24}$$

The velocity of the slipstream at the quarter chord needs to be evaluated. Therefore, the axial position of the propeller as a fraction of its radius needs to be computed (Equation 10.25 [33]). For this, the propeller radius-wing chord ratio is needed (Equation 10.26 [33]).

$$\frac{x_p}{R_p} = \frac{\frac{x_p}{c} + 0.25}{\frac{R_p}{c}} \tag{10.25}$$

$$\frac{R_p}{c} = \frac{1}{2} \cdot \sqrt{\frac{D_p^2}{W} \cdot \frac{W}{S} \cdot A} \tag{10.26}$$

The contraction ratio of the slipstream at the wing can be calculated (Equation 10.27 [33]), and finally, the velocity increase at the quarter chord of the wing (Equation 10.28 [33]).

$$\frac{R_{\frac{c}{4}}}{R_p} = \sqrt{\frac{1+a}{1+a \cdot \left(1 + \frac{\frac{x_p}{R_p}}{\sqrt{(\frac{x_p}{R_p})^2+1}}\right)}} \tag{10.27}$$

$$a_{\frac{c}{4}} = (1+a) \cdot \left(\frac{R_p}{R_{\frac{c}{4}}}\right)^2 - 1 \tag{10.28}$$

Finally the increase in lift and drag per propeller can be derived [33]:

$$dc_l = 2 \cdot \pi \cdot \left(\left(\sin(\alpha) - a_{\frac{c}{4}} \cdot \beta \cdot \sin(i) \right) \cdot \sqrt{(a_{\frac{c}{4}} \cdot \beta)^2 + 2 \cdot a_{\frac{c}{4}} \cdot \beta \cdot \cos(\alpha + i) + 1} - \sin(\alpha) \right) \tag{10.29}$$

$$dc_{d_0} = a_{\frac{c}{4}}^2 \cdot c_f \tag{10.30}$$

$$dc_{d_i} = \frac{(dc_l)^2}{\pi \cdot A \cdot e} \tag{10.31}$$

$$dc_d = dc_{d_0} + dc_{d_i} \tag{10.32}$$

In Equation 10.29, α is taken as the average angle of attack during the different flight phases, i is the propeller incidence angle and β represents the finite-slipstream correction factor. This factor is needed to avoid overestimation of the lift and is calculated using [34]. This model is a surrogate model of OVERFLOW simulations constructed at four different $\frac{V+\Delta v}{V}$: 1.25, 1.50, 1.75 and 2.00. In addition, $\frac{x_p}{c}$ values of 0.25, 0.5, 1.0 and 1.5 are fitted in a vector equation. In order to find β, the constructed surrogate model is summarized in Equation 10.33. The input variables needed for using the OVERFLOW surrogate model are $\frac{R_p}{c}$ provided by Equation 10.26, $\frac{x_p}{c}$ deducted from Equation 10.25, as well as $\frac{V+\Delta v}{V}$ coming from Equation 10.24. The coefficients and corresponding vector defining the surrogate model are shown in Equation 10.34 and Equation 10.35. It is apparent that this finite-slipstream correction factor is increasing with propeller diameter, which means that large propellers relatively give higher lift than small propellers [34].

$$\beta = \sum_{i=0}^{4} \cdot K_i \cdot X \left(\frac{R_p}{c}\right)^i \tag{10.33}$$

$$X = \begin{bmatrix} 1 & \frac{x_p}{c} & \left(\frac{x_p}{c}\right)^2 & \frac{x_p}{c} \cdot \frac{V+\Delta v}{V} & \frac{V+\Delta v}{V} & \left(\frac{V+\Delta v}{V}\right)^2 \end{bmatrix}^T \tag{10.34}$$

$$\begin{aligned} K_0 &= \begin{bmatrix} 0.378269 & 0.748135 & -0.179986 & -0.056464 & -0.146746 & -0.015255 \end{bmatrix} \\ K_1 &= \begin{bmatrix} 3.071020 & -1.769885 & 0.436595 & 0.148643 & -0.989332 & 0.197940 \end{bmatrix} \\ K_2 &= \begin{bmatrix} -2.827730 & 2.054064 & -0.467410 & -0.277325 & 0.698981 & -0.008226 \end{bmatrix} \\ K_3 &= \begin{bmatrix} 0.997936 & -0.916118 & 0.199829 & 0.157810 & -0.143368 & -0.057385 \end{bmatrix} \\ K_4 &= \begin{bmatrix} -0.127645 & 0.135543 & -0.028919 & -0.026546 & 0.010470 & 0.012221 \end{bmatrix} \end{aligned} \tag{10.35}$$

Furthermore in Equation 10.30, c_f is the friction coefficient and is assumed to be 0.009 [33]. Finally, the three dimensional coefficients can be computed:

$$dC_L = \frac{dc_l}{\bar{b}_{dp} \cdot \frac{b}{2}} \tag{10.36}$$

$$dC_{D_0} = \frac{dc_{d_0}}{\bar{b}_{dp} \cdot \frac{b}{2}} \tag{10.37}$$

$$dC_{D_i} = \frac{dc_{d_i}}{\bar{b}_{dp} \cdot \frac{b}{2}} \tag{10.38}$$

Since the propeller induces drag on the wing, this drag has to be fed back to the thrust calculation, resulting in an increase in thrust, etc. This needs to be iterated to get an accurate result. Furthermore, this method is also used to obtain the amount of blown wing propellers through an iterative process.

The additional lift and drag coefficients for the takeoff flight phase are summarized in Table 10.7 for the blown wing (i.e. the distributed smaller propellers) and the main propellers (i.e. the two larger propellers located at the wing root). Specifications about the propulsion system design can be found in chapter 12.

10.5.4. Wing Loading Distribution

Now that all of the contributing forces have been identified, the forces need to be decomposed in the specified reference frame. A general vertical (z-direction) and horizontal (x-direction) load distribution along the wing span can be generated by adding/subtracting the decomposed forces. In Figure 10.11, all of the vertical contributions are shown separately and are added in Figure 10.12. The same can be seen for the horizontal loads (Figure 10.13 and Figure 10.14). The black dotted lines are indicating the fuselage boundary.

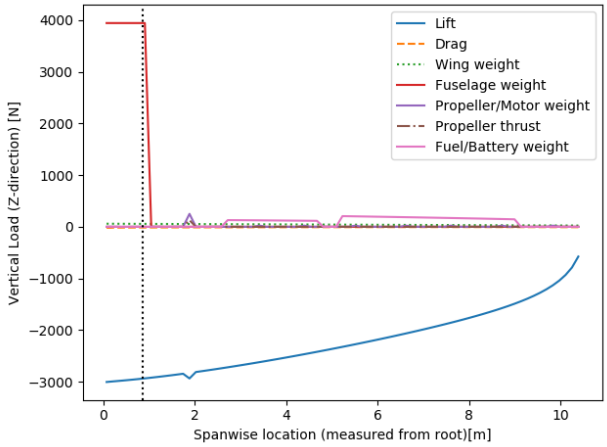

Figure 10.11: Wing loading for ultimate loading condition of different contributions in z-direction.

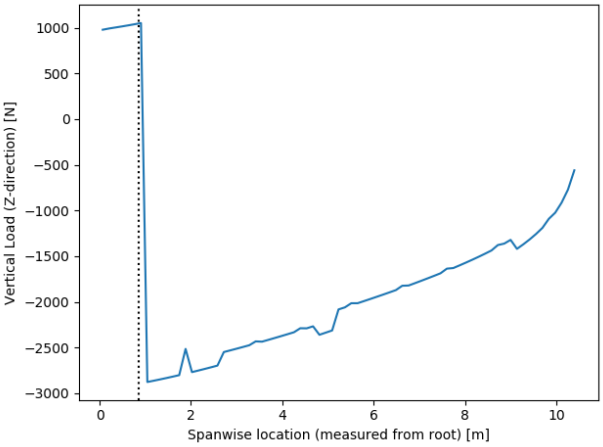

Figure 10.12: Total wing loading for ultimate loading condition in z-direction.

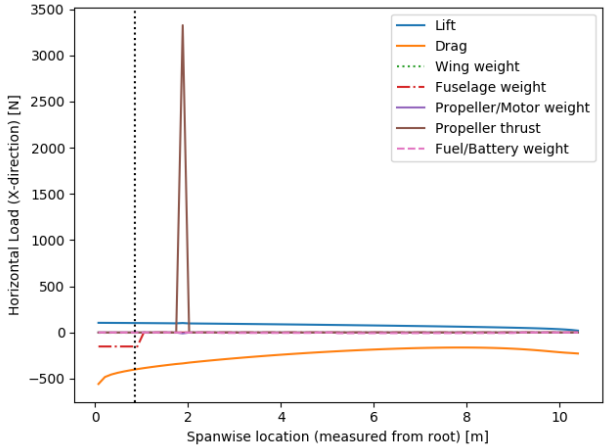

Figure 10.13: Wing loading for ultimate loading condition of different contributions in x-direction.

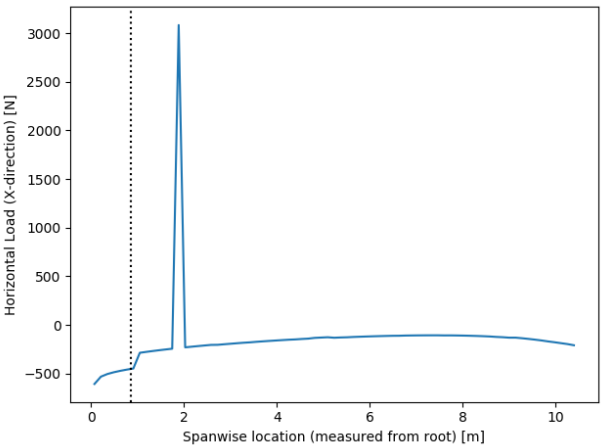

Figure 10.14: Total wing loading for ultimate loading condition in x-direction.

10.5.5. Reaction Forces and Bending Moments along the Wing

Using the identified loads on the wing, internal forces and moments at every section of the wing span can be obtained. These are needed to design a sufficiently strong and stiff wing box.

Reaction Forces Along the Wing

Using the identified loads on the wing from subsection 10.5.2, the reaction forces acting on the wing can be calculated. In order to obtain these reaction forces, a cut is made at different locations along the span, each containing a reaction force in x- and z-direction. Starting from the non-clamped tip and proceeding to the clamped root, the reaction force is obtained by summing all the preceding loads. The result of this analysis is shown in the shear force diagrams in Figure 10.15 (z-direction) and Figure 10.16 (x-direction). It is visible that the lift force in the z-direction has a major influence on the shear reaction force acting on the wing. The shear reaction force at the wing root rises above 0 again due to the presence of the fuselage including its weight, payload etc.

From Figure 10.15 and Figure 10.16, it can be seen that the reaction force attains a maximum along the span. This is shown for the design loading conditions, which refers to the ultimate loading. In addition to this, different propulsion system usage is present at these different phases. In the z-direction, the highest loading condition is at $y = 0.91$ m from

the root chord where $F_Z = -135.862\,\text{N}$. For the x-direction, the critical shear is present at the root with a shear force $F_X = -10.300\,\text{N}$. The shear conditions are used as an input for the upcoming design of the load carrying structure in section 10.6.

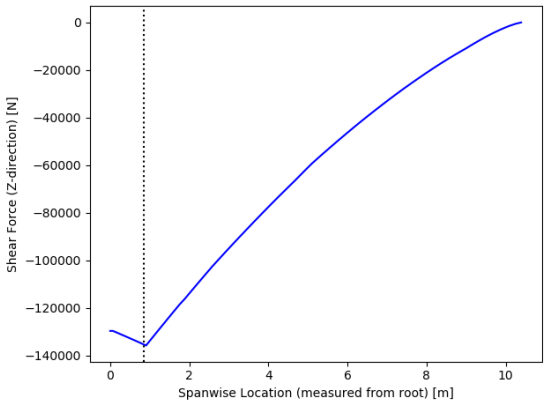

Figure 10.15: Shear diagram for ultimate loading in z-direction.

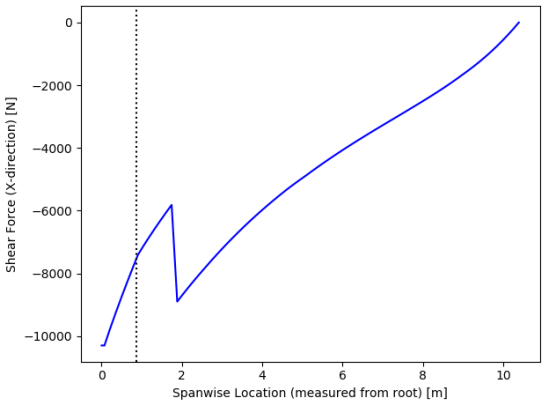

Figure 10.16: Shear diagram for ultimate loading in x-direction.

Bending Moments Along the Wing

Following the reaction forces calculated in subsection 10.5.5, the bending moment along the wing span is calculated. The reaction moment acting at the wing tip is zero as this is an unsupported point. Starting from the wing tip, the integral of the shear force diagram is calculated along the wing span to obtain the reaction moments around the x- and z-axis. The bending moment diagrams are given in Figure 10.17 around the x-axis and Figure 10.18 around the z-axis for the critical loading condition, which is the maximum load factor. For the moment about x, the highest moment is present at the root, where $M_X = 658.960\,\text{N m}$. For the z-direction, the critical moment is also positioned at the root, where the moment builds up to $M_Z = -50.043\,\text{N m}$.

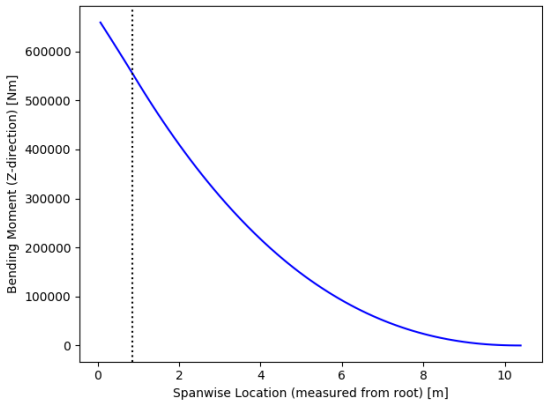

Figure 10.17: Moment diagram for ultimate loading around x.

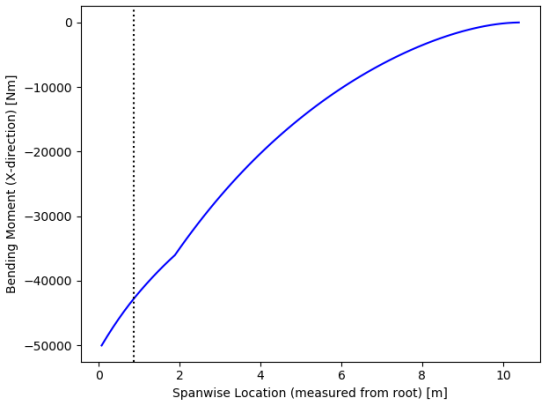

Figure 10.18: Moment diagram for ultimate loading around z.

10.6. Wing Box Design

The wing is subjected to large forces, as became clear from previous sections. A load bearing structure needs to be designed to ensure that those forces are sustained. This section explains the design approach for a wing box.

Assumptions

AS-STR-10: The cross-section is idealized: the stringers are represented as booms.
AS-STR-11: The number of stringers on the upper and lower skin and along the wing span are equal. This leads to redundancy, but also to a heavier wing structure.
AS-STR-12: The skin is assumed to only carry shear stresses. This simplifies the shear flow calculations, but also makes them less accurate.
AS-STR-13: The wing box is assumed to be rectangular during all skin, spar and stringer thickness calculations.

10.6.1. Design Approach

A wing box capable of carrying all the loads it is subjected to needs to be designed. This means that all stresses induced in the wing box need to be sustained. An iterative process is proposed, visualized in Figure 10.19. First, an initial wing box sizing is done: dimensions are chosen based on the wing geometry, ribs and spars are placed, and thicknesses of the skin, spars, rib webs and stringers are estimated. Simultaneously, the wing loading is investigated: the maximum loading case is used for the design. It is decided to idealize the cross-section to simplify the stress calculations: stringers are replaced by booms with equivalent areas. These take up all the direct stresses, while the skin and the spars only carry shear stresses. The process starts with four stringers, or booms: one in each corner of the wing box. With these, the direct stresses are computed in the booms in every cross-section along the wing span based on the ultimate loading. The stresses are compared to the yield stress of the chosen material and to the critical buckling load. If these are exceeded, a stringer on both the upper and lower skin is added. Stringers are added until the stresses do not exceed the yield and buckling limits anymore. It is assumed that the number of stringers remains constant along the entire span. The shear flow is calculated in between the booms for every cross-section along the span. This is fed back into the thickness calculations to update the wing box dimensions.

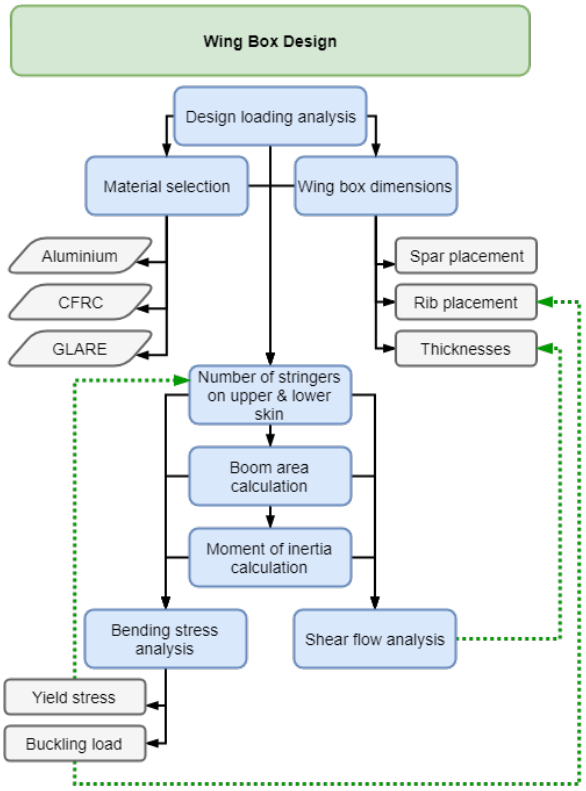

Figure 10.19: Approach for the wing box design.

10.6.2. Material Selection

The wing is a highly loaded structure and thus needs to be made out of appropriate material. Three options are considered: an Aluminum alloy, carbon fiber reinforced polymer composite (CFRP) and glass reinforced Aluminum (GLARE). Multiple factors have to be take into account:

- Ultimate stress
- Yield stress
- Stiffness
- Temperature limits
- Fatigue resistance
- Conductivity
- Affordability
- Mass density
- Fabricability
- Recyclability

Aluminum Alloy

Aluminum alloys are the mostly used material in the aerospace industry. In general, different alloys have different properties: when one property is improved, another one is sacrificed. For aerospace applications, the most commonly used Aluminum alloy is Al2024-T3, it is considered of high grade aircraft quality, because of its high strength and fatigue resistance.

Table 10.1: Properties of Al2024-T3.

Parameter	Evaluation	Value
Ultimate stress	High tensile strength [28]	496 MPa
Yield stress	High yield strength [28]	393 MPa
Stiffness	Low stiffness [28]	73 GPa
Temperature limits	Low elevated temperature capabilities [28]	$< 130°C$
Fatigue resistance	Low fatigue strength	90 MPa[3]
Conductivity	Excellent electrical conductivity [28]	
Affordability	Relatively low cost compared to the other two options [28]	
Mass density	Relatively high [28]	2700 kg m^{-3}
Fabricability	Easily fabricated, may be fabricated in every form [28]	
Recyclability	Known methods on recyclability	± 90%

CFRP

Composite materials are made out of fibers in a matrix of epoxy resin, protecting the fibers. The fibers can either be continuous or discontinuous, but either of them show very high tensile strength and stiffness (exceeding that of steel). The composite is anisotropic: it is stronger in the direction of the fiber orientation. Therefore, the fibers must be orientated in the direction that shows the greatest loads. In aircraft, a commonly used composite is CFRP, so this is considered in the material selection. The properties shown in Table 10.2, are properties of a single ply with fibers in one direction. A composite laminate is build up out of multiple plies oriented in different directions, to enhance to shear behaviour of the composite [36].

Table 10.2: Properties of CFRP.

Parameter	Evaluation	Value
Ultimate stress	High longitudinal/ low transverse [36]	1.8 GPa/0.02 GPa
Yield stress	High longitudinal/ low transverse [36]	1.8 GPa/0.02 GPa
Stiffness	High longitudinal/ low transverse [36]	270 GPa/5.53 GPa
Temperature limits	Depends on the temperature performance of the resin: conventional epoxy resins [37]	$180°C$
Fatigue resistance	Complex, involves many damage modes: fiber/matrix debonding, matrix cracking, delamination, fiber fracture, but more resistant to fatigue than Aluminum [37]	
Conductivity	Low conductivity [37]	
Affordability	High material costs, high production costs, but lower assembly costs [37]	
Mass density	Low [36]	1760 kg m^{-3}
Fabricability	Difficult: high probability of layup mistakes, resulting in lower quality, but bigger parts can be produced at once, resulting in lower assembly costs [37]	
Recyclability	Able to recycle carbon fibers and used in other applications [37]	

GLARE

GLARE is a laminated material consisting of thin layers of Aluminum metal sheets and a prepeg, glass fiber embedded in an epoxy resin [38]. It combines the best properties of Aluminum and glass fibers (see Table 10.3). The prepeg layers can be aligned to match the major loading, meaning the properties of GLARE can be tailored to fit their application. For the comparison, GLARE 3 is used; this is the material used in the A380.

Table 10.3: Properties of GLARE.

Parameter	Evaluation	Value
Ultimate stress	High strength [39]	717 MPa
Yield stress	High strength [39]	292 MPa
Stiffness	Low stiffness [39]	56 GPa
Temperature limits	Better resistance to fire than the other two options [40]	$210°C$
Fatigue resistance	Better resistance to fatigue than the other options: fibers restrain crack opening [41]	
Conductivity	Mediocre conductivity: in case of lightning only the outer layers are damaged [42]	
Affordability	High costs, higher compared to the other options [43]	
Mass density	Low density due to thin layers of metals and composite plies [39]	$2500\,kg\,m^{-3}$
Fabricability	GLARE laminates can be machined in the same way as Aluminum alloys, production of large panels is possible [41]	
Recyclability	Able to recycle glass fibers and Aluminum, see section 21.2	

Selection

For the wing structure, the material to be used is GLARE 3. The wing is highly loaded and the combination of mechanical properties of Aluminum and composites is therefore beneficial. Moreover, fuel tanks and batteries have to be stored in the wing, which makes the wing a flame sensitive area. Using GLARE there, may provide more time to evacuate, increasing passenger safety [42]. GLARE also has a lower density than Aluminum, leading to a weight reduction of approximately 20%. The greatest disadvantage of GLARE is its high cost [43]. Therefore, only the wing is made of GLARE, to minimize the manufacturing and material costs. Another downside, is that it is such a novel material: recyclability is still under investigation, but shows great potential [38].

Carbon fiber reinforced polymer composites show high strength and stiffness, but its anisotropic character is a disadvantage: the wing is loaded in many directions and therefore needs to be strong enough in all directions. Furthermore, it is difficult to produce, and is susceptible to ply orientation mistakes, leading to decreased material quality. Also, recyclability is not well-developped yet, making this material less sustainable.

Aluminum is proven to work. However, the possibility to combine its properties with the best qualities of a composite material is very attractive. Moreover, it has a low temperature limit and is not resistant to fire. Since the E-COmmuter uses a great amount of batteries, fire safety is an important factor to consider, especially if the batteries are stored in the wings.

10.6.3. Wing Box Design

An initial wing box geometry is decided upon. This leads to the calculation and addition of booms, in which normal stresses can be calculated and compared to the yield stresses and critical buckling loads. Afterwards, a shear stress analysis is performed to iterate through appropriate wing box dimensions.

Design Loading

The loading conditions resulting in the highest loads and moments on the wing box are those for the limit load factor. This limit load factor is multiplied with a safety factor of 1.5 arising from CS-23 regulations to obtain the maximum and minimum ultimate load factor n_{ult}. As the same number of stringers are added on the lower and upper skin, and because the thicknesses for upper and lower skin are equal, the maximum load factor multiplied with the loads resulting from the level cruise flight condition (L = W for $\alpha = 2.2°$) is the design loading condition. The shear and moment diagrams for this design case are the ones given in Figure 10.15, Figure 10.16, Figure 10.17 and Figure 10.18.

Initial Wing Box Sizing

Since the propeller and electrical motors are mounted on the leading edge, and the trailing edge is almost entirely occupied by high lift devices and control surfaces, it is decided to limit the load bearing structure to the center part of the wing. The wing box consists out of a front (at 30% of the chord) and a rear spar (at 70% of the chord). These are connected to the upper and lower skin of the wing, and together they form the load bearing structure, or the wing box. The spars take up the shear and torsional loading, while the skin resists direct stresses, caused by bending and direct loading. Ribs are positioned along the wing box with a spacing of 0.5 m. These serve as a prevention for column buckling and are loaded in shear. Stringers are distributed on the upper and lower skin to resist direct stresses as well.

Figure 10.21 shows the wing box location and shape for a normalized cross-section of the wing. The wing box is indicated in blue.

An initial thickness estimation is performed. This is later updated via iteration using the direct and shear stresses. For the skin, stringer and spar thicknesses, a rectangular wing box is assumed. For this rectangular wing box, the sectional width (between the spars) is $w_{s,i}$ and the height (between the skins) is $h_{s,i}$. These are dependent on the sectional chord length.

The loading acting in the wing skin due to bending and shear is calculated first. The skin load due to bending is obtained using Equation 10.39. Furthermore, the shear flows are first assumed to be zero in every cross-section. These shear flows, q_T, are updated after the first iteration to update the skin thicknesses [44].

$$\left(\frac{P}{w}\right)_{s,i} = \frac{M_{s,i}}{w_{s,i} \cdot h_{s,i}} \tag{10.39}$$

Using the above mentioned q_T and $\left(\frac{P}{w}\right)_{s,i}$, the upper and lower wing skins can be designed for strength. Doing so, it is important to have an idea of the material that will be adopted. In this case, GLARE 3 is used as discussed in subsection 10.6.2. This is a composite material, for which the smeared thickness of the wing skins (consisting of the combination of stringer and skin itself) can be estimated as in Equation 10.40, where shear and direct loading are considered separately. A safety factor of 1.5 is applied to the entire design to account for design uncertainties. The variable $k_s = \frac{t_{\text{skin}}}{t_{\text{stringer}} + t_{\text{skin}}}$ is estimated to be 0.6 [44]. Moreover, the yield tensile stress and shear maximum allowable stress of GLARE 3 is used, which are $\sigma_y = 292\,\text{MPa}$ and $\tau_{max} = 115\,\text{MPa}$ respectively [44][45].

$$(t_{\text{e,strength}})_{s,i} = \text{SF} \cdot \max\left(\left|\frac{(\frac{P}{w})_{s,i}}{\sigma_y}\right|, \left|\frac{(q_T)_{s,i}}{k_{skin} \cdot \tau_{max}}\right|\right) \tag{10.40}$$

In addition to the thickness of the stringers, which is determined using k_s and the obtained smeared thickness $t_{\text{e,strength}}$, the thickness of the spar webs can be obtained using Equation 10.41. The maximum allowable shear stress is a given value for GLARE 3, and again a safety factor of 1.5 is applied to these calculations [44][45].

$$(t_{\text{w, strength}})_{s,i} = \frac{\text{SF}}{\tau_{max}} \cdot \left(\frac{S_{s,i}}{2 \cdot h_{s,i}} + (q_t)_{s,i}\right) \tag{10.41}$$

The obtained thicknesses of stringers, skin and spar webs are used during the boom area calculations to append stringers and skin into the different booms.

Boom Area Calculation

Based on the buckling and bending stresses, stringers are to be added to the upper and lower skin to resist the stresses. To simplify the calculations, the cross-section is idealized: the stringers are represented as booms with equivalent areas. The wing box design iteration is initiated with only four stringers: one in each corner of the wing box. Stringers are added based on the bending stresses and whether or not yielding and/or buckling occurs. These stringers are evenly distributed over the upper and lower skin and replaced by booms to re-evaluate the calculations. This is repeated until the wing box can resist all stresses.

Idealization of the structure leads to some inaccuracies:

- The bending stiffness is underestimated because the contribution of the web is neglected.
- The maximum direct stress is overestimated because of the lower bending stiffness. This serves as a safety factor in the calculations.
- The maximum shear flow is underestimated. This only has a limited effect on the final results, since shear is less critical than direct stress in thin-walled structures.

To idealize a panel into direct stress carrying booms and shear stress carrying skin, the boom areas need to be calculated. Using the example shown in Figure 10.20, the boom areas can be calculated following Equation 10.42 and Equation 10.43 [46].

$$B_1 = \frac{t \cdot b}{6} \cdot \left(2 + \frac{\sigma_2}{\sigma_1}\right) \tag{10.42}$$

$$B_2 = \frac{t \cdot b}{6} \cdot \left(2 + \frac{\sigma_1}{\sigma_2}\right) \tag{10.43}$$

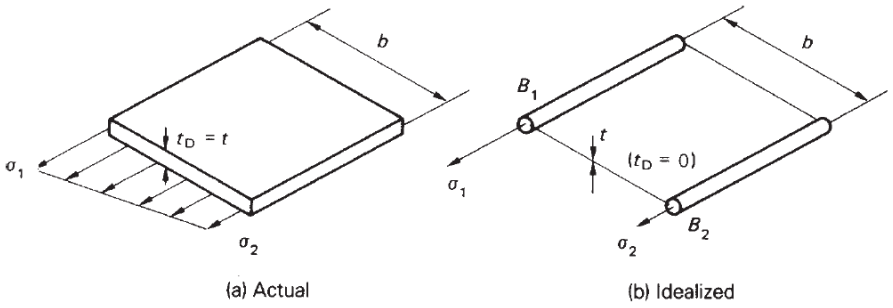

Figure 10.20: Idealization of a panel [46].

The ratio of the direct stresses, σ_1 to σ_2 or the other way around is not known at this point, but it can be assumed. Its is assumed that the direct stresses are proportional to the boom's distance from the neutral axis. This would imply that

the wing box cross-section is symmetrical and no moment about the z-axis is applied. In reality, this is not the case, leading some uncertainty in the design. This is accounted for by applying a safety factor in the thickness calculations.

The final result of the iteration shows 14 stringers on both the upper and lower skin. Figure 10.21 shows the normalized wing cross-section and wing box, with the boom locations indicated as red dots. Furthermore, the final boom areas are given in Table 10.4. The booms are numbered, from the top right corner to the bottom right corner.

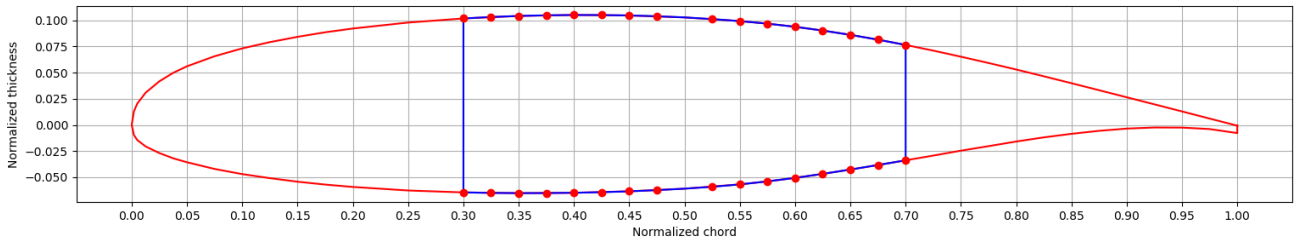

Figure 10.21: Normalized wing cross-section with wing box and boom/stringer locations.

Table 10.4: Boom areas.

Boom	Area	Boom	Area	Boom	Area	Boom	Area
B_1	537.61 mm^2	B_9	598.09 mm^2	B_{17}	642.9 mm^2	B_{25}	603.32 mm^2
B_2	453.35 mm^2	B_{10}	453.51 mm^2	B_{18}	453.55 mm^2	B_{26}	453.35 mm^2
B_3	453.33 mm^2	B_{11}	453.52 mm^2	B_{19}	453.57 mm^2	B_{27}	453.391 mm^2
B_4	453.38 mm^2	B_{12}	453.52 mm^2	B_{20}	453.57 mm^2	B_{28}	453.38 mm^2
B_5	453.31 mm^2	B_{13}	453.51 mm^2	B_{21}	453.56 mm^2	B_{29}	453.49 mm^2
B_6	453.35 mm^2	B_{14}	453.35 mm^2	B_{22}	453.55 mm^2	B_{30}	453.54 mm^2
B_7	453.43 mm^2	B_{15}	453.48 mm^2	B_{23}	453.54 mm^2	B_{31}	453.61 mm^2
B_8	602.84 mm^2	B_{16}	662.9 mm^2	B_{24}	597.66 mm^2	B_{32}	515.88 mm^2

Moment of Inertia Calculations

The moment of inertia is calculated using the boom areas and locations calculated above. Because a boom is an area appended in a single point, only the Steiner terms are to be calculated to come up with a moment of inertia I_{xx}, I_{zz} and I_{xz}. However, the centroid location for each section is needed as input, which is obtained from Equation 10.44 and Equation 10.45 . Once the location of the centroid is known, the moment of inertia for each section can be calculated using Equation 10.46.

$$\bar{x}_s = \frac{\sum_{i=0}^{n} A_{s,i} \cdot x_{s,i}}{\sum_{i=0}^{n} A_{s,i}} \tag{10.44}$$

$$\bar{z}_s = \frac{\sum_{i=0}^{n} A_{s,i} \cdot z_{s,i}}{\sum_{i=0}^{n} A_{s,i}} \tag{10.45}$$

$$\begin{aligned} (I_{xx})_s &= \sum_{i=0}^{n} A_{s,i} \cdot (z_{s,i} - \bar{z}_s)^2 \\ (I_{zz})_s &= \sum_{i=0}^{n} A_{s,i} \cdot (x_{s,i} - \bar{x}_s)^2 \\ (I_{xz})_s &= \sum_{i=0}^{n} A_{s,i} \cdot (x_{s,i} - \bar{x}_s) \cdot (z_{s,i} - \bar{z}_s) \end{aligned} \tag{10.46}$$

Bending Stress Analysis

The design condition bending moments introduce tensile stresses in the lower skin as well as compressive stresses in the upper skin. Therefore, a first criteria is that the lower skin is to be stiffened to make sure that tensile stresses do not exceed the GLARE yield stress. The stress acting at each boom location is calculated using Equation 10.47. The sectional moments are inputs for this, as well as the previously calculated moment of inertia [47].

$$\sigma_{s,i} = \frac{(M_z)_s \cdot (x - \bar{x})}{(I_{zz})_s} + \frac{(M_x)_s \cdot (z - \bar{z})}{(I_{xx})_s} \tag{10.47}$$

$$(\sigma_{b,cr})_s = (K_c)_s \cdot E \cdot \left(\frac{t_s}{b_s}\right)^2 \tag{10.48}$$

In addition to the lower skin, the compressive stresses in the upper skin are designed such that the critical buckling stress and/or the maximum compressive stress of GLARE are not exceeded. The buckling stress at each section is calculated using Equation 10.48. In this formula the compression buckling coefficient for the skin-stiffener panel is calculated using loading case 5 of Figure 10.22. The a in this figure refers to the rib spacing, while b refers to the stringer spacing [48].

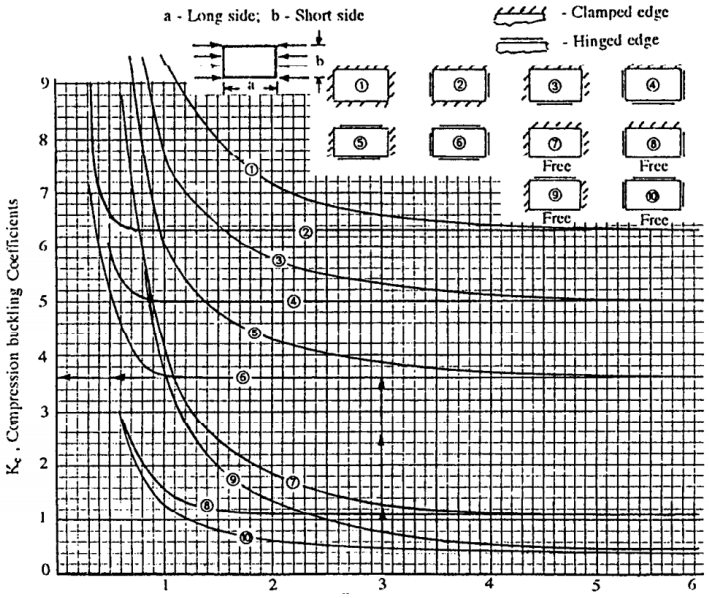

Figure 10.22: Compression buckling coefficient for skin-stiffener panel K_c [48].

If either of the above mentioned conditions is not met, a stringer is added to the upper and lower skin in each sectional cut. Doing so, the stiffness of the wing box is increased, which in turn decreases the tensile, compressive and buckling stresses in the cross-section.

Shear Stress Analysis

In order to size the skin and spars such that they can resist the shear loading, a shear analysis needs to be performed. The shear flows are fed back into the wing box thickness calculation to take into account the shear stresses. The shear flow at any point in the cross-section of the wing box can be computed using Equation 10.49 [46].

$$q_s = -\left(\frac{S_x \cdot I_{xx} - S_z \cdot I_{xs}}{I_{zz} \cdot I_{xx} - I_{xz}^2}\right) \cdot \left(\int_0^s t \cdot x \cdot ds + \sum_{i=1}^{n} B_i \cdot x_i\right) - \left(\frac{S_z \cdot I_{zz} - S_x \cdot I_{xs}}{I_{zz} \cdot I_{xx} - I_{xz}^2}\right) \cdot \left(\int_0^s t \cdot y \cdot ds + \sum_{i=1}^{n} B_i \cdot y_i\right) + q_{s,0} \tag{10.49}$$

This equation can be simplified. Since it is assumed that the skin only carries shear stress, it can be said that $t = 0$, removing the integral from Equation 10.49. This results in a constant shear flow in between the booms. The equation can be reduced to:

$$q_s = q_b + q_{s,0} \tag{10.50}$$

Here, q_b is the basic or open section shear flow. It is obtained by making a "cut" in the cross-section and treating it as an open section. Then, $q_{s,0}$ is a constant shear flow throughout the cross-section and accounts for the torque in the closed section. It can be obtained by equating the internal and external torsional moments about a point. In Equation 10.51, η_0 and ξ_0 represent the moment arms of the external shear forces to the point about which the moment is taken. Taking the moment about the shear center would result in Equation 10.53. However, the shear center differs along the wing span, since the shear loading and geometry of every cross-section is different. Nevertheless, the shear center is calculated to evaluate the torque and twist of the wing. This is discussed later. Since, $q_{s,0}$ is constant, its induced shear force can be calculated by multiplying it by twice the internal cross-sectional area. Rewriting this equation, results in a value for the constant shear flow, and thus the total shear flow, at each point of the cross-section.

$$S_x \cdot \eta_0 + S_z \cdot \xi_0 = \oint p \cdot q_b \cdot ds + 2 \cdot A \cdot q_{s,0} \tag{10.51}$$

This analysis is done for every cross-section along the wing span. The maximum shear flow in the skin and spar is calculated at every spanwise location and fed into the thickness calculation. Moreover, the maximum shear stress value can be seen in section 10.10.

Wing Deflection

The bending deflection of the wing in the z-direction v(z) under ultimate load conditions can be calculated using Equation 10.52. The result of this is given in Figure 10.23. It is visible that the tip is deflected 1.1 m in negative z-direction, which is an upward deflection. Deflection of the wing in x-direction is neglected, as I_{zz} is relatively large and the moment very small [47].

$$v(z) = \int_0^{b/2} \left(\int_0^{b/2} \frac{M_x(y)}{E \cdot I_{xx}(y)} \cdot dy \right) \cdot dy \tag{10.52}$$

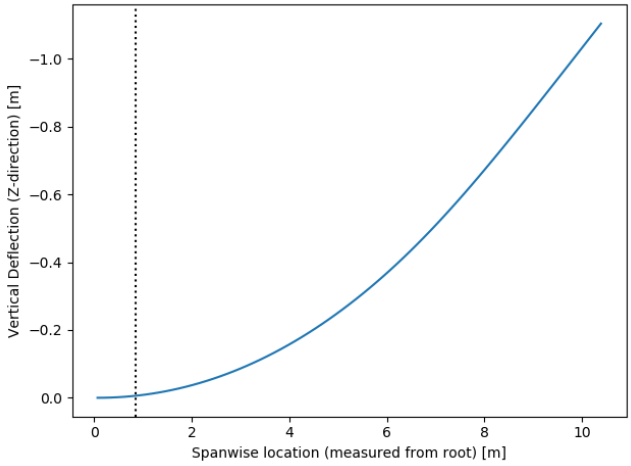

Figure 10.23: Vertical (z-direction) deflection of the wing at ultimate loading conditions.

Wing Twist

In order to evaluate the twist of the wing, the shear center needs to be obtained. This is the point about which the wing torques: if the shear forces are applied in the shear center, there is no torsion. The shear center can be found by applying dummy forces S_x and S_z through it. Afterwards, the basic shear flow is calculated using the same method as discussed above. The constant shear flow $q_{s,0}$ is found by using the fact that a shear force acting through the shear center produces zero twist, resulting in Equation 10.53. Thus, Equation 10.54 can be used to calculate $q_{s,0}$.

$$0 = \oint \frac{1}{G \cdot t} \cdot (q_b + q_{s,0}) \cdot ds \tag{10.53}$$

$$q_{s,0} = \frac{\oint q_b \cdot ds}{\oint ds} \tag{10.54}$$

Here, G is the shear modulus. The distance to the shear center can be found by equating the external moments (caused by the dummy forces S_x and S_z) and the internal forces about a point in the cross-section.

It becomes clear that the shear center differs along the wing span: every cross-section is loaded differently and has a different geometry.

The shear center plays an important part in computing the twist along the wing span. Using Equation 10.55, the twist angle at every point of the wing span can be found. Here, J is the polar moment of the wing and is approximated by Equation 10.56 [46]. This is the polar moment for a rectangular thin walled cross-section (a and b being the sides). This results in an overestimation of the twist.

$$\phi = \int_0^L \frac{T(y)}{J(y) \cdot G} \tag{10.55}$$

$$J = \frac{a \cdot b \cdot t}{3} \cdot (a + b) \tag{10.56}$$

The torque is obtained by taking the moments of the shear forces about the shear center at every section along the span. Then, an interpolating spine is made to create the function $T(y)$ and $J(y)$. Assuming the root of the wing is clamped, the twist angle increases starting from zero to the tip. The twist at the wing tip should preferably be between 2 to 5°. No exact value for the twist is calculated due to time constraints.

10.7. Battery and Fuel Tank Integration

The battery to supply power to the E-COmmuter is situated in the wing. As the battery volume takes up a significant part, and because it is easily connected with wires instead of larger fuel ducts, the batteries are located more outboard than the fuel tank. Doing so, it is offering a significant bending relief to the aircraft wing during all flight phases as an invariable weight. The battery volume is calculated in section 12.6 to equal 0.457 m^3. A battery weight of 587 kg is determined as well, consisting of 2346 cells in total. These batteries are located between 5.2 m and 9.1 m measured from the root in both wings taking into account a factor of 2 on the volume to account for fireproof casing and thermal control. A clearance near the tip is accounted for to prevent damage resulting from lightning strikes on the wing tip. The cells are split up in different compartments between the evenly spaced wing ribs for safety and battery bending reasons. Puncture protection is provided by the GLARE wing box, which is a material showing favourable impact resistance characteristics. In addition, the GLARE ribs with high flame resistance serve as a firewall between the compartments [49]. Cooling for the batteries is provided by leaving a freestream possibility for cold air to reach the batteries.

The replacement of the batteries is still to be designed in more detail. However, it is determined that the batteries can be replaced by opening the lower wing skin. Doing so, the batteries can be changed quickly on the ground and are reachable for ground crews. The batteries are held fixed in the wing using clips carrying the weight of the battery. A more detailed design of the wing box lower skin shall be performed, where a hinge can provide opening of the wing box, and the stringers stop near the ribs to have the ability to transfer loads. Currently, the wing near the ribs is slightly over designed for this issue, as more stringers are present than necessary assuming the constant wing box geometry. An advantage of accessing the batteries via the lower wing skin is that the flow over the upper wing skin remains undisturbed, which is favourable for the aerodynamic efficiency of the wing.

Finally, the fuel tanks of the aircraft capable of carrying 369 kg of fuel are positioned more inboard than the batteries in both wings. They are positioned from 2.7 m up to 4.8 m from the root. This offers bending relief, while still providing enough space for the large motor connection, as well as limited fuel duct length. The fuel tanks are positioned within the wet GLARE wing box offering good corrosion, flame resistance and impact resistance characteristics. The compartments of the wing box are between the wing ribs to control the lateral c.g. of the aircraft.

The integration of batteries and fuel into the wing are displayed visually in Figure 10.24. Space for the inverters is left between the wing root and the large motor integration part.

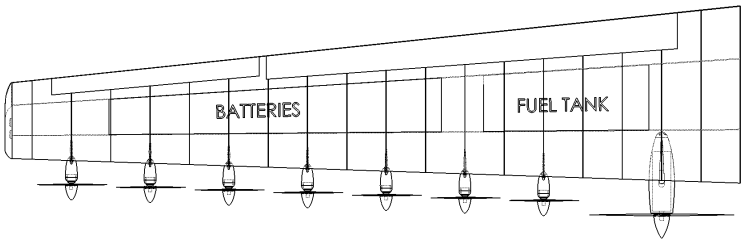

Figure 10.24: Fuel tank and battery location in the wing.

10.8. Weight of the Wing Structure

To calculate the structural weight of the wing, the following formula is used: $M = \rho \cdot V$. Using the mass density of GLARE 3 of 2500 kg m^{-3} and the volume of the wing, the weight can be computed. First, the volume of the wing box is found, by calculating its area on every section along the wing span and multiplying this by the spacing between two spanwise positions. Adding these gives the total wing box volume. This includes: skin, spars, stringers and ribs. Since the wing consists of more than just the wing box, this value is multiplied by a factor. Since the rest of the wing is not load carrying, it can be considered as secondary structure. The mass of the secondary structure is assumed to be 25% of the primary structure (the wing box). This results in a total wing mass of 596.32 kg. This is approximately 7% lighter than the Class II weight estimation. Nevertheless, the difference between the Class II and the detailed estimation is very little and therefore, the weight estimation from Class II can be considered validated. The weight of structural parts that are not calculated in detail, such as the tail or landing gear, are thus considered equal to the Class II estimations.

10.9. Verification and Validation

Below, the verification and validation of is explained for each of the analyses discussed above.

Wing and Power Loading Constraints

The constraint analysis is verified by comparison to calculations by hand, in which a small rounding error deviation is taken into account. Furthermore, conversions from and to imperial units are verified by hand and checked with reliable unit conversion tools.

To validate the wing surface and power, a look is taken at the wing and power loading of reference aircraft: the relationship between the wing surface/power and the MTOW is derived and a regression line is found. Using the MTOW from the first weight estimations, the wing and power loading can be validated. For the wing loading, a linear regression line with R^2=0.57 is found, because the data is scattered. The data cannot be accurately validated using this, but looking at the power loading, a regression line with R^2=087 is found. It is shown that the power is way lower than estimated. This can be explained because the reference aircraft have conventional propulsion systems rather than the blown wing concept. The power is assumed valid.

Wing Planform

Unit tests are performed to ensure that unit conversion are applied correctly. The mean aerodynamic chord is verified using graphical methods. The planform is validated by comparing it to reference aircraft. As can be seen in [4], high-wing regional turbopropeller driven aircraft always have a quarter chord sweep of zero, the taper ratio is often around 0.4 and the dihedral is slightly positive.

Airfoil Selection

In order to validate the airfoil, XFLR5 has to be validated. Using the XFoil Direct Analysis tool, different polars can be analyzed and obtained. The results can be compared to tests performed in the Langley low-turbulence pressure tunnel. The analyses are done at $Re3 = 3.7 \cdot 10^6$ and M = 0.1. The results of the wind tunnel tests can be found in [4], while the results from XFLR5 are shown in Figure 10.3 and Figure 10.4. As can be seen, XFLR5 tends to overestimate: the actual maximum lift coefficient is only 90% of the estimated one. Therefore, the actual $C_{l_{max}} = 0.9 \cdot 1.93 = 1.74$. This still meets the desired lift coefficient of the airfoil, so both XFLR5 and the airfoil are validated.

Wing Propeller Interaction

The method to evaluate the propeller wing interaction is based on [33]. The code is verified by calculations by hand and unit tests ensuring that the number of propellers fit on the wing and there is enough clearance between them. Moreover, extreme values are inputted: a thrust of zero results in zero additional drag/lift, an angle of attack of zero also results in zero lift/drag, since the wing airfoil is assumed to be symmetrical. Using [34], calculated values are compared: $\frac{x_p}{c}$, $\frac{V_j}{V}$, β and dc_l. For an angle of attack of 3°, the following results are obtained.

Table 10.5: Validation of the propeller-wing interaction.

Parameter	Patterson value	Calculated value	Discrepancy
$\frac{x_p}{c}$	0.35	0.28	20%
$\frac{V_j}{V}$	2	1.32	34%
β	0.6114	0.648	5.64%
dc_l	0.9542	0.8598	9.89%

The first two parameters in the table are values set at the beginning of the program: the distance of the propeller in front of the leading edge and the velocity increase over the actual velocity (this depends on the freestream velocity). Discrepancies there are the result of different design choices and have to be taken into account. It can be seen that the β and dc_l term have very low discrepancies and can thus be validated. They can be explained however by the difference in propeller location and free stream velocity.

Reaction Forces and Moments Along the Wing

The load distribution in z-direction are validated to match the weight of the aircraft in level flight conditions at cruising angle of attack, which means that the total goes to 0. In a similar fashion, the x-direction was automatically verified on correctness, as those are correlated to the z-direction with the angles.

The reaction force diagrams are constructed immediately for the ultimate loading condition, and those are verified by manual calculations at a location of 1 m inboard, as the procedure afterwards remains the same. The bending moments are verified using 2 different methods, a first one by integration of the shear forces, the other one by taking the multiplication at each point manually. Doing so, the code for the reaction forces and moments along the span is verified on the correctness.

Boom Area Calculation

The boom area code is verified by hand and validated by implementing an exercise from [46], that calculates the boom areas in a similar fashion. Moreover, the code to automatically distribute the added booms evenly and calculate the boom area accordingly is extensively verified by testing different stringer combinations and number and plotting these on the wing box, to ensure that they are indeed added and evenly distributed. An example of this can be observed in Figure 10.21.

Moment of Inertia Calculation

The code for the moment of inertia is validated in a similar fashion as the boom area calculation. Using the same exercise, the moment of inertia using the booms is obtained and validated on correctness using the solution provided in [46]. This is done for I_{xx} and I_{zz}.

For I_{xz}, no solution is available. Therefore, this is verified by manual calculation of the moment of inertia formulas provided in [46]. The results of this analysis were identical because the applied formulas are identical.

Bending Stress Analysis

The bending stresses acting upon the wing are verified manually by calculating those for a specific boom located at a given distance from the neutral axis. Doing so, the sign of the stress, as well as its magnitude is verified.

Furthermore, using the bending deflection, a reasonable number shall be obtained in comparison to other aircraft for the tip deflection of the wing. It is apparent that the wing deflection is also correct, as value of 1.1 m is reasonable compared to [50, Equation 41] giving 1.14 m as result. This is a 3.6% error, which is reasonable considering the simplifications made. Due to this verification, the entire bending stress block is verified.

Shear Stress Analysis

To verify the shear stress analysis, small calculations are verified by hand. Moreover, when analyzing a closed section, a cut needs to be made to compute the basic shear flow. At the cut, the shear flow is zero. This can be verified by calculating the shear flows in between the booms until ending up at the cut again. Also, a careful look is taken that no floating errors are made. Furthermore, the code is validated by using it to solve a shear exercise from [46] (Example 20.4). The discrepancies can be seen below. None of the discrepancies are above 1%. Therefore, the program calculating the shear flow can be verified.

Table 10.6: Validation of the shear stress code.

Parameter	Megson	Calculated value	Discrepancy	Parameter	Megson	Calculated value	Discrepancy
q_{12}	12.7	12.64	0.47%	q_{56}	-34.3	-34.26	0.12%
q_{23}	-5.4	-5.4	0%	q_{67}	-5.4	-5.4	0%
q_{34}	-34.3	-34.26	0.12%	q_{78}	12.7	12.64	0.47%
q_{45}	-37.9	-37.87	0.08%	q_{81}	17.0	16.97	0.18%

10.10. Results

Here, all the results from the wing design are summarized. Furthermore, a rendering of the complete wing can be seen in Figure 10.25.

Table 10.7: All the results obtained from the wing design.

Parameter	Symbol	Value	Unit	Parameter	Symbol	Value	Unit
Wing Planform							
Wing surface	S	36.48	m^2	Wing span	b	20.92	m
Root chord	c_r	2.49	m	Tip chord	c_t	0.996	m
Taper ratio	λ	0.4	-	Quarter chord sweep	$\Lambda_{c/4}$	0	°
Dihedral angle	Γ	1	°	Mean aerodynamic chord	MAC	1.85	m
Lateral position MAC	y_{MAC}	4.48	m	Aspect ratio	A	12	-
Airfoil	NASA/LANGLEY			Flapped area	$S_{W_{\text{flap}}}$	29.7	m^2
Max delta lift coefficient flaps	$\Delta C_{l_{max_{\text{flap}}}}$	1.0	-	Flapped span	$b_{W_{\text{flapped}}}$	8.5	m
Fuel tank location	y_{fuel}	2.7 - 4.8	m	Battery compartment location	y_{bat}	5.2 - 9.1	m
Wing-propeller interaction							
Lift coefficient blown wing	$\Delta C_{L_{\text{blown}}}$	0.871	-	Drag coefficient blown wing	$\Delta C_{D_{\text{blown}}}$	0.0159	-
Lift coefficient main props	$\Delta C_{L_{\text{main}}}$	0.318	-	Drag coefficient main props	$\Delta C_{D_{\text{main}}}$	0.00392	-
Structural Wing Design							
Front spar location	$x_{\text{front spar}}$	30	% chord	Rear spar location	$x_{\text{front spar}}$	70	% chord
Rib spacing	d_{ribs}	0.5	m	Number of stringers	$n_{\text{stringers}}$	14	-
Max skin thickness	t_{skin}	5.2	mm	Max spar thickness	t_{spar}	5.0	mm
Max stringer thickness	t_{stringer}	3.5	mm	Max rib thickness	t_{rib}	5.0	mm
Max bending stress	σ_{max}	240	MPa	Max shear stress	τ_{max}	41	MPa
Max wing tip deflection	v_{tip}	1.10	m	Wing tip twist	ϕ	2-5	°
Wing structural weight	W_{W}	596.3	kg	Wing material	GLARE		

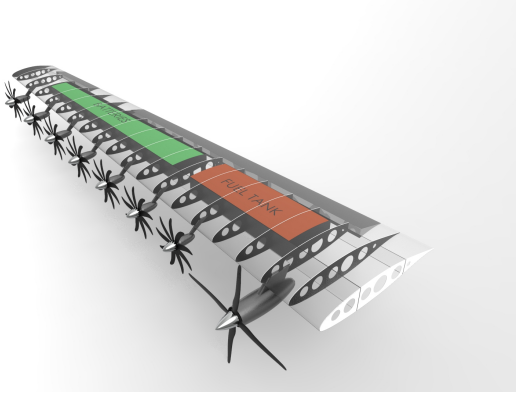

Figure 10.25: Rendering of the wing with the battery compartment (green) and fuel tank (red).

11
Performance Analysis

From the wing and the fuselage design it has become more clear what the aircraft will eventually look like, but how will it perform? The performance of any aircraft is almost always its most distinguishing aspect compared to other, similar aircraft. To assess if this is true for the E-COmmuter, a performance analysis is carried out in this chapter. First, the mission profile will be discussed in more detail than in chapter 5, after which a detailed analysis of each flight phase is carried out. Second, an aerodynamic analysis of the aircraft is carried out that serves as an input for the detailed analysis of the flight phases of the E-COmmuter. Last, the range performance is analyzed for the E-COmmuter. In the end of the chapter the verification methods used and final results are given.

11.1. Mission Profile

The mission profile depicted in Figure 5.1 is one of the most determining factors in the design of the E-COmmuter. It highlights certain sustainable features such as the hybrid design and the accessibility provided to rural areas. In this section the construction of the mission is elaborated and the problem of hybrid flying is tackled with a hybridization factor balancing the power for the hybrid flight phases. This all results in the optimal fuel and battery weights for the desired mission.

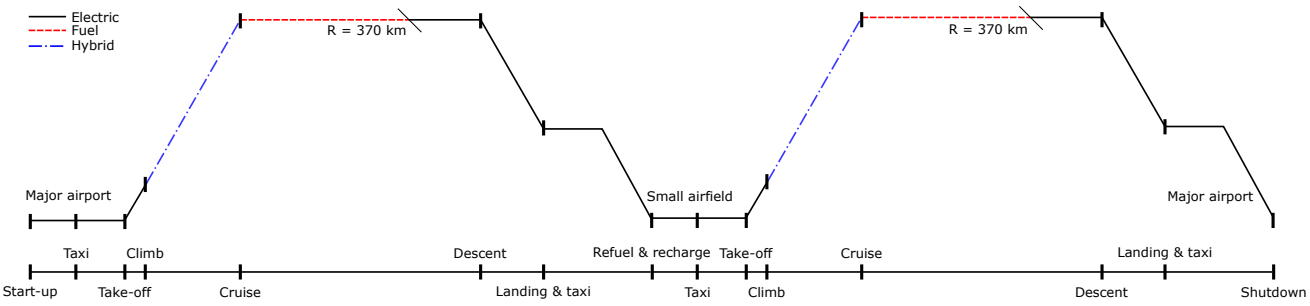

Figure 11.1: Mission profile for the E-COmmuter.

11.1.1. Construction of the Mission Profile

The mission profile is constructed while keeping the important requirements in mind. Requirement **HEF-OPR-03** sets the range of the aircraft at 370 km. **HEF-PROP-02** limits the takeoff and landing phases to pure electric power. Climb, cruise, and descent are the remaining flight phases up for hybrid electric propulsion. Fuel has a higher specific energy, 43 MJ kg^{-1}, compared to batteries, 2.7 MJ kg^{-1} [51][1]. As a result, using the maximum amount of fuel allowed by **HEF-MAN-02**, roughly 202 kg of aviation gasoline (Avgas), and complete the mission with batteries only could be a preferable choice.

However, simply dividing the energy between fuel and electricity storage neglects one of the large benefits of a hybrid system. This the hybrid ability to limit the amount of energy the internal combustion engines (ICEs) have to provide. For example, if one sizes the aircraft by using only fuel to power the climb phase to burn fuel as quickly as possible and reduce weight, one overlooks that then the internal ICEs have to be sized to produce the full required climbing power, adding unnecessary weight. Hence, an optimum is to be found between burning fuel as quick as possible while keeping the ICE size small by compensating the high power loads with battery power. This results in the mission profile as shown in Figure 11.1.

Hybridization Factor

To optimize the combination of battery, fuel, and the ICE weights an ideal hybridization factor for each flight phase can be determined. These factors determine how much energy provided to the motors comes from the batteries or the

[1] URL: `https://hypertextbook.com/facts/2003/EvelynGofman.shtml` [cited 24 June 2018]

ICEs [2]. As takeoff and landing shall be fully electric due to requirement **HEF-PROP-02**, climb and cruise are the flight phases for which the ideal hybridization factor are to be found. Descent, as will be discussed in subsection 11.3.6, can be done unpowered.

First the energy and power required to complete climb and cruise have to be determined. This is done in section 11.3. Then, it can be evaluated how different hybridization factors for climb and cruise affect the sum of the battery, fuel, and ICE weights. These affect each other inversely. If the battery weight, and therefore their total capacity increases, less of the required energy and power needs to be provided by the engine. Engines are heavy and take up a significant amount of space within the aircraft, so smaller lighter engines are preferred. On the other hand, batteries are heavy as well and if most of the energy needs to be provided by them, they will become too heavy to be useful as a power source. As said before, another important consideration is that using up fuel quickly reduces the in-flight weight and therefore also the amount of energy required to keep the aircraft flying.

It is found that during the climb phase, which requires a large power output, a hybridization factor of 0.39 is ideal to provide the lowest propulsive weight. This because this factor assures that the ICEs do not have to be sized too large. To achieve the lowest energy required for cruise, the cruise phase is split up in two. During the first cruise phase the vast majority of the power comes from the ICEs, such that the fuel gets used up first. During the second cruise phase, once all the fuel is used up and the aircraft is at its minimum operational weight, all the energy for flight is provided by the batteries. It was found that the first cruise phase should last 72.82 min with a hybridization factor of zero, meaning that it is most efficient to complete the first phase with only fuel and ICE power. The second electric cruise phase should then last for 15.98 min.

Recharging the batteries during cruise with the help of the ICEs is also considered, but it was decided not to use this approach as this would be an inefficient and unsustainable use of fuel when compared to greener alternatives like charging on the ground with clean energy. Instead, during the unpowered decent the propellers can theoretically be used to extract energy from the air and recharge the E-COmmuter batteries. This could reduce turnaround time and increase the overall efficiency of the aircraft, which is discussed in detail in Equation 11.3.6.

11.2. Aerodynamic Analysis

An important factor for the performance of the aircraft is the aerodynamic analysis of the aircraft as a whole. A limited analysis of the wing and airfoil is already done in section 10.2, but for a performance analysis a C_L and C_D of the whole aircraft is often required. This section describes how they are obtained and calculated.

11.2.1. 3D Wing Lift Coefficient

From the analysis in section 10.2, sectional lift coefficients of the wing are provided. One then has to convert these sectional C_l coefficients to a single C_L. The lift over a single wing section can be defined as

$$l = \frac{1}{2} \cdot \rho_\infty \cdot V_\infty^2 \cdot C_l \cdot c \tag{11.1}$$

Where c is the chord of the airfoil at a specific location s along the wing. One can then integrate Equation 11.1 over the entire wingspan b to obtain the total lift, which is shown in the following sequence of equations.

$$L = \int_{-s}^{s} \frac{1}{2} \cdot \rho_\infty \cdot V_\infty^2 \cdot C_l(s) \cdot c(s) \cdot ds \tag{11.2}$$

$$L = \frac{1}{2} \cdot \rho_\infty \cdot V_\infty^2 \cdot C_L \cdot S \tag{11.3}$$

$$C_L = \frac{\int_{-s}^{s} C_l(s) \cdot c(s) \cdot ds}{S} \tag{11.4}$$

The calculated C_L needs to be slightly corrected. From the verification done in section 10.9 on the XFLR5 model, it is required to apply a factor of 0.9 to the lift coefficients in order to account for XFLR5 slightly overestimating lift coefficients. Then, as the XFLR5 model does not take into account the average tail down load, the lift coefficients need to be divided by 1.08. The resulting C_L can be found in Figure 11.2, which shows the $C_L - \alpha$ curve for the cruise phase of the E-COmmuter.

11.2.2. Airframe Drag

The drag of the airframe of the E-COmmuter consists of parasitic and lift-induced drag. This subsection discusses the sources of both types of drag and their calculation.

Wing Lift Induced Drag

The lift-induced drag of the aircraft is a direct result of a similar analysis as done in subsection 11.2.1, however now for C_{d_i} which is also a result of the XFLR5 aerodynamic analysis. This produces a C_{D_i} for the total wing per flight phase.

Component Drag

The component drag of the aircraft consists of the parasitic drag caused by the wing, fuselage, nacelles and tail. As a full computation fluid dynamic (CFD) analysis of the aircraft is outside the scope of this project, a simplified estimation is done to get the parasitic drag or C_{D_0} of the aircraft. Elham [52] provides such a method for propeller aircraft:

$$C_{D_0} = \frac{1}{S_{\text{ref}}} \cdot \sum_c C_{D_c} \cdot A_c + C_{D_{\text{misc}}} \tag{11.5}$$

In Equation 11.5, C_{D_c} denotes the parasitic drag due to the various components in the aircraft and A_c denotes their frontal area. $C_{D_{\text{misc}}}$ denotes the miscellaneous drag due to interference and roughness. Standard values for propeller aircraft are stated in Table 11.1. For $C_{D_{\text{misc}}}$, Elham [52] states that it should add 15% on top of the calculated C_{D_0}.

Table 11.1: Component drag coefficients provided by Elham [52].

Component	C_{D_c}
Wing	0.007
Fuselage: multi-engine	0.080
Nacelles	0.060
Tail (horizontal and vertical)	0.008

As a result of this estimation, a C_{D_0} of 0.0225 is found.

Landing Gear

Another significant source of airframe drag is that of the landing gear of the E-COmmuter. In section 14.2 the landing gear is designed and it is now time to assess its drag impact on the aircraft using another method from Elham [52]. For retractable landing gears with closed wheel wells, Equation 11.6 is used.

$$\Delta C_{D_{S_{\text{closed}}}} = 0.04955 \cdot e^{5.616 \cdot \frac{S_A}{S_{A_{\text{ref}}}}} \tag{11.6}$$

In Equation 11.6, S_A is the exact frontal area of the landing gear while $S_{A_{\text{ref}}}$ is the reference area of the landing gear (total width x total height). To convert the ΔC_{D_S} to an actual ΔC_{D_0}, it has to be multiplied by $\frac{S_{A_{\text{ref}}}}{S_{\text{ref}}}$. This produces a $\Delta C_{D_{0-lg}}$ of 0.0145.

The total combination of the lift-induced drag (C_{D_i}) and the parasitic drag (C_{D_0}) can be seen in the $C_D - \alpha$ curve in Figure 11.3. This excludes the landing gear, as Figure 11.3 only shows the drag for the cruise flight phase. Additionally, a $C_L - C_D$ curve is provided in Figure 11.4.

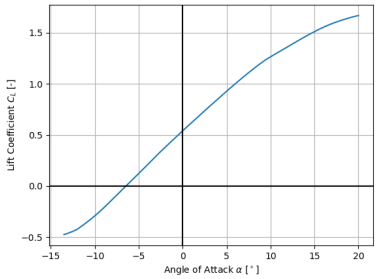

Figure 11.2: $C_L - \alpha$ curve for the aircraft at cruise velocities.

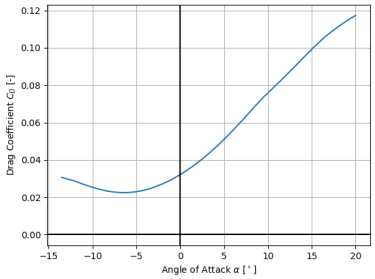

Figure 11.3: $C_D - \alpha$ curve for the aircraft at cruise velocities.

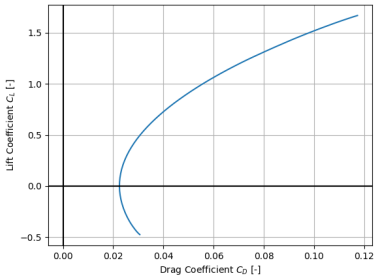

Figure 11.4: C_L-C_D curve for the aircraft at cruise velocities.

11.3. Analysis of Flight Phases

To be able to determine the optimum combination of fuel powered flight, electric flight and hybrid flight in subsection 11.1.1, it is required to have an idea of the required power and energy for all flight phases in the mission profile. In this section this is calculated for each flight phase of the mission profile displayed in Figure 11.1.

11.3.1. Motor Sizing

The size of the motors is based on required performance during motor failure. When one of the main motors or its power train fails during cruise flight, the aircraft should be capable of achieving a 4% climb gradient. This corresponds to a climb angle of 2.2°. To have a margin of safety 3° is chosen. This value is based on the standard approach angle of 3° which is commonly used in aviation. If 3° is a good value for the approach angle it is assumed this value is also sufficient for climb.

First, the big motors are sized for flight in clean configuration, then the power for the small motors is determined by the engine inoperative climb gradient requirement in takeoff configuration. The assumption is made that the cruise

altitude will be reduced in case this happened. The minimum cruise altitude is taken as the altitude of Europe's highest airport, Samedan airport. Therefore, the density is set to $\rho = 1.0366\,\mathrm{kg\,m^{-3}}$.

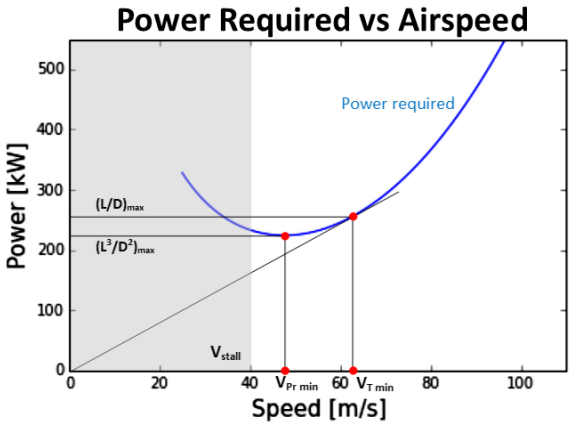

Figure 11.5: Power required vs airspeed

Cruise Motors

The choice is made to design the cruise motors for the power required at the airspeed which corresponds to maximum lift over drag. Figure 11.5 shows the power required over airspeed. This way the E-COmmuter is still capable of a relatively high cruise speed at this altitude and a margin exists for climb to higher altitudes.

The power at maximum lift over drag is found at the point on the curve where the tangent passes through the origin. The lift and drag coefficients corresponding to this condition are found using Equation 11.7 and Equation 11.8, assuming the simplified drag model.

$$C_{L_{\left(\frac{L}{D}\right)_{\max}}} = \sqrt{C_{D_0} \cdot \pi \cdot A \cdot e} \tag{11.7}$$

$$C_{D_{\left(\frac{L}{D}\right)_{\max}}} = 2 \cdot C_{D_0} \tag{11.8}$$

Hence, a single cruise motor power of 255 kW is obtained for an airspeed of $63\,\mathrm{m\,s^{-1}}$ or 122 kts. The total power of both cruise motors is then 510 kW. With an estimated power density of $10\,\mathrm{kW\,kg^{-1}}$ these motors weigh in at 25.5 kg each [2].

Blown Wing Motors

To find the power needed for the blown wing motors, the required engine inoperative climb angle is set to 3°. Equation 11.9 is used to find the thrust required and iterated to compensate for the changing lift and drag coefficients due to that thrust. This is done for a range of airspeeds. The airspeed for minimum thrust needed to climb at an angle of 3° is then set as the climb speed with one cruise motor inoperative and corresponding power is calculated from the thrust. The airspeed corresponding to the minimum thrust required is found to be $50\,\mathrm{m\,s^{-1}}$ or 97 kts. The power required for this airspeed is subtracted with the power of one cruise motor to find the power for all the blown wing motors. This results in a total power for the blown wing of 257 kW and, devided by 14 motors, a power of 18.3 kW per blown wing motor. These smaller motors have a power density of $8\,\mathrm{kW\,kg^{-1}}$, meaning they will each weigh 2.3 kg [3]. All 14 motors together then weigh 32.1 kg.

$$\text{Thrust} = \sin(\theta_{\text{climb}}) \cdot W_{TO} + \text{D} \tag{11.9}$$

11.3.2. Takeoff

Takeoff is split into several segments: first ground roll, followed by the rotation, transition, and climb to obstacle height [25]. The distances for each of these segments are calculated and added up to obtain the total takeoff distance. A visual representation of the takeoff segments is shown in Figure 11.6. This phase of the flight relies on the blown wing for lift augmentation. The lift coefficients, from the blown wing effect, are a function of the thrust. The thrust itself, however, is a function of speed. At the same time, speeds are calculated using lift coefficients. To overcome this loop, the calculations are iterated to obtain a final value. To make sure operation is possible from every airfield in Europe, again, calculations are done assuming the air density at Samedan airport (Europe's highest airport) where $\rho = 1.0366\,\mathrm{kg\,m^{-3}}$.

Ground Roll

Before starting the calculations for the ground roll distance, first the stall speed in takeoff configuration, liftoff speed, and average/reference ground speed are calculated using Equation 11.10 to 11.12. The lift coefficient is the sum of the

[2] URL: `https://www.compact-dynamics.de/en/aviation/` [cited 21 June 2018]
[3] URL: `https://www.compact-dynamics.de/en/aviation/` [cited 21 June 2018]

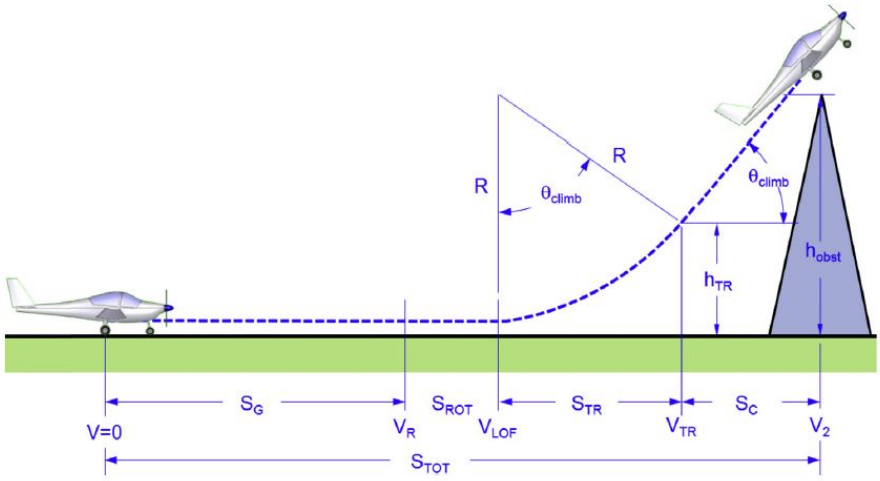

Figure 11.6: Takeoff segments as defined by Gudmundsson [25].

lift coefficient of the clean wing and the increase in lift coefficient due to the blown wing. The increase in lift generated by the propeller interaction with the wing is obtained using the method described in subsection 10.5.3. A maximum $\Delta C_{L_{\text{blown wing}}}$ of 1.6 is achieved. Note that this value depends on thrust which reduces with airspeed for propeller aircraft.

$$V_{s_1} = \sqrt{\frac{W_{TO}}{S} \cdot \frac{2}{\rho} \cdot \frac{1}{C_{L_{\max_{\text{clean}}}} + \Delta C_{L_{\text{blown wing}}}}} \tag{11.10}$$

$$V_{\text{lof}} = 1.1 \cdot V_{s_1} \tag{11.11}$$

$$V_{\text{ref}} = V_{\text{average}_{\text{ground}}} = \frac{V_{\text{lof}}}{\sqrt{2}} \tag{11.12}$$

After iteration, a stall speed in takeoff configuration of $V_{s_1} = 34\,\text{m s}^{-1}$ or 66 kts is found, which leads to a liftoff speed of $V_{\text{lof}} = 37\,\text{m s}^{-1}$ or 72 kts and an average ground roll speed of $V_{\text{ref}} = 26\,\text{m s}^{-1}$ or 51 kts. The distance for the ground roll is found using Equation 11.13 where V_{lof} is the liftoff speed and $\bar{a}$ is the average acceleration.

$$s_g = \frac{V_{lof}^2}{2 \cdot \bar{a}} \tag{11.13}$$

From the equations of motion it follows that the acceleration is given by Equation 11.14 where $\bar{T}$, $\bar{D}$ and $\bar{L}$ are the average thrust, drag and lift during the ground roll. They are calculated in Equation 11.15 and 11.16. μ is the ground friction coefficient (0.08 for takeoff on wet grass [25]).

$$\bar{a} = \frac{g_0}{W_{TO}} \cdot \left(\bar{T} - \bar{D} - \mu \cdot (W_{TO} - \bar{L})\right) \tag{11.14}$$

The average thrust, drag, and lift are calculated at the reference ground speed V_{ref}. The lift coefficient is found by summing the lift coefficient at zero angle of attack, C_{L_0} found from the $C_L - \alpha$ curve, and the increase in C_L due to the incidence angle α_i. The drag is corrected for the ground effect using McCormick's correction factor for the induced drag. This correction factor, calculated in Equation 11.17 [25], is a function of wing span and the height of the wing above the ground, found in section 9.1.

$$\bar{L} = \frac{1}{2} \cdot \rho \cdot V_{\text{ref}}^2 \cdot S \cdot (C_{L_0} + \Delta C_{L_\alpha} \cdot \alpha_i + \Delta C_{L_{\text{blown wing}}}) \tag{11.15}$$

$$\bar{D} = \frac{1}{2} \cdot \rho \cdot V_{\text{ref}}^2 \cdot S \cdot (C_{D_0} + k \cdot C_L^2 \cdot \phi + \Delta C_{D_{\text{landing gear}}}) \tag{11.16}$$

$$\phi = \frac{\left(16 \cdot \frac{h_{\text{wing}}}{b}\right)^2}{1 + \left(16 \cdot \frac{h_{\text{wing}}}{b}\right)^2} \tag{11.17}$$

Thrust is calculated using the methods as described in section 12.5. All motors run at maximum power during the whole takeoff which leads to an acceleration distance of 277 m.

Rotation

To account for rotation, the assumption is made that it takes one second at liftoff speed for the aircraft to actually lift of the ground. This adds 37 m to the ground segment by using Equation 11.18, leading to a total ground run from brake release until liftoff of 314 m.

$$s_{\text{rot}} = |V_{\text{lof}}| \tag{11.18}$$

Transition

The transition segment starts at liftoff and ends when the Climb angle is achieved. Usually this climb angle is obtained by flying the airspeed for maximum climb gradient, V_x. According to Gudmundsson [25] the theoretical V_x for small aircraft is usually lower than the stall speed. When putting the equation for climb angle (Equation 11.19) and the equation for airspeed with the weight corrected for climb angle (Equation 11.20) in an iterative loop, indeed a value of V_x = 31 m s^{-1} or 61 kts is found, which is indeed lower than the stall speed.

$$\theta_{\text{climb}} = \arcsin\left(\frac{T}{W} - \frac{1}{\frac{L}{D}}\right) \tag{11.19}$$

$$V_{\text{climb}} = \sqrt{\frac{W_{TO}}{S} \cdot \frac{2}{\rho} \cdot \frac{1}{C_L} \cdot \cos(\theta_{\text{climb}})} \tag{11.20}$$

Instead, it is assumed the initial climb will be performed at the safety speed, V_2, which is the minimum safe airspeed to fly with a motor/engine inoperative. Regulations dictate this speed should not be less than 1.2 times the stall speed. Hence, $V_{\text{climb}} = V_2 = 1.2V_{s_0} = 40.5$ m s^{-1} or 79 kts. This speed is kept constant and using Equation 11.19 with the respective C_L and C_D values, a climb angle of 7.58° is found after iteration. Now, Equation 11.21 and Equation 11.22 can be used to determine that the transition distance is 127 m and the transition height is 7 m [25]. Equation 11.17 is again used to account for the ground effect, assuming the wing height is the average height between when the aircraft is on the ground and when it reaches the transition altitude h_{tr}.

$$s_{tr} = 0.2156 \cdot V_{s_1}^2 \cdot \sin(\theta_{\text{climb}}) \tag{11.21}$$

$$h_{tr} = 0.2156 \cdot V_{s_1}^2 \cdot (1 - \cos(\theta_{\text{climb}})) \tag{11.22}$$

Climb to Screen/Obstacle Height

In general aviation the screen height or obstacle clearance height is usually set to 50 ft or 15.2 m. The distance needed to climb from the transition height to the screen height is obtained using the equation below.

$$s_{scr} = \frac{h_{scr} - h_{tr}}{\tan(\theta_{\text{climb}})} \tag{11.23}$$

This gives a climb distance for obstacle clearance of 62 m. Adding up all the values found gives a total takeoff distance from brake release until obstacle clearance height of 503 m.

Time and Energy

The energy is found by multiplying the time needed to complete each section with the total power. Following equations give the time per segment.

$$t_{lof} = \sqrt{\frac{2 \cdot s_g}{\bar{a}}} + 1 \tag{11.24}$$

$$t_{tr} = \frac{s_{tr}}{\cos(\theta_{(\text{climb})}) \cdot V_{tr}} \tag{11.25}$$

$$t_{scr} = \frac{s_{scr}}{\cos(\theta_{\text{climb}}) \cdot V_2} \tag{11.26}$$

With a total power of 767 kW and a time of 21 s from brake release until the obstacle height is reached this requires a total energy of 4.4 kW h.

11.3.3. Climb

Climb is, next to takeoff, one of the most performance-constraint phases. As the takeoff phase of the E-COmmuter is the most demanding, the large motors are sized to provide the necessary takeoff power. For climb, it is assumed that only the large motors are used and that they are used at their full power. Hence, $P_{\text{cl}} = P_{\text{large motors}}$. To evaluate climb performance and to calculate the total energy expended during climb, it is required to find the optimal climb speed, V_y (see Equation 11.28), and the corresponding maximum rate of climb (ROC).

The optimal climb speed is defined for quasi-steady climb as the point in the power curve where $P_a - P_r$ is at its maximum. According to Ruijgrok [53], this occurs at $\left(\frac{C_L^3}{C_D^2}\right)_{\text{max}}$. The $C_{L_{\text{cl}}}$ is then equal to:

$$C_{L_{\text{cl}}} = \sqrt{3 \cdot C_{D_0} \cdot \pi \cdot A \cdot e} \tag{11.27}$$

$$V_y = \sqrt{\frac{2}{\rho} \cdot \frac{W}{S} \cdot \frac{1}{C_{L_{\text{cl}}}}} \tag{11.28}$$

As one can see from Equation 11.27, it is clear that the speed is dependent on both the air density and the weight of the aircraft. This means that it is impossible to define only one optimal climb speed, as there exist multiple, all at different altitudes. A relatively simple approximation to this problem is to calculate the climbing speed at the altitude at the start of the climb maneuver and the altitude at the end of the climb maneuver, then average the two. This will overestimate the climbing speed, as the aircraft spends more time during the climb maneuver at higher altitudes than it does at lower altitudes [25]. The average V_{y_a} for the E-COmmuter equals 59.5 m s^{-1}.

Using the averaged climbing speed V_{y_a} one can then approximate the time required to climb to the cruising altitude of 3048 m using again $t_{\text{cl}} = \frac{h_{\text{cr}}}{V_{y_a}}$. t_{cl} can then be used in tandem with P_{cl} to calculate E_{cl} using Equation 11.29. This results in a E_{cl} of 133 kW h. Additionally, Gudmundsson [25] provides Equation 11.30 to obtain the maximum ROC$_s$ at the optimal climbing speed in feet per minute.

$$E_{\text{cl}} = P_{\text{cl}} \cdot \frac{t_{\text{cl}}}{3600} \tag{11.29}$$

$$\text{ROC}_{s_{\max}} = \frac{\eta_p \cdot P}{W} - V_y \cdot \frac{1.1547}{\left(\frac{L}{D}\right)_{\max}} \tag{11.30}$$

However, all calculations done thus far assume quasi-steady climb. The impact of this assumption consists of an overestimation of the ROC of the aircraft. This can be corrected using the kinetic energy correction factor provided by Ruijgrok [53], which corrects the ROC from Equation 11.30 to account for the change in altitude, given in Equation 11.31.

$$\text{ROC} = \frac{\text{ROC}_s}{1 + \frac{V_y^2}{2} \cdot \frac{\rho}{p} \cdot \left(\frac{R}{g} \cdot \frac{dT}{dH} + 1\right)} \tag{11.31}$$

Using Equation 11.31, ROC is approximated to be 3.3 m s^{-1} or 647 ft min^{-1}. This is a low climb rate for an aircraft, which is mostly due to the high MTOW combined with the assumption that only the cruise motors are used for climbing. However, the slower climb rate is partially compensated due to the low cruise time, so that requirement **HEF-PAX-02** can still be satisfied.

11.3.4. Cruise

To calculate the power and energy required during cruise, one can assume the aircraft is in a steady, stable flight. Hence, $L = W$, and $P_r = P_a = D \cdot V$ so the following equations can be used to calculate the required cruise power P_{cr}.

$$C_{L_{\text{cr}}} = \frac{W}{\frac{1}{2} \cdot \rho_{\text{cr}} \cdot V_{\text{cr}}^2 \cdot S} \tag{11.32}$$

$$C_{D_{\text{cr}}} = C_{D_0} + \frac{C_{L_{\text{cr}}}^2}{\pi \cdot A \cdot e} \tag{11.33}$$

$$P_{\text{cr}} = \frac{D_{\text{cr}} \cdot V_{\text{cr}}}{\eta_p} = \frac{1}{2} \cdot \frac{1}{\eta_p} \cdot \rho_{\text{cr}} \cdot V_{\text{cr}}^3 \cdot C_{D_{\text{cr}}} \cdot S \tag{11.34}$$

In Equation 11.34, η_p denotes the propeller efficiency. V_{cr} is calculated using the travel times from section 2.5. There, a car travel time of 3 h 30 min is estimated. For the trip by E-COmmuter, next to the flight times, a car travel time of 30 min and a time at the airfield of 40 min are estimated. In order to be 20% faster than the car travel time (**HEF-PAX-02**), an average speed of 63.1 m s^{-1} or 123 kts is required. A safety factor of 1.1 is applied on this to account for deviating travel times, resulting in a speed of 69.4 m s^{-1} or 135 kts. Using Equation 11.34, P_{cr} was found to be 282 kW. As now the power is known and using $t_{\text{cr}} = \frac{R}{V_{\text{cr}}}$, E_{cr} can be calculated in a similar way to Equation 11.30. This gives an E_{cr} of 416.8 kW h, which makes cruise by far the most energy intensive phase of the whole mission.

Maximum airspeed

An important performance parameter for any aircraft is the maximum level airspeed $V_{\max}$ that is attainable. $V_{\max}$ occurs when the E-COmmuter provides maximum thrust although the actual $V_{\max}$ is usually restricted by structural and regulatory limits.

For propeller aircraft the maximum thrust is a function of the airspeed and hence, an iteration is required to solve for $V_{\max}$ as it is by itself a function of the airspeed. The function for $V_{\max}$ is provided by Gudmundsson [25] and is given in Equation 11.35.

$$f(V_{\max}) = \rho_{\text{cr}} \cdot S \cdot C_{D_0} \cdot V_{\max}^3 - \eta_p \cdot P_a - \sqrt{(\eta_p \cdot P_a)^2 - 4 \cdot W^2 \cdot V_{\max}^2 \cdot C_{D_0} \cdot k} \tag{11.35}$$

Using the bisection method to find the roots on Equation 11.35 gives a $V_{\max}$ of 122.7 m s^{-1}. This $V_{\max}$ is much higher than the regulatory cruise speed of $V_{\text{max-rg}} = 1.4 \cdot V_{\text{cr}} = 97.22$ m s^{-1} but it is useful as the input for thrust calculations as used in subsection 12.5.1.

11.3.5. Turning

In order to be maneuverable the aircraft has to be able to turn at a reasonable rate. The E-COmmuters' turn performance of maximum bank angle, minimum turn radius and maximum turn rate are evaluated in this chapter.

The factor determining the bank angle and the turn radius a specific aircraft can turn is its ultimate load factor, which is 4.5 for this aircraft. Commercial aircraft usually do not apply a load factor higher than 2 during a cruise as this would cause discomfort for the passengers. Using this lower load factor and evaluating from Equation 11.36 the maximum bank angle ϕ is 60°. To compute the minimum sustainable turn radius with Equation 11.38, the corresponding speed must be determined first using Equation 11.37, requiring Equation 11.39. Finally the maximum turn rate is calculated. Similar to the turn radius the appropriate speed has to by determined with Equation 11.40 before ψ can be computed using Equation 11.41. All results are displayed in the results table at the end of this chapter.

$$\phi_{max} = \arccos\left(\frac{1}{n_{max}}\right) \tag{11.36}$$

$$V_{R_{min}} = 2 \cdot \sqrt{\frac{\frac{W}{S} \cdot k}{\frac{T}{W} \cdot \rho}} \tag{11.37}$$

$$R_{min} = \frac{V_{R_{min}}^2}{g \cdot \sqrt{n_{R_{min}} - 1}} \tag{11.38}$$

$$n_{R_{min}} = \sqrt{2 - \frac{1}{n_{max}^2}} \quad (11.39) \qquad V_{\psi_{max}} = \sqrt{\frac{2}{\rho} \cdot \frac{W}{S} \cdot \sqrt{\frac{k}{C_{D_{min}}}}} \quad (11.40) \qquad \psi_{max} = \frac{g \cdot \sqrt{n_{max}^2 - 1}}{V_{\psi_{max}}} \quad (11.41)$$

11.3.6. Descent

First, unpowered descent is assumed. If the resulting descent angles prove too steep power will be added. Two conditions are looked at: descent at best glide speed and descent at minimum sink speed.

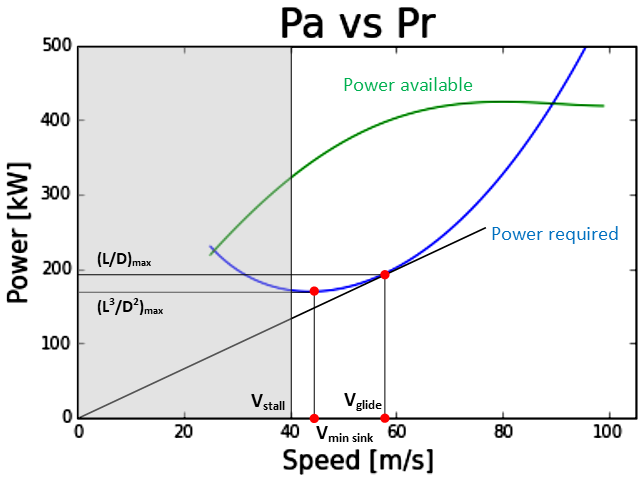

Figure 11.7: Power available and power required plotted against equivalent airspeed.

Best Glide

Best glide speed corresponds to the speed for minimum descent angle or minimum thrust required. This speed is achieved by flying at $(\frac{L}{D})_{max}$ or the airspeed for minimum thrust required [25][53]. On the power curve, shown in Figure 11.7, this corresponds to the speed for which the tangent of the power required curve crosses the origin. Using the simplified drag model, the values for lift and drag coefficients corresponding to $(\frac{L}{D})_{max}$ are given by Equation 11.7 and Equation 11.8, used before in subsection 11.3.1.

Since this airspeed is not constant with altitude, the equivalent air speeds are calculated. This means air density at sea level is used. If instrument error is neglected, this will be the indicated airspeed the pilot should fly at regardless of altitude.

From the lift equation (and the polar) the best glide speed is found to be $V_{glide} = 58\,\mathrm{m\,s^{-1}}$ or 112 kts. Flying at this speed with no thrust will result in maximum range. The glide angle and rate of descent are given by Equation 11.42 and Equation 11.43.

$$\theta_{\text{best glide}} = \arctan\left(\frac{1}{\left(\frac{L}{D}\right)_{max}}\right) \quad (11.42) \qquad \text{ROD}_{\text{best glide}} = \frac{V_{\text{glide}}}{\left(\frac{L}{D}\right)_{max}} \quad (11.43)$$

This returns 3.34° for the glide angle and a descent rate of $3.36\,\mathrm{m\,s^{-1}}$ or $662\,\mathrm{ft\,min^{-1}}$. Note that the angle has a positive value but is in fact a negative flight path angle. If the true airspeed is needed for a certain altitude, Equation 11.44 can be used to convert the equivalent airspeed to true airspeed.

$$\text{TAS} = \text{EAS} \cdot \sqrt{\frac{\rho_0}{\rho}} \quad (11.44)$$

Minimum Sink

The airspeed for minimum sink or minimum rate of descent allows the aircraft to stay in the air the longest. It is the airspeed corresponding to minimum power required, as indicated in Figure 11.7. This airspeed as achieved for the following relation of lift and drag: $(\frac{C_L^3}{C_D^2})_{max}$ [25][53]. Using the simplified drag model to obtain the values for C_L and C_D:

$$C_{L_{\left(\frac{L^3}{D^2}\right)_{max}}} = \sqrt{3 \cdot C_{D_0} \cdot \pi \cdot A \cdot e} \quad (11.45) \qquad C_{D_{\left(\frac{L^3}{D^2}\right)_{max}}} = 4 \cdot C_{D_0} \quad (11.46)$$

The equivalent airspeed for minimum rate of descent equals $44\,\mathrm{m\,s^{-1}}$ or 85 kts. Using Equation 11.47 and Equation 11.48 results in a minimum descent rate of $2.95\,\mathrm{m\,s^{-1}}$ or $581\,\mathrm{ft\,min^{-1}}$ and a corresponding descent angle of 3.85°. Again, the actual flight path angle has a negative value since the aircraft is descending.

$$\theta_{minsink} = \arctan\left(\frac{1}{\left(\frac{L}{D}\right)_{\left(\frac{L^3}{D^2}\right)_{max}}}\right) \quad (11.47) \qquad ROD_{minsink} = \frac{V_{minsink}}{\left(\frac{L}{D}\right)_{\left(\frac{L^3}{D^2}\right)_{max}}} \quad (11.48)$$

Since both these air speeds result in relatively small descent angles, no power will be added and the descent will be unpowered.

Recharging During Descent

Recharging during descent is a highly desirable feature of an electric propelled aircraft, as it saves energy usage, as well as ground charging time, thus turnaround time. It is, however, a topic not elaborated upon in many papers on electric aircraft propulsion. This discussion thus only provides a theoretical approach to the concept. Using propellers for recharging is, from a general view on the problem, much like electricity generated by windmills. Therefore, theory from wind energy methods is used as a basis to this approach.

In order to derive the required equations, the rotor or propeller is considered an actuator disk [54]. Using the principles of mass flow, momentum flow and kinetic energy flow rates, a simplified derivation can be done. The following Equation 11.50 and Equation 11.51 show the power (P) extracted from the flow and thrust (T) exerted on the flow. In the first Equation 11.49, a is the induction factor: the change in flow velocity between free stream (U) and at the rotor (U_r), divided by the free stream velocity. Furthermore, the density of the air (ρ) and the actuator disk area (area of the propeller or rotor, A) are required.

$$a = \frac{U - U_r}{U} = \frac{\Delta U}{U} \quad (11.49) \qquad T = \frac{1}{2}\cdot\rho\cdot U^2\cdot A\cdot 4\cdot a\cdot(1-a) \quad (11.50) \qquad P = \frac{1}{2}\cdot\rho\cdot U^3\cdot A\cdot 4\cdot a\cdot(1-a)^2 \quad (11.51)$$

Using the entries with a in Equation 11.51, defined as the power coefficient ($C_P = 4\cdot a\cdot(1-a)^2$), the optimal point can be found, thus maximizing C_P. The optimum is found at $a = \frac{1}{3}$, known as the Betz limit [54]. Note that this limit is to be taken between $a = 0$ and $a = 0.5$ [54].

Using the derived relations for power extraction, as well as the dimensions of the propellers and efficiencies of the electric system, the power of recharging can be determined. Then setting a certain time in which the recharging is to take place results in the energy the system is capable of extracting from the wind.

The theory described, along with the current state of wind energy technology shows that recharging using the electric motors is possible. There are, however, large setbacks in the application of the technology for aircraft.

Firstly, the rotors of a windmill are designed for optimal power extraction, much like aircraft propellers. They are, however, designed to slow down the wind, instead of accelerating it to provide thrust like propellers. Therefore, the aerodynamic shapes of rotors and propellers are the exact opposite. Propellers thus are in no way efficient to recharge, only with possible (complex) systems rotating the propellers around their longitudinal axis in order to resemble windmill rotors more closely.

Secondly, the thrust from a rotor is not to be underestimated. It an be seen as a form of drag, as the thrust force of recharging rotors is directed into the direction of the wind (thus decelerating it). To show the added drag from recharging, the following referential values are used: $\rho = 1.0\,\mathrm{kg\,m^{-3}}$ (density of the air just below cruise altitude), $U = 50\,\mathrm{m\,s^{-1}}$. The propeller radius (for area calculation) is determined from the calculations in the following chapter. With these values, the added drag per propeller is approximately 800 N. With 14 propellers recharging and an estimated recharging efficiency of 10%, the added drag equals 540 N. In order to keep velocity above stall, the two large propellers thus could be required to provide thrust.

Lastly, the power extracted from the wind is relatively low with respect to the added drag. As said before, the propellers are very limited in recharging capabilities. Using the same referential values used before, the power extracted by 14 small propellers equals 38.3 kW. Recharging during descent, assuming the velocity is constant and the recharging time equals 10 min, provides 6.39 kW h energy.

Concluding, approximately 1.5% of the total capacity can be recharged during descent with current technology and assumptions. With the high added drag and the low efficiency of the propellers, the recharging is not considered feasible to be implemented into the design of the E-COmmuter at this moment. The model is, however, very basic, using very large uncertainties. Further research can prove the feasibility of the concept and later on possible implementation.

11.3.7. Landing

Just like the takeoff, landing is split into several segments (see Figure 11.8). First the approach, where the E-COmmuter descents from obstacle height to flare height, followed by the flare, touchdown and ground roll. After trying several different methods to operate the blown wing, it became clear that using the blown wing during landing would not be possible. The added thrust reduces the approach angle or increases approach speed too much. Instead, the flaps are used to increase the lift coefficient needed to landing.

To start some speeds are defined. First, the stall speed given by Equation 11.52. The approach and flare speed, the touchdown speed, and average ground speed are then given by Equation 11.53, Equation 11.54 and Equation 11.55 respectively [25]. Many of the equation that follow are very similar to the ones used for the takeoff calculations in subsection 11.3.2. The value for $\Delta C_{L_{\text{flaps}}}$ was determined in section 10.3.

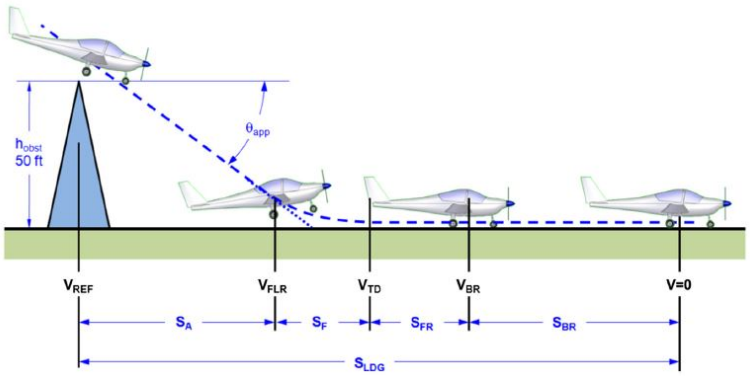

Figure 11.8: Landing segments as defined by Gudmundsson [25].

$$V_{s_0} = \sqrt{\frac{W_L}{S} \cdot \frac{2}{\rho} \cdot \frac{1}{C_{L_{\max_{\text{clean}}}} + \Delta C_{L_{\text{flaps}}}}} \tag{11.52}$$

$$V_{app} = V_{flr} = 1.3 \cdot V_{s_0} \tag{11.53}$$

$$V_{TD} = V_{\text{brake}} = 1.1 \cdot V_{s_0} \tag{11.54}$$

$$V_g = V_{\text{average}_{\text{ground}}} = \frac{V_{\text{brake}}}{\sqrt{2}} \tag{11.55}$$

This results in a stall speed in takeoff configuration $V_{s_0} = 34\,\text{m}\,\text{s}^{-1}$ or 66 kts. The stall speed without flaps in clean configuration would have been $V_s = 43.5\,\text{m}\,\text{s}^{-1}$ or 85 kts. The approach speed and touch down speed are then equal to $V_{\text{app}} = 44\,\text{m}\,\text{s}^{-1}$ or 86 kts and $V_{TD} = 37.5\,\text{m}\,\text{s}^{-1}$ or 73 kts respectively.

Approach

For the approach, first the approach angle is determined based on C_L and C_D, taking into account contributions of the flaps and landing gear, using Equation 11.56 through Equation 11.58. For the drag, only the $\Delta C_{D_{0_{flaps}}}$ is added, since the flaps' contribution to the induced drag is already included in the term $kC^2_{L_{app}}$.

$$C_{L_{\text{app}}} = \frac{W_L}{\frac{1}{2} \cdot \rho \cdot V^2_{app} \cdot S} \tag{11.56}$$

$$C_{D_{\text{app}}} = C_{D_0} + k \cdot C^2_{L_{app}} + \Delta C_{D_{0_{\text{flaps}}}} + \Delta C_{D_{\text{landing gear}}} \tag{11.57}$$

$$\theta_{\text{app}} = \arctan\left(\frac{\frac{1}{2} \cdot \rho \cdot V^2_{\text{app}} \cdot S \cdot C_{D_{\text{app}}}}{W_L}\right) \tag{11.58}$$

An approach angle of 5.5° is achieved. Like before, the angle has a positive value but this corresponds to a negative flight path angle of -5.5°. When approaching the ground, the aircraft needs to flare, i.a. round off its descent in order to touch down gently. Using Equation 11.59 and Equation 11.60 the flare height and approach distance are obtained [25]. The flare height turns out to be 2.6 m and the approach distance measures 131 m. The obstacle height, h_{obs}, is again 50 ft or 15 m. The flare distance is found to be 55 m, using Equation 11.61. Equation 11.17 is used to account for the ground effect during flare and ground roll.

$$h_{\text{flr}} = 0.1512 \cdot V^2_{s_0} \cdot (1 - \cos(\theta_{\text{app}})) \tag{11.59}$$

$$s_{\text{app}} = \frac{h_{\text{obs}} - h_{flr}}{\tan(\theta_{\text{app}})} \tag{11.60}$$

$$s_{\text{flr}} = 0.1512 \cdot V^2_{s_0} \cdot \sin(\theta_{\text{app}}) \tag{11.61}$$

After the flare, the aircraft touches down and the assumption is made it will roll freely at the touchdown speed for one second before the brakes are applied. Hence the free roll distance $s_{\text{free roll}} = |V_{TD}| = 37.5\,\text{m}$.

Brakes alone would not suffice to stop the E-COmmuter within the available runway length. Therefore, the two main motors are fitted with variable pitch propellers capable of producing reverse thrust. According to Gudmundsson, reverse thrust is about 40% of the static thrust (Equation 12.2). Braking distance is then found using following equations.

$$\bar{L}_{\text{ldg}} = \frac{1}{2} \cdot \rho \cdot V^2_g \cdot S \cdot \left(C_{L_0} + \Delta C_{L_\alpha} \cdot \alpha_i + \Delta C_{L_{\text{flaps}}}\right) \tag{11.62}$$

$$\bar{D}_{\text{ldg}} = \frac{1}{2} \cdot \rho \cdot V^2_g \cdot S \cdot \left(C_{D_0} + k \cdot C^2_L \cdot \phi + \Delta C_{D_{\text{landing gear}}} + \Delta C_{D_{0_{flaps}}}\right) \tag{11.63}$$

$$s_{br} = -\frac{V^2_{br} \cdot W_L}{2 \cdot g \cdot \left(-0.4 \cdot T_{\text{stat}} - D_{\text{ldg}} - \mu_L \cdot (W_L - L_{\text{ldg}})\right)} \tag{11.64}$$

The negative sign at the right side of Equation 11.64 compensates for the negative acceleration. μ_L equals 0.2 for braking on wet grass. The final value for the braking distance is 343 m. This gives a total ground roll distance of 381 m and a total landing distance from obstacle height to stand still of 566 m.

Time and Energy

The time needed for landing is again determined using Equation 11.26, Equation 11.25 and Equation 11.24, but replacing the takeoff speeds and distances with the respective landing speeds and distances. This gives a total landing time of 38.8 s. The energy is found by multiplying the time with the power. Since the approach is assumed to be unpowered, the only energy needed is the one for the reverse thrust. This gives an energy required for landing of 1 kW h.

11.4. Payload Range Diagram

Following from the mission profile defined in chapter 5 and subsection 11.1.1 it is clear that there are different flight phases with respect to the power source used. There are three different parts, conventional propulsion by means of burning Avgas, electric flying with the power coming from the batteries, and a combination of both hybrid electric flying. During climb the aircraft is operated by means of hybrid propulsion. The cruise phase of the mission consists of a conventional propulsion part and a fully electrical propulsion part.

The nominal mission range follows from the requirements. The aircraft should be able to have a range of at least 370 km, **HEF-OPR-03**. This range is considering an aircraft which is fully loaded with 14 passengers with luggage, and added fuel until the maximum takeoff weight (MTOW) is reached. Now the question is raised: "what will the range be for a different loading case?". This section discusses the analysis of the nominal mission and three optional additional missions for the E-COmmuter. The additional missions are: adding extra fuel, extra batteries, and adding both extra fuel and batteries. First the nominal mission is discussed, then the additional missions will be treated.

Each of the missions produce CO_2 emissions, per mission the emissions will be discussed in the end of this section.

Nominal Mission

The nominal mission consists out of two parts. First, conventional flight phase using Avgas. Second, fully electric flight phase making use of the energy stored in the batteries. For the range only the cruise is taken into account, as takeoff and landing distances are small compared to the mission range. To calculate the range of these flight phases the following equations are used. First for conventional and then electrical in Equation 11.65 and 11.66 respectively [2].

$$R_{\text{conv}} = \frac{\eta_{\text{propsystem}}}{c_p \cdot g} \cdot \frac{C_L}{C_D} \cdot \ln\left(\frac{W_{\text{initial}_{\text{fuel}}}}{W_{\text{end}_{\text{fuel}}}}\right) \quad (11.65)$$

$$R_{\text{elec}} = \frac{\eta_{\text{propsystem}} \cdot \eta_{\text{electrical}}}{g} \cdot \frac{C_L}{C_D} \cdot \ln\left(\frac{W_{\text{initial}_{\text{electric}}}}{W_{\text{end}_{\text{mission}}}}\right) \quad (11.66)$$

The initial weight $W_{\text{initial}_{\text{fuel}}}$ equals the MTOW and the $W_{\text{end}_{\text{fuel}}}$ is the MTOW minus the fuel used for the conventional flight phase. Continuing with the range calculation, $W_{\text{initial}_{\text{electric}}}$ equals $W_{\text{end}_{\text{fuel}}}$ and the $W_{\text{end}_{\text{mission}}}$ equals $W_{\text{end}_{\text{fuel}}}$ minus the equivalent weight of the batteries for the energy needed during cruise.

Figure 11.9 depicts the payload range diagram concerning only the nominal mission. This diagram shows the range of the aircraft versus the weight of the aircraft. From top to bottom the diagram shows, fuel, payload, cruise batteries, rest of the batteries, and the remaining weight. In the diagram only the fuel weight increases causing the range to increase. With the fuel weight of 163.0 kg and a battery weight of 117.0 kg for cruise, the aircraft has a range of 389 km. Of which 321 km is flown during the conventional phase and 68.9 km fully electric.

Extra Full Fuel Mission

The fuel tanks are sized for a total of 369.0 kg of fuel. The nominal mission only requires 269.0 kg of fuel, of which 50 kg is reserve and 17 kg trapped fuel. This leaves room for 100 kg of additional fuel. However, adding fuel to the nominal mission without any compensation would mean that the MTOW will be exceeded, so the payload needs to be changed accordingly.

The aforementioned range equation is used to determine the additional range with added fuel. The range is extended with 200.94 km. Furthermore, the maximum range becomes 761.23 km, if no payload were to be transported at all. The payload range diagram for this mission is presented in Figure 11.10. The first part of the diagram consists of the nominal mission up to 389.12 km.

Concluding, the additional fuel is just a little more than one passenger with luggage. This means that the operator can choose to take two passengers less on board and distribute the remaining 94 kg remaining payload among the twelve remaining passengers as additional luggage, or one can take all the passengers with just 12 kg of luggage each instead of 20 kg.

Extra Battery Pack Mission

The nominal mission requires a total of 577.69 kg of batteries. Of this, 117.5 kg of batteries are used for cruise and the remaining are used during takeoff and climb. The batteries are placed in the wing, for bending relief and safety reasons. One of the options that is considered is replacing the cargo compartment with a battery compartment. Doing so, a total of 280 kg of batteries could be placed where the cargo compartment would be. Replacing the cargo by the same amount of batteries in the same location is done for stability & control reasons. The center of gravity range does not significantly change this way.

With the additional battery pack an increase in range of 175.5 km and a maximum range of 738.94 km is possible. The payload range diagram concerning the placement of the extra battery pack is given in Figure 11.11.

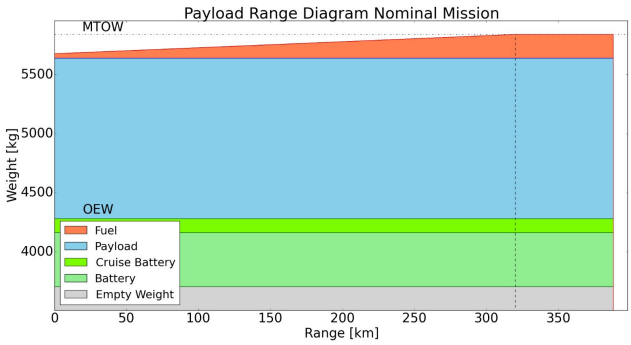

Figure 11.9: Payload-Range diagram for nominal mission.

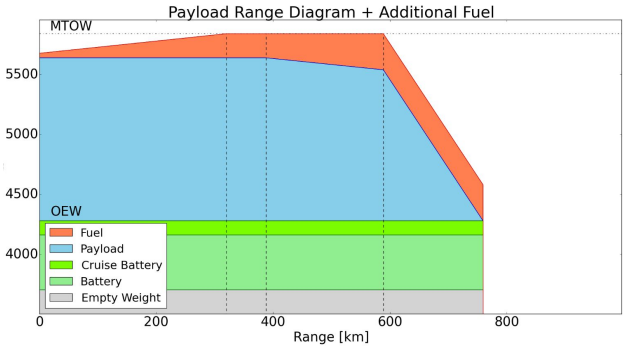

Figure 11.10: Payload-Range diagram with fuel tanks fully filled.

However, the 280 kg of additional batteries leaves multiple options concerning the payload. The aircraft could be loaded with fourteen passengers without any luggage. Reducing the number of passengers to eleven implies that every passenger can take just a little more than 20 kg of luggage each, or thirteen passengers with little room for luggage.

Full Fuel Tank and Extra Battery Pack Mission

As a third option the E-COmmuter can carry both extra fuel and a battery pack added to the nominal mission. This will extend the range of the aircraft with 376.44 km and is capable of a maximum range of 989.03 km. Due to the addition of 100 kg extra fuel and 280 kg extra battery pack the payload weight has to be reduced to 978 kg. With this amount of payload the number of passengers can be reduced to ten passengers with each 20 kg of luggage, or a total of twelve passengers are transported, each carrying 4.5 kg of luggage. Figure 11.12 shows the payload range diagram for the mission with extra fuel and battery pack.

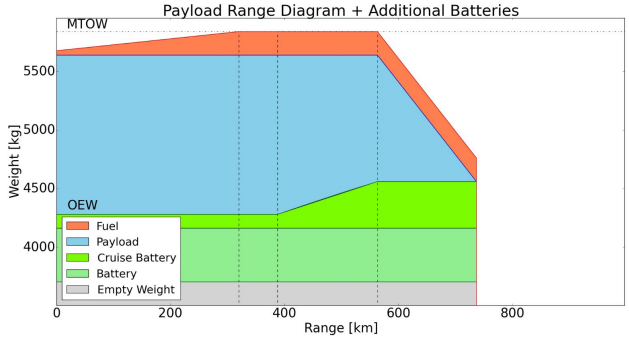

Figure 11.11: Payload-Range diagram adding extra battery pack.

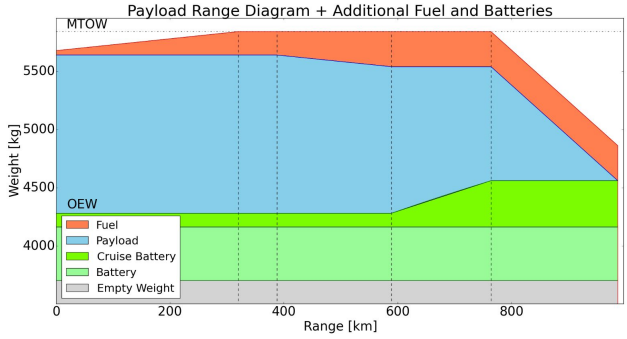

Figure 11.12: Payload-Range diagram with both extras.

11.4.1. CO_2 Emissions

In terms of sustainability all the missions have been analyzed with respect to the CO_2 emissions per passenger per kilometer. In Table 11.2 all the missions together with their range and emission of CO_2 are shown. This is the actual CO_2 production during a flight and does not consider the impact battery charging has. It is assumed that the batteries are charged at airport or airfield with renewable energy sources, such as wind energy and/or solar energy.

The total emissions of CO_2 produced by the E-COmmuter are calculated in a straightforward way. First, the weight of the total fuel is taken into account. This weight is divided by the density of Avgas and this is multiplied by the emission coefficient of Avgas, resulting in a total amount of CO_2 produced in kilograms per kilometer.

Requirement **HEF-MAN-02** states that the CO_2 emissions shall be lower than 0.1185 kg km^{-1} seat^{-1} for the nominal mission. The range of the nominal mission is 389.12 km resulting in 0.1127 kg km^{-1} seat^{-1} of CO_2 emissions. Therefore, the requirement is met.

For the additional missions this is slightly different. The mission with extra fuel obviously has a higher CO_2 production per kilometer than the nominal mission due to the extra fuel. For the additional battery pack mission this is not the case. The emissions during flight are reduced compared to the nominal mission. This makes it a more sustainable mission compared to the nominal mission. Moreover, the mission is extended by almost the same range as for adding extra fuel. The addition of fuel and battery pack also drops the CO_2 emissions down and of course extends the range the most out of the three additional mission options. Remarkably, it drops the CO_2 emission to the lowest.

Conclusion

From all the additional missions adding fuel and batteries seems to be the most sustainable and profitable mission. Sustainable since this mission emits the least amount CO_2 in kg km^{-1} seat^{-1}. Profitable as the range is extended with

almost twice the nominal mission range while keeping the amount of passengers over ten. The extension of the range makes it interesting for the operator, as the E-COmmuter can be used for multiple applications.

Although the range is not exactly the range that it designed for, the additional mission are assumed to be viable. Mainly due to the use of different methods in calculating the range of the aircraft. Further research has to be done with electric flying, cause this is a rather new type of air transportation. Also, it could be interesting to analyze the endurance of the E-COmmuter. With the knowledge of the endurance of the aircraft coastal surveillance could be an option as well, instead of just transporting passengers from A to B. This could make the E-COmmuter even more interesting to a larger group of operators. This subject is an interesting topic for future investigation with regard to operations of the aircraft.

11.5. Verification and Validation

This section discusses the verification and validation of each of the analyses explained above.

Hybridization

The algorithm which finds the ideal hybridization factor to achieve to lowest operational empty weight (OEW) outputs fuel-and battery weight and ICE engine. To verify these results the total combined energy required for all flight phases is compared to the energy stored within the onboard batteries and fuel (efficiencies are taken into account). The error was 0.38%. The code is therefore considered verified.

Payload Range Diagram

The equations that are put into the payload range diagram program have been checked by hand in terms of units used and correctness itself. The program takes inputs and out puts which first have been used in the hand calculations. Resulting in the same values as the program gives.

11.6. Results

The results obtained in this chapter are summarized below in Table 11.2.

Table 11.2: All the results obtained from the performance analysis.

Parameter	Symbol	Value	Unit	Parameter	Symbol	Value	Unit
Aerodynamic Analysis							
Maximum clean lift coefficient	$C_{L_{\max_{\text{clean}}}}$	1.6	-	Zero lift drag coefficient	C_{D_0}	0.0225	-
Landing gear drag coefficient	$C_{D_{0-lg}}$	0.0145	-				
Takeoff							
Total takeoff distance	s_{to}	503	m	Total takeoff power	P_{to}	767	kW
Rotation distance	s_{rot}	37	m	Transition distance	s_{tr}	127	m
Distance to screen height	s_{scr}	62	m	Climb angle	θ_{climb}	7.56	deg
Ground roll distance	s_{g}	277	m	Energy required	E_{to}	4.4	kWh
Stall speed in takeoff conf.	V_{s_1}	33.8	m s^{-1}	Lift off speed	V_{lof}	37.2	m s^{-1}
Climb speed in takeoff conf.	V_2	40.5	m s^{-1}				
Motor sizing							
Cruise motor power	P_{cm}	255	kW	Blown wing motor power	P_{bl}	18.3	kW
Amount Cruise motor	$N_{\text{motor}_{\text{cr}}}$	2	-	Amount blown wing motor	$N_{\text{motor}_{\text{bw}}}$	14	-
Total cruise motor power	P_{cm}	510	kW	Blown wing motor power	P_{bl}	257	kW
Climb							
Power required	P_{climb}	510	kW	Energy required	E_{climb}	132.5	kWh
Climb speed	V_{climb}	59.5	m s^{-1}	Time to climb to cruise altitude	t_{climb}	15.5	min
Rate of climb	ROC	3.3	m s^{-1}				
Cruise							
Power required	P_{cr}	282	kW	Energy required	E_{cr}	416.8	kWh
Cruise speed	V_{cr}	69.4	m s^{-1}	Maximum level airspeed	$V_{\max}$	122.7	m s^{-1}
Stall speed in clean conf.	V_s	43.5	m s^{-1}				
Turning							
Minimum turn radius speed	$V_{R_{\min}}$	50.9	m s^{-1}	Maximum turn rate speed	$V_{\phi_{\max}}$	57.3	m s^{-1}
Minimum turn radius	$R_{\min}$	305	m	Maximum turn rate	$\phi_{\max}$	16.9	$^\circ\,\text{s}^{-1}$
Descent							
Power required	P_{descent}	0	kW	Energy required	E_{descent}	0	kWh
Optimal glide speed (EAS)	$V_{\text{best glide}}$	57.6	m s^{-1}	Glide speed for $\text{ROD}_{\text{min sink}}$ (EAS)	$V_{\text{min sink}}$	43.8	m s^{-1}
Descent rate at best glide speed	$\text{ROD}_{\text{best glide}}$	3.4	m s^{-1}	Minimum descent rate	$\text{ROD}_{\text{min sink}}$	3.0	m s^{-1}

Glide angle at $V_{\text{min sink}}$	$\theta_{\text{min sink}}$	3.9	deg	Glide angle	$\theta_{\text{best glide}}$	3.3	deg
Landing							
Power required for reverse thrust	P_{landing}	193	kW	Energy required	E_{landing}	1.0	kW h
Total landing distance	s_{la}	566	m	Approach distance	s_{app}	131	m
Flare distance	s_{fl}	55	m	Free roll distance	s_{fr}	38	m
Breaking distance	s_{br}	343	m	Total ground roll distance	s_{gr}	381	m
Approach angle	θ_{app}	5.5	deg	Stall speed in landing conf.	V_{s_0}	34.1	m s^{-1}
Approach speed	V_{app}	44	m s^{-1}	Touchdown speed	V_{TD}	37.5	m s^{-1}
Payload range							
Range nominal mission	R_{nominal}	389	km	CO_2 emissions nominal mission	$\Upsilon_{\text{nominal}}$	0.1127	$\text{kg km}^{-1}\text{ seat}^{-1}$
Range extra fuel	$R_{\text{extra fuel}}$	590	km	CO_2 emissions extra fuel	$\Upsilon_{\text{extra fuel}}$	0.1590	$\text{kg km}^{-1}\text{ seat}^{-1}$
Range extra battery	$R_{\text{extra battery}}$	565	km	CO_2 emissions extra battery	$\Upsilon_{\text{extra battery}}$	0.0988	$\text{kg km}^{-1}\text{ seat}^{-1}$
Range extra both	$R_{\text{extra both}}$	766	km	CO_2 emissions extra both	$\Upsilon_{\text{extra both}}$	0.0802	$\text{kg km}^{-1}\text{ seat}^{-1}$

12
Propulsion System Design

One of the most unique characteristics of the E-COmmuter is its propulsion system. Hence, a detailed design study is done on its layout and function which is presented in this chapter. First, the general architecture and layout of the propulsion system will be discussed after which an engine, propeller and battery selection take place in order to obtain a full picture of the most important components that make up the propulsion system.

12.1. Propulsion System Architecture and Layout

In section 7.2 and section 7.3 it is decided that the aircraft will use a series hybrid electric propulsion system with a distributed electric propulsion layout. This means that combustion engines are used for power generation and, together with batteries, will power electric motors spread over the wing. The internal combustion engines are linked to electrical generators to convert mechanical power to electrical power. These generators can also be used as starters for the engines, as their layout is very similar to that of electric motors.

Since the hybrid system is basically a chain of components, the whole system will fail if one link or component does. To avoid this, a number of redundancies are inserted into the system. The propulsion system architecture and the communications flow is shown in Figure 12.1. Since the propulsion system is a hybrid system and it consist for a large part out of electrical components, the electrical block diagram is obtained by simply removing the internal combustion engines, fuel tanks and fuel pump from Figure 12.1.

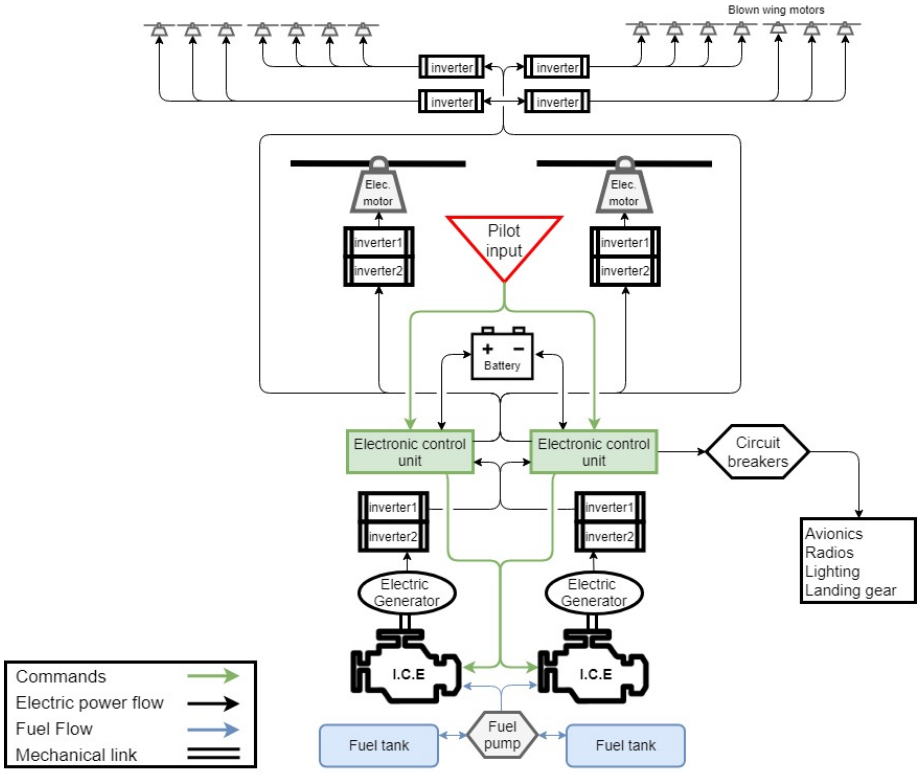

Figure 12.1: Propulsion system architecture.

In subsection 7.3.3 the choice is made to go with a distributed electric propulsion system. Because of this the aircraft is characterized by 14 small blown wing propellers, distributed over the leading edge of the wing, and two larger propellers sized for cruise performance. The amount of blown wing propellers is decided through an iterative calculation

process using the equations discussed in section 10.5 and the noise analysis, discussed in more detail in section 19.2.

At the center of the system are two electric/engine control units (ECU). These are completely redundant and one of them can take over all tasks if the other were to fail. In normal conditions, one of them is active, while the other is in stand-by. The stand-by one also monitors both the system and the active ECU. If the stand-by ECU detects a fault in the the active ECU it will take over. This way ECU failure should have no effect on performance. The communications flow is indicated by the arrows and their colors. The (green) arrows from the ECUs to the internal combustion engines (ICEs) indicate the ECUs controlling the engines throttle setting and thus their power output. The (blue) arrows from the fuel tanks and fuel pump indicate fuel lines. All other (black) arrows show current or electric power flow.

The ECUs read the control inputs from the pilots and make sure the requested power is delivered by the motors. They do this by drawing power from the batteries or increasing the power setting of the ICEs or a combination of the two and then directing this power to the electric motors. Inverters, converters and transformers make sure the current and voltage are adjusted according the component needs and limits. In Figure 12.1 inverters, converters and transformers are indicated as only 'inverters' for simplicity. Also in further explanations the inverter and converters assemblies are simply referred to as inverters.

The ECUs also monitor the whole systems and all its components. They protect the batteries from overdischarging during flight and included an overcurrent protection. Overcharge or overdischarge rates could occur if too high currents are drawn when a lot of power is demanded by the pilot. This also protects the inverters, converters and electric motors from electrical overload.

Overcharge and overdischarge rate protections are included in the charging station on the ground. Overcharging occurs when more energy is put in the batteries than they can handle. Overcharge rates occur when to high currents are used during charging, basically charging the batteries faster than they can handle. The ECUs monitor the engines as well, keeping track of RPM and temperatures, making sure the engine can not go in overspeed or overheat. In general, temperatures from all components are monitored to avoid any kind of overheating. All this information is also fed into the cockpit instruments for the pilot to consult.

12.1.1. Full Electric Operation

During full electric operation the ECUs control the power drawn from the batteries and provided to the motors which in turn determines the RPM and thus the power the motors run at.

For the main motors two redundant inverter assemblies are in place, each handling half of the power. This way if one of them fails, half of the power remains available for that motor. The ECU would recognize the inverter failure and compensate by only allowing half the normal amount of current to flow to that motor to keep the remaining inverter from overloading.

The blown wing motors motors are most crucial during takeoff. During climb and cruise they are not used and fold away. To reduce complexity these motors are not all equipped with separate inverters. Instead there are two inverters per wing which each power half of the motors. Since there is an odd number of motors per wing, one inverter powers four motors versus three for the second inverter. If one of these motors fails, the moment generated due to the thrust differential is only minimal. If one of the inverters fails however, half of the blown wing motors lose power on one wing. This will also reduce the augmented lift effect they have. The thrust differential in this case generates a moment correctable with the rudder, as is analyzed in section 13.5 for the failure of the entire blown wing on one side. If a longer runway is available and the full effect of the blown wing is not needed (i.e. if the required ΔC_L is lower), the same inverter on the other side can limit or even shut off power to the respective motors, removing the need for control input. The flap system can also be partially used to slightly increase the lift coefficient while keeping the drag increase low at small deflections.

Blown Wing Operation

Once a safe altitude and speed are reached, the blown wing is shut off and the main motors power the aircraft for the rest of the climb and cruise phase of the flight. Switching the blown wing motors on and off is done using a simple switch in the cockpit. As the blown wing replaces the flap system during takeoff, switching it on and off should be as simple as raising and lowering the flaps during takeoff. The power is then increased by the power lever which also controls the main engines. The power will however not increase equally with the main motor power, but will increase very fast and reach its maximum long before the main motors reach there maximum power setting. This way the added lift effect is kept even when the thrust lever is set to lower power settings.

12.1.2. Hybrid and Engine Only Operation

Once the aircraft passes a certain altitude and distance where zero emissions are no longer a requirement, the internal combustion engines are started. There are two piston engines connected to generators to convert their mechanical power into electrical power. The generators have intrinsic redundancy through the use of two independent winding systems in each generator. This way if one of the winding's in the generator fails, part of the generator can still operate

using the second winding system producing partial power. Again, a set of inverters, two per generator each handling half of the power, make sure the output voltage and current are adjusted as needed. Power setting of the engines is controlled by the ECU. The engines and generators are placed in the tail, behind the luggage compartment. A fuel pump connects the fuel tanks in the wings with the engines and makes sure that the fuel pressure is always kept at a level needed for the engines to run at. Most engines have built in fuel pumps but this adds an extra level of redundancy. It also allows cross-feed between the fuel tanks in the wings to keep the fuel level and thus the weight balanced.

12.1.3. Cooling

The engines produce a lot of excess heat from the combustion process. Also the electric motors, inverters and batteries heat up significantly when handling large currents. Therefore, cooling is needed to not wear these components unnecessarily. Cooling of the engines is done using air cooling. Air intakes on the sides and top of the E-COmmuter redirect ram air to the engines. In addition, the engines are cooled slightly by oil. The electric motors, placed on the wings, are air cooled by the free stream they encounter. The batteries and inverters, placed in the wing, are cooled by ram air just like the engines. Two air intakes are placed in the center of the wing, above the fuselage. This air is then guided over the batteries and inverters, cooling them, and is then expelled at the wingtip. Further design of this system should be done in the future.

12.2. Engine Selection

The choice of engine is based on the power required to be delivered and the specific fuel consumption. Using the hybridization algorithm described in subsection 11.1.1 it is determined that a maximum power of 433 kW required from the engines is necessary. Furthermore, due to the requirement demanding the capability of refueling at every airport, the choice of fuel is limited to Avgas, which in turn limits the engine choice to piston engines. Two 224 kW Continental IO-550's, with a weight of around 200 kg per engine, are chosen as it best matches. It is a certified aircraft engine used in popular general aviation aircraft like the Cirrus SR22[1], the Beechcraft Bonanza[2] and the Mooney Ovation Ultra[3].

12.3. Inverter and Generator Weights

Each engine puts out 224 kW of power. Assuming a generator rated power density of $7\,\mathrm{kW\,kg^{-1}}$ this requires 32 kg of generator per engine. The generators have an estimated efficiency of 0.95, meaning the inverters after the generators weigh about 12 kg each. This is based on the assumptions the inverters can handle 10 kW of power per kg of mass and that each of the two engine/generator combinations are equipped with two inverters each handling half of the power.

The cruise motors are capable of 255 kW of power each. Using the same assumptions as before, and that the inverters have an efficiency of 0.98, meaning they are supplied with more power to make sure the output power equals the maximum motor power. This results in a mass of 13 kg per inverter. Again, each motor is supplied by two inverters, each delivering half of the total power.

The blown wing motors should each be capable of outputting 18.3 kW of power. Per wing, there is one inverter handling the power for 3 motors and another one handling the power for the four remaining motors. Using the same values as before means the inverter connected to 3 motors will weigh 5.6 kg and the one connected to 4 motors will weigh 7.5 kg.

12.4. Propeller Selection

An important part of the propulsion system consists of the propellers mounted to both the cruise motors and the blown wing. This section discusses their sizing and selection.

12.4.1. Cruise Propellers

The propeller diameter of the cruise propellers is determined by both the thrust and the noise they produce. As the aircraft iteration loop is written such that it takes thrust as a variable, the noise performance of the propellers is the limiting criteria for determining its diameter (e.g. a lower thrust due to a smaller diameter would cause the program to try and lower the weight of the aircraft).

Starting off with a larger propeller diameter of 2.1 m and a lower blade count of 3, the propeller sizes are iterated for best cruise performance. Then, the estimated noise emissions with these propellers are checked if they satisfy requirement **HEF-ARP-01**. This is explained in section 19.2. If not, the diameter is gradually reduced and the blade count and RPM are increased in the iteration until this requirement is met. The end result are propellers of 1.7 m with 4

[1] URL: `https://cirrusaircraft.com/aircraft/sr22/` [cited 21 June 2018]
[2] URL: `http://beechcraft.txtav.com/en/bonanza-g36#specs` [cited 21 June 2018]
[3] URL: `https://www.mooney.com/aircraft` [cited 21 June 2018]

blades, which match the design of the Hartzell HC-C4YR-2's[4]. The Hartzell propellers are rated for a maximum power of 261 kW, which is a little more than the maximum power of 256 kW which the cruise motors are sized for. The HC-C4YR-2 are constant speed, variable pitch propellers which allows for high efficiencies for a large range of different airspeeds.

12.4.2. Blown Wing Propellers

The 14 smaller electric motors, distributed over the leading edge, are mounted with custom, 9-blade, high-lift propellers with a diameter of 0.98 m. The diameter, number and also location of the blown wing propellers are a result of the analysis done in subsection 10.5.3 and are verified using the noise analysis method in section 19.2 to ensure they do not breach requirement **HEF-APR-01**. From the noise analysis it quickly becomes clear that the cruise propellers produce more noise than the blown wing propellers, and so noise is not a major concern in the sizing of the blown wing propellers.

As propellers specifically designed for high-lift are mostly in the experimental development stages, it is not possible to find a practical propeller currently on the market that provided the necessary efficiency during takeoff and landing of the E-COmmuter. However, Lenfers et al. [55] have designed a high-lift propeller specifically for short takeoff and landing aircraft, which is suitable for use on the E-COmmuter.

The high-lift propellers have hinged blades so they can fold back during cruise flight and create minimal drag. In emergencies however, they can still be used during the cruise phase to provide additional stability or power in a one engine inoperative (OEI), or in this case one motor inoperative, scenario. The folding mechanism used is similar to the one used on the X-57 Maxwell designed by NASA [56] and is of relatively low complexity. Detailed design of the folding mechanism is left for further studies.

12.5. Propeller Thrust

The propeller thrust is a crucial component for the performance calculations done in chapter 11. Hence, this section details how the propeller thrust is calculated for both the cruise and the blown wing propellers, as these methods differ due to the experimental nature of the blown wing propellers.

In general, to calculate the thrust of a propeller, Equation 12.1 is often used with a constant η_p. However, although Equation 12.1 is quite true to life at higher airspeeds, below 41.16 m s^{-1} the deviation from experimental data is simply too high to make the equation usable [25]. Hence, a different method is to be found that takes into account that propeller efficiency decreases with lower airspeeds, making η_p not a constant but a variable based on the airspeed.

$$T = \frac{\eta_p \cdot P_a}{V} \tag{12.1}$$

12.5.1. Cruise Propellers

For the cruise propellers, it can be assumed that their design is based on reaching its maximum efficiency at cruise speeds. To successfully find an alternative to Equation 12.1, a quadratic interpolation can be done between the thrust at 0 airspeed and the thrust at $V_{\max}$ for the cruise propellers. This method assumes that the cruise propellers reach a maximum efficiency at the cruise airspeed.

The thrust at 0 airspeed is the static thrust T_{static} and can be calculated based on a method resulting from the Rankine-Froude momentum theory, given by Equation 12.2 [25]. For the density, the density is taken for the highest airport in Europe, namely Samedan airport where $\rho = 1.0366\,\text{kg m}^{-3}$. This ensures that the aircraft can perform at all airports in Europe.

$$T_{\text{static}} = 0.85 \cdot P^{\frac{2}{3}} \cdot \left(2 \cdot \rho \cdot A_{\text{prop-disc}}\right)^{\frac{1}{3}} \cdot \left(1 - \frac{A_{\text{spinner}}}{A_{\text{prop-disc}}}\right) \tag{12.2}$$

As the spinner is not specifically selected for the propeller, it is taken as 10% of the propeller frontal area.

The thrust at $V_{\max}$ is simple to calculate using Equation 12.1 as the maximum airspeed of the E-COmmuter has been calculated in subsection 11.3.4 and is much higher than 41.16 m s^{-1}. For Equation 12.1, η_p for the cruise propellers at $V_{\max}$ is taken as 0.8 due to the use of a constant speed propeller which keeps its high efficiency at higher airspeeds than the cruise airspeed.

12.5.2. Blown Wing Propellers

As the blown wing propellers are experimental high-lift propellers [55], not much is known about its performance at different airspeeds. It is certain that a method similar to the one used in subsection 12.5.1 cannot be used, as the method used in that section assumes a maximum efficiency of the propellers at cruise velocities, which is not what the high-lift propellers have been designed for. Hence, to calculate the thrust generated by the high-lift propellers,

[4] URL: `https://hartzellprop.com/wp-content/uploads/159-0000-R63-WA.pdf` [cited 23 June 2018]

experimental data is used from Lenfers et al. [55] that provides a list of η_p for a range of advance ratios J. The advance ratio of a propeller is defined as:

$$J = \frac{V_\infty}{n \cdot D} \tag{12.3}$$

Where n is the RPS of the propeller and D its diameter. To optimize the thrust produced by the propellers, the program that calculates the thrust iterates through the allowed RPS of the motor until the advance ratio is found that produces the maximum efficiency at a certain airspeed. Then, as the propeller efficiency is not constant anymore but dependent on the airspeed, Equation 12.1 can be used to calculate the propeller thrust for the blown wing propellers at every airspeed.

12.6. Battery Selection

This section elaborates on the choice of the batteries. The most important requirement for this power source is the energy and the power it can deliver. For the E-COmmuter, a total energy of 440.25 kW h and a maximum power (for takeoff) of 769.73 kW are required (subsection 11.3.4). In order to achieve these targets with a battery weight as low as possible, batteries with a high specific energy density are searched for. Four batteries are looked into: Lithium-ion, Lithium-polymer, Lithium-air and Lithium-sulfur.

12.6.1. Battery Comparison

Lithium-ion is currently being used in electric cars[5]. After 30 years of development, its specific energy is levelling out around 280 W h kg^{-1} [51]. This is regarded not sufficient for aerospace applications, and is therefore not used in E-COmmuter[6].

Next, Lithium-polymer batteries are considered, as it is currently used in some small electric aircraft[7]. One of the main advantages is the high continuous and peak discharge rates[8]. However, the specific energy is rather limited to below 300 W h kg^{-1} [57]. Since the battery is already implemented in several aircraft, the technology is readily available and further development is expected in the coming decades.

Furthermore, Lithium-air batteries are gaining interest due to their very promising specifications. Currently, specific energy values of 1000 W h kg^{-1} seem achievable in the future [58][59]. Unfortunately, experiments in realistic environments have not shown any operational use yet because of the production of undesirable byproducts, which block the cathode and consequently unable functioning of the battery[9]. Moreover, the battery gains weight during discharge due to extraction of air from the ambient, for which has to be accounted in the design [60]. It is decided to not use Lithium-air batteries because of its still conceptual design stage.

Finally, Lithium-sulfur batteries are a possibility. It has a high specific energy, simple processing techniques and is more sustainable than the existing Lithium-ion batteries. Its raw materials are cheap, abundant and relatively environmentally friendly [51]. For example, the carbon-sulfur can be extracted from waste of petroleum processes [61]. The main disadvantages arise from currently limited research. The reaction mechanism is very complex, which makes integration of multiple cells rather complicated [51][61]. The cycle life is limited by degradation mechanisms in the cells. However, the latter is balanced by the previously mentioned low cost [51][61]. Almost every global battery developer is investing in research for Lithium-sulfur batteries, major developments are expected in the near future [51]. A more in-depth analysis is performed to see whether this sustainable and innovative battery complies with the E-COmmuter requirements.

12.6.2. Lithium-sulfur Battery Analysis

Lithium-sulfur (Li-S) cells have a theoretical specific energy of 2500 to 2600 W h kg^{-1} [51][62]. In practice, 25% to 33% of this value can be reached. Most optimistically, a specific energy of 858 W h kg^{-1} is achievable. As this does not seem feasible by 2035, a more realistic value of 750 W h kg^{-1} is used. Some prototypes Li-S cells have been manufactured and expected developments for the following three years are predicted [51][63]. The cell specifications expected for the coming decades are given in Table 12.1.

$$E_{\text{bat}} = n_{\text{total}} \cdot V \cdot Q \tag{12.4}$$

$$P_{\text{bat}} = (n_{\text{series}} \cdot V) \cdot (n_{\text{parallel}} \cdot Q) \cdot C \tag{12.5}$$

With these values, the weight and volume of the total battery is estimated. Equation 12.4 and Equation 12.5 are used to calculate required amount of cells and arrangement to meet the aforementioned energy and power requirements [64]. In these equations, n refers to the number of cells. In order to meet the energy requirement, at least 2346 cells are needed. It is decided to place 8 cells in series. In this way, if one of the cells fails, at most eight cells are lost. This

[5]URL: http://www.businessinsider.com/here-comes-teslas-missing-piece-battery-announcement-2015-4?international=true&r=US&IR=T [cited 21 June 2018]
[6]URL: https://www.insidescience.org/news/brief-where-are-electric-airplanes [cited 21 June 2018]
[7]URL: http://www.pipistrel.si/plane/taurus-electro/faq [cited 21 June 2018]
[8]URL: http://www.szaspower.com/industry-news/The-advantages-and-disadvantag.html [cited 21 June 2018]
[9]URL: https://www.sciencedaily.com/releases/2018/03/180321141345.htm [cited 21 June 2018]

means 292 (2330/8) parallel connections have to be made. A disadvantage of this configuration is the corresponding high current, implying losses, requiring large cables and causing high temperatures. In order to mitigate this risk, sufficient insulation around the wires has to be provided [64]. The maximum power output is calculated using Equation 12.5 and equals 2.38 MW. Thus, the power requirement is easily met. As the available power is three times larger than the required power, the discharge rate of the batteries will be lower. Hence, the batteries will suffer from less degradation, increasing the life cycle.

A battery volume and weight of respectively 0.457 m^3 and 587 kg are obtained. The latter value is indeed 10 kg larger than the initial estimation. This is probably due to the packaging of the cells, which is not taken into account in the first estimation, as it is based on the specific energy of the battery. With the current developments in Lithium-sulfur batteries, the cycle life is very limited [51][62]. However, when effective protection is applied and with the expected discharge rate, the cycle life increases significantly [51]. At the same time, large progress is required both in power rate and in cycle life. In the very near future, it is not expected that both of these can be increased simultaneously [51][61]. As the power rate is of main importance for aerospace vehicles, it is thought that this will be of priority. Consequently, the cycle life will remain limited in the first years. For now, it is assumed that by 2035 Lithium-sulfur will have caught up on the Lithium-ion batteries regarding life cycle. Thus, the life cycle is estimated at 1500 cycles [51][65]. This means the aircraft can complete 1500 flights before the batteries need to be replaced.

Table 12.1: Expected Lithium-sulfur battery specifications for the coming decades [51][63].

	Electric Charge Q	**Discharge rate C**	**Nominal voltage V**	**Specific energy E_{sp}**	**Dimensions**	**Cell weight W**
Value	90 A h	5.4 C	2.1 V	750 W h kg^{-1}	0.174 m x 0.112 m x 0.01 m	0.25 kg

12.7. Results

All of the results obtained above are summarized in the table below.

Table 12.2: All the results obtained in the propulsion design.

Parameter	**Symbol**	**Value**	**Unit**	**Parameter**	**Symbol**	**Value**	**Unit**
Engine Selection							
Engine weight	W_{eng}	200	kg	Number of engines	n_{eng}	2	-
Power per engine	P_{eng}	224	kW	Used fuel weight	$w_{fuel\text{-}used}$	201	kg
Reserve fuel weight	$w_{fuel\text{-}reserve}$	50	kg	Type of fuel	Avgas		
Engine type	Continental IO-550						
Battery Selection							
Battery weight	W_{bat}	587	kg	Battery volume	V_{bat}	0.457	m^3
Number of battery cells	n_{cells}	2330	-	Battery type	Lithium-sulfur		
Battery configuration	8S292P						
Propeller Selection							
Cruise propeller model	Hartzell HC-C4YR-2			Cruise propeller diameter	d_{cr}	1.7	m
Blown wing propeller model	Experimental high-lift			Cruise propeller blade count	$\#_{cr}$	4	-
Blown wing propeller diameter	d_{bl}	0.98	m	Blown wing propeller blade count	$\#_{bl}$	9	-
Blown wing propeller TO RPM	$n_{bl\text{-}to}$	3060	RPM				
Inverters and generators							
Generator efficiency	η_g	0.95	-	Inverter efficiency	η_i	0.98	-
Generator weight	W_{gn}	32	kg	Single inverter weight (after generator)	$W_{i_{gen}}$	12	kg
Single inverter weight cruise motors	$W_{i_{cm}}$	13	kg	Single inverter weight 3x blown wing motor	$W_{i_{3bl}}$	5.6	kg
Single inverter weight 4x blown wing motor	$W_{i_{cm}}$	7.5	kg				

13

Stability & Control

After the design of all other subsystems, the main geometry of the aircraft and other performance characteristics that affect the flight behaviour of the E-COmmuter are known. With this information, the stability & control subsystem can be designed and analyzed. This subsystem is very widely encompassing. This chapter starts with the placement of the wing and horizontal tail sizing, which is a result of operational c.g range and stability and controllability. With this info empennages and the landing gear can be sized. Next the dynamic stability is analyzed by use of estimated stability derivatives. Last, the turning behaviour and control surface sizing is performed. This chapter ends with verification and validation of the used models.

13.1. Aircraft Loading

Concerning the aircraft loading, the several possible locations of center of gravity are evaluated. These are required to evaluate the stability and controllability of the aircraft, which is discussed in section 13.2.

13.1.1. Location of Center of Gravity for Operating Empty Weight

As a starting point for both the aircraft loading & balance diagram and the scissor plot, an estimation of the center of gravity (c.g.) location of the Operating Empty Weight (OEW) is needed. In this subsection, the estimation of this c.g. location is discussed step-by-step. The datum for the distances is the aircraft's nose.

For effective control of the c.g. location at OEW while moving the wing position with respect to the fuselage during sizing, it is convenient to arrange the various weight components. The components are divided in:

- **Fuselage group**
  - Fuselage
  - Equipment
  - Vertical tail
  - Horizontal tail
  - Nose landing gear
  - Internal combustion engines
  - Generators
- **Wing group**
  - Wing
  - Batteries
  - Fuel system
  - Electric motors
  - Main landing gear

In order to make it possible to iterate the OEW c.g., the estimation is done by use of a program. The program uses the parameters from the preliminary sizing and weight estimation of the aircraft which can be found in Brill et al. [4, Table 10.1] as initial values. The used equations and incorporated parameters in the equations, along with the most important assumptions, will be elaborated below.

Fuselage Group

The longitudinal c.g. locations of the fuselage, vertical tail and horizontal tail are given by Oliviero [66], in which the parameters from the initial sizing are used as input. For the horizontal tail, the equation has been altered to account for the additional horizontal distance due to the usage of a T-tail in the E-COmmuter design. The fuselage c.g. contains the fuselage structure, but also the built-in systems. Therefore, the fuselage and equipment weight found in the Class II weight estimation are considered. For the horizontal and vertical tail, the weight is directly given by the Class II weight estimation.

The initial nose landing gear position is given in the preliminary parameter table. The weight is provided by the Class II weight estimation.

Next, the c.g. location of the internal combustion engines (ICE) is estimated to be behind the fuselage cargo compartment. The weight of the ICE is the installed-engine weight from the Class II weight estimation. The generators are placed 1 m aft of those, which is a fraction of the electrical propulsion system weight.

After the calculation of all separate components, the c.g. location and weight of the total fuselage group can be calculated by Equation 13.1.

$$X_{\text{total}} = \frac{\sum_{\text{components}}(W_{\text{component}} \cdot X_{\text{component}})}{\sum_{\text{components}}(W_{\text{component}})} \tag{13.1}$$

Wing Group
The position of the c.g. of the wing is determined by equations from [66]. The wing weight is found in the Class II weight estimation.

The batteries are located in the wing of the aircraft. The detailed dimensions of the battery package are not yet known. Therefore, the c.g. location of the batteries is assumed to be in the middle of the Mean Aerodynamic Chord (MAC). The battery weight is found in the Class I weight estimation.

The remaining fraction of the electric propulsion system weight (also used for the generators in the fuselage group) are the inverters, which are placed halfway down the MAC.

The last component of the wing group are the electric motors that drive the propellers. As these motors are evenly distributed along the leading edge of the main wing, it is assumed that on average these are placed just aft of the Leading Edge of the Mean Aerodynamic Chord (LEMAC). The weight of the motors is the installed electric motor weight from the propulsion system sizing and Class II weight estimation.

Just as for the fuselage group, the c.g. location of the total wing group is given by Equation 13.1.

Operating Empty Weight
The last step before the loading & balance diagram and scissor plot can be constructed is to find the c.g. location of the OEW. This is the two weight groups, in addition of the crew and trapped fuel and oils. The crew is assumed to be seated three quarters of the cockpit length from the nose and the trapped fuel at the location of the ICEs. The crew and trapped fuel and oils weight is found in the Class I weight estimation. The total OEW c.g. location is given by a derivative of Equation 13.1, by means of Equation 13.2.

$$X_{\text{OEW}} = \frac{X_{\text{fuselage group}} \cdot W_{\text{fuselage group}} + X_{\text{wing group}} \cdot W_{\text{wing group}} + X_{\text{crew}} \cdot W_{\text{crew}} + X_{\text{tfl}} \cdot W_{\text{tfl}}}{W_{\text{fuselage group}} + W_{\text{wing group}} + W_{\text{crew}} + W_{\text{tfl}}} \tag{13.2}$$

13.1.2. Aircraft Loading Diagram

The loading diagram shows the range of the aircraft c.g. location during loading of fuel and payload (cargo and passengers), up to the Maximum Takeoff Weight (MTOW). The construction of such a diagram can be used in combination with the scissor plot to finalize the position of the main wing relative to the fuselage. In turn, this will allow the final sizing of the horizontal tail and placement of landing gear.

In order to be conservative to guarantee a safe and robust design, the loading diagram is made for multiple cases with different orders of loading such that the most critical loading can be found. This is done by selection of the most forward and most aft position of all diagrams. This will provide the widest c.g. range.

The construction of the diagram follows the same procedure as in subsection 13.1.1, where Equation 13.1 is used for every addition of fuel, one row of passengers, or cargo to calculate the incremental change in c.g. location and gross weight of the aircraft. The location of these components is given by the following equations.

$$X_{\text{cargo}} = l_{\text{fuselage}} - l_{\text{tailcone}} + 0.5 \tag{13.3}$$

$$X_{\text{passenger seat row n}} = l_{\text{nosecone}} + n \cdot \text{seat pitch} \tag{13.4}$$

$$X_{\text{fuel}} = X_{\text{LEMAC}} + 0.5 \cdot \text{MAC} \tag{13.5}$$

The cargo c.g. position is approximately 0.5 m aft of the cabin. The first seat is placed on a nosecone length from the aircraft's nose. The fuel c.g. location is assumed to be halfway down the MAC, assuming no change in location during fueling or burning. The weight of the cargo is given by $14 \cdot 20\,\text{kg} = 280\,\text{kg}$, which is the luggage weight of 14 passengers. The weight of one passenger row is given by $2 \cdot 77\,\text{kg} = 154\,\text{kg}$; the weight of two passengers. Last, the fuel weight is given by the maximum fuel capacity from the Class I weight estimation.

Following the procedure as outlined above, one finds the loading & balance diagrams as depicted in Figure 13.1. These are the two loading diagrams for the final design from after the iteration.

In the loading diagrams, one can readily see the incremental change of c.g. location and aircraft gross weight. For the left, the critical, most forward point is the front-to-back loading of the third passenger row when passengers are loaded first with a $\frac{\text{c.g.}}{\text{MAC}}$ ratio of 0.188. The critical, most aft point for the middle diagram is the back-to-front loading of the fourth row after cargo and fuel have been loaded with a $\frac{\text{c.g.}}{\text{MAC}}$ ratio of 0.505. The most forward and aft c.g. are indicated with a margin of 2%.

After one c.g. range has been found for one X_{LEMAC}, the construction of the loading diagrams can be repeated with different wing positions. The X_{LEMAC} range considered in this report is 2 m front and 1.5 m aft of the initial placement from Brill et al. [4, Table 10.1]. The most forward and aft c.g. positions of the entire X_{LEMAC} range can be plotted against the X_{LEMAC} over the length of the fuselage l_{fuselage}, which results in the green graph in Figure 13.3. This graph is used in combination with the scissor plot to find the optimal wing placement and horizontal tail size.

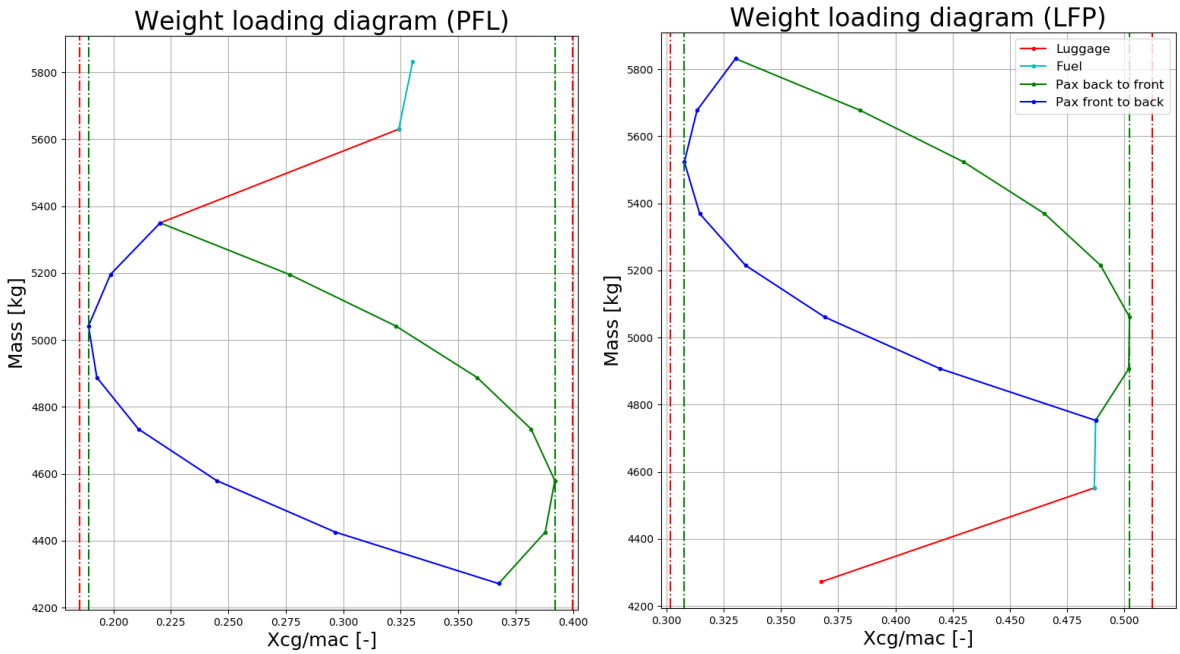

(a) C.g. range for loading sequence 'passengers, fuel, luggage'.

(b) C.g. range for loading sequence 'luggage, fuel, passengers'.

Figure 13.1: Aircraft loading & balance diagrams for the final X_{LEMAC} of 6.911 m. The most forward c.g. location is found in the left diagram and the most aft c.g. location in the right diagram (P: Passenger, L: Luggage, F: Fuel). The final OEW is 4280 kg.

13.2. Stability & Controllability

To evaluate the stability and controllability of the aircraft, both of these constraints should be evaluated individually. After evaluation of these constraints, the exact location of the wing is determined together with a more accurate required horizontal tail surface area.

13.2.1. Stability

First the stability is discussed which focuses on the ability to return to the previous state of equilibrium after a disturbance. A disturbance will cause a resultant force which acts in the neutral point. The neutral point will always need to be positioned aft of the center of gravity. If the neutral point is located behind the center of gravity a counteracting moment is created in and the aircraft will return to its previous state of equilibrium. Since there should always be a sufficient margin between the neutral point and the center of gravity, a stability margin of 0.05 $\frac{X_{c.g.}}{MAC}$ is chosen. By evaluating the stick-fixed stability of a conventional aircraft the following equation of the c.g. as function of $\frac{S_h}{S}$ is obtained [67]:

$$\frac{S_h}{S} = \frac{\overline{x}_{c.g.} - \overline{x}_{a.c.} + 0.05}{\frac{C_{L\alpha_h}}{C_{L\alpha_{A-h}}} \cdot \left(1 - \frac{d\epsilon}{d\alpha}\right) \cdot \frac{l_h}{\bar{c}} \cdot \left(\frac{V_h}{V}\right)^2} \tag{13.6}$$

In order to plot Equation 13.6 with $\frac{S_h}{S}$ as a function of $X_{c.g.}$ several coefficients need to be determined first. The unknown coefficients are $X_{a.c.}$, $C_{l\alpha_h}$, $C_{l\alpha_{A-h}}$ and $\frac{d\epsilon}{d\alpha}$. They are determined by using semi-empirical relations which are provided by Torenbeek [23], Raymer [31] and slides provided by Oliviero [67][68]. The relations are given in Table 13.1. All of the elements which are given in the relation are either dependent on the geometry of the aircraft or are based on aerodynamic coefficients which are determined in chapter 10.

Since most of the coefficients of Table 13.1 depend on the geometry of the aircraft, the evaluation of stability and control needs to be iterated. This is since the geometry is also updated as an output of the stability and control. However, for some of the coefficients it is assumed to stay constant throughout the iteration. $X_{a.c._w}$ is assumed to be constant at 0.25 since the aircraft has no sweep at quarter cord line [23]. Also, $\frac{V_h}{V}$ is assumed to be equal to 1 because the aircraft has a T-Tail configuration. All the other coefficients are updated during the iteration process. Lastly, the equation for C_{l_α} can also be used for determining the lift slope for the horizontal tail.

The stability constraint is evaluated at cruise altitude together with the cruise speed which is obtained from the loading diagram. This scenario is used for determining stability because the neutral point moves forward by increasing the airspeed. The closer the neutral point comes towards the center of gravity, the less stable the aircraft will be. All the

aerodynamic coefficients are therefore evaluated at cruise altitude and at high speeds. By using Equation 13.6 for a range of c.g. values, the red line with a positive slope in Figure 13.3 is obtained.

Table 13.1: Values of coefficients which are used for controllability and stability determination.

Parameter	Symbol	Value	Unit	Parameter	Symbol	Value	Unit
Stability							
Aerodynamic center	$x_{a.c}$	0.129	% MAC	Downwash	$\frac{d\epsilon}{d\alpha}$	0.2982	-
Tail lift coefficient slope	$C_{L\alpha_h}$	3.811	-	Tail/wing speed ratio	$\frac{V_h}{V}$	1	-
Lift coefficient slope	$C_{L\alpha_{A-h}}$	5.692	-				
Controllability							
Moment coefficient	$C_{m_{a.c.}}$	-0.0661	-	Tail/wing speed ratio	$\frac{V_h}{V}$	1	-
Maximum lift coefficient	$C_{L_{A-h}}$	1.505	-	Aerodynamic center	$x_{a.c}$	0.1234	% MAC
Max tail lift coefficient	C_{L_h}	-0.5561	-				

13.2.2. Controllability

In case of controllability the aircraft is designed such that it is possible to fly in trimmed condition. To evaluate this, the should be a moment equilibrium around the center of gravity. The moment created by the main wing needs to be compensated by the vertical tail. By having a moment equilibrium around the center of gravity the aircraft is controllable since, a deflection of the control surfaces will result in a desired moment.

Opposite to stability, controllability needs to be evaluated at minimum stall speeds at sea level. During this flight condition the tail plane is less effective and is therefore constraining the design of the tail surface area. By deriving the moment equilibrium around the center of gravity for a conventional aircraft, Equation 13.7 can be obtained. The equation expresses the ratio of tail surface area w.r.t to the main wing surface as a function of several centre of gravity locations: [68]

$$\frac{S_h}{S} = \frac{\overline{x}_{c.g.} + \frac{C_{m_{a.c.}}}{C_{L_{A-h}}} - \overline{x}_{a.c.}}{\frac{C_{L_h}}{C_{L_{A-h}}} \cdot \frac{l_h}{\overline{x}} \cdot \left(\frac{V_h}{V}\right)^2} \tag{13.7}$$

To evaluate the controllability the following coefficients need to be determined first: $x_{a.c.}$, $C_{m_{a.c.}}$, $C_{L_{A-h}}$, C_{L_h}. $\frac{V_h}{V}$ is again equal to 1 because of the T-Tail configuration. $x_{a.c.}$ can be determined by using the same method which is used for evaluating stability. The equations that are used for determining the other unknown coefficients are given in the controllability section of Table 13.1. Since these equations again depend on the geometry of the aircraft iteration is required. However, some values are assumed to be constant. The maximum lift coefficients are determined in section 10.3 and their values don't change throughout the iteration. However, these lift coefficients are valid for an infinite wing and thus need to be transformed to a finite wing by using methods which are described by Raymer [31]. All the other parameters are updated during iteration since the geometry is updated as well.
Since the aircraft consists of a blown wing concept, the controllability constraint needs to be evaluated at multiple configurations. Due to CS-23 regulation, the aircraft is also equipped with flaps for redundancy. During regular flight conditions these won't be necessary since the blown wing will provide the required extra lift. However, since the lift coefficients and the moment coefficient are different for the different configurations, they both need to be evaluated. After the first iteration it became apparent that the scenario with the flaps fully extended is constraining. Therefore, this in the only configuration that is used for further analysis.

Since the output and input for both Equation 13.6 and Equation 13.7 is the same they can be plotted in the same graph. This is displayed by the red lines in Figure 13.3, where the positive slope corresponds to stability and the negative to controllability.

From the two lines in Figure 13.3 a feasible region can be obtained. For an aircraft to be controllable, the center of gravity should always be placed aft of the controllability line. Otherwise the aircraft cannot be properly trimmed. For an aircraft to be stable, the neutral point should always be placed aft of the center of gravity. Therefore, the center of gravity should always be in front of the stability line. By considering both requirements the feasible design region is shaped by the triangle between the two red lines in Figure 13.3.

13.2.3. Wing Placement

Using the combined plot of the c.g. to longitudinal wing placement and the scissor plot, the optimal wing placement and horizontal tail size can be found. The procedure for this is to compare both graphs by positioning them over each other, with on the x-axis the $\frac{\text{c.g.}}{\text{MAC}}$. Next, the goal is to find the smallest horizontal tail area for an operational c.g. range that satisfies the stability and controllability lines. Simultaneously, the optimal corresponding wing placement along the fuselage is found.

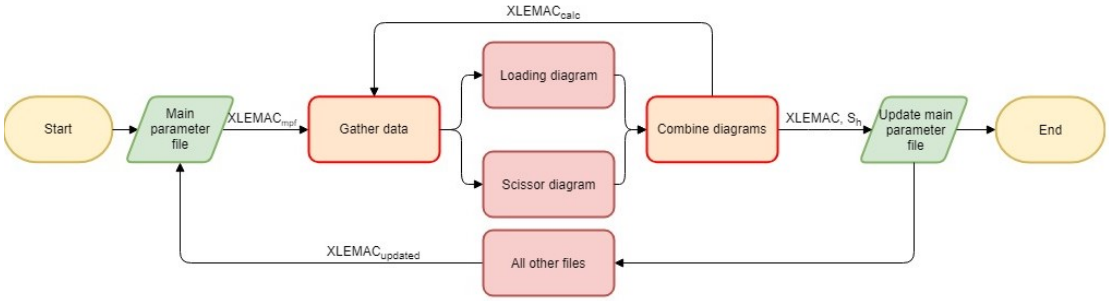

Figure 13.2: Code flow diagram for the scissor plot generation.

The manner that the X_{LEMAC} is found in the program is visualized in Figure 13.2. The lines of the c.g. graph are given by a large list with both the forward and aft $x_{\text{c.g.}}$ and the X_{LEMAC}. As mentioned, this list is from 2 m front and 1.5 m aft of the initial X_{LEMAC} placement. For every X_{LEMAC}, the most forward $x_{\text{c.g.}}$ is taken and that is used as input for the controllability curve, giving a certain $\frac{S_h}{S}$. This y-value is searched for in the stability curve and its corresponding aft $x_{\text{c.g.}}$ is taken. Next, the difference between this value and the aft c.g. of the c.g. graph of the considered X_{LEMAC} is assessed. The X_{LEMAC} and $\frac{S_h}{S}$ which result in the smallest difference between the c.g.'s of both plots is then the most optimal one, as depicted in Figure 13.3.

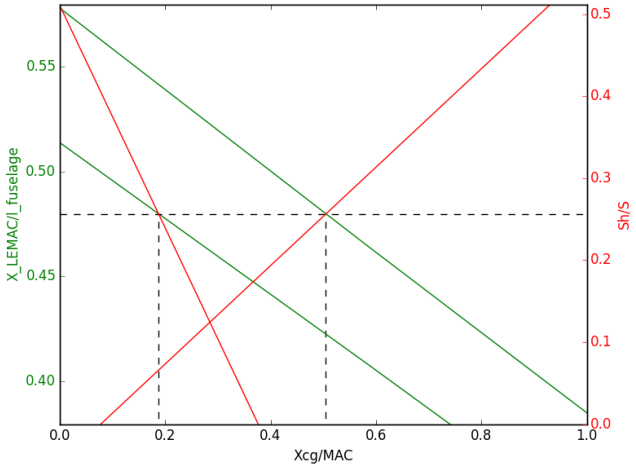

Figure 13.3: Graph showing the final combination of the c.g. range vs. wing placement and scissor plot. The found parameters are $X_{\text{LEMAC}}/l_{\text{fuselage}} = 0.480$ and $S_h/S = 0.256$. The corresponding operational c.g. range is from 0.188 to 0.505 $x_{\text{c.g.}}$/MAC.

In order to converge to a final wing position, the combination of the graphs as described in this section finds a new X_{LEMAC}. This one is cross-referenced with the preliminary estimated X_{LEMAC}. If the difference is more than 0.1%, scissor plot is reconstructed with the newly found X_{LEMAC} and corresponding new tail arm and the two graphs are matched again. This method is repeated until the difference is less than 0.1%. This results in the final values for wing position and horizontal tail area, which are indicated in the final graph of the last iteration in Figure 13.3. Note that the optimal c.g. range is the same as in Figure 13.1.

Using the aforementioned design for stability & control, the tail and landing gear are designed in chapter 14.

13.3. Estimating Stability Derivatives

The stability and blown wing analyses considered in section 13.4 and section 13.5 both make use of the symmetric and asymmetric equations of motion (EOM) of the aircraft. These EOM include a large number of stability derivatives, which need to be estimated for the E-COmmuter.

One of the most known and trusted methods to estimate these derivatives for conceptual aircraft is the USAF Stability and Control DATCOM [69]. The numerous extensive equations in the book have been incorporated into a program published simultaneously called Digital DATCOM, nowadays publicly available online[1].

The input values of the program rely on so-called Data Cards containing a detailed description of the aircraft geometry and flight conditions the user wants to find the derivatives for. These Data Cards are constructed for the E-COmmuter by the method described in the Digital DATCOM User Manual [70]. These are based on the final geometry found after

[1] URL: `http://www.pdas.com/datcom.html` [cited 6 June 2018]

the iteration phase of the aircraft design process. Therefore, the estimated derivatives can be expected to accurately represent the derivatives of the actual aircraft, as they will probably only slightly change in the further design process (see tables in "Results" section of each of the design chapters).

For the E-COmmuter, the stability derivatives are estimated for cruise conditions and MTOW for seven different angles of attack around the cruise angle of attack of 2.2°. The Mach number is 0.21 and the cruise altitude 3048 m. This is the most common flight condition of the aircraft. The derivatives are given in Table 13.2. These values have been compared to derivatives of different reference aircraft and it is found that these are in fact similar. Also, the values have been checked for multiple speeds and altitudes and show no significant differences, and therefore the derivatives in the table are assumed to be representative for all flight phases of the aircraft.

Table 13.2: E-COmmuter stability derivatives for cruise conditions as estimated by Digital DATCOM. All units in [rad^{-1}].

Derivative	Value	Derivative	Value
C_{Z_α}	-6.370	$C_{Z_{\dot{\alpha}}}$	-2.476
C_{m_α}	-2.328	$C_{m_{\dot{\alpha}}}$	-9.835
C_{Y_β}	-0.676	C_{l_p}	-0.511
C_{n_β}	0.047	C_{Y_p}	-0.098
C_{l_β}	-0.101	C_{n_p}	-0.068
C_{Z_q}	-9.989	C_{n_r}	-0.072
C_{m_q}	-29.73	C_{l_r}	0.166

However, a number of derivatives which occur in the EOM of the aircraft are not directly estimated by DATCOM. Therefore the following assumptions have been incorporated to still be able to analyze the EOM, without having to simplify the EOM themselves (which would compromise accuracy more):

- $C_{X_u} = -2C_D$, $C_{Z_0} = -C_L$, and $C_{Z_u} = -2C_L$ as given by Mulder et al. [32], in which DATCOM outputs for C_L and C_D for cruise angle of attack can be used;
- C_{m_u} is normally either zero or very small, it is therefore set to 0 [32];
- C_{X_α} can be derived from the change of the axial force as result of increasing alpha, given by the DATCOM output;
- C_{X_0} can be derived from the axial force at cruise angle of attack from DATCOM output;
- $C_{n_{\dot{\beta}}}$ can be neglected due to the E-COmmuter's high aspect ratio [32];
- $C_{Y_{\dot{\beta}}}$ and C_{Y_r} are assumed negligible as they are also of minor importance [32].

With the listed assumptions, the remaining assumed stability derivatives in addition to Table 13.2 for the E-COmmuter are given in Table 13.3.

Table 13.3: Remaining E-COmmuter stability derivatives for cruise conditions as assumed or derived from Digital DATCOM. All units in [rad^{-1}].

Derivative	Value	Derivative	Value	Derivative	Value
C_{X_u}	-0.062	C_{X_0}	-0.004	C_{X_α}	0.659
C_{Z_u}	-1.372	C_{Z_0}	-0.686	$C_{Y_{\dot{\beta}}}$	0
C_{m_u}	0	$C_{n_{\dot{\beta}}}$	0	C_{Y_r}	0

13.4. Static & Dynamic Stability and Control

To analyze the behaviour and handling of the aircraft it is essential to perform research on its flight dynamics. These include longitudinal and lateral static stability, and symmetric and asymmetric dynamic stability.

The longitudinal static stability of the aircraft has been extensively discussed in section 13.1 and with the horizontal tail sizing and wing placement result, it can be concluded that longitudinal stability and controllability is guaranteed. Lateral static stability and controllability is largely influenced by the blown wing characteristics, which is discussed in section 13.5. Thus in this section only the dynamic stability will be discussed.

13.4.1. Radius of Gyration Determination

Before the Dynamic stability can be assessed, the non-dimensional radius of gyration for the aircraft needs to determined first. For symmetric and asymmetric the flight, the radii of gyration are required: K_X^2, K_Y^2, K_Z^2 and K_{XZ}. K_{XZ} can assumed to be equal to zero since the aircraft design is symmetric. The remaining non dimensional radii of gyration can directly be obtained from the moment of inertia around the corresponding axis with the following equations [32]:

$$K_x^2 = \frac{I_{XX}}{m \cdot b^2} \quad (13.8) \qquad K_Y^2 = \frac{I_{YY}}{m \cdot \bar{c}^2} \quad (13.9) \qquad K_Z^2 = \frac{I_{ZZ}}{m \cdot b^2} \quad (13.10)$$

The aircraft is subdivided in several mass components to determine the moment of inertia around all three axis. For each of these mass components the location of the center of gravity is determined together with their dimensions. The subdivision of the mass components is displayed in Table 13.4. Each component with (2x) means that this is present on both sides of the center line of the fuselage. This is crucial for determining the moment of inertia since it should be evaluated separately for both sides. The passengers are modelled as two rectangular cuboid, one for each side of the aircraft. Therefore, each cuboid consists of 7 passengers. The mass components are subdivided in four categories

Table 13.4: Assumed shapes for moment of inertia determination.

DATCOM	**Cylinder**	**Cuboid**		**Point Mass**
Fuselage	Main motors (2x)	Blown wing motors (2x)	Fuel system	Nose landing gear
Wing	Generators	Cabin equipment	Reserve fuel (2x)	Trapped fuel and oil
Horizontal tail		Internal combustion engines	Crew (2x)	Main landing gear (2x)
Vertical tail		Inverters (2x)	Passengers (14x)	
		Battery (2x)	Cargo (2x)	
		Used fuel (2x)		

before evaluation. Elements which can be closely modelled as a simplified shape, are either modelled as a cylinder or cuboid. Elements for which the shape is difficult to determine and have a small mass are modelled as point mass since their moment of inertia excluding Steiner term will be negligible.

For the fuselage, wing, horizontal stabilizer and vertical stabilizer a more accurate method is required to determine the moment of inertia. This is due to their complex shape, size and significant mass contribution. The DATCOM method is applied for these elements. DATCOM provides a specific method to determine the moment of inertia for these elements within 10% of the actual value. As an input for the DATCOM method, general geometric parameters of the aircraft are required. From here on a set of semi-empirical relations are used to determine the moment of inertia for roll (x-axis), pitch (y-axis) and yaw (z-axis) [69].

However, also for the DATCOM method, the locations of the center of gravity are required. For all the elements which are stored in the wing, an even mass distribution is assumed and the center of gravity locations is determined by evaluating a trapezoidal shape. The location of the center of gravity for elements inside the fuselage is obtained by evaluating the cabin layout.

The final results which are obtained from this analysis are given in Table 13.5.

Table 13.5: Moments of inertia of the E-COmmuter.

	K_X^2	K_Y^2	K_Z^2	K_{XZ}
Value	0.02135	3.031	0.04219	0

13.4.2. Dynamic Stability

The EOM for symmetric and asymmetric flight respectively are given in matrix form in Equation 13.11 and Equation 13.12 [32].

$$\begin{bmatrix} C_{X_u} - 2\mu_c \cdot D_c & C_{X_\alpha} & C_{Z_0} & 0 \\ C_{Z_u} & C_{Z_\alpha} + (C_{Z_{\dot{\alpha}}} - 2 \cdot \mu_c) \cdot D_c & -C_{X_0} & C_{Z_q} + 2 \cdot \mu_c \\ 0 & 0 & -D_c & 1 \\ C_{m_u} & C_{m_\alpha} + C_{m_{\dot{\alpha}}} \cdot D_c & 0 & C_{m_q} - 2 \cdot \mu_c \cdot K_Y^2 \cdot D_c \end{bmatrix} \begin{bmatrix} \hat{u} \\ \alpha \\ \theta \\ \frac{q\bar{c}}{V} \end{bmatrix} = \vec{0} \quad (13.11)$$

$$\begin{bmatrix} C_{Y_\beta} + (C_{Y_{\dot{\beta}}} - 2 \cdot \mu_b) \cdot D_b & C_L & C_{Y_p} & C_{Y_r} - 4 \cdot \mu_b \\ 0 & -\frac{1}{2} \cdot D_b & 1 & 0 \\ C_{l_\beta} & 0 & Cl_p - 4 \cdot \mu_b \cdot K_X^2 \cdot D_b & C_{l_r} + 4 \cdot \mu_b \cdot K_{XZ} \cdot D_b \\ C_{n_\beta} + C_{n_{\dot{\beta}}} \cdot D_b & 0 & C_{n_p} + 4 \cdot \mu_b \cdot K_{XZ} \cdot D_b & C_{n_r} - 4 \cdot \mu_b \cdot K_Z^2 \cdot D_b \end{bmatrix} \begin{bmatrix} \beta \\ \phi \\ \frac{p \cdot b}{2 \cdot V} \\ \frac{r \cdot b}{2 \cdot V} \end{bmatrix} = \vec{0} \quad (13.12)$$

In order to analyze the dynamic stability of the aircraft the eigenvalues that define the eigenmotions of the aircraft need to be found. This can be done by programming the matrices into Python with the stability derivatives as found by DATCOM as in Table 13.2 and Table 13.3.

Now, the eigenvalues of the matrices can be found in Python by replacing the D_c and D_b by eigenvalues λ_c and λ_b respectively, taking the determinant characteristic equation and solving for the unknown eigenvalues. These eigenvalues can be used to calculate the eigenmotions of the E-COmmuter. The results are given in Table 13.6.

Table 13.6: E-COmmuter eigenmotions.

Eigenmotion	Eigenvalue	P	$T_{\frac{1}{2}}$	ω_0	ζ
Symmetric eigenmotions					
Short period	$\lambda_{c_{1,2}} = -1.8839 \pm 2.0596i$	2.9822 s	0.3584 s	2.8596 Hz	0.6762
Phugoid	$\lambda_{c_{3,4}} = -0.0104 \pm 0.0919i$	37.159 s	247.25 s	0.1691 Hz	0.0166
Asymmetric eigenmotions					
Aperiodic roll	$\lambda_{b_1} = -4.2328$	-	0.1591 s	-	-
Spiral	$\lambda_{b_2} = 0.0007$	-	–958.3 s	-	-
Dutch roll	$\lambda_{b_{3,4}} = -0.1754 \pm 0.9760i$	5.4097 s	4.0561 s	1.1740 Hz	0.1455

From Table 13.6 it can be concluded that all motions are stable, except for only the spiral motion. Three of these motions have to comply with CS-23 regulations. The short period should be heavily damped, as is the case. Namely, the half time is significantly shorter than the period. The phugoid is stable, thus it complies too. Last, the Dutch roll motion damps to less than $\frac{1}{10}$ of its original amplitude within 7 cycles, as can be easily calculated. As a result, the dynamic stability of the aircraft is sufficient.

13.5. Blown Wing Integration and Control Applications

The choice of a novel distributed blown wing propulsion system offers a significant number of benefits to the performance and aerodynamics of the aircraft, as is extensively discussed in chapter 11. Additionally, distributed propulsion might also prove to be beneficial to the control system, especially for lateral dynamics. It could take on a partial role as 'control surface', (partially) replacing the conventional systems. Moreover, it is assessed on its ability to offer a sustainable redundancy in case of failure of aircraft components. Here, these applications are investigated.

13.5.1. Equations of Motion

For the analyses described, it is needed to find and alter the equations of motion for asymmetric flight given in Equation 13.12 to fit the novel aircraft's lateral motion. For the sake of simplicity it is assumed that during asymmetric flight, the aircraft remains in horizontal, steady flight conditions. Furthermore, an addition has to be made to the standard set of equations to account for the contribution of the distributed propulsion. With the assumptions made in section 13.3, the result is the following set of equations:

$$\begin{bmatrix} C_{Y_\beta} & C_L & -4\cdot\mu_b & 0 & C_{Y_{\delta_r}} & 0 \\ C_{l_\beta} & 0 & C_{l_r} & C_{l_{\delta_a}} & 0 & C_{l_m} \\ C_{n_\beta} & 0 & C_{n_r} & 0 & C_{n_{\delta_r}} & C_{n_m} \end{bmatrix} \begin{bmatrix} \beta \\ \phi \\ \frac{r\cdot b}{2\cdot V} \\ \delta_a \\ \delta_r \\ 1 \end{bmatrix} = \begin{bmatrix} 0 \\ 0 \\ 0 \end{bmatrix} \tag{13.13}$$

The coefficient C_{n_m} represents the total moment around the top axis (yaw) caused by the distributed propulsion, which is given by:

$$C_{n_m} = \sum_{\text{motors}} k \cdot \frac{T_{\text{motor}} \cdot y_{\text{motor}}}{\frac{1}{2}\cdot\rho\cdot V^2\cdot S\cdot b} \tag{13.14}$$

In this equation k is the scale factor, which is assumed to be 2 for high-wing propeller aircraft [32], T is the thrust of one motor, and y is the distance from the line of action of the thrust vector of the considered motor to the plane of symmetry of the aircraft. It is divided by $\frac{1}{2}\rho V^2 Sb$ to make the coefficient dimensionless.

The coefficient C_{l_m} is the second addition due to the distributed propulsion. It represents the caused moment around the longitudinal axis (roll) of the aircraft. It is given by:

$$C_{l_m} = \sum_{\text{motors}} \frac{\Delta C_{L_{\text{motor}}} \cdot y_{\text{motor}} \cdot d_{\text{prop}_{\text{motor}}} \cdot c_{\text{motor}}}{S\cdot b} \tag{13.15}$$

In which ΔC_L is the change in lift coefficient of due to one motor and y is its distance to the longitudinal axis. The parameters d and c are the diameter of the propeller and chord at the location of the propeller respectively, which multiplied define the affected area behind the motor. The reference area S and span b are added to make the coefficient non-dimensional.

These two equations give the contributions to the equations of motion of all motors combined in a compact form, which can easily be used in further analyses. In python, this structure is represented by three lists for T_{motor}, $\Delta C_{L_{\text{motor}}}$, and y_{motor} for all motors along the span.

13.5.2. Turning Behaviour

The most promising application for the blown wing is to be used as a feature that can control the roll and yaw and, subsequently, turns of the aircraft. For the assessment a right-hand turn is considered for stall speed at sea level at MTOW. This is the least controllable speed, altitude and weight. The turn consists of three parts: initiating the turn, steady turn, and roll-out. Also, these calculations can later be used to size the ailerons of the aircraft.

First, the required moment coefficients for the turn are calculated. For initiation of the turn, the following idealized equation is used:

$$C_{l_{m,\text{initiate}}} = -C_{l_p} \cdot \frac{p \cdot b}{2 \cdot V} \tag{13.16}$$

In which $\frac{p \cdot b}{2 \cdot V}$ is the non-dimensional roll rate, which follows from CS-23 regulations. By CS-23, $p_{\max}$ is 60° in 7 s for the E-COmmuter. This is equal to 0.15 rad s^{-1} which is rather conservative. According to Gudmundsson [25], a more common higher number for $p_{\max}$ is 0.5 rad s^{-1}, which is used for the analysis here. Solving the equation, a needed roll coefficient is found of $C_{l_{m,\text{initiate}}} = 0.0765$.

For the constant in-turn analysis, Equation 13.13 can be altered to represent coordinated turns. This means that $\beta = 0$. Also, in order to fully analyze the capabilities of the blown wing, the aileron and rudder deflections are set to 0 ($\delta_a = 0$ and $\delta_r = 0$), so that all control moments result solely from the blown wing motors. Also, to check the most constraint turn for control purposes, roll angle ϕ is set to 60°; the angle for a steep turn, the largest angle that needs to be achieved for a commuter aircraft via CS-23 regulations. In the EOM three unknowns $\frac{r \cdot b}{2 \cdot V}$, C_{l_m}, and C_{n_m} remain. Solving for these, one finds the coefficients $C_{l_{m,\text{turn}}} = -0.0015$, and $C_{n_{m,\text{turn}}} = 0.0007$.

Last, the aircraft needs to roll out of the turn. In this procedure the blown wing roll moment needs to provide both the moment to stay in turn, additional to the moment required for the regulated roll rate. Therefore, turn roll-out is the most important constraint, and is given by:

$$C_{l_{m,\text{roll-out}}} = C_{l_{m,\text{minimum}}} = -C_{l_{m,\text{initiate}}} + C_{l_{m,\text{turn}}} = -0.0781 \tag{13.17}$$

In order to check the feasibility of using the blown wing as aileron or rudder control, the maximum values of C_{l_m} and C_{n_m} that the blown wing motors can provide need to be calculated. This is achieved by turning the blown wing propellers on the left wing on maximum thrust and the right wing off. The large motors do not provide asymmetric thrust and are both normally operated on maximum power. For C_{l_m}, the maximum ΔC_L values are given in chapter 10, which are 0.15 for the large motors and 0.0437 for the small motors. For C_{n_m} the maximum thrust is 3120 N for the large motors and 250 N for the small motors. By Equation 13.14 and Equation 13.15, the maximum attainable coefficients are $C_{l_m} = 0.0040$ and $C_{n_m} = 0.0420$.

Unfortunately, the roll moment generated by the blown wing is not large enough to be able to actively provide primary roll control. However, what can be concluded is that the blown wing produces a significant yawing moment when activated. This might cause some complications if motors fail, and should thus not be overlooked. Therefore, an engine failure analysis is performed later in this chapter.

13.5.3. Aileron Sizing

As follows from the assessment of the blown wing control applications, the aileron need to be sized as well for the speed regimes in which the blown wing cannot be used. The starting point for the aileron sizing is the minimum required roll moment to roll out of a turn, as this was found to be the most constraining parameter. For use with ailerons, the following equation holds:

$$C_{l_{m,\text{roll-out}}} = C_{l_{\delta_a}} \cdot \delta_{a,\text{roll-out}} \tag{13.18}$$

The sizing of the aileron dimensions is dependent on the value of $C_{l_{\delta_a}}$. Thus, an expected aileron deflection $\delta_{a,\text{roll-out}}$ needs to be assumed. Common maximum aileron deflections of similar aircraft are around 20° [71]. According to Gudmundsson [25], the in-flight deflection may be as much as 75% of this maximum. Therefore, $\delta_{a,\text{roll-out}}$ is assumed to be 15° or 0.262 rad. This results in a aileron effectiveness of $C_{l_{\delta_a}} = -0.298$.

For the sizing of the aileron, Equation 13.19 is used for the straight tapered wing of the E-COmmuter [25], with dimensions as in Figure 13.4.

$$C_{l_{\delta_a}} = \frac{c_{l_{\delta_a}} \cdot c_{\text{root}}}{S \cdot b} \cdot \left(\left(b_2^2 - b_1^2\right) + \frac{4 \cdot (\lambda - 1)}{3 \cdot b} \cdot \left(b_2^3 - b_1^3\right) \right) \tag{13.19}$$

In Equation 13.19 the parameter that needs to be estimated is the inboard position of the aileron b_1. The parameters c_{root}, S, b, and λ are all known from the sizing of the aircraft. Parameter b_2 is the outboard edge of the aileron and is set to 0.5 m from the edge of the wing to leave some spacing for the structures of the wing tip, thus $b_2 = 9.98$ m. This leaves the unknown $c_{l_{\delta_a}}$.

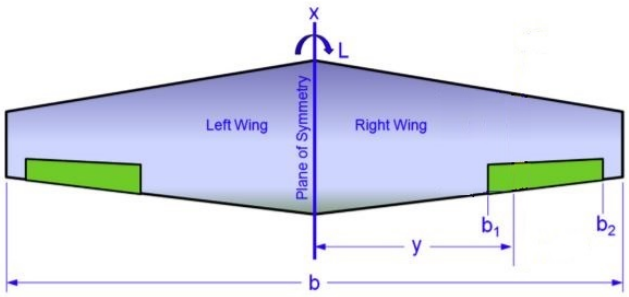

Figure 13.4: Definition of aileron geometry [25].

The parameter $c_{l_{\delta_a}}$ gives the increase in airfoil lift coefficient with aileron deflection. In order to estimate this value, an aerodynamic analysis was done to assess the effect of the aileron by use of XFoil[2]. The coordinates of the NASA/LANGLEY LS(1)-0417 (GA(W)-1) airfoil are loaded into the program, which are available online[3]. In XFoil, the aileron is simulated via addition of a flap. The flap hinge point is set on the camber line at an $\frac{x}{c}$ of 0.8 of the chord as to not interfere with aft spar which is located at 0.72 of the chord (see section 10.3). Then, for five different flap deflections ranging from -15° to +15°, the C_L is assessed for stall speed at sea level. The five points are fitted with a linear relationship which results in $c_{l_{\delta_a}} = 4.01\,\text{rad}^{-1}$.

Now, one can solve Equation 13.19 for the unknown b_1, which is found to be 7.343 m. This results in a aileron width of 2.64 m, with a length of 0.2 of the local chord.

13.5.4. Engine Failure Analysis

As is concluded from the blown wing control applications, an important part of the blown wing integration in the stability & control subsystem is to perform an engine failure analysis. For this analysis, the same EOM are used as given in Equation 13.13 at low speed at sea level. To check the effect of engine failure, these are altered such that the state of flight is coordinated straight flight such that $\beta = 0$ and $\frac{rb}{2V} = 0$. The roll and yaw effects of the engine failure C_{l_m} and C_{n_m} are calculated per respective engine failure case. For this, the most critical engine failure characteristics needs to be identified. The remaining unknowns are the required aileron deflection δ_a, rudder deflection d_r and roll angle ϕ. For the aileron, $C_{l_{\delta_a}}$ was found with the aileron sizing. The rudder deflection coefficients $C_{n_{\delta_r}} = -0.1$ and $C_{Y_{\delta_r}} = 0.3$ were taken from reference aircraft in Mulder et al. [32].

The cases are the two most critical engine failures that are most likely to occur in flight follow from the propulsion system architecture from chapter 12. These involve the failure of one of the main engines, one of the main blown wings, or both. Failures of the right wing motors are considered. For all cases, the T and ΔC_L lists are appended in Python to represent the case to find the corresponding C_{l_m} and C_{n_m}, and the EOM are solved for the stated unknowns. The results are depicted in Table 13.7.

Failure case	δ_a	δ_r	ϕ
Main motor failure	0.2068°	13.386°	−17.46°
Blown wing failure	0.7688°	24.073°	−31.39°
Full failure	1.0993°	37.459°	−48.85°

Table 13.7: Required aileron and rudder deflection and roll angle in order to maintain straight coordinated flight during engine failures.

From Table 13.7, a number of observations can be made. See the list below.

- All engine failure cases require only small aileron deflection, which follows from the small roll moment the motors generate.
- Main motor failure on one side of the wing is not critical, as it requires a rudder deflection of 13.4°, which are easily achievable by normal aircraft.
- Blown wing failure results in more constraining values. A rudder deflection of 23.1° is substantially large, although not entirely impossible, as many rudders can provide deflections up to 30°. A roll angle of 31° is also significantly large. But this value is not unexpected with the large lateral force due to the rudder deflection to counteract the large blown wing yawing moment.
- A full wing motor failure would almost certainly result in unrecoverable loss-of-control of the aircraft. Required rudder deflections of up to 37.5° are too large for normal rudders and roll angles of 48.9° are very high, and furthermore

[2]URL: `http://web.mit.edu/drela/Public/web/xfoil/` [cited 19 June 2018]
[3]URL: `http://airfoiltools.com/airfoil/details?airfoil=ls417-il` [cited 19 June 2018]

close to upset bank angles of over 60°.

In conclusion, a situation with the failure of all motors of one wing should be avoided at all cost. For this reason, in chapter 12 a large number of redundancies have been built in with regard to the failure of motors. First, for both the outboard and inboard blown wing motors, the inverters are installed such that if they fail, the blown wing motors fail symmetrically. Also, the main wing engines both have two inverters, making failure less likely. The odds of the third case occurring in flight are thus extremely small. It also makes the second case less critical. From this, it can be concluded that the E-COmmuter has been properly designed to be redundant to motor failures from a control perspective.

13.5.5. Rudder Sizing

The rudder sizing of the aircraft can be done similarly to the aileron sizing. The difference with aileron sizing is however that the rudder sizing is based on the engine inoperative asymmetric thrust requirements [25]. Thus, with the failure analysis performed in the previous section, the rudder of the E-COmmuter can be sized.

The starting point is the needed yaw moment coefficient for second motor inoperative case, as it was found that the third case was too unlikely and extreme to reasonably size for. Therefore, the next to most critical second case is chosen sizing requirement. Evaluating the results from this case, the required yaw moment coefficient is found to be $C_{n_m} = 0.0420$. This logically is the same as the maximum yaw moment as found for blown wing turning behaviour. Then the following equation can be applied:

$$C_{n_m} = C_{n_{\delta_r}} \cdot \delta_r \tag{13.20}$$

Which is rudder variant of Equation 13.18. Maximum rudder deflection of 30° and 75% of that in-flight is assumed, resulting in $\frac{22.5°}{0.393\,\text{rad}}$, so that the sizing is slightly more conservative as found in the engine failure analysis (23.1°). The required rudder effectiveness is found to be $C_{n_{\delta_r}} = 0.107$.

Then, again XFoil is used to find the deflection effectiveness of the rudder. The used airfoil is the symmetric NACA 0012 airfoil, which is integrated in XFoil. The hinge is set at 0.8 and the C_L is evaluated from -30° to +30°. In the same way as for the aileron, the effectiveness found is $c_{l_{\delta_r}} = 3.75\,\text{rad}^{-1}$.

Then, for the rudder size the following equation from Sadraey [71] can be used, assuming the pressure ratio of the wing and vertical tail is 1:

$$C_{n_{\delta_r}} = -c_{l_{\delta_r}} \cdot \frac{l_{VT} \cdot S_{VT}}{S \cdot b} \cdot \frac{b_R}{b_{VT}} \tag{13.21}$$

Filling in this equation and calculating, the required rudder width is found: $b_R = 1.37\,\text{m}$.

13.6. Safety and Pilot Interface

For the stability & control subsystem, some extra consideration should be taken into account with respect to safety and sustainability. From investigation in the baseline and midterm reports [4][6], it was found that loss-of-control due to upset conditions, including stall, are one of the main threats to the safety of the stability & control subsystem. As a result, a number of technical risk requirements are added to the requirement list in chapter 4. In the light of upset prevention, requirements **HEF-SC-09** through **HEF-SC-12** should be considered.

- **HEF-SC-09 & HEF-SC-10.** The stability & control subsystem does actively deter pilots from causing upset conditions and can inherently recover, as the aircraft is designed to be longitudinally stable. When a stall is to occur or actually occurs, the aircraft has a nose-down tendency, that can recover from the stall.
- **HEF-SC-11 & HEF-SC-12.** Actual sizing has not yet taken place to meet these two requirements. However, it is decided that in further design stages, the flight interface of the aircraft should be chosen and a stall warning should be installed.

In general, these requirements apply to the flight deck design of the E-COmmuter. As mentioned, the design of this system is out of the scope of this report. However, it is recommended that the flight deck design should start as soon as possible after continuing the project, in combination with the design of an electronic control unit to control the aircraft in normal and unusual flight conditions. This is important as the pilot interface is one of the most essential components required for safe operation of the aircraft, including navigation, communication and avionic systems.

A second consideration performed with regard to the safety of the stability & control of the aircraft is the possibility of a deep stall. In this situation the main wing of a T-tailed aircraft stalls, after which the horizontal tail is in its wake, such that this loses its recoverable function. For the E-COmmuter, no detailed analysis of this problem has been done yet, but a number of considerations are taken into account that might mitigate the risk of a deep stall slightly.

First, the blown wing re-energizes the boundary layer of the wing, or at least directs its flow. This might provide flow over the horizontal tail, even when the wing has stalled. Second, the wing of the E-COmmuter is placed very aft. This means that the possibility of a deep stall are significantly lowered, as the angles of attack needed for the horizontal tail to be in the stalled wing wake become unusually large.

13.7. Verification and Validation

Location of Center of Gravity for Operating Empty Weight

The main landing gear is placed with respect to the positioning of the main wing. All of the elements in the calculation for the center of gravity location in longitudinal location where correct. However, for the determination of the vertical position of the c.g. the assumption has been made that the weights inside the wing coincide with the center line of the root cord. This is a reasonable assumption because the wing has a dihedral angle of only 1°. However, for the main landing gear this is not valid since this is placed underneath the fuselage. This has been changed in the Python program.

Loading & Balance Diagram

The program that is able to generate the loading & balance diagram is verified by means of using an example. This example considers a surveillance aircraft. The aircraft falls within a different category, but the loading & balance diagrams are based on the same principles for every aircraft. It is checked whether or not the program is able to generate the same loading diagram as in the example. The exact same loading diagram could be made. Furthermore, part of the calculations are checked by hand.

Scissor Plot

Before the scissor plot is created, all of the coefficient are checked to see if their magnitude and sign is feasibility. These checks are performed comparing the values of reference aircraft. Moreover, one full iteration is done by hand to check if the output of the Python program matched the calculations. Last of all, outputs of Torenbeek and DATCOM are compared. The obtained scissor plot is checked by looking at the locations of both lines, with respect to the x- and y-axis.

After combining the scissor plot with the loading diagram, the obtained values for the horizontal tail surface are checked with reference aircraft. Compared to these aircraft, the main wing is placed more aft. This is can be explained by the fact that the engines are placed in the tail cone section of the aircraft. Also, a lot of weight moves along with the wing since they are placed in the wing box. Since the main wing is placed more to the back of the aircraft, the tail arm is decreasing. The required area for the horizontal tail is slightly higher compared to reference aircraft.

Moment of Inertia

The moment of inertia determination is verified by comparing the obtained results with the example calculation which is provided by DATCOM [69]. The example given is slightly bigger and it is therefore not suitable to compare the results by using absolute values. Instead, a relative comparison is performed. For each component a moment of inertia is obtained for roll, pitch and yaw. The ratio between these three values should be roughly the same by comparing the example results with the calculated values. However, it is also possible that the overall magnitude for a certain component is off. To check for this the ratio of the moments of inertia of different components is compared with the data from the example. In order to verify the value of the elements for which DATCOM is not applied the input values are checked, to see if they are feasible. All the obtained moments of inertia are put into Excel to detect any outliers. Both their size and location on the aircraft is taken into consideration to determine if the obtained moments of inertia are feasible or not.

After the verification of the individual elements, the obtained radii of gyration are verified. To perform verification these values they are compared to radii of gyration which are given in appendix D of Mulder et al. [32]. From here no issues were found with K_X^2 and K_Y^2 since they matched the reference data. However, the value for K_Y^2 was not close to the values for comparable aircraft. After some research a mistake is found in the list of symbols of Mulder et al. [32]. To obtain the non-dimensional factor K_Y^2, I_Y should be divided by $m\bar{c}^2$ instead of mb^2. After correction of this mistake the correct value of K_Y^2 is obtained.

Eigenmotions

For the verification of the dynamic stability of the E-COmmuter, the aircraft model with the same dimensions as input in DATCOM is built in the XFLR5 program[4]. One drawback of the program is that XFLR5 does not support fuselage inputs accurately. Therefore, only the wing and empennages of the aircraft are loaded into the program. This affects the reliability of the aircraft, which needs to be assessed. XFLR5 has a dynamic stability analysis tool, which after input of the cruise flight conditions and mass moments of inertia outputs the eigenvalues of the aircraft model. For the analysis of the E-COmmuter, the eigenvalues of Table 13.8 are found.

As can be seen in the table significant differences exist between the used method and XFLR5. However, all differences are within 100%. In a dynamics context this means that all eigenmotions still have the same characteristics. In both methods all motions are stable, with exception of the spiral mode. This result is is ultimately the most important goal of the eigenmotion analysis. For all eigenmotions, XLFR5 gives less stable values, with higher frequencies. Judging from the fact that XFLR5 is less accurate due to not including the effect of the fuselage, but still meeting the stability requirements, the method used in subsection 13.4.2 is verified.

Validation of dynamic stability should take place in the further design process by use of wind tunnel or flight tests.

[4] URL: `http://www.xflr5.com/xflr5.htm` [cited 19 June 2018]

Table 13.8: XFLR5 E-COmmuter eigenmotions.

Eigenmotion	Eigenvalue	Difference real part	Difference imaginary part
Symmetric eigenmotions			
Short period	$\lambda_{c_{1,2}} = -1.2849 \pm 3.2114i$	-32%	+55%
Phugoid	$\lambda_{c_{3,4}} = -0.0002 \pm 0.1532i$	-98%	+67%
Asymmetric eigenmotions			
Aperiodic roll	$\lambda_{b_1} = -2.9909$	-29%	-
Spiral	$\lambda_{b_2} = 0.0233$	+32%	-
Dutch roll	$\lambda_{b_{3,4}} = -0.1749 \pm 1.7591i$	0%	+80%

Control Surface Sizing

For the verification of the control surface sizing, XFLR5 can also be used. To the model in the program as described in the verification of the eigenmotions, aileron and rudder surfaces are added with the dimensions as calculated. Then, a control deflection analysis is performed at maximum in-flight aileron and rudder deflection, and low speed at sea level. Then XFLR5 can calculate the generated moment coefficients. The results are given in Table 13.9.

Table 13.9: XFLR5 control surface moment analysis

Control surface	Coefficient	Needed coefficient	Difference
Aileron deflection	$C_l = -0.10997$	$C_{l_{m,\text{roll out}}} - 0.0781$	+41%
Rudder deflection	$C_n = 0.04355$	$C_{n_m} = 0.0420$	+4%

From the table it can be concluded that the aileron sizing performed in section 13.5 is more conservative than needed according to XFLR5. But again, due to accuracy issues with XFLR5 with regard to the fuselage, conservativeness is required. Next to this, it can be immediately concluded that the rudder sizing is accurate with a difference between the coefficients of +4%. With these results, it can be concluded that the control surface sizing is verified. However, to also validate the used methods, wind tunnel tests and flight tests are needed in further design phases.

13.8. Results

The analyses carried out above results in the values given in Table 13.10. Here, MZFW is the maximum zero fuel weight.

Table 13.10: Results obtained from the stability & control analyses.

Parameter	Symbol	Value	Unit	Parameter	Symbol	Value	Unit
Stability & controllability							
Max forward c.g. location	$x_{\text{c.g.}_{\text{min}}}$	18.8	% MAC	Wing position	X_{LEMAC}	48.0	% l_{fuselage}
Max aft c.g. location	$x_{\text{c.g.}_{\text{max}}}$	50.5	% MAC	MTOW c.g. position	$x_{\text{c.g.}_{\text{MTOW}}}$	33.0	% MAC
Horizontal tail size	$\frac{S_h}{S}$	25.6	% S	MZFW c.g. position	$x_{\text{c.g.}_{\text{MZFW}}}$	32.5	% MAC
OEW c.g. position	$x_{\text{c.g.}_{\text{OEW}}}$	37.0	% MAC	Operational Empty Weight	OEW	4280	kg
Dynamic stability							
Radius of gyration x-axis	K_X^2	0.021	-	Radius of gyration y-axis	K_Y^2	3.031	-
Radius of gyration z-axis	K_Z^2	0.042	-	Radius of gyration xz-axis	K_{XZ}	0	-
Short period eigenvalue	$\lambda_{\text{c}_{1,2}}$	$-1.8839 \pm 2.0596i$		Aperiodic roll eigenvalue	λ_{b_1}	-4.2328	
Phugoid eigenvalue	$\lambda_{\text{c}_{3,4}}$	$-0.0104 \pm 0.0919i$		Spiral eigenvalue	λ_{b_2}	0.0007	
				Dutch roll eigenvalue	$\lambda_{b_{3,4}}$	$-0.1754 \pm 0.9760i$	
Blown wing integration and control							
Max roll rate	p	0.5	rad s^{-1}				
Turn initiation roll moment	$C_{l_{m,\text{initiate}}}$	0.077	-	Stay-in-turn roll moment	$C_{l_{m,\text{turn}}}$	-0.0016	-
Roll-out roll moment	$C_{l_{m,\text{roll-out}}}$	-0.078	-	Stay-in-turn yaw moment	$C_{n_{m,\text{turn}}}$	0.0007	-
Blown wing roll moment	C_{l_m}	-0.0040	-	Blown wing yaw moment	C_{n_m}	0.0420	-
Control surface sizing							
Max aileron deflection	$\delta_{a_{\text{max}}}$	20.0	°	Max rudder deflection	$\delta_{r_{\text{max}}}$	30.0	°
In-flight aileron deflection	$\delta_{a,\text{roll-out}}$	15	°	In-flight rudder deflection	δ_r	22.5	°
Aileron length	c_a	20.0	% c	Rudder length	c_R	20.0	% c_{VT}
Aileron width	b_a	2.64	m	Rudder width	b_R	1.37	m

14

Tail & Landing Gear Design

Based on the chapter 13 on stability & control, the tail and landing gear can be positioned and sized. In this chapter, first the tail design is explained and afterwards, both the main and nose landing gear are positioned and sized, based on the static loads they have to be able to sustain.

14.1. Tail Design

In the following section, the design of the tail section of the aircraft is discussed. During the design trade-off, a T-Tail configuration is chosen. The horizontal tail is designed first since this also influences the design of the vertical tail. Last of all, the dorsal fin is designed to improve directional stability of the aircraft. The obtained dimensions of all tailplanes are given at the end of this chapter in Table 14.4.

Some wing parameters are based on values of reference aircraft. From literature, a list is created of reference aircraft with a T-Tail configuration. For the determination of the required vertical tail area, aircraft are selected which have a similar passenger capacity and mission profile. The data set for this list are given in Table 14.1 and Table 14.2.

The tail design is preliminary and primarily based on stability and control requirements. No structural analysis of the tail is performed.

14.1.1. Horizontal Tail Design

In subsection 13.2.3, the required horizontal tail area is determined. From here the final geometry of the horizontal tail can be determined. From the reference aircraft, given in Table 14.1 the average aspect ratio, taper ratio and leading edge sweep angle is extracted. Together with the required wing area, the other geometry parameters such as span, root and tip chords, are determined.

From the detailed weight calculations in chapter 9 and chapter 10, it becomes clear that the Class II weight estimation can be considered validated. Since no structural analysis is performed on the horizontal tail, its weight is taken to be the one resulting from the Class II weight estimation.

The material to be used to construct the horizontal tail is Aluminum alloy Al2024, similarly to the fuselage. This is a commonly used material for aircraft structures: it s relatively lightweight, provides high strength and has good fatigue resistance. It is also cheaper than other options (such as GLARE).

14.1.2. Vertical Tail Design

After the horizontal tail is designed, in subsection 14.1.1, the design of the vertical tail can be evaluated. Because of the T-tail configuration, the horizontal stabilizer needs to be connected on top of the vertical stabilizer. The tip cord of the vertical stabilizer will therefore be equal to the root cord of the horizontal stabilizer. Besides the determination of the tip chord, some other general parameters of the vertical tail need to be determined. From the reference aircraft data, an average aspect ratio and leading edge sweep is determined [25]. However, since the wing is placed relatively aft of the fuselage, the average parameters are resulting in an ineffective shape. The aspect ratio is therefore increased to 1.2 and the sweep is decreased to 35°. By having a larger aspect ratio, the aircraft encounter deep stall at higher angles of attack. A change of these parameters does not cause a significant effect in the performance of the vertical tail, and is still within the advised range provided by Roskam [72].

The last parameter for designing the vertical tailplane is the required vertical tail area. This is determined by using the tail volume coefficient method, given in Equation 14.1. This method relates the required vertical tail area, by using the vertical tail arm (l_{VT}), span of the main wing (b_{REF}), and main wing area (S_{REF}) [25].

$$S_{VT} = \frac{V_{VT} \cdot b_{REF} \cdot S_{REF}}{l_{VT}} \tag{14.1}$$

The vertical tail volume coefficient (V_{VT}) is obtained from the same set of reference aircraft, given in Table 14.2. Since all the other parameters are known, the required tail area can be obtained. From here the other parameters of the vertical are determined and given in the results section.

Similarly to the horizontal tail, the vertical tail's mass is based on the Class II weight estimation and the structure is made out of Al2024.

14.1.3. Dorsal Fin

In front of the aircraft, a dorsal fin is added. This provides additional directional stability at high yaw angles. The sweep of a dorsal fin is higher than the sweep of the regular vertical tail. Due to the dorsal fin, the sideways force coefficient locally decreases in magnitude but the stall angle increases. The dorsal fin can therefore be used to prevent rudder-locking. Rudder-locking occurs when the aircraft the vertical tail stalls and the pilot must apply reverse rudder forces to get out of stall. Since the dorsal fin has a higher stall angle, the rudder-lock can be postponed [25][73].

To size the dorsal fin, reference values are obtained from other aircraft. For these aircraft the sweep of the dorsal fin is roughly equal to double the sweep at the leading edge of the vertical tail. The high sweep angle is required to provide enough benefit for preventing rudder locking. To limit the size of the dorsal fin, the sweep is equal to 80°. The chord extension is equal to 0.6 times the root cord of the vertical tail. The values are within the conventional regions which are described in Nicolosi et al. [73].

The dorsal fin is made out of Al2024.

Table 14.1: Tail parameters for reference aircraft with a T-tail configuration [25].

Aircraft	A_h	λ_h	Λ_{LE_h}	A_v	λ_{LE_v}
Yakovlev	4.33	0.43	11.5°	0.81	47.5°
Fokker VFW	3.83	0.48	27.5°	1	40°
BAC-111	3.38	0.6	25°	0.91	41°
DC-9	4.21	0.31	32°	0.95	43.5°
B727	3.4	0.4	35°	0.78	55°
Lockheed C-5A	4.89	0.364	24.5°	0.84	34.9°
Average	4.01	0.43	25.92°	0.93	44.84°

Table 14.2: Tail volume coefficients of comparable sized aircraft [25].

Aircraft	**Tail volume coefficient**
Beechcraft Baron G58	0.0464
Beechcraft Duchess	0.0477
BN-2 Islander	0.0489
Partenavia P68	0.0488
MD415	0.0414
Average	0.0466

14.2. Landing Gear Design

The landing gear configuration for the aircraft is a tricycle configuration. This the most conventional configuration of similar sized aircraft. After creating Figure 13.3, a range of possible center of gravity locations is obtained. The locations of the center of gravity form the basis of placing the landing gear, which is described in subsection 14.2.1. Afterwards, the landing gear struts, wheels, dampers and tires are designed in subsection 14.2.2.

14.2.1. Landing Gear Positioning

Together with the final position of the wing, the longitudinal location of the main landing gear can be determined. The main requirement for placing the nose & main gear are the minimum and maximum loads on the nose landing gear. According to Roskam [27] the nose gear loads should be between 8-15%, for the most aft and forward c.g. locations respectively. By looking at Figure 13.3, as significant range of centers of gravity is visible. The nose landing gear loads are therefore increased to 8-17%.

The vertical position of the landing gear is based on the required scrape angle for takeoff and landing. The scrape angle should be at least 15° to guarantee safety during a landing with flaps deployed. Furthermore, the landing gear should be at least 65 cm from the ground due to size of the nose wheel tires. For the main landing gear this is not a requirement since this is placed on the outside of the fuselage. After the height of the fuselage is set, a final check for the location of the centre of gravity needs to be performed. By rotating the aircraft at the scrape angle, the center of gravity is not allowed to rotate aft of the main landing gear. This requirement is met when the angle between main gear and the center of gravity is greater than the scrape angle. This angle is referred to as the Beta angle, see Figure 14.2.

The last element that is left for determining the location of the landing gear is the lateral location of the main gear. To determine this, there are two requirements. First of all there should be enough propeller clearance, both clearance distance and in roll angle, as can be seen in Figure 14.1. Requirement CS-23.925 states that there should be at least 18 cm clearance between the tips of the propeller blades and the ground [24]. Moreover, there should also be enough ground clearance when the aircraft rolls during landing. Given that the total distance from the lowest propeller to the ground is about 1 m, there is always enough clearance, both in terms of angles and distance. Therefore, the lateral clearance is not constraining the lateral position of the main gear.

Another requirement for the lateral position of the main gear, is that the aircraft should not overturn when it is making sharp corners. Since a significant amount of the weight is stored in the high wing, the vertical position is also relatively high. The so-called overturn angle Ψ should not exceed 55° [27]. The overturn angle can be evaluated by using

methods described in Torenbeek [23]. The final location of the lateral position of the center of gravity is obtained by taking the maximum amount of required distance for the propeller clearance as well as the overturn angle.

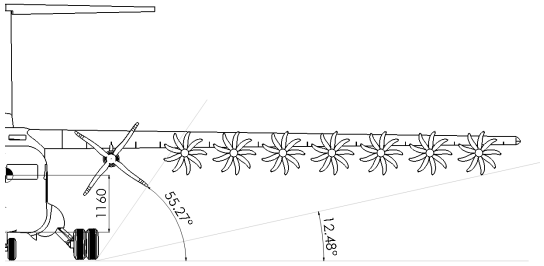

Figure 14.1: Main and outside propeller clearance angles, Φ_1 and Φ_2.

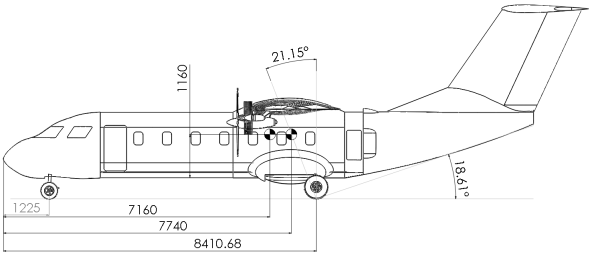

Figure 14.2: Scrape and beta angles, θ and β.

14.2.2. Landing Gear Sizing

After determining the location of the main and nose gear, the actual sizing and retracting mechanisms can be performed. First the loads on the gear elements are determined. These influence how strong the landing gear needs to be. By using these loads the wheels, brakes, struts and damper are designed. The results of these sections are given in Table 14.4.

Loads on Landing Gear

The loads that the landing gear needs to be able to handle are dependent on its location as well as CS-23 requirements. The nose gear and the main gear therefore need to be evaluated separately. In subsection 14.2.1 it is determined that the maximum load on the main gear is 92% of the Maximum Takeoff Weight (MTOW). For the nose gear this is equal to 17% of the MTOW.

Furthermore, CS-23.485 states that the main gear should be designed for 1.33 times the maximum loads in vertical direction. Likewise CS-23.499 states that the nose gear should be designed for 2.25 times the maximum loads in vertical direction [24]. And the pressure of the tire is allowed to be at most 414 kPa in order to be capable of landing at grass paved runways [27].

Tire Design

From the obtained loads on the landing gear, a set of tires is chosen which are capable of handling the loads under the specified pressure. By using the Global Aviation Tires Catalogue from Goodyear a specific type of tire is obtained[1]. In the tire catalogue no tires where available of acceptable sizes which had the correct tire pressure rating combined with the required loads. Therefore, each landing gear strut will consists of two wheels. By choosing a tire, a linear relationship thought the origin is assumed between the tire pressure rating and the load rating. The verification of this assumption is discussed in section 13.7.

Struts Design

The landing gear struts are assumed to be of a cylindrical shape. They are made of Titanium 6AL-4V. It has excellent material properties compared to magnesium and aluminum. The weight and storage space advantages outweigh the cost factors [74]. The material properties for Titanium 6AL-4V are given below.

Table 14.3: Yield stresses for load cases and density of Titanium 6AL-4V[2].

	Shear	**Tension**	**Compression**	**Density**
Value	760 MPa	880 MPa	880 MPa	4430 kg m^{-3}

To determine the required strength of the landing gear, CS-23 regulations are used.Requirements CS-23.485 and CS-23.493 provides required load factors for the main gear in the longitudinal and lateral direction due to drag and side forces during landing. CS-23.499 provides similar requirements which apply to the nose landing gear. The normal stresses, shear stresses and bending moments are evaluated to determine the required radius of the landing gear strut. For the analysis a cylindrical shape is assumed. The stress is assumed to be evenly distributed among the cross-section. Therefore, a safety factor of 1.5 is added, which is standard for a structural analysis [24].

Brakes

For aircraft of similar size, there are normally two types of brakes used: disc brakes or drum brakes. Disc brakes are more often used since they are lighter, better accessible, easier to maintain and have a better friction to heat conversion

[1] URL: `https://www.goodyearaviation.com/resources/pdf/databook_7_2016.pdf` [cited 12 June 2018]
[2] URL: `http://asm.matweb.com/search/SpecificMaterial.asp?bassnum=mtp642` [cited 24 June 2018]

compared to drums [25]. For the material of disc brakes, carbon will be used. The heat sink performance characteristics of carbon are better compared to conventional metals that formerly often used, according to Currey [75]. Also the use of carbon brakes is preferred since that material characteristics are easily capable of meeting the kinetic energy per wheel requirement (KE) from CS-23.735 [24][75].

Shock Absorbers

For the design of the shock absorbers different systems are used for the nose and main gear. For the nose landing gear Oleo pneumatic shock absorbers are used, as displayed in Figure 14.5. This type of absorbers is preferred as symmetrical loading will be present for a dual wheel nose gear design [25].

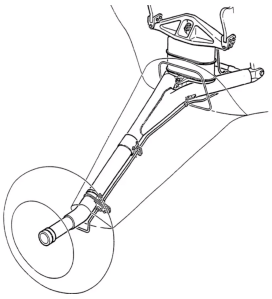

Figure 14.3: Shock absorber layout for De Havilland Canada DHC-6 Twin Otter [75].

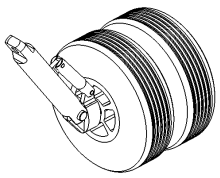

Figure 14.4: Oleo-pneumatic trailing link shock absorber for main gear.

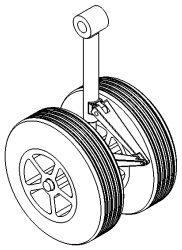

Figure 14.5: Oleo-pneumatic shock absorber for nose gear.

The main shock absorber for the main gear will be located at the connection to the fuselage. It is a leaf spring shock absorber, where the design will be similar to the one which is present at the *De Havilland Canada DHC-6 Twin Otter*. This is also displayed in Figure 14.3. The Twin Otter is the heaviest aircraft which uses this type of shock absorbers. The maximum landing weight of the Twin Otter is similar to the one of the E-COmmuter. However the E-COmmuter will also make use of a secondary shock absorber.

Closely mounted to the wheel an oleo-pneumatic trailing-link landing gear is used. However, the configuration is slightly unconventional since the wheel is placed perpendicular to the shock absorber. This is also visible in Figure 14.4. Before landing the landing the wheels will still be placed at an angle of 10° with respect to the ground. In case the aircraft would land within an allowed bank angle, the aircraft will still be able to land safely on its wheels and the shock absorber will still function. The main shock absorber will minimally influence the bank angle requirements since the deflection is very small [25].

Folding Mechanism

In order to achieve optimal cruise performance the landing gear needs to be able to retract. The nose landing gear will fold backwards into the nose landing gear. The nose wheel will be stored in a compartment between the two pilots. This is possible without interfering with cockpit systems. The hinge point of the nose gear is 10 cm above the fuselage skin.

The main gear will be stored in the fuselage as well. By retracting the main gear it will fold forward into blister which stores the main gear during cruise. By retracting the main gear, the wheel will turn perpendicular with respect to the strut. This will be done by using the oleo-pneumatic trailing-link absorber. The retraction is also visualized in Figure 14.6. In the left picture the landing gear is displayed in extracted position. It will then move forward inside the blister as displayed in the right picture. Then the landing gear door closes to maximize noise reduction. Since the largest part of the landing gear is stored inside the blister, no sacrifices have to made with passenger comfort.

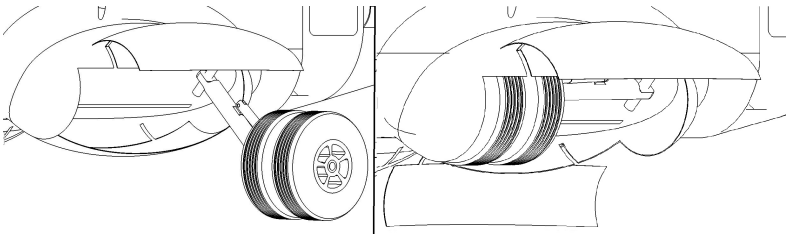

Figure 14.6: Folding mechanism for the main landing gear.

14.3. Verification and Validation

Landing Gear

The placement of the landing gear is verified by comparing the values which are obtained from the iterative Python program with calculations that are performed by hand. At a later stage in the design the CAD model is used for verification.

The landing gear is placed at the correct location and from here the propeller clearance, scrape angle, and overturn angle are measured. The obtained values are compared with the programmed values and checked if they coincided.

Tire Determination
As explained in subsection 14.2.2 a linear relation, which passes through the origin, is assumed between the rated loads and the rated inflation pressure. This assumption was required since there are no wheels of reasonable size currently out on the market which have both the required inflation and load rate. The assumption is verified by looking up tires which are certified for multiple inflation levels. For two different tires, the ratio between the certified load and certified inflation for different inflations was less than 1%. From here it was assumed that these assumptions would also hold for tires which are not rated for different inflation pressures.

Tail Design
The required horizontal tail area is based on data from reference aircraft with a similar configuration. The obtained vertical tail area was compared with this same set of data to check if the aircraft is actually comparable to the other aircraft. After defining the geometry of the vertical and horizontal tail, the data is implemented into the CAD model. The tail is modelled into the CAD without specifying the area. The calculated area area from the CAD model is used as validation to check that it equals the calculated area.

14.4. Results

The results of this chapter are summarized in Table 14.4. Please note that the vertical location of the landing gears, Z_{NLG} and Z_{MLG}, are measured from the bottom of the fuselage.

Table 14.4: Tail & landing gear design results.

Parameter	Symbol	Value	Unit	Parameter	Symbol	Value	Unit
Horizontal tail							
Surface	S	8.52	m^2	Span	b	5.84	m
Root chord	c_r	2.04	m	Tip chord	c_t	0.88	m
Aspect ratio	A	4.01	-	Leading edge sweep	$\Lambda_{c/4}$	25.9	°
Mean aerodynamic chord	MAC	1.53	m	Horizontal tail arm	l_h	7.09	m
Horizontal tail mass	W_{HT}	57.8	kg				
Vertical tail							
Surface	S	5.99	m^2	Span	b	2.68	m
Root chord	c_r	2.43	m	Tip chord	c_t	2.04	m
Aspect ratio	A	1.20	-	Leading edge sweep	$\Lambda_{c/4}$	35.0	°
Mean aerodynamic chord	MAC	2.24	m	Vertical tail arm	l_v	5.90	m
Dorsal fin cord	c_{r_d}	1.70	m	Dorsal sweep	Λ_d	80.0	°
Vertical tail mass	W_{HT}	41.1	kg				
Clearance angles							
Scrape angle	θ	18.6	°	Beta angle	β	21.2	°
Outside propeller clearance	Φ_2	12.5	°	Main propeller clearance	Φ_1	55.3	°
Overturn angle	Ψ	55.0	°				
Nose gear							
Longitudinal location	X_{NLG}	1.25	m	Lateral location	Y_{NLG}	0	m
Vertical location	Z_{NLG}	0.6	m	Number of wheels	$n_{\text{NLG}_{\text{wheels}}}$	2	-
Diameter tire	$D_{\text{NLG}_{\text{tire}}}$	0.44	m	Width tire	$W_{\text{NLG}_{\text{tire}}}$	0.16	m
Diameter rim	$d_{\text{NLG}_{\text{tire}}}$	0.15	m	Radius strut	h_{NLG}	0.021	m
Nose landing gear mass	W_{NLG}	46.9	kg				
Type of shock absorber	Oleo-pneumatic shock absorber						
Tire	Smooth 17.5x6.25-11						
Main gear							
Longitudinal location	X_{MLG}	8.37	m	Lateral location	Y_{MLG}	1.41	m
Vertical location	Z_{MLG}	0.6	m	Number of wheels (per strut)	$n_{\text{MLG}_{\text{wheels}}}$	2	-
Diameter tire	$D_{\text{MLG}_{\text{tire}}}$	0.65	m	Width tire	$W_{\text{MLG}_{\text{tire}}}$	0.22	m
Diameter rim	$d_{\text{MLG}_{\text{tire}}}$	0.25	m	Radius strut	h_{MLG}	0.037	m
Main landing gear mass	W_{MLG}	237.0	kg				
Type of shock absorber	Oleo-pneumatic trailing-link shock absorber & Leaf spring shock absorber						
Tire	Aircraft Rib 25.5-8.75-10						

15 System Integration

Everything is now combined and integrated into one design. First, a sensitivity analysis of the program is carried out, after which the subsystem interaction and integration is elaborated upon.

15.1. Sensitivity Analysis

In order to check the dependency of the aircraft design on certain parameters, a sensitivity analysis is performed. Several design parameters are changed with +5.00% and -5.00% to check their influence on important aircraft characteristics. For this, the code, visualized in Figure 8.3, is run again with some parameters changed in the "Main Parameter File". As can be seen in Table 15.1, the changed parameters are battery specific energy, payload weight, range and specific fuel consumption of the internal combustion engine (ICE). The first and last one heavily depend on design choices and are therefore evaluated. Moreover, the payload and range are inputs from the stakeholders. Analyzing changes in these variables allows for a preliminary estimation of alternative missions.

The evaluated variables are maximum takeoff weight (MTOW), energy consumption, operating cost, wing span and emissions. Energy consumption and emissions clearly represent sustainability and corresponding requirements. The span and MTOW are chosen as the main sizing parameters of the E-COmmuter. The operating cost represents the operational side of the mission. In Table 15.1 the results of the sensitivity analysis are given for the final aircraft design.

Table 15.1: Sensitivity analysis changing the original values of parameters with percentages shown below them.

		Battery specific energy		**Payload weight**		**Range**		**ICE specific fuel consumption**	
	Original value	750 W h kg^{-1}		1358 kg		370 km		$9.48 \cdot 10^{-8}$ kg J^{-1}	
		-5.00%	+5.00%	-5.00%	+5.00%	-5.00%	+5.00%	-5.00%	+5.00%
MTOW	5835 kg	+1.16%	-0.96%	-2.92%	+3.04%	-0.40%	+0.43%	-1.36%	+1.28%
Energy consumption	553 995 W h	+0.67%	-0.36%	-3.31%	+3.27%	-0.16%	+0.13%	-1.08%	+1.01%
Operating cost	€ 2686794	+0.37%	-0.28%	-1.56%	+1.71%	-1.54%	+1.57%	-0.37%	+0.78%
Span	20.9 m	+0.58%	-0.48%	-1.47%	+1.51%	-0.20%	+0.21%	-0.68%	+0.64%
Emissions	0.113 kg km^{-1} seat^{-1}	-0.035%	+0.017%	+7.73%	+0.05%	-0.006%	+0.076%	+0.11%	-0.14%

By evaluating the results, the consequences of changes in battery specific energy are as expected. If this value reduces, the weight of the battery increases, so that the MTOW also increases. It is as expected that the MTOW shows the largest change of all evaluated dependent variables. As a consequence of this MTOW increase, the energy consumption is also larger, and larger wings are required to lift the plane of the ground. More batteries, but with the same price per kg, imply that the operating cost also increases. The influence on the emissions is rather ambiguous. One would expect that if the MTOW increases due to a lower battery specific energy, the emissions also increase, as more fuel would be required. At this point, it cannot be explained why the emissions decrease when the specific energy decreases. Further analysis of how these variables are interrelated should be carried out.

Furthermore, one can obtain that a change in payload weight, i.e. adding or removing a passenger, has a significant influence on the main parameters. This can be explained by the fact that the payload weight forms the basis of sizing the aircraft. The payload weight therefore directly influences the important aircraft characteristics. The reason the emissions go up when both adding and removing a passenger is that the emissions are defined as kilogram per kilometer per seat. For the calculation is it assumed as if with this change, the seat number changes accordingly. Adding a passenger will increase the MTOW, as shown in the table, which will require more power and thus results in more emissions. The opposite is expected to happen when the payload weight is decreased. However, this is not the case. A possible explanation arises from the emissions per passenger calculation. This program uses the payload weight to

determine the number of passengers. By decreasing the weight, the program assumes there are less passengers, and thus less seats. This may result in a higher emission per passenger (or seat), if other values are not changed in a similar way. This should be investigated and if needed, corrected for in the program. The second largest change is obtained for the the energy consumption. A change in payload directly influences the MTOW. Due to the snowball effect, the amount of energy required can change with a certain additional factor.

For a change in range, the obtained changes are smaller compared to the other parameters. With the current design, there is still space left for additional fuel inside the tanks. For an increase in range, extra fuel can be added without any major design changes. The change in wing span shows that the ideal wing shape would change slightly in this case too. Since this is measured in $\mathrm{kg\,km^{-1}\,seat^{-1}}$, the emissions are almost linearly dependent on the range. A change in range will have the largest effect on operating cost due to additional expenses required for navigation and extra fuel.

By changing the ICE specific fuel consumption, expected results are obtained, apart from the emissions. A decrease in specific fuel consumption will make the ICE more efficient. This will cause the MTOW, energy consumption, operating cost and span to decrease. However, one would also expect the emissions to decrease since the engine becomes more fuel efficient. Similar to the change in battery specific energy, it cannot be explained t this point why a decrease in specific fuel consumption causes an increase in emissions. The largest change is observed for the MTOW. This is due to the fact that less fuel is required.

From this analysis, it becomes clear that the emissions vary in an unexpected manner. A possible cause can be a flaw in the iteration algorithm. This should be investigated and adjusted in future development. The other results are as expected and realistic and do not require any further analysis.

15.2. Subsystem Interaction

This section contains the hardware- and software block diagrams. They serve as an illustration to show how different subsystems and components interrelate. The hardware diagram is shown in Figure 15.1.

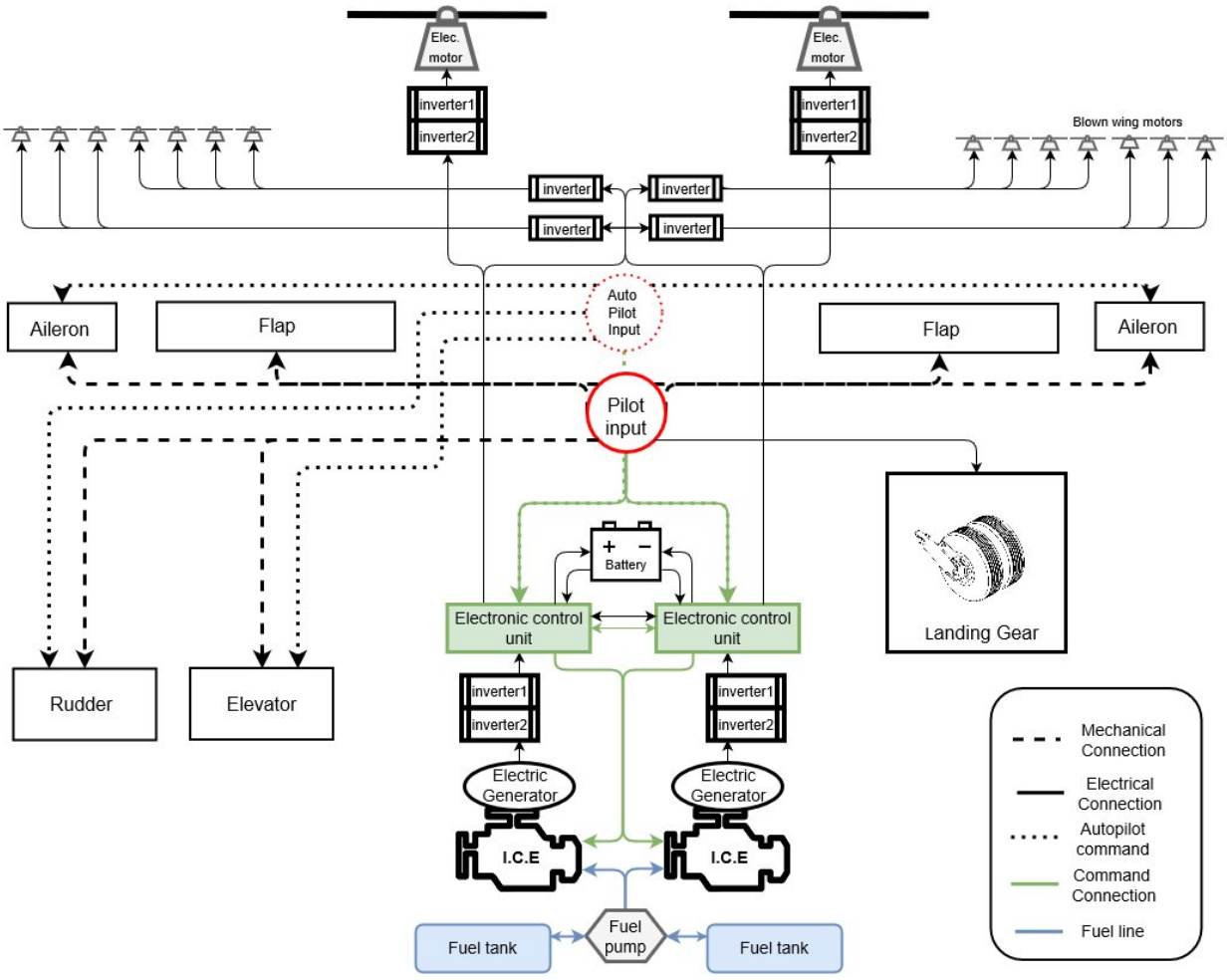

Figure 15.1: Hardware block diagram.

The software diagram is displayed in Figure 15.2. In the diagram, the avionics system is displayed with navigation,

communication and autopilot as subsystems. These subsystem are not designed at this point of the design. However, since they need be present in the actual aircraft, they are taken into account for the software block diagram.

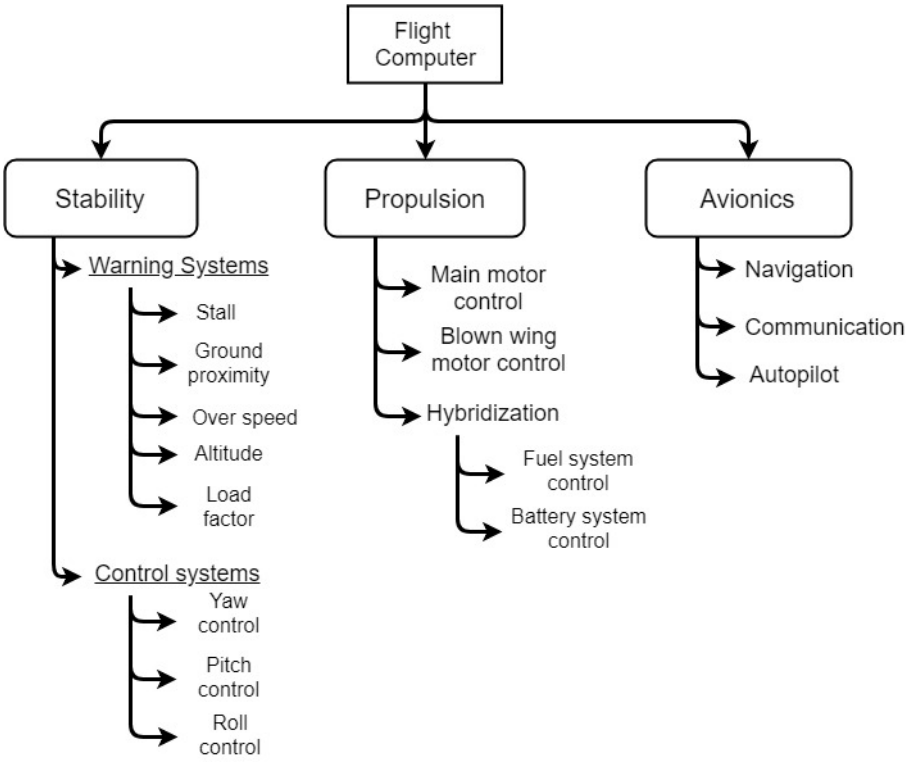

Figure 15.2: Software block diagram.

15.3. Integration of the System

The combination of all design aspects that are explained in chapter 8 to chapter 12 can now by integrated in one aircraft design. The result can be observed in the front view (Figure 15.3), top view (Figure 15.4) and side view (Figure 15.5) of the E-COmmuter.

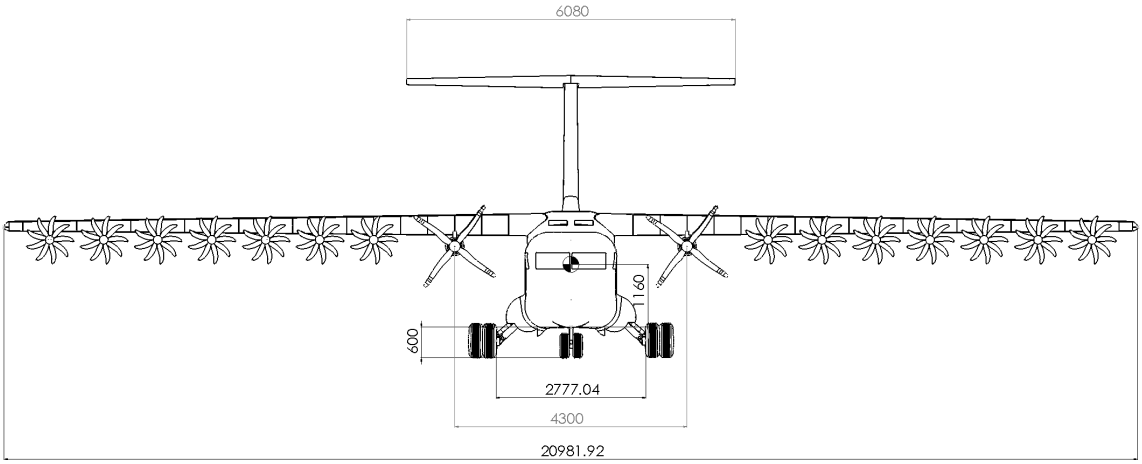

Figure 15.3: Front view of the E-COmmuter (dimensions given in mm).

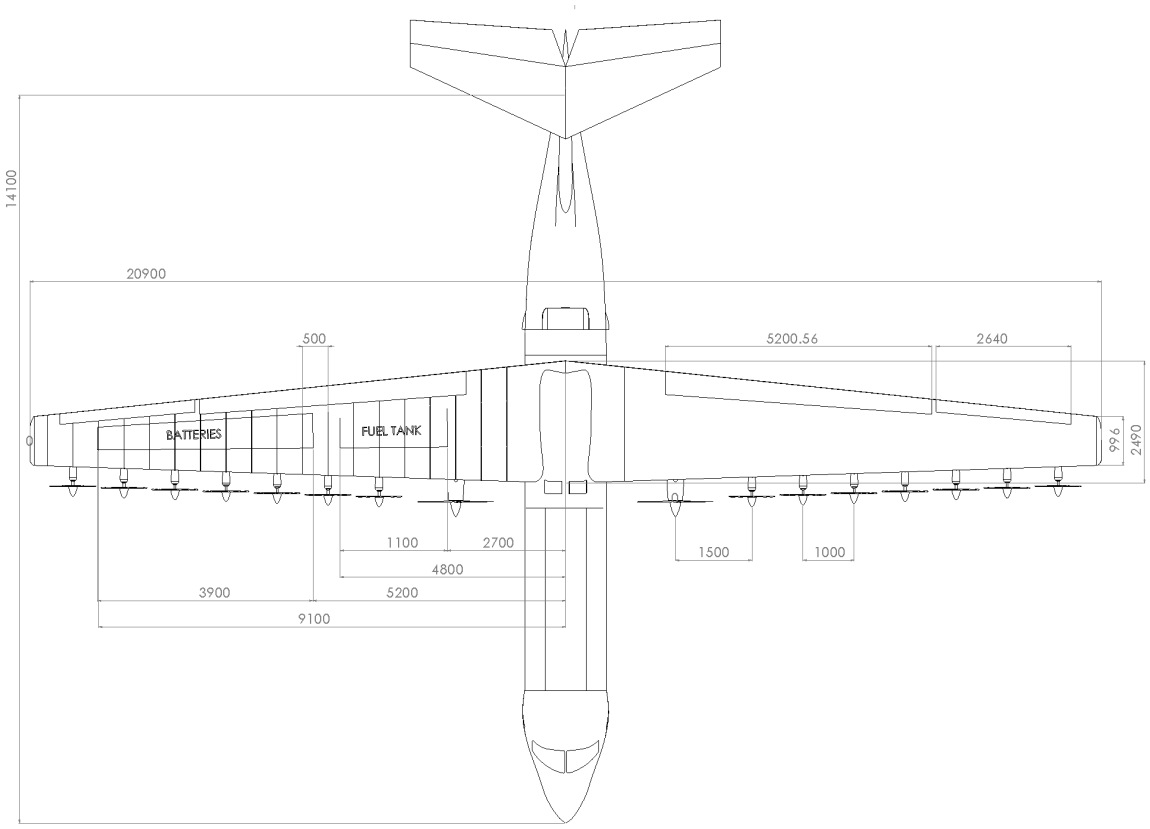

Figure 15.4: Top view of the E-COmmuter (dimensions given in mm).

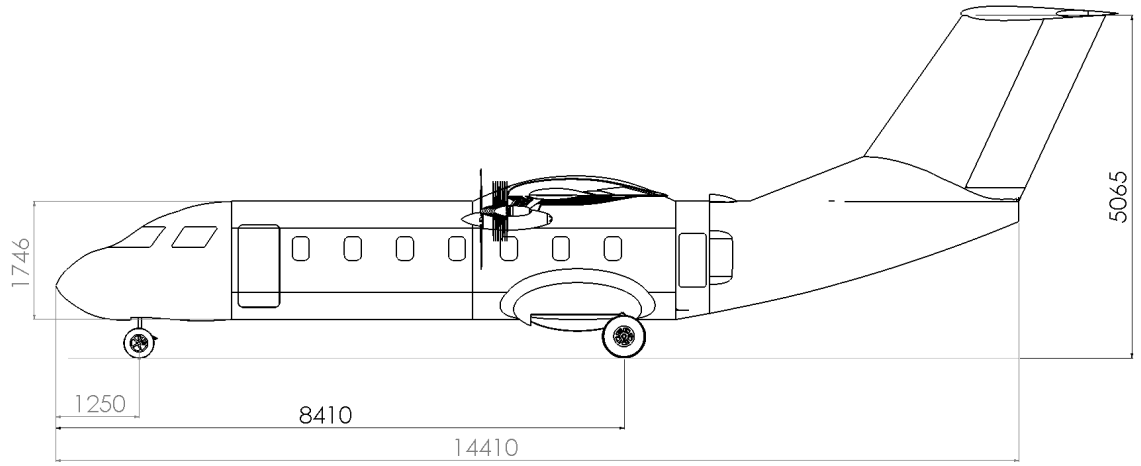

Figure 15.5: Side view of the E-COmmuter (dimensions given in mm).

16

Operations and Logistics

Now that all systems are integrated in the design, it is investigated how operations are to be carried out and whether the aircraft can compete with ground transportation. First, an operations concept is set up, identifying the required ground infrastructure. This is followed by a time analysis of the ground handling time and of the total travel time of the passengers. Finally, a more in-depth analysis of battery handling on ground is performed.

16.1. Operations Concept

When the aircraft is in operation, it has to be checked, fueled and charged. The passengers and their luggage must go through a safety check, embarked and disembarked at both the airfields and airports. To ensure a smooth and fast ground handling, an operation concept is set up. The goal is to have a strategy for minimizing both the operating cost and the turnaround time. **HEF-OPR-01** shows that especially the latter is of main importance for this mission. The ground handling activities are separated into two groups: aircraft handling and passenger handling. These actions can, to some extent, be carried out simultaneously, as can be seen in Figure 16.1. Here, departing means departing by the E-COmmuter and arriving means arriving by the E-COmmuter. Some of the activities in this diagram are elaborated upon below.

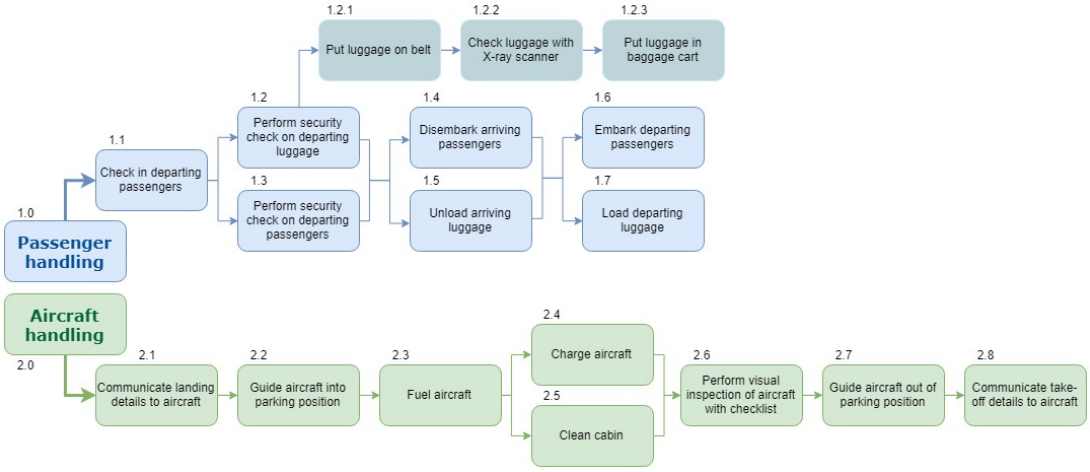

Figure 16.1: Flow diagram of the operational activities at the airports and airfields [4].

- **Perform security check on departing passengers (1.3):** Monitor passengers and their hand luggage for unallowed objects by use of a metal detector and an X-ray scanner, respectively.
- **Communicate landing/takeoff details to aircraft (2.1 & 2.8):** By radio on the airfield.
- **Charge and fuel aircraft (2.3 & 2.4):** This implies that every airfield and airport should be equipped with charging and fueling facilities.
- **Perform visual inspection with checklist (2.6):** Daily inspection; visually inspect the aircraft for damage (see section 17.2).

It becomes clear that some support systems must be put in place in order to process the passengers and service the aircraft. Especially on the airfields, investments are required for successful operation of the aircraft, as there are currently only limited resources available. Below, the most important support systems are detailed. For each item, it is added where it has to be provided: at the airfield, airport or at both.

- **Personnel:** Ground crew of three people to ensure fast ground handling, a minimum of one person is trained for E-COmmuter handling (to be provided at airfield and airport)
- **Building:** Building for the security checks, for the personnel...(to be provided at airfield).
- **Passenger facilities:** Bathrooms, waiting rooms... (to be provided at airfield).
- **Metal detector and X-ray scanner:** One of each should be enough, two in case of a busy airfield where multiple E-COmmuter's are operated (to be provided at airfield).
- **Baggage cart:** To bring luggage from building to aircraft and back (to be provided at airfield).
- **Radio communication:** Radio to communicate with aircraft for takeoff and landing instructions (to be provided at airfield if not present already).
- **Fuel facility:** Fuel reservoir and pump, including fire protection, such as fire extinguishers (to be provided at airfield).
- **Charging facility:** Charging station capable of sufficiently high power and charge rates (to be provided at airfield and airport).
- **Inspection checklist:** Checklist for daily inspection (to be provided at aircraft).
- **Maintenance building:** To perform more extensive maintenance (to be provided at the airport, or to be outsourced to other maintentance facility or MRO.
- **Maintenance personnel:** Trained and certified personnel to perform maintenance on the E-COmmuter specifically (to be provided at airport).
- **Spare parts:** To be provided in the maintenance building (to be provided at the airport).
- **IFR procedures:** If operations are to take place at airfields during the night or in bad weather, IFR procedures should be made up for these airfields.
- **Runway lights:** Lights for landing and/or takeoff in bad weather or in the dark (to be provided at airfield).
- **De-icing facilities:** For the aircraft and for the runway, (to be provided at the airfield).
- **Others:** Security material, office supplies, etc. (to be provided at the airfield).

Regarding the security level, it is for now assumed that the checks performed on the airfields are of the same safety level as the ones performed on the airports. If this is not the case, the passengers would have to be checked again at the airports upon arrival, before transferring to their actual flight. The overall security level of the airfields is considered out of the scope of this project, as it depends on the airfield operators and cannot be analyzed at this stage.

16.2. Time Analysis

A time analysis is carried out in order to investigate whether the aircraft can be competitive with the car. First, an analysis of the ground handling time is carried out, followed by the total travel time of the passengers using the E-COmmuter.

16.2.1. Ground Handling Time

This subsection analyzes the ground handling time. As explained in section 16.1, passenger handling and aircraft handling can be carried out simultaneously. First, the passenger handling at the airfield is discussed. This covers the activities in blue and identifier "1" in Figure 16.1. Secondly, the aircraft handling is treated. After the passengers disembark, the aircraft must be cleaned, charged, fueled and then the new passengers embark. Finally, the ground handling at the airport is covered.

Check-in

It is expected that passengers can check in online at home. A self check-in apparatus is provided at the airfield as well. However, it is expected that most passengers do their check in at home. Thus, the passenger check-in should not take longer than 5 min per flight.

Security Checks

Now, continuing with security checks. Current metal detectors and X-ray scanners can check around 150 bags per hour[1] and 200 passengers per hour[2]. These values are limited by the personnel and passengers, rather than by the machines. Trained personnel is capable of detecting threats in luggage within 7 s [76]. Assuming there is one departing flight with 14 passengers (i.e. full aircraft), there is a maximum of 28 bags to check; 14 hand luggage and 14 hold luggage items. This can theoretically be checked in less than 4 min. Nevertheless, taking into account extra checks due to false alarms and other irregularities, a factor of 2.5 is applied, leading to a luggage security check time of 10 min. After the security check, the hold luggage is separated from the hand luggage, and checked in (also for the flight departing from the airport).

Simultaneously, the passengers are checked. Although the metal detector has a high capacity, it is assumed that this is not reachable in real life. A duration of 1 min per passenger is estimated, resulting in a total duration of 14 min, which is rounded to 15 min including a minute of margin. It is assumed that this can be done (partially) in parallel with the check-in.

[1] URL: `https://www.wired.com/story/tsa-tests-ct-scanners-airport-security/` [cited 12 June 2018]
[2] URL: `http://www.sds.l-3com.com/advancedimaging/provision-2.htm` [cited 12 June 2018]

Passenger Embarking and Luggage loading
Finally, the passengers board and the luggage is loaded. This is expected to take at most 10 min (including walking and bringing luggage to aircraft) [77].

Total Passenger Handling Time
This results in a total passenger handling time of 27 min. Taking into account irregularities, such as passengers arriving late, a total time of 40 min is obtained.

Passenger Disembarking and Luggage Unloading
disembarking and unloading luggage is expected to take around 10 min, similar to boarding and loading luggage.

Cleaning
Cleaning the cabin is the removal of trash, which takes at most 5 min. More extensive cleaning can be performed when the aircraft is not operational.

Charging
The most time-consuming activity is certainly the charging. It is assumed a charging power of 2 MW can be delivered by the charging facility[3]. The analysis of the capabilities of charging points is considered out of the scope of this project. It is therefore assumed that the limiting factor for the charging time is the charge rate of the Lithium-sulfur battery. The charge rate of this battery equals $3\,h^{-1}$, also noted as a charge rate of 3C [78], meaning charging can be done in 20 min. In order to account for limited charging efficiency, environmental conditions and unexpected incidents, a margin of 10 min is added, resulting in a total charging time of 30 min.

Fueling
Next, the aircraft has to be fueled. Fuel flow rates at airfields are comparable to fuel rates at car fuel station, so around $50\,L\,min^{-1}$ [4]. For the maximum amount of 200 kg of fuel, i.e. 277 L [79], 6 min of fueling is required. 2 min are added as a margin. In order to limit the ground handling time, fueling can be done in parallel with cleaning, boarding and luggage embarking. Unboarding and luggage disembarking can be done at the charging facility. For safety and practical reasons, fueling and charging cannot be done simultaneously.

Total Aircraft Handling Time
In order to limit the ground handling time, fueling can be done in parallel with unboarding and luggage disembarking. Cleaning, boarding and luggage embarking can be done at the charging facility. A margin of 2 min is added in between fueling and charging for moving the aircraft from one facility to the other and for unexpected incidents. This results in a total aircraft handling time of 40 min.

Total Ground Handling Time
As said earlier, passenger and aircraft handling are carried out simultaneously. This is summarized in the Gantt chart, given in Figure 16.2. The analysis carried out above is for the trip from airfield to airport. For the other case, a part of the passenger handling was already carried out at the departing airport of the passengers, namely the check-in and the security check. Looking at Figure 16.2, this does not influence the ground handling time, Since this time is entirely depending on charge and refuel time. Not that it is now assumed that charging and fueling takes place with passengers on board. According to regulations, refueling is not allowed with people present in the aircraft. However, complying with this rule would mean that meeting the turn around time requirement would be impossible.

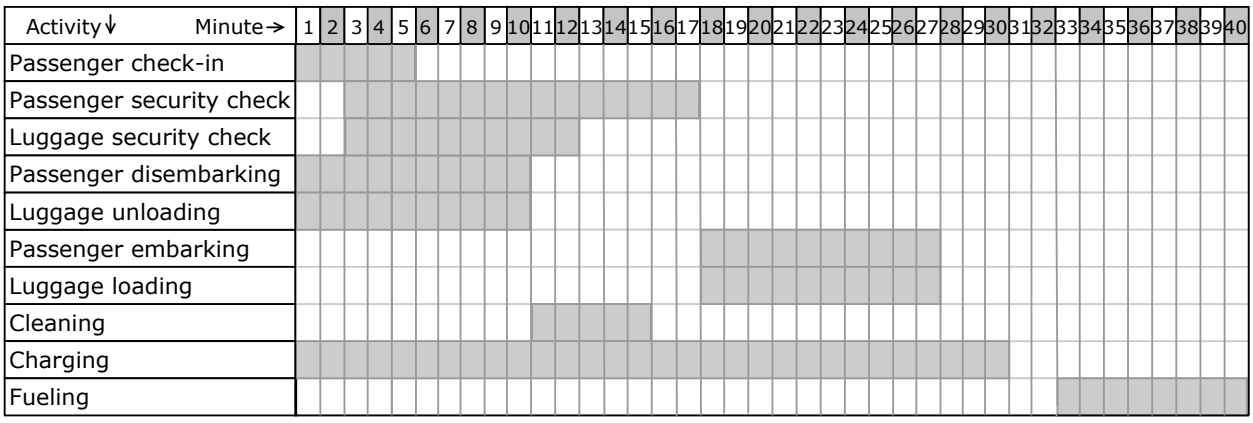

Figure 16.2: Gantt chart for the ground handling operations.

[3] URL: https://electrek.co/2018/05/10/chargepoint-2-mw-charger-electric-aircraft-and-semi-trucks/ [cited 23 June 2018]
[4] URL: https://www.quora.com/What-is-the-flow-rate-of-gasoline-station-fuel-dispensers-in-liters-per-second [cited 13 June 2018]

16.2.2. Travel Time of Passengers

The travel time of the passengers is estimated in order to check whether the E-COmmuter service is competitive with the car, in terms of time. For the analysis, the target countries derived from the case studies in section 2.5 are used (i.e. France, Spain and Poland), together with the determined range of 370 km. Different distances and travel times are used, as a more detailed analysis is performed, based on the presence of both airports and airfields.

As check-in and security check are also performed on the airfield, this has not to be done at the airport anymore. Thus, this time is taken into account for the comparison as well. The boarding time at the airport is excluded, as this is the same for both cases.

Travel Time by Car

In order to estimate a travel time range circles of 370 km (i.e. the maximum range of the E-COmmuter) around the large airports of each of the case countries (and neighbouring countries) are drawn, as in Figure 2.2(b). For locations which are at a straight line distance of 370 km of any large airport, the travel time is determined. This results in 4 h 35 min in France, 3 h 30 min in Spain and 4 h 29 min in Poland.

Depending on the airport and the moment of travel (e.g. holiday or ordinary weekday), the required time for check-in and security checks can vary significantly. Typically, airlines advise their passengers to be at the airport 2 and 3 h before their flight for intra- and intercontinental flight, respectively[5]. This includes gate closure 30 and 45 min before the departure time, respectively, which has to be subtracted from the airport time, as this time does not change when traveling by E-COmmuter. Furthermore, an extra margin of 15 min is added. Now, the most conservative value of 1 h 15 min is assumed for the time it takes from arrival at the airport until the gate. The resulting travel times are given in Table 16.1 and are used as travel times to compete with by the E-COmmuter.

Table 16.1: Summary of travel time by car to airport.

	France	**Spain**	**Poland**
Car trip to airport	4 h 35 min	3 h 30 min	4 h 29 min
Time at airport	1 h 15 min	1 h 15 min	1 h 15 min
Total travel time	5 h 50 min	4 h 45 min	5 h 44 min

Table 16.2: Summary of travel time by the E-COmmuter from airfield to airport.

	France	**Spain**	**Poland**
Car trip to airfield	0 h 32 min	0 h 21 min	0 h 36 min
Time at airfield	0 h 40 min	0 h 40 min	0 h 40 min
E-COmmuter flight	2 h 10 min	2 h 10 min	2 h 10 min
Total travel time	3 h 22 min	3 h 11 min	3 h 26 min

Travel Time by E-COmmuter: Trip to Airfield

The travel time to the airfields is estimated based on the airfields in Figure 16.3. Clearly, there is a high density of airfields (4786 in Europe[6]). In order to gain insight into the average travel time to airfields, the average maximum distance to an airfield is calculated. The following approach is used. It is assumed that the airfields are evenly distributed in a country. Of course, this is not the case, but it is considered an acceptable assumption to get a rough idea of the travel time. The average coverage area of each airfield is calculated (km^2 per airfield). Then, this coverage area is assumed to be a circle around the airfield, from which the radius is calculated. This is the maximum distance to an airfield to have full coverage of a country. For the three cases, the straight line distances are all very close to 23 km. For each, an average travel time is determined, based on the analysis of some airfields in Figure 16.3. The travel times by car are calculated to be 32 min, 21 min and 36 min for France, Spain and Poland, respectively.

Travel Time by E-COmmuter: Time at Airfield

From subsection 16.2.1, it is found that passenger are expected to be at the airfield 40 min in advance of their flight.

Travel Time by E-COmmuter: Flight

Based on the takeoff, climb, cruise, descent and landing speed and distance, the corresponding time is estimated (see chapter 11). A flight time of 2 h is obtained. Together with taxiing, and start-up, a total flight time of 2 h 10 min is found.

Travel Time by E-COmmuter: Total Travel Time

The results above are now summed to the total travel time by E-COmmuter. This is shown in Table 16.2.

Comparison Between Ground Transportation and the E-COmmuter

HEF-PAX-02 requires that the total travel time of the passengers by the E-COmmuter is at least 20% less than the travel time by car. The comparison is shown in Table 16.3. Clearly, for each of the cases the requirement is easily met.

For the reverse trip (i.e. from airport to airfield), a slightly different analysis has to be performed. The total travel time by ground transportation consists of the luggage reclaim and the car trip. Luggage reclaim takes around 30 min [80]. The car travel time remains the same. For the E-COmmuter, the boarding time is increased to 40 min in accordance with the gate closure time for intracontinental flights, including a margin of 10 min. The flight time and car drive time remain the same. Consequently, the time by E-COmmuter remains the same as for the trip from airfield to airport.

[5] URL: `https://www.klm.com/travel/nl_en/prepare_for_travel/checkin_options/dropoff_times/index.htm` [cited 14 June 2018]
[6] URL: `https://github.com/datasets/airport-codes` [cited 15 June 2018]

Figure 16.3: Airports and airfields in Europe. Explanation: red – large airport, blue – medium airport, green – small airport (airfield)[6].

This is summarized in Table 16.3. Again, **HEF-PAX-02** is met, but with smaller margins than for the initial analysis.

This analysis shows that the E-COmmuter increases the airport accessibility for people from rural areas. This means that the design fulfills an important task in transport sustainability in the aviation industry.

Table 16.3: Comparison of travel times by car and by E-COmmuter from airfield to airport.

	Airfield to airport			**Airport to airfield**		
	France	**Spain**	**Poland**	**France**	**Spain**	**Poland**
Travel time by car	5 h 50 min	4 h 45 min	5 h 44 min	5 h 5 min	4 h 0 min	4 h 59 min
Required travel time by E-COmmuter	4 h 40 min	3 h 48 min	4 h 35 min	4 h 4 min	3 h 12 min	3 h 59 min
Actual travel time by E-COmmuter	3 h 22 min	3 h 11 min	3 h 26 min	3 h 22 min	3 h 11 min	3 h 26 min
Percentage E-COmmuter / car time	57.6%	65.9%	59.7%	66.1%	79.4%	68.7%

Further Recommendations
This time analysis focused on the range of 370 km and assumed an even distribution of airfields. For further research, one can investigate what the results are for other ranges and for a more representative airfield distribution. Also other target countries can be analyzed and a time analysis of alternative missions can be researched.

16.3. Battery Handling

This section elaborates on the battery handling, including accessibility for inspection and for replacement, and charging.

In order to inspect and replace the batteries, an access hatch on the lowerskin of the wing is installed for aerodynamic and practical reasons, as explained in section 10.7. The hatch can be opened for inspection. For replacement, the holders are opened as well, enabling removal of the battery. Care should be taken to not damage the batteries during handling. As explained in section 17.2, the batteries are to be replaced every 1500 cycles, so every 1500 flights (charge after every flight).

For charging the battery, one charging cable per wing is connected. A control system built in to the charger monitors the temperature and charge level of every group of eight cells. The design of the charging infrastructure is considered out of the scope of this project and is therefore not treated.

17
RAMS Characteristics

Along with designing the aircraft to meet all requirements on performance, structures and stability, the ability to operate the aircraft safely is an important part to be considered during design phases. Because safety is a key factor in aviation, it is of utmost importance for the design. Furthermore, safety is an essential sustainability metric, which is highly valued in this project. This chapter discusses the reliability, availability, maintainability and safety analysis performed for the aircraft. These are performed to show what parts of the aircraft are expected to require regular checks. section 17.1 discusses the reliability assessment, performed with a qualitative analysis on aircraft failure. With the results from this part, the maintainability is discussed in section 17.2. The section shows the expected required maintenance, both scheduled and unscheduled. After maintainability, availability is analyzed. This shows how much the aircraft is available, which is directly linked to operational costs, discussed in chapter 22. Lastly, an analysis on safety of the design is performed. Here all safety measures in the design are discussed.

17.1. Reliability

Reliability is defined, in engineering terms, as "the ability of a system or component to perform its required functions under stated conditions for a specified period of time" [81]. Analysis of reliability is key to find the critical parts of a system and then use preventive tools to decrease the risk of failure, directly influencing sustainability. Quantitative measures of reliability are performed to find the probability of failure after a certain time, for instance by calculating failure rates from probability density functions [82]. As failure of components can be seen as stochastic events, the actual failure rate cannot be determined exactly until the aircraft is already operational and actual data can be analyzed. This section thus discusses the reliability of the aircraft based on an analysis described in subsection 17.1.1. The results provide an expectation on the reliability of subsystems, which can be used in the design to minimize failure rates. The reliability can furthermore be used in the planning of maintenance activities.

17.1.1. Aircraft Failure Analysis

The aircraft failure analysis is done in order to find the main causes of accidents and incidents in aviation. The data used in the analysis are retrieved from the National Transportation Safety Board (NTSB)[1], a US independent federal agency. The database provides detailed information for each accident or reported incident, for instance on the involved aircraft and the causes of failure. It should be noted that the database may provide multiple entries for the same accident if the investigation findings show multiple causes and factors. This is because a single event (an event being one entry in the database) can cause other parts to fail or multiple events can contribute together to the occurrence of an accident.

In order to get an overview of the sensitivity to failure of subsystems, all entries (if present) are used in the analysis. In order to structure the data and analyze reliable data, the following data restrictions are determined:

- **Occurrence date:** Only occurrences between 1990 and 2018 are used. The data before 1990 are not considered feasible due to the rapid development of aviation in past decades.
- **Aircraft type:** The aircraft considered are not home-built. They can carry between 10 and 30 passengers. This is used rather than using CFR categories as commuter type aircraft were redefined in 1997[2]. Comparing data from only CFR-135 category aircraft would result in less reliable results in the set date range.
- **Investigation status:** Only closed investigations are used in the analysis, as many data of accidents still under investigation provide no detailed information. As the investigation is ongoing the cause of these accidents is considered the possible cause, thus they are not considered sufficiently reliable and left out.
- **Contribution of events:** The database assesses all findings on its contribution to the accident. They are given a code for cause, factor or no code at all. Entries without a code are excluded from the analysis as they merely describe an event which is neither a cause of, nor a factor to the accident.

[1] URL: `https://www.ntsb.gov/` [cited 7 June 2018]
[2] URL: `https://www.bts.gov/content/transportation-accidents-mode` [cited 7 June 2018]

- **Factors and causes:** In the analysis, cause is defined as an event that produces an effect which can lead to an accident. A factor is something that influences the effect but not directly produces it. Factors thus do not directly cause a failure or accident. The analysis is performed with both inclusion and exclusion of factors, in order to fully evaluate the data.

Using the set restrictions the analysis is performed in two successive divisions of data. The NTSB categorizes findings in three major groups, given with their respective sections [83]: non person-related findings (section IA), person-related findings (section IB) and underlying events (sections II and III). The first describe the events in which no person is involved directly in the failure. In the second group, people can be linked directly to the event. Underlying events further describe the primary events of the other two groups, they thus do not directly provide information on the direct accident cause. They are therefore left out of the analysis.

The remaining two categories then can be analyzed separately to show their main contributors. They are internally categorized by grouping the (very detailed) findings codes of the NTSB into more general groups, for instance the major subsystems. Of the two groups the non person-related findings are most important for the reliability, as they show what parts failed or caused an accident without relation to a person. The results of non person-related analysis are chosen for further discussion. The major categories are structure (fuselage, landing gear, wing, control surfaces including stabilizers and remaining structure), powerplant, aircraft internal systems (AC system, electrical system and remaining systems and equipment), external findings (weather, air traffic control and airports) and rotorcraft.

As said before, the analysis is performed two times, one including and one excluding the factors contributing to the accident. In the following parts both analyses are discussed. First the whole data set, including the factors, is analyzed, then the factors are left out and the analysis is done again.

17.1.2. Analysis Results

Continuing from the set up of the analysis, the results will be discussed in this subsection. Both analyses are discussed separately on their respective outcomes. Afterwards concluding remarks and a comparison of results is provided.

Factors Included Analysis

Beginning with the analysis including the factors, the two steps of the analysis described in subsection 17.1.1 are shown in Figure 17.1 and Figure 17.2. Figure 17.1 shows the internal division of non person-related causes from Figure 17.2. It can clearly be seen that accidents have a majority of person-related findings, with 52.9%. The non person-related findings are, however, still a large part, meaning their influence on aviation accidents is significant.

Figure 17.2 then shows the different subsystems chosen to be categorized. Firstly the external findings contribute largely to accidents. This is to be expected, as the category includes a large part of the groups' findings codes. However, these do not directly show the reliability of the subsystem as the aircraft reported could be functioning perfectly when the accident happened. Furthermore the category "Rotorcraft" is not of importance in this analysis. The rest of the categories show what subsystems failed most in the reported accidents. From this plot it becomes clear that the powerplant (14.2%), landing gear (8.7%) and control surfaces (6.2%) are to be considered most when designing or planning maintenance for reliability.

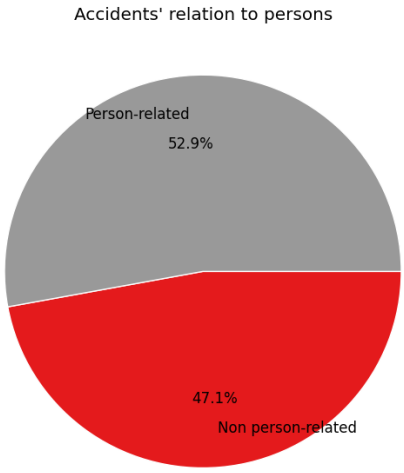

Figure 17.1: Factors included division of person- and non person-related accident findings within the described dataset and restrictions.

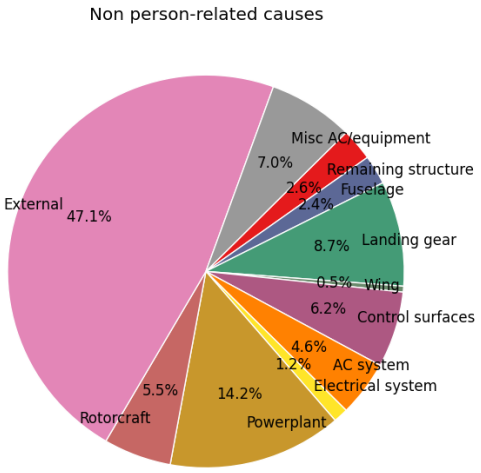

Figure 17.2: Detailed division of non person-related accident findings with factors included.

Factors Excluded Failure Analysis

Following the previous analysis the factors are now excluded from the failure analysis. This results solely in causes of accidents being analyzed, providing a more detailed insight. Figures 17.3 and 17.4 show the results of the analysis. It immediately becomes clear that person-related findings have large contribution to the causes of accidents, accounting

for almost two thirds of all causes (see Figure 17.3. However, the non person-related findings are still a significant part of accident causes.

From Figure 17.4 can be concluded that accidents are caused more by the aircraft itself than external contributors. The powerplant, landing gear and control surfaces are the main categories to be considered, being the larger parts of internal causes.

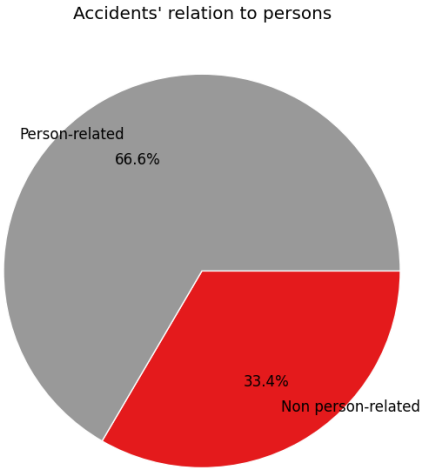

Figure 17.3: Factors excluded division of person- and non person-related accident causes within the described dataset and restrictions.

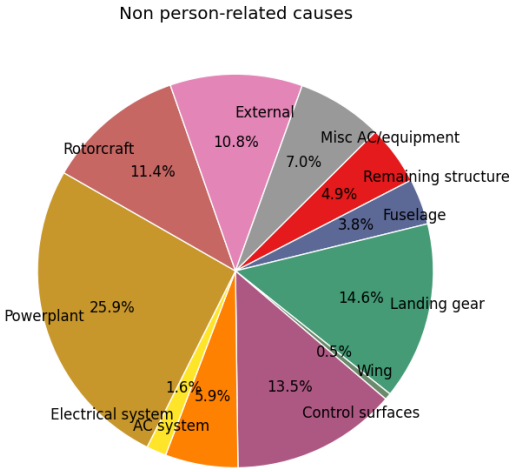

Figure 17.4: Detailed division of non person-related accident causes with factors excluded.

Comparison and Conclusion

The two analyses show significant differences in the division of findings, both in the relation to persons in Figures 17.1 and 17.3 and the non person-related findings in Figures 17.2 and 17.4. The results show that persons cause the majority of accidents, but many non person-related findings are a factor (thus not directly influencing) contributing to accidents. It furthermore shows that external contributors mostly are factors to the accident but not directly cause them, the percentage dropping drastically from 47.1% to 10.8%. This drop is to be expected from the change an data, as for instance solely bad weather does not directly mean an accident will happen. It can however contribute to the possibility of an accident happening if a possible cause (person-related or not) comes up.

From both analyses can be concluded that non person-related findings contribute significantly to accidents with aircraft carrying between 10 and 30 passengers, although the analysis shows that persons are more involved. Both analyses show that the landing gear, powerplant and control surfaces are the main aircraft subsystems contributing to accidents, thus having larger failure rate than others. Other than the landing gear, structural parts of the aircraft show relatively small failure rates. This is in line with the expectation of maintenance on subsystems as discussed in Brill et al. [4].

As a last remark, it can be seen in both analyses that the electrical systems of the aircraft involved in the research have very small contribution to accidents. Most (if not all) of these aircraft however do not have any type of (hybrid-) electric propulsion. The only electrical system they require is to power the internal systems of the aircraft, for instance avionics. As the E-COmmuter will have this type of propulsion the failure rate of the electrical system is expected to be significantly higher. This is due to the novelty of the design, thus expectancy of "child diseases" of the system, and the much larger system involved in comparison to conventional propulsion type aircraft.

The data obtained in this section are required and used to find the critical subsystems of an aircraft. The data are firstly used in the design phases of the project to critically assess which subsystems require extra attention. This with respect to redundancies and safety factors, to improve the reliability of such subsystems. Improving the reliability can for instance be done by improving component reliability or implementing lean design, designing such that the total number of components is reduced. Improving component reliability can, however, be more expensive [82]. This relates to sustainability, and a trade-off has to be made between improving safety at the expense of affordability. Moreover, the results can also be used to make a preliminary maintenance planning on subsystem level. The data show which subsystems are expected to be less reliable, thus require extra inspection and maintenance. This is required in order to mitigate risks concerning the failure of these subsystems. By making sure the failure rate stays low, for instance by adding safety factors or doing extra maintenance on the subsystems, the aircraft reliability can be increased.

17.2. Maintainability

In order to provide a safe service, maintenance and overhaul is to be performed on the aircraft. Plans are to be set up, such that a standardized approach can be used for these activities, which increases the reliability even more. First, a

scheduled maintenance plan, also known as preventive maintenance, is established, in combination with an overhaul plan. This is followed by an unscheduled maintenance plan, i.e. corrective maintenance.

17.2.1. Scheduled Maintenance & Overhaul Plan

The maintenance and overhaul plan is set up in accordance with CS-23 regulations and the European Aviation Safety Agency (EASA) regulations and recommendations. For example, the maintenance manual contains a clearly distinguishable section showing approval by airworthiness [24], and maintenance is to be carried out by a Part-145 certified organization [84][85]. Note, that if the aircraft is operated in other regions, local regulations have to be consulted and applied. Next, the maintenance and overhaul intervals are based on the reliability of the subsystems. For this, the reliability analysis above is used (section 17.1, Figure 17.4) in combination with failure rates reported earlier in the baseline report [6]. The structural and propulsion failure rates can be found in Table 17.1. The latter is based on **HEF-PROP-05**, the others on reference commuter aircraft [86]. It can be seen that the propulsion system is more critical than the fuselage, wing and tail. From the reliability analysis, it is found that landing gear failure is responsible for a large amount of accidents [87]. This is in agreement with the analysis performed above. Also, due to the unpaved runways at airfields, the risk of landing gear failure and damage increases even more. A similar result is obtained for propulsion system and control surfaces failures. Consequently, maintenance of these subsystems is to be performed more frequently and extensively. As explained in section 17.1, the electrical system is also expected to require more maintenance due to the novel design. In order to ensure completeness of the maintenance activities, manuals of two aircraft (Twin Otter DHC-6 and Diamond DA20-C1) are used as a guideline [88][89].

Table 17.1: Failure rates per flight hour for the major aircraft systems [86].

	Fuselage	**Wing**	**Tail**	**Propulsion system**
Failure rate per flight hour	$6.8 \cdot 10^{-8}$	$6.8 \cdot 10^{-8}$	$3.4 \cdot 10^{-8}$	$1.0 \cdot 10^{-6}$

Six types of scheduled maintenance activities are distinguished, listed below [4]. Note that the maintenance intervals are given in number of flight hours. A more elaborate analysis is provided in the next section on availability. It is assumed here that the E-COmmuter is operational 10 flight hours per day. Next to these maintenance activities, the pilot always performs a quick check before flight. This is not discussed here, as it is merely an operational check and typically not included in maintenance manuals [90]. For each of the maintenance activities, the interval, the expected duration of the maintenance task is given. Note that in each more extensive maintenance activity, the less extensive activities are also performed.

- **Service check:** Every 20 flight hours (FH). Expected duration: ± 1 h [90].
- **Line maintenance:** Every 100 FH [4]. Expected duration: ± 1 h [90].
- **Type A maintenance:** Every 500 FH [4]. Expected duration: ± 10 h [90][91].
- **Type B maintenance:** Every 2500 FH. Expected duration: ± 30 h (aircraft out of operation) [90][91].
- **Type C maintenance:** Every 5000 FH [4]. Expected duration: ± 7 d (aircraft out of operation) [90][91].
- **Type D maintenance:** Every 20000 FH [4]. Expected duration: ± 21 d (aircraft out of operation) [90][91].

In Appendix B, a first step towards a maintenance manual is made. This table is to be updated and extended during a more detailed design phase. Upon sale and operation, a full manual is to be set up, in compliance with CS-23 regulations. Furthermore, the manual needs to be reviewed and updated frequently when the aircraft is already in full operation, in order to remain reliable.

Note that, if a system is dismounted for inspection and testing, and it becomes clear that it is damaged and irreparable, it can be replaced, depending on the cost, time and influence on the rest of the aircraft. For example, the landing gear and the battery most likely need to be replaced before the end-of-life of the aircraft.

As explained in section 12.6, the life cycle is estimated at 1500 cycles, which corresponds to 250 operational days, or in total 260 days (see section 17.3). Consequently, during a type B maintenance, testing has to be performed to check the status of the batteries. It can then be decided to replace the batteries, or to extent its use. A cycle life of 260 days is indeed very low, but with the current developments in batteries, a higher cycle life cannot be obtained yet. Further research should be carried out in order to investigate whether alternative solutions to this problem can be found.

17.2.2. Unscheduled Maintenance Plan

If abnormalities occur during testing or flights, or if any kind of damage is found during scheduled maintenance, further investigation is required. Due to the novelty of the design, it can be expected that "child diseases" occur, especially in the first operational years. Therefore, a corrective maintenance plan is to be created.

The required maintenance depends on the type and severity of the abnormality. Consequently, the maintenance duration can vary a lot. A limited plan is set up for now, focusing on the possible failures and their severity. Attention is paid to the differences with conventional aircraft failures. Some E-COmmuter related failures are discussed below with their causes, consequences, required maintenance and expected duration of maintenance. They are merely based on

logical reasoning and the duration of scheduled maintenance actions.

Hard landing
- Causes: Bad runway condition (unpaved), weather conditions, malfunctioning shock absorbers, pilot error, etc. [92].
- Consequences: From slight discomfort to unrepairable aircraft damage [92].
- Required action: Inspection of the landing gear and underside of wing and fuselage for damage, before next flight. If damage is detected, aircraft is taken out of operation for detailed overhaul, and replacement, if necessary [92].
- Expected duration: From ± 30 minutes to 1 week.

Surface damage
- Causes: Runway debris (unpaved runways), weather conditions, bird strike, etc.
- Consequences: From small cracks and dents to irreparable aircraft damage.
- Required action: Inspection of the aircraft surface, before next flight. If damage is detected, aircraft is taken out of operation for more detailed inspection with sensors and scanners. If necessary, the aircraft is (partially) stripped.
- Expected duration: From ± 30 minutes to 2 weeks.

Battery overheating
- Causes: Malfunctioning cooling system, malfunctioning thermostat, early wear-out, electric overload, battery cell imbalance, etc. [93].
- Consequences: Loss of power, fire, battery failure, battery rupture (expansion), etc. [93].
- Required action: Aircraft out of operation for extensive inspection and testing, and (part) replacement, if required.
- Expected duration: From ± 3 days to 2 weeks.

Engine overheating
- Causes: Malfunctioning cooling system, malfunctioning thermostat, early wear-out, lack of oil, etc.
- Consequences: Loss of power, fire, detonation, engine failure, vapor lock etc.
- Required action: Aircraft out of operation for extensive inspection and testing, and (part) replacement, if required.
- Expected duration: From ± 3 days to 2 weeks.

Battery leaking
- Causes: Overcharging, physical damage due to debris, frozen acid due to cold weather, etc.[3].
- Consequences: Fire, damage to surrounding systems, battery failure, etc.[4].
- Required action: Replacement of battery, cleaning of casing, inspect surrounding for acid.
- Expected duration: ± 3 days.

Fuel leaking
- Causes: Excessive flexing of tank, early wear-out of sealing, physical damage of tank due to debris or damage of adjacent subsystems (cracks, wholes, etc.), wrong initial manufacturing, etc. [94].
- Consequences: Fire, explosion, damage to surrounding systems, etc. [94].
- Required action: Replacement of (parts of) fuel system, cleaning of surrounding systems.
- Expected duration: From ± 3 days to 2 weeks.

Propeller damage
- Causes: Bird/debris strike, unintended stress concentrations, lightning strike, overspeed conditions, corrosion, etc. [95].
- Consequences: Reduction of power, wing damage, etc.
- Required action: Removal of surface damage, replacement of (parts of) propellers, inspection of wings for damage.
- Expected duration: From couple of hours to ± 1 week.

17.3. Availability

From the maintenance plan described in previous section, the availability of the aircraft can be determined. The scheduled maintenance plan described in section 17.2 shows a full cycle of maintenance and overhaul of 20000 FH. The calculation of expected availability thus is done in this time frame as well. This section first discusses the method used to assess availability. Then planned maintenance (or scheduled) availability is provided, after which a discussion on the actual availability, including unscheduled maintenance, is discussed. Assessing availability is key in the sustainability of the aircraft, as operating costs are directly influenced by availability.

[3] URL: `https://www.racshop.co.uk/advice/car-battery-leaking-leak-advice-and-tips` [cited 11 June 2018]
[4] URL: `https://www.skybrary.aero/index.php/Aircraft_Batteries` [cited 11 June 2018]

Availability can be assessed in more than one way, as the conditions in which it is considered available are debatable. This section discusses the availability from a maintenance based point of view. Subsection 17.3.2 will, however, also discuss total availability.
Availability of an aircraft is calculated by determining the ratio between the time an aircraft is operable and the total time. Total time can be given in, for instance, a year, total life time or another time frame. As discussed before, the total time considered in this section is the overhaul cycle of 20000 FH. Operating time then is defined as the time the aircraft is fit for operation [96]. This thus includes actual servicing time as well as transits, night stops and if the aircraft is available, but not used for flight.

To calculate the availability, some assumptions are made, discussed below. These restrict the analysis and provide a preliminary framework for the assessment of availability.

- **Flight hours per day:** The aircraft is assumed to perform 10 FH per day. This number is acquired by excluding nightly flying of the aircraft (as is the case for most regional or commuter type services). With the 40 min turnaround time, the aircraft can perform six two-hour flights per day, i.e. 12 FH. Taking into account possible delays and shorter flights, this number is reduced to 10 FH. Looking at other regional and commuter type aircraft, their flight times are mainly between one and two hours and they generally perform six to eight flights per day[5].
- **Nightly maintenance:** Maintenance is assumed to be performed on a 24/7 basis in order to reduce the unavailability of aircraft [91]. Smaller checks and maintenance are planned overnight to ensure full operational availability in operational hours. These are estimated to be between 06:00 and 23:00 every day[5].
- **Overlapping maintenance checks:** All maintenance checks are planned such that they overlap with the lower level checks. It is assumed that the larger checks also cover the smaller ones. Thus they are not required to be performed and they are not counted in the total duration calculation. The exception to this assumption is the daily check, performed before each first flight of the day to visually check if the aircraft is airworthy.

17.3.1. Scheduled Availability

Using the assumptions and the planned maintenance discussion from previous section, a preliminary calculation can be performed. Table 17.2 provides the total maintenance duration planned per overhaul cycle of 20000 FH divided into the different maintenance principles discussed before. The table shows the duration and expected occurrence of all checks, as well as their expected total time in one cycle. Moreover, it shows if the aircraft will be available for regular operation, thus if the checks can be performed overnight or, if possible, between two flights.

Table 17.2: Planned maintenance duration in 20000 FH cycle [90][91].

	Duration of check	**Times performed**	**Total duration**	**Available during day**
Daily (pilot) check	20 min	2000	667 h	Yes
Service check	1 h	800	800 h	Yes
Line maintenance	1 h	160	160 h	Yes
Type A	10 h	32	320 h	Yes
Type B	30 h	4	120 h	No
Type C	168 h	3	504 h	No
Type D	504 h	1	504 h	No
		Total	3075 h	

The availability of the aircraft now can be calculated using the assumptions and the data from Table 17.2. Note that the availability at this point only considers planned maintenance. A discussion on the results and implementation of the unscheduled maintenance will be given later on. Using the assumption that 10 FH are performed each day the aircraft is operable, the aircraft operates a total of 2000 days in one overhaul cycle. Furthermore, the planned maintenance in which the aircraft is not operable during the day adds another 46 days (type B, C and D maintenance). Total time of the considered time frame thus equals 2046 days, or 49 104 h. The total unavailable hours due to planned maintenance and inspection is 3075 h, seen in Table B.1. Operating time thus equals 49 104 h − 3075 h = 46 029 h.

Availability of the aircraft then can be calculated as the ratio between operating time and total time [97]. The result is a scheduled availability of 93.7%. This result is to be expected, as the definition of availability shows that operating time can be considered to be very large.

17.3.2. Actual Availability

As said in previous subsection, the availability assessment is now only performed using planned maintenance. It is however to be expected that an aircraft subsystem fails during its operational lifetime or that faulty components are discovered during inspections and maintenance. Moreover, planned maintenance checks have an expected time to

[5]URL: `https://www.flightradar24.com/` [cited 12 June 2018]

complete, but they might require more time due to heavier maintenance required than planned, or missing parts. If parts required for reparation are not in stock, the aircraft is grounded until they are delivered, delaying the time until available. Lastly, if the aircraft is grounded on an airfield, it can be assumed that maintenance will take much longer, as no specialized equipment is available at the airfield. Accessing the airfield with the required tools, repairing the aircraft with fewer resources and other conditions constraining the maintainability will further reduce availability. All described unscheduled maintenance actions reduce the availability of the aircraft.

In order to reduce the unavailability it is of importance to regularly check the aircraft for possible faulty components, as is done with the maintenance planning. Furthermore, a maintenance hangar requires a specialized parts and components management strategy to make sure the maintenance can be done as efficiently as possible to reduce waiting time. Making sure the technicians are well trained and that their quality of work is sufficient further reduces the possibility of failure.

Apart from maintenance, other restrictions can reduce the availability of aircraft, namely non-maintenance related down time. This includes, among others, labour strikes, bad weather, diversions due to medical conditions and the time when the aircraft is parked on the ground, not to be used [96]. As these propose another type of unavailability, the percentage is again expected to reduce. Many of these cannot be influenced by the operator. To reduce the non-maintenance unavailability, the usage of aircraft can be optimized such that aircraft storage and parking is minimized.

Concluding, the total availability includes all parameters restricting the usage of an aircraft, both maintenance related and other causes. The availability percentage discussed in subsection 17.3.2 thus decreases. In order to maximize the availability it is key importance to have good management on maintenance planning, spares stock and fleet usage. If restrictions can not be influenced by the operator, the consequences of those restrictions have to be assessed, for instance with risk mitigation, to reduce impact on operation.

17.4. Safety

The safety of the passengers and crew is not ensured by measures during operation only, such as maintenance and security checks. Already during the design, actions must be undertaken in order to mitigate and/or prevent the consequences of hazardous events. Regarding redundancy, a clear philosophy is followed. It is decided to implement redundancy as a fail-safe method in the form of duplication for the critical components. For the E-COmmuter, this means that, next to the typical aircraft critical components (e.g. avionics) and especially the novel parts of the design, redundancy is applied. Thus, it is mainly implemented in the propulsion system. However, redundancy also has some drawbacks: it increases the cost, maintenance and weight of the aircraft. Therefore, the increased reliability related to redundancy has to be traded off against its disadvantages. The applied redundancies are explained below, together with safety factors and other measures taken into account in the design.

Structures
- Safety factor of 1.5 to obtain the ultimate load factor from the limit load factor [24].
- Safety factor of 1.5 on the thickness of the wing box to account for uncertainties in the design (subsection 10.6.3).
- Redundancy of stringers on the topside of the wing box (subsection 10.6.3).
- Safety factor of 2 on the battery compartment volume to account for cabling and protection (section 10.7).
- Factor of 0.9 on the $C_{l,max}$ extracted from XFLR5 to account for a possible overestimation (section 10.2).

Fuselage & Cabin
- Margin of 5 cm on the width of the cabin (section 9.1).
- The luggage packing density is estimated to be 85% to account for inefficient packing (section 9.1).
- Factor of 1.15 on the luggage compartment volume to account for unexpected extra luggage (section 9.1).
- Margin on engine compartment length to account for cabling and protection (section 9.1).

Propulsion System
- Redundancy of inverters and electronic control units (Figure 12.1).
- Intrinsic energy redundancy due to the use of two energy sources (batteries and internal combustion engines).
- Motors are sized for maximum range (min. thrust), instead of maximum endurance (min. power) (subsection 11.3.1).

Stability & Control and Landing Gear
- Wing location and tail sizing designed for most critical flight conditions, i.e. high cruise speed for stability and stall speed for controllability.
- Safety factor on ultimate loads to be carried by the landing gear in accordance with CS-23 [24].
- Factor of safety of 1.5 for the structural design of the landing gear to account for material flaws (subsection 14.2.2).
- Two wheels and two dampers per landing gear strut (subsection 14.2.2).
- In-flight deflection of control surfaces limited to 75% of maximum deflection (section 13.5).
- Safety factor of 3.33 on the minimum roll rate the E-COmmuter should be able to obtain (section 13.5).

18

Technical Risk Assessment

A technical risk assessment is of significant importance throughout the design process of the E-COmmuter. A preliminary technical risk assessment from previous reports [4][6] has already been taken into account while doing the detailed design of many subsystems. Nevertheless, many risks remain that can be identified and which have to be mitigated to produce a safe and sustainable aircraft, fit for daily usage. This chapter identifies the risks associated with the design and their impact and discusses techniques for mitigation in future design studies of the E-COmmuter.

18.1. Risk Identification and Assessment

The risk identification and assessment of the E-COmmuter design consists of two parts: the risks identified in the previous reports of Brill et al. [4][6] and the new risks identified for the detailed design in this report. In this section, both of these will be identified and described.

18.1.1. Risk Mitigation Performed

The risks that have been assessed to be critical in previous reports resulted in multiple mitigation strategies [4][6]. These risk mitigation strategies are taken into account in the E-COmmuter design in this report.

Certain risk mitigation strategies from previous reports are easier to apply than others and hence not all mitigation strategies have been applied in the detailed design phase of the E-COmmuter and are left for further studies. The following risk mitigation strategies have been applied during the design up to this point:

1. **Stability & control:** The E-COmmuter is fitted with an electronic stability and protection system, as described chapter 13. Additionally, an analysis is done on the blown wing to identify its use during a control surface failure in section 13.5. From the analysis, it is clear that the blown wing can replace the rudder in emergency cases due to its high influence on the yawning moment of the aircraft. However, it has only a marginal influence on the rolling moment of the aircraft, requiring the ailerons to be more the redundant than the rudder.
2. **Structural failure:** The use of appropriate safety margins is applied in the design during the wing and fuselage design (chapter 10 and chapter 9 respectively). For example, the limit load factor n_Z is multiplied with a factor of 1.5 according to CS-23 regulations [24]. Also, as the methods used to calculate the skin thickness of the wingbox are valid only for a rectangular wingbox (and the wingbox of the E-COmmuter is not rectangular), a safety factor of 1.5 is applied to the skin thickness of the wing. Additionally in section 14.2, the ground clearance of the aircraft is analyzed and it is determined that the aircraft has ample ground clearance in all flight phases.
4. **Electrical power source failure:** In the wing design (see chapter 10), a margin is applied for space needed to provide active battery cooling. As the batteries are located in the wing, they are compartementalized by the ribs which act as a firewall.
5. **Human Error:** The design furnishes the aircraft with two pilot seats as explained in the cabin design (section 9.1). Having two pilots allows the pilots to check on each other to reduce the risk of human error. Furthermore, a door is provided to restrict passenger accessibility to the cockpit. In addition to the extra pilot seats, the avionics system of the aircraft includes a computer system that controls how the division of energy between the ICEs and batteries, and the division of power between the large propellers and the blown wing. This allows a pilot trained for normal GA aircraft to also be able to fly an aircraft with a propulsion system as complex as the one of the E-COmmuter.
6. **Environmental Factors:** The E-COmmuter is designed for gust loads specified in the CS-23 specifications. In addition, the aircraft is designed to climb over obstacles of a maximum size of 50 feet (or 15.24 m in its design takeoff distance. Other environmental factors such as wildlife are mainly the responsibility of the airport, although the aircraft should be able to handle a bird strike and not fail catastrophically. A system like Pulselite[1] can help to reduce the chance of bird strikes (from an aircraft perspective) up to 60%.

[1] URL: `https://www.preciseflight.com/pulselite-pulsing-aircraft-lights/` [cited 22 June 2018]

The above mentioned risk mitigation strategies are used in the detailed design up to this point. However, these risks are still present and need to be addressed for future studies. Hence, they are still assessed and displayed in the risk map. In addition, newly identified risks from the detailed design are treated in more detail in subsection 18.1.2.

18.1.2. Risk Identification and Assessment of Detailed Design

During the detailed design in this report, new risks have come too light that have to be assessed in addition to the already identified risks from previous design stages. For clarity, this section only presents those risks that are still unmitigated for the design presented in this report. The most important newly identified risks are:

1. **Stability & control:** The T-tail introduces stability & control risk due to the inability to recover from a deep stall. The probability of losing control due to deep stall is therefore increased and the consequence is catastrophic. No analysis has been done on this risk as of yet. In addition to this, if either the elevator or the aileron gets stuck at its maximum deflection, there is currently no mitigation in place to recover from such an event.
2. **Structural failure:** As the fuselage design in chapter 9 is relatively limited in scope, no attention has been given to protect the wing, cabin and in general the airframe from a propeller strike. Propeller strikes generally happen due to (a part of) a propeller blade coming lose and hitting the fuselage. If the fuselage is not protected, this is a catastrophic accident. If the blade does not hit the fuselage but flies away, the imbalance of the propeller can cause severe damage to the motor and the structural integrity of the pylon and wing[2].
   In addition, no assessment of stress concentrations is done with regard to the many cutouts in the aircraft for the doors, windows, batteries, etc. Structural failure due to stress concentrations is almost always catastrophic.
   Next to the limited scope of the fuselage design, some important analyses have been neglected as well during the wing design. These consist of a flutter and a fatigue analysis, both having a tremendous impact on the safety of the aircraft. Structural failure due to flutter happens very quickly and is usually catastrophic. Structural failure due to fatigue is much slower but still crucial as it can cause catastrophic failure as well.
3. **Propulsion system failure:** From the reliability analysis became clear that the propulsion system is a system with relatively high failure rate. This requires extra attention with respect to risk identification and mitigation. However, due to the use of a hybrid system, many redundancies are already built into the design due to the use of multiple motors, generators, inverters and ICEs. Care has been taken to size the system for a one engine inoperative (OEI) scenario so it can still perform safely. All electric systems have a very low failure rate, much larger than 10^{-6} which makes the ICEs the most failure prone part of the propulsion system. However, due to the use of dual ICEs and the strong certification of the selected Continental engines, this should not pose a risk to the design. Hence, propulsion system failure is evaluated as unlikely but marginal.
4. **Electrical power source failure:** A failure of the batteries can be both damaging to the integrity of the aircraft as a whole (battery fire) or to the performance of the aircraft (loss of power). The first case is already partially mitigated in the detailed design (see subsection 18.1.1) but said measures have not been verified or validated. Hence, the likelihood of a battery fire is still at medium with a catastrophic impact.
   The second case, concerning a loss of power due to a short or failure in the battery management system, is already mitigated due to the redundancies provided by the hybrid system. In case of a loss of battery power, the 50 kg of reserve fuel can be used to start the ICEs and provide the missing power until an emergency landing has been made.
5. **Human Error:** The risk of human error can be classified as unlikely but catastrophic. As the control computer takes care of the special aspects of the hybrid propulsion system, pilots do not have to worry about motor power balance or running out of power. However, failure due to foregoing startup checks, forgetting the lower the landing gear or pulling up into deep stall are still considerable risks. Hence, human error is classified as likely and catastrophic.
6. **Environmental Factors:** Besides gust loading, the aircraft is (as of yet) not designed for icing conditions or to handle bird strikes. Icing conditions have a medium probability and can have a critical effect on the aircraft structure and controllability. Bird strikes also have a medium probability and also have a critical effect, due to the damage than can be done on the airframe and propulsion systems.
7. **Operations & logistics:** Operations & logistics mainly revolves around the turnaround time. As the turnaround time is dependent on a multitude of factors, it is very sensitive to delays due to problems with cleaning, fueling or charging the aircraft. It is not uncommon for a flight to be delayed because luggage is lost on the way or because de-icing is required. Hence, the risk is categorized as very likely but negligible.

18.1.3. Risk Map

In subsection 18.1.1, the mitigation strategies used during the detailed design are stated. Moreover, some new risks are identified and assessed for the E-COmmuter during the detailed design phase in subsection 18.1.2. The performed risk mitigation and newly identified risks can be summarized in a risk map as displayed in Table 18.1. The following parameters are used on the vertical and horizontal axis [6]:

[2] URL: `https://www.aopa.org/-/media/files/aopa/home/pilot-resources/asi/safety-advisors/sa06.pdf?la=en` [cited 22 June 2018]

Probability of Occurrence:
- **Very likely:** the event occurs on a daily basis.
- **Likely:** the event occurs regularly; one is not surprised when the event occurs.
- **Medium:** the event occurs only sometimes; one is surprised when the event occurs.
- **Unlikely:** the event rarely occurs.
- **Negligible:** the probability that the event occurs is so low that it does not need to be considered.

Severity of the Consequence:
- **Catastrophic:** the consequence of the event is a fatal accident.
- **Critical:** the consequence of the event is an accident resulting in structural damage.
- **Marginal:** the consequence of the event leads to a loss in performance.
- **Negligible:** the consequence of the event does not affect the aircraft significantly.

Table 18.1: Risk map resulting from the current technical risk assessment.

Probability of Occurrence	*Very likely*	7			
	Likely				5
	Medium			6	1, 4
	Unlikely		3		2
	Negligible				
		Negligible	*Marginal*	*Critical*	*Catastrophic*
		Severity of the Consequence			

18.2. Risk Mitigation

In the current risk map displayed in Table 18.1, all risk categories except for propulsion system failure (number 3), environmental factors (number 6) and operations & logistics (number 7) are in the red critical zone showing high risk. This means that those (number 1, 2, 4 and 5) need to be mitigated during further studies to reduce the probability and/or consequences of the event. In order to do so, the following risk mitigation strategies can be defined:

1. **Stability & Control:** The severity of losing stability & control can be reduced as well as the probability:
   - Detailed analysis on the effect of the wing wake on the horizontal and vertical tail in deep stall. Mitigation may be provided by the added airflow due to the blown wing propellers but detailed analysis needs to be done as well.
   - Monitoring and checking the c.g. range before takeoff.
   - Introduce redundancy into the elevator and aileron systems to allow the aircraft to recover from an elevator/aileron stuck at full deflection.
2. **Structural Failure:** The probability of structural failure can be mitigated by:
   - The detailed analysis of fatigue and flutter of the airframe.
   - Detailed analysis of stress concentrations around windows, doors, etc.
   - Fortifying areas that can be damaged by a prop strike.
   - Careful monitoring the application of the MRO plan elaborated upon in section 17.2.
4. **Electrical Power Source Failure:** The probability of the batteries to fail and the severity can be reduced by:
   - Short-circuit protection on all power sources, as well as providing redundancy on critical inverters, generators etc.
   - Effective design of a puncture-proof casing under the battery storage in the fuselage.
   - Presence of a firewall between battery compartment and cabin floor for the passengers to reduce the severity of consequence of batteries catching fire.
   - Active environmental control to control the temperature in the battery compartment.
5. **Human Error:** Reduce the probability of occurrence of human errors:
   - The development of clear and consistent checklists for blown wing operations and failures.
   - Offering pilot training specific to using a blown wing.
   - Installation of a stick pusher/shaker for the pilots to prevent high α that results in deep stall of the T-tail.

Applying the risk mitigation strategies, the mitigated risk map of all critical events is constructed as shown in Table 18.2.

Table 18.2: Risk map resulting from the technical risk mitigation.

Probability of Occurrence	*Very likely*	7			
	Likely				
	Medium			6	
	Unlikely		3	4	
	Negligible			1	2, 5
		Negligible	*Marginal*	*Critical*	*Catastrophic*
		Severity of the Consequence			

19
Sustainability Assessment

This chapter aims to give an overview of all sustainable features of the E-COmmuter in a compact manner. First, the most important technical sustainable design features will be discussed in section 19.1. Second in section 19.2, an elaborate assessment will be performed of the noise production of the aircraft, since it is one of the most impactful sustainability metrics.

19.1. Assessment of Technical Sustainability

With the defined metrics from chapter 6, sustainability could be implemented into the technical design of the E-COmmuter. This section will give a concise overview of the most important measures taken during the technical design, and is to be used as a retrospect. For further, more elaborate reasoning the reader should refer to the analyses performed throughout the respective chapters and subsystems.

Accessibility

The entire mission of the aircraft has been specifically developed in order to provide rural, poorly accessible regions with a fast, reliable connection to the global network. All subsystems have been designed in order to be able to perform this mission. For example: the weight estimation and performance sizing in chapter 11 are entirely based on the ability for the E-COmmuter to perform the mission.

Furthermore, for the operations and logistics subsystem described in chapter 16, a very extensive travel time and availability analysis have been performed. This results in an availability percentage of the E-COmmuter of 93.7%, and average travel time of roughly 66% of corresponding ground transport. Thus, the aircraft can play a substantial role as transport mode supporting the development of individuals and companies using it.

Last, in the performance analysis in section 11.4, multiple versions of the aircraft are considered. These versions have different fuel and battery capacities, which make it possible for the aircraft to perform different missions than the nominal mission. These missions increase the reach of the E-COmmuter even further, increasing its accessibility capabilities even further.

Safety

Safety has been one of the most important drivers throughout the design of all subsystems. For example, for the propulsion & performance of the aircraft in chapter 11 and chapter 12, one-engine-inoperative cases have been studied, analyses have been done for the altitude of the highest European airport where lower performance is to be expected, and numerous failure scenario's have been investigated resulting in a large number of redundancies in the propulsion system architecture.

For the structures of the wing and fuselage in chapter 10 and chapter 9, safety factors are continuously throughout the entire subsystem applied for designing for loads, maintenance accessibility has been a priority and the material choice of GLARE has outstanding fatigue characteristics.

In stability & control in chapter 13, engine failure analyses have been performed, and stability, controllability and additional technical risk requirements have been met. Next, the blown wing configuration of the aircraft directs the flow behind the wing in stall, which guarantees airflow over the tail, preventing deep stall. Moreover, in the landing gear design safety is provided in the form of two wheels per strut. Each strut is also equipped with two types of dampers.

Last, for operations, an elaborate RAMS analysis is performed in chapter 17 that discusses a large number of reliability insurance, a very extensive maintenance plan and all applied safety factors throughout the entirety of the design.

In conclusion, with all the above mentioned measures and verification and validation activities performed, the safety of the design is assessed as very high.

Ecosystem Health

Probably the broadest subject within sustainability is the the ecosystem health. As has been discussed in the sustainability strategy, this concerns local emissions of NO_x and global emissions of CO_2. In the E-COmmuter design, these have been reduced in a simple but very effective manner.

First, the local emissions are reduced to zero by the zero-emission takeoff and landing which has been extensively designed for in the propulsion and performance subsystems of chapter 12 and chapter 11. To reduce the global emissions of CO_2, additional measures have been taken.

This goal is one of the requirements which states that the maximum CO_2 emission of $118.5\,g\,km^{-1}\,seat^{-1}$ for the nominal mission profile. To assure that this requirement is met, the total amount of fuel, which can be burned to not exceed that emission, was determined first. The performance and propulsion subsystems were then designed using this maximum amount of fuel as an input. Due to the finding the ideal hybridization factor and carrying just the right amount of batteries the aircraft is still able to complete its mission, which is ultimately the largest eco-friendly factor of the E-COmmuter.

Furthermore, for the different mission profiles that the derived versions of the E-COmmuter are able to fly from section 11.4, recommendations are made on how to make sure the design is still as eco-friendly as possible, e.g. by using green energy for charging the batteries.

Lastly, the structures subsystem of the wing and fuselage in chapter 10 and chapter 9 has a contribution to reducing the CO_2 emissions of the aircraft. Namely, the maximum emission performance has been based on the weight estimation of the aircraft. In the structures subsystem however, a primary goal is the reduction of the structural weight. With this reduction, the emissions will also reduce, resulting in an even more eco-friendly aircraft.

Resource Use

The resource use of the aircraft is primarily addressed in the wing and fuselage design, the manufacturing plan, and End-Of-Life (EOL) plan for the aircraft. The leading requirement for resource use is the recyclability of the materials used in the production of the aircraft.

From the wing and fuselage design, chapter 9 and chapter 10, the material choice has the largest influence on resource use. For the wing, GLARE is used which can be almost entirely recycled and re-used. The same goes for the aluminum used for the structure of the fuselage.

In the manufacturing plan of section 21.1, extra care is taken for minimizing waste material and re-using of waste that cannot be prevented. Next to this, at the EOL strategy of section 21.2, an elaborate plan has been developed to arrange the recycling of at least 85% of the used aluminum, GLARE and batteries of the aircraft.

Noise

For propeller aircraft there are three noise sources: engines, propellers, and the airframe of the aircraft. The engines of the E-COmmuter are placed within the fuselage, therefore the noise emitted by the internal combustion engines is discarded as being not a main source of aircraft noise. Keeping the serious noise requirements set by the International Civil Aviation Organization (ICAO) in mind, a substantial number of measures have been taken in the propulsion chapter and landing gear sizing section in order to reduce the noise.

The landing gear is retractable, which will greatly improve the noise characteristics of the airframe as discussed in section 14.2. Propeller sizing has been done in chapter 12 with noise reduction as driver. Including the high blade count of the propellers, four for the main and nine for the blown wing propellers, and relatively low Revolutions Per Minute (RPM), 2575 for the large and 3060 for the blown wing. Next to this, the propeller choice and diameter selection are purely based on noise reduction. Last, during the zero emission takeoff and landing the aircraft makes use of electric motors only, which are very silent.

The result of the noise reduction measures and their modeling will be elaborated in section 19.2.

Affordability

The last metric to be discussed is the affordability of the E-COmmuter. The affordability of the aircraft is a direct result of the cost analysis performed in chapter 22. Here, it was found that the direct operating cost slightly exceeds the requirement of €545 $flight^{-1}$ h, ending up at €640 $flight^{-1}$ h. While this is very unfortunate, a number of design decisions have helped to get this number down as much as practically possible.

The factors that increase the operation costs are mainly maintenance, ground handling and navigation fees. However, these costs cannot be mitigated. Ground handling and navigation fees are costs which are set by third parties, but these must be paid in order to operate the aircraft. Maintenance cost might be mitigated, but will have a negative effect on safety, thus mitigation is not possible here either.

Fortunately some of the factors which decreases the cost are also increase the sustainability of the aircraft. The first are capital battery cost due to low depreciation values of about 15000 cycles. This is a result of a meticulous choice of batteries with a high capacity so that less batteries are needed, and low unit cost. The second big factor is savings on energy use, which is due to the hybridization of the aircraft. Fuel is one of the most expensive factors for direct operating costs, which the E-COmmuter is not directly reliant on. The aircraft can use cheaper, green, electric charge, which also increases ecosystem health.

Finally, it can be concluded from the above assessment that sustainability has been a driver for the E-COmmuter design. As a result, the aircraft complies with all but one (HEF-OPR-05) sustainability requirements, the defined mission, and extra factors. Where this is not the case, the aircraft has been designed such that it comes as close as possible to the

requirement. All in all, it is believed that the E-COmmuter will prove to be a sustainable transport mode, viable to meet the needs and wants of the involved stakeholders for the years to come.

19.2. Noise

Noise emission is one of the most important and publicly debated issues in aviation industry in present day. This is mainly due to the very high number of affected people living in the vicinity of airports and because the results of noise nuisance can be very substantial. The emitted noise of the E-COmmuter is analyzed in this section.

Causes of Aircraft Noise

Aircraft noise can be categorized into two groups: propulsive noise and air-frame noise.
Airframe noise, or aerodynamic noise, is all noise generated by the non-propulsive components of an aircraft. In modern-day high-bypass turbofan engine aircraft, the air-frame noise represents the largest contribution to the overall noise level [98]. For a propeller aircraft, this contribution might be less but could still be very substantial. The main sources of air-frame noise for the E-COmmuter are the following [98]:

- **Wing trailing edge noise:** Main contribution to air-frame noise in clean configuration. It is caused by the scattering of the kinetic energy of the turbulent wing boundary layer at the trailing edge of the wing into acoustic energy. This also applies to the tail surfaces.
- **Flap side edge noise:** This noise type is is very substantial at takeoff and landing conditions. It exists due to the sideways movement of air from the bottom side of the flap to the side edge causing a vortex. This generates noise via interaction between side moving air and the sharp flap edge, and via unstable oscillations in the vortex. This noise also applies to the elevator and rudder.
- **Landing gear noise:** The noise of the landing gear is generated due to the complex vortex-force generated by the separation of unsteady flow behind the different structural components of the landing gear. This noise applies to both main and front landing gear.

The main source of the propulsive noise component is generated by the propellers. There are two main causes for propeller noise generation [99].

- **Rotational noise:** It is caused by the pressure differences due to the difference in airspeed for blades going up and down. The pressure differences on the blade between different moments in the rotations causes a noise of oscillatory nature. Additionally, extra rotational noise is caused by a propeller blade encountering the turbulent air of the preceding blade.
- **Vortex noise:** Which is caused by the formation and shedding of vortexes in the flow past a blade. These create an interaction of the air mass past the propeller which causes a broad-band noise.

19.2.1. Noise Models

Modeling aircraft noise accurately is a rather difficult task and an art in itself. Due to limited resources simplified noise models are used to evaluate whether this aircraft design will be able to meet the ICAO requirements or not. A preliminary method for propeller noise estimations is used. To analyze airframe noise the Aircraft Noise Prediction Program (ANOPP) is used [5]. Both will be treated respectively in this section.

Airframe Noise

One rather straight forward method to model the noise emitted by the airframe is the ANOPP method developed by NASA. For this method each aircraft component of interest is computed with a semi-empirical model. The core-equation for this model, a acoustic pressure equations, is shown below [5].

$$p_e^2(f,\theta,\phi) = \frac{\rho_\infty \cdot c \cdot P \cdot D(\theta,\phi) \cdot F(S)}{4 \cdot \pi \cdot r^2 \cdot \left(1 - M \cdot cos(\theta)\right)^4} \tag{19.1}$$

Where P is a acoustic power function , D is the directivity function and empirical spectral function versus Strouhal number S. With this model the noise induced by the wings, the flaps, and the landing gear can be determined separately and then later added to the applicable flight phase as described below. The noise calculations for airframe considers: wingspan, flap span, wing chord, and flap chord as geometrical input and the number of wheels and blisters, and tire diameter for the landing gear.

Propeller Noise

There has been a high demand for a method to estimate propeller noise in early design phases for a long time. Therefore, NASA had developed a simply preliminary modeling method with reasonable accuracy, which is described in [100]. This method uses empirical data to output a near-field and far-field noise level. From propeller input power in brake horse power, the starting sound level, called L1, is determined using the graph shown in Figure 19.1. This L1 sound level is then adjusted by applying a number of correction factors to it. These correction factors are influenced by the propeller diameter, blade count, RPM, air speed, directional characteristic of sound spreading and the attenuation due to the normal spherical spreading of sound and are read of of similar graphs as Figure 19.1 and can be found in Made and

Kurtz [100]. With the last two correction factors mentioned the sound pressure level at any point from the propeller can be calculated. When implementing this method into Python a sound pressure map can be generated and the noise at certain distances from the propeller can be determined.

The noise emitted by the large rotors and by the blown wing rotors is computed separately and then added to together. This is done with Equation 19.2 where SPL the sound pressure level and L_i is the noise emitted by each component emitted. The result is plotted onto a polar plot, which is shown in the noise map of Figure 19.2. In this noise map the aircraft is at the center and moving towards the 0° mark. The white spaces are due to the limited empirical data, which was only available from 45° to 160°. The thin black rings represent the distance from the aircraft in meters.

$$SPL = 10 \cdot \mathrm{Log}_{10}\left(\sum_{n}^{i=1} 10^{\frac{L_i}{10}}\right) \tag{19.2}$$

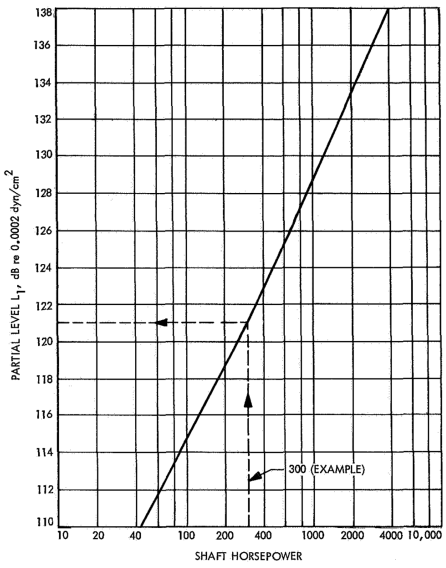

Figure 19.1: Reference noise level

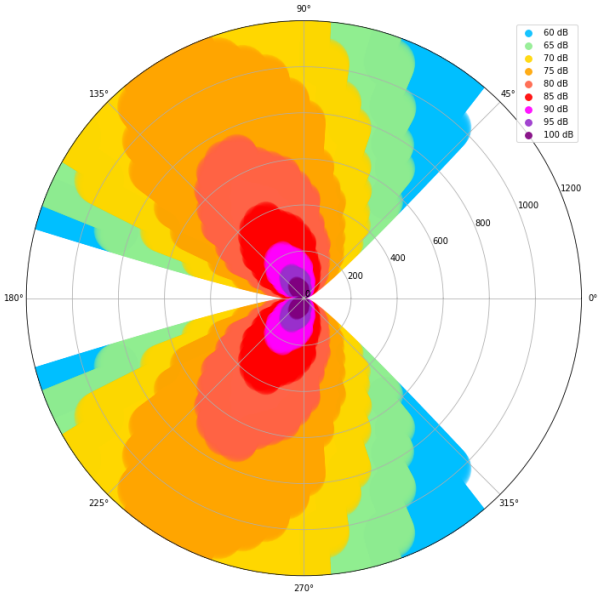

Figure 19.2: Noise map of main propellers and blown wing propellers

19.2.2. Noise Assessment

Guidelines for noise certification and assessment of aircraft used by many aviation authorities are defined by the ICAO in Annex 16, Volume I [101]. Chapter 10 in this Annex is applicable to the design of the E-COmmuter, with maximum noise levels defined in 10.4b). This noise level is applicable for propeller driven aircraft with a Maximum TakeOff Weight not exceeding 8618 kg and application for type certificate on or after 4 November 1999.

The noise emitted by the aircraft, propeller and airframe, is measured from three specifically defined points: the Lateral full-power reference point, the Fly-over reference point and the Approach reference point. Each of these points are shown as a red dot in the figures Figure 19.3,Figure 19.4 and Figure 19.5 below.

The Lateral full-power reference runs parallel to the center line of the runway at a distance of 450 m. The noise measured here shall not exceed 94 dB. The Fly-over reference point is at 6500 m distance from the start of the roll, the noise level measured here shall be less than 89 dB. The final measurement point for approach is located 120 m beneath the aircraft when approaching the airfield at a three degree angle. Here noise not higher than 98 dB shall be measured. It is important to note that the ICAO evaluated the effective perceived noise in decibel or EPNdB. This is a correction to the real noise level taking into account how the human ear perceives noise. Due to the limited model used here it was not possible to convert the noise level to EPNdB. In general the EPNdB is lower than the actual sound level. Therefore it is assumed that if the requirements are met using this model they will certainly be met when measured in EPNdB.

To asses if these requirements were met we will look at the noise maps to check whether the noise at the given distance exceeds the permitted sound pressure level. The noise map only consists of the propulsive noise. noise emitted by the E-COmmuter is more than 10 dB lower compared to the noise emitted by the propellers at the same distances.

Lateral Full-Power Measurement

During takeoff and initial climb the thrust settings are on full power, at this phase the noise produced by the main and blown wing propellers is the most intense. No flaps are used during takeoff but the landing gear at this point is still extended. The transition speed between lift-off and climb of 39 m s^{-1} is considered for the calculations. The sound pressure level allowed to pass this requirement is 94 dB at a 450m distance. In the noise map below Figure 19.6 one can see that the noise at this distance does not exceed 85 dB.

Fly-over Measurement

At the fly-over measurement point the aircraft is in its climb phase, the power setting are reduced and the blown wing turned off. The noise map below shows now the combination of the main propellers and wing noise. At a distance of 6500 m from start the aircraft flies at a speed of 59 m s^{-1} and has reached an altitude of 640 m, which is indicated in the blue circle in the Figure 19.7 below. It is obvious that the line does not cross the region of 85 dB or higher, therefore this requirement is met.

Approach Measurement

The approach reference point is the one measured the closest to the aircraft and can therefore be the most critical one. The E-COmmuter is descending unpowered using flaps only with an approach speed of 44 m s^{-1}. The main noise during this operation originates from the airframe only. The noise map is shown below in Figure 19.8 with the distance of 120 m indicated by the blue circle. The noise is well below the maximum of 98 dB.

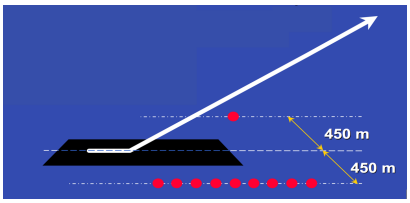

Figure 19.3: Lateral full-power point.

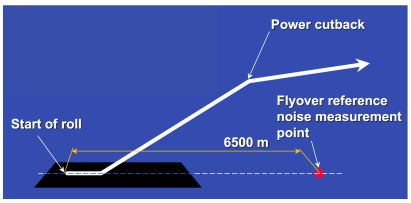

Figure 19.4: Fly-over point.

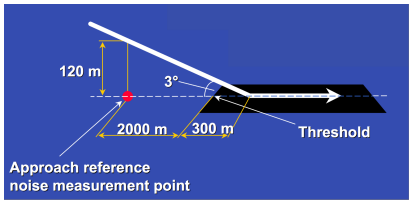

Figure 19.5: Approach point.

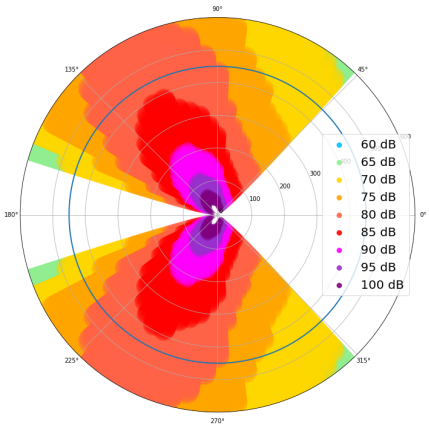

Figure 19.6: Takeoff noise map.

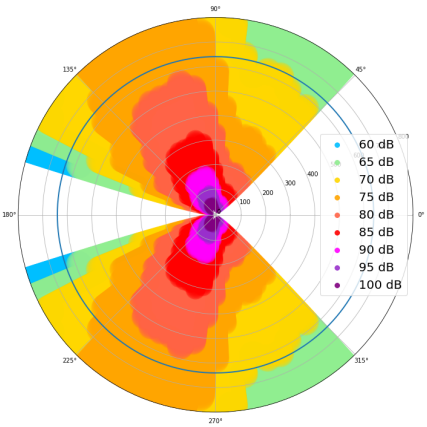

Figure 19.7: Fly-over noise map.

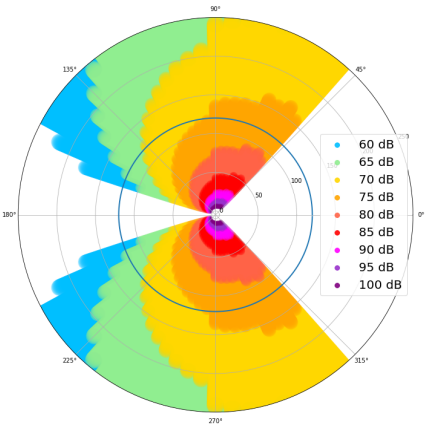

Figure 19.8: Approach noise map.

Verification

The NASA noise models are used to create a program which is able to map the noise emitted by the propulsive system and the airframe. Both the noise models from NASA are verified by making use of an example. The ANOPP method code is verified by means of putting in the parameters of an example case and check if the output coincides with the example case results. To verify the model code an example calculation given in the NASA paper [100] was used as comparison for he results of the program. The error was 0.6%, therefore the code is assumed verified.

The preliminary noise analysis needs some further development, as in the next design stages noise mitigation actions are still taken into account. A more detailed noise analysis needs to be conducted once the design is more finalized. The more detailed analysis needs a form of verification, this will be done by implementing the noise affecting characteristics of similar general aviation aircraft. Validation will be done by performing noise measurements at the three reference points defined by ICAO.

Moreover, a more detailed noise analysis has to be performed including noise emissions during ground operations and inside the cabin, instead of only during flight.

20

Further Project Development

After completing the DSE, the design still needs to be refined to a higher level of detail. In case of continuation of the design, several steps have to be taken to deliver a design which is capable to fulfill market demands and obtain certification. First, an initial overview will be given to show which tasks have to be performed over time. A schematic overview is given in the project design flow diagram, given in section 20.1. This is translated into a time planning which is provided in the project Gantt chart in section 20.2.

In the current design, battery technology expected to be available in 2035 is used. However, in case of continuation of the design, the battery capacity will need to be adapted to current available technology. This will result in a change of general aircraft parameters. However, it will not have a significant effect on the design planning since this is easily implemented in the upcoming design iteration loops.

The aircraft will be released already in 2023 since the current market analysis shows that there is already significant amount of demand for this aircraft. If the release were to be postponed to wait for development of the 2035 technologies, there will be a risk of competitors entering the market, which will result less favourable operating conditions. Furthermore, analysis has shown that the aircraft will still be sustainable and comply to all requirements adopting current battery technology.

20.1. Project Design Flow Diagram

The project is subdivided in five major phases. The first phase considers the creation of the detailed design. This is the most time consuming phase to deliver a certified aircraft. At this point in time the technical familiarization with EASA should also take place. This consists of personally discussing the aircraft with EASA. The second phase consists of subsystem testing. At the beginning of this stage, individual parts will be tested individually. From this point onwards, small assemblies of multiple parts are tested. This will slowly progress to testing of larger systems and finally complete subsystems. Simultaneously with testing the larger subsystem, a start will be made on developing the manufacturing process. The design and testing takes place in parallel for most of the subsystems. The manufacturing process for smaller subsystems can also be developed while it is tested. However, it should be taken into account that some parts will need a redesign after testing. In Figure 20.1 this is indicated by the blue dotted arrows.

If larger subsystems are produced, the manufacturing process will start to focus on creating the first aircraft prototype. Since part manufacturing processes are already defined for the subsystems, the prototype production can be performed in a time efficient manner. After production, the regulator needs to provide an experimental type certification. This will be provided based compliance demonstration that is performed during the test phase.

After receiving the experimental type certification, test flights can be performed and performance and stability & control characteristics can be evaluated. If for all the individual subsystem there is shown that they comply with the regulations, the final set of test flights can be performed to receive the airworthiness certificate. However, the certificate is only valid for that specific airplane. In order to receive a certificate for aircraft that you would like to sell to airlines, a production certificate needs to be obtained. The manufacturing process needs to be evaluated to receive this certification. Over time the manufacturing standards will need to be maintained in order to keep the production certificate as discussed in chapter 21.

After receiving the certification, the manufacturer stills needs to provide services to accommodate maintenance processes and end-of-life procedures. These are indicated in Figure 20.1 by level number 6.

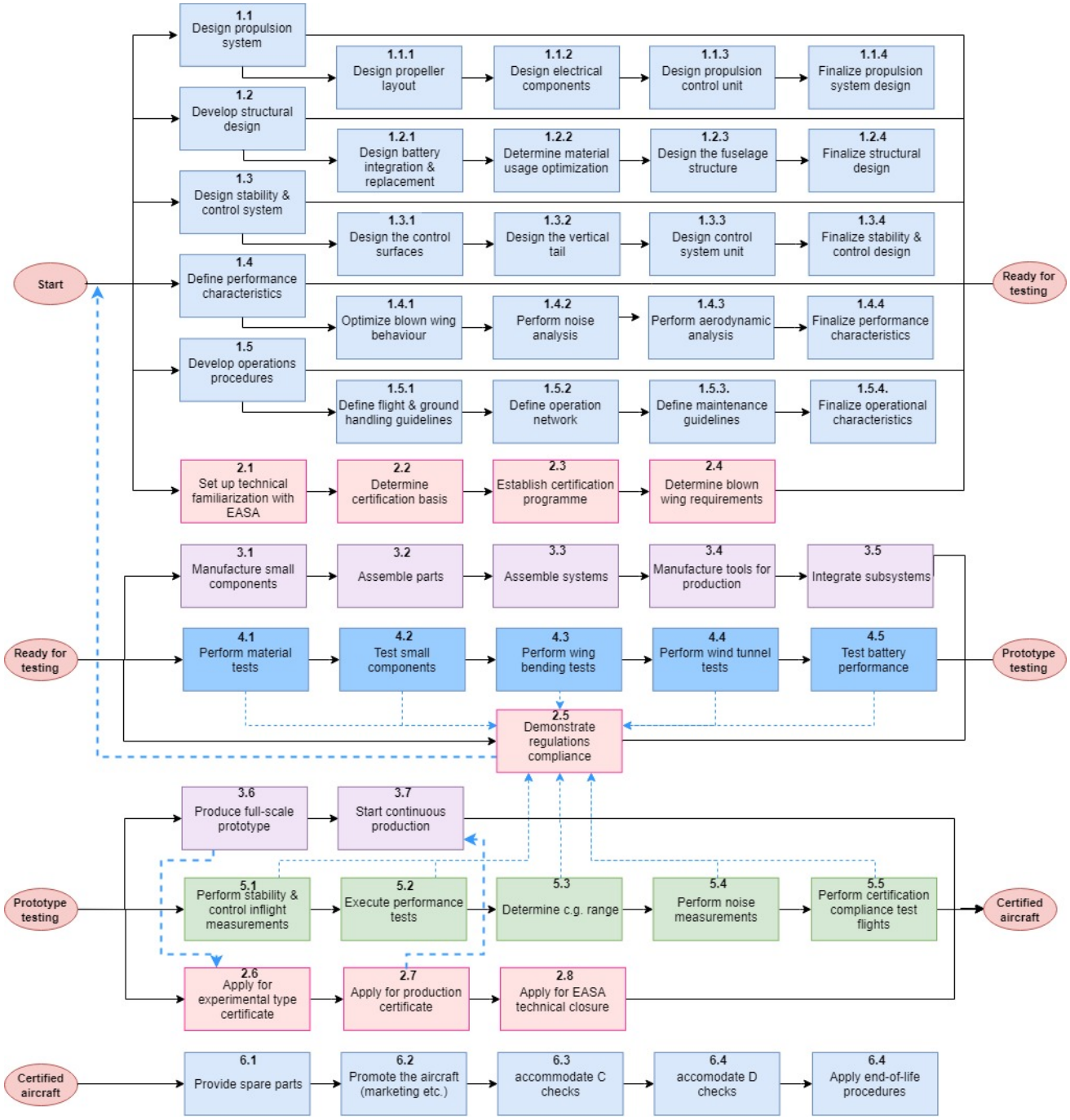

Figure 20.1: Phase block diagram for E-COmmuter project.

20.2. Project Gantt Chart

A realistic time planning, would suggest that the first commercial aircraft can be delivered in the summer 2023 to a customer. The time planning takes buffer time into account to compensate for any possible issues with the design of certain parts. By adding buffer time, the chances that customers will receive their aircraft with delay are minimized.

In figure Figure 20.2 a couple of milestone are defined. The first milestone will be achieved when the production of the first prototype starts. To achieve this, all subsystems need to have passed their test. The second milestone will be achieved if the first test flight is allowed. An experimental type certificate is required to achieve this. When the final certification test flights start, the design is frozen and no changes are allowed. This results in a final design. After receiving the aircraft certificate and production certificate, the final milestone is achieved and continuous production is allowed to start.

As can be seen in Figure 20.2, the detailed design takes is spread out over a large time frame. During the aircraft testing and manufacturing phases, the design is still likely to be revised. Extra time is reserved to revise design flaws or adjust the design for manufacturing purposes. By growing towards a more detailed design, more processes will be executed in parallel. As a consequence more manpower will be required as well.

The EASA will be involved in the design process of the aircraft from the start until the delivery of the first aircraft. Keeping connection with the EASA is crucial due to the novelty of the design. The design consists of components which have not been used before for a CS-23 regulated aircraft. Requirements need to be altered or added to ensure that the aircraft is safe to operate[1].

Also, the phases (indicated by 6 in Figure 20.1) after the receiving the EASA certification are not mentioned in the Gantt chart. These will take place over a long period of time and will therefore take place outside the time scale of the Gantt chart.

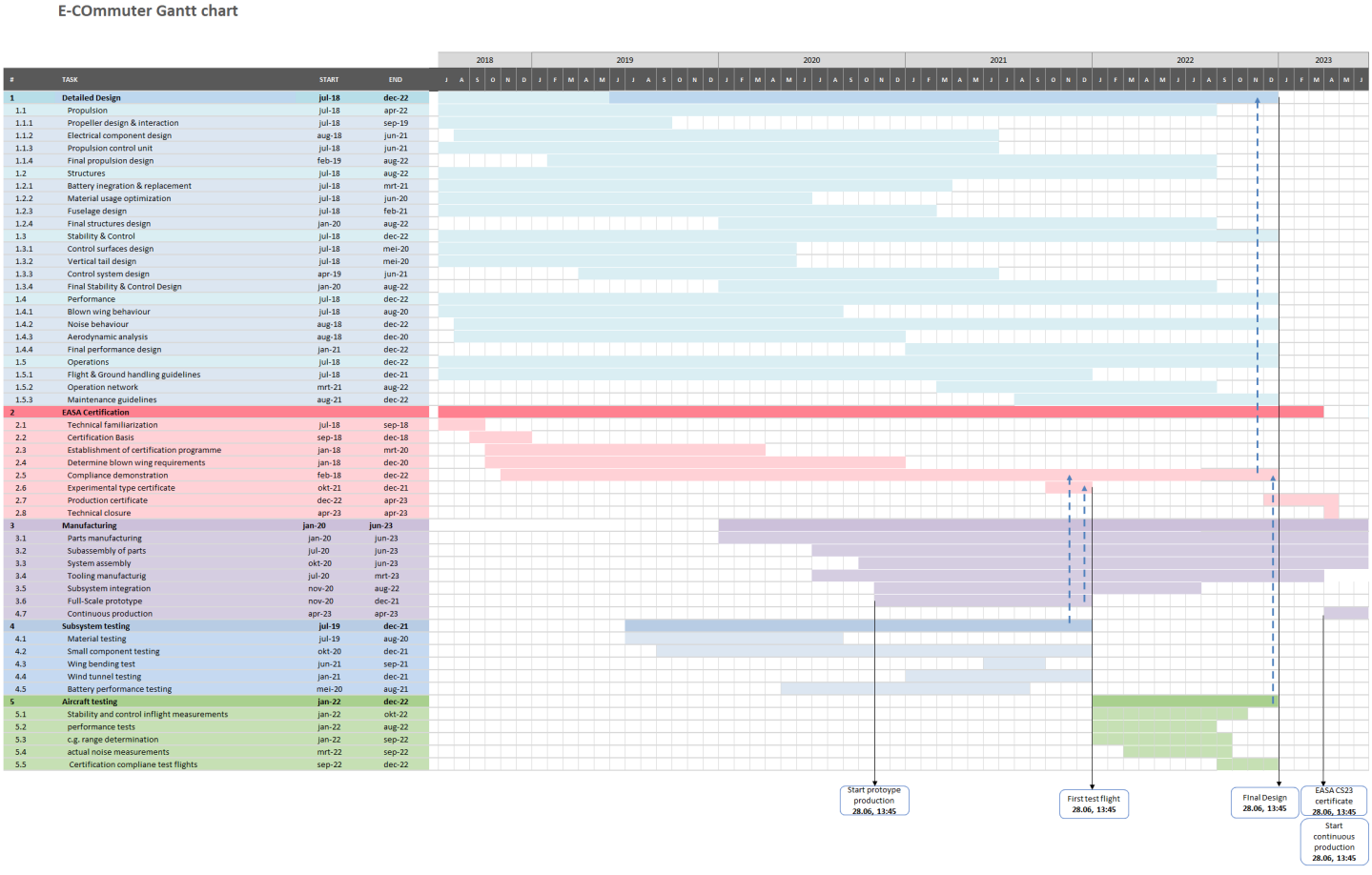

#	TASK	START	END
1	**Detailed Design**	**jul-18**	**dec-22**
1.1	Propulsion	jul-18	apr-22
1.1.1	Propeller design & interaction	jul-18	sep-19
1.1.2	Electrical component design	aug-18	jun-21
1.1.3	Propulsion control unit	jul-18	jun-21
1.1.4	Final propulsion design	feb-19	aug-22
1.2	Structures	jul-18	aug-22
1.2.1	Battery inegration & replacement	jul-18	mrt-21
1.2.2	Material usage optimization	jul-18	jun-20
1.2.3	Fuselage design	jul-18	feb-21
1.2.4	Final structures design	jan-20	aug-22
1.3	Stability & Control	jul-18	dec-22
1.3.1	Control surfaces design	jul-18	mei-20
1.3.2	Vertical tail design	jul-18	mei-20
1.3.3	Control system design	apr-19	jun-21
1.3.4	Final Stability & Control Design	jan-20	aug-22
1.4	Performance	jul-18	dec-22
1.4.1	Blown wing behaviour	jul-18	aug-20
1.4.2	Noise behaviour	aug-18	dec-22
1.4.3	Aerodynamic analysis	aug-18	dec-20
1.4.4	Final performance design	jan-21	dec-22
1.5	Operations	jul-18	dec-22
1.5.1	Flight & Ground handling guidelines	jul-18	dec-21
1.5.2	Operation network	mrt-21	aug-22
1.5.3	Maintenance guidelines	aug-21	dec-22
2	**EASA Certification**		
2.1	Technical familiarization	jul-18	sep-18
2.2	Certification Basis	sep-18	dec-18
2.3	Establishment of certification programme	jan-18	mrt-20
2.4	Determine blown wing requirements	jan-18	dec-20
2.5	Compliance demonstration	feb-18	dec-22
2.6	Experimental type certificate	okt-21	dec-21
2.7	Production certificate	dec-22	apr-23
2.8	Technical closure	apr-23	apr-23
3	**Manufacturing**	**jan-20**	**jun-23**
3.1	Parts manufacturing	jan-20	jun-23
3.2	Subassembly of parts	jul-20	jun-23
3.3	System assembly	okt-20	jun-23
3.4	Tooling manufacturig	jul-20	mrt-23
3.5	Subsystem integration	nov-20	aug-22
3.6	Full-Scale prototype	nov-20	dec-21
4.7	Continuous production	apr-23	apr-23
4	**Subsystem testing**	**jul-19**	**dec-21**
4.1	Material testing	jul-19	aug-20
4.2	Small component testing	okt-20	dec-21
4.3	Wing bending test	jun-21	sep-21
4.4	Wind tunnel testing	jan-21	dec-21
4.5	Battery performance testing	mei-20	aug-21
5	**Aircraft testing**	**jan-22**	**dec-22**
5.1	Stability and control inflight measurements	jan-22	okt-22
5.2	performance tests	jan-22	aug-22
5.3	c.g. range determination	jan-22	sep-22
5.4	actual noise measurements	mrt-22	sep-22
5.5	Certification compliane test flights	sep-22	dec-22

Figure 20.2: Gantt chart for E-COmmuter project.

[1] URL: `https://www.easa.europa.eu/easa-and-you/aircraft-products/aircraft-certification` [cited 23 June 2018]

21
Manufacturing Approach

With design at this stage it is time to take a look at the manufacturing of the E-COmmuter. The E-COmmuter is a series production aircraft. A Manufacturing, Assembly, and Integration (MAI) plan is an integral part of the design. The MAI plan provides a time line for all activities performed in order to build the final product from its different components. Furthermore, what will be done with the aircraft when it is out of service? This is treated in an End-Of-Life (EOL) strategy. The MIA plan and the EOL strategy will be treated in this chapter, respectively.

21.1. Manufacturing, Assembly and Integration Plan

The estimation of 100 sales in a 5-year time span will require an efficient organization, which includes parallel activities. First, the manufacturing of different parts is done. Afterwards, the assembly of the different parts to obtain the entire subsystem is elaborated upon. Finally, the the different subsystem assemblies are integrated into the aircraft system.

21.1.1. Manufacturing

For part manufacturing, parts are considered in the different subsystem, which elaborated upon using their allocated material. If a subsystem or large parts of a subsystem are manufactured by third parties, this is mentioned including a possible manufacturer. The different subsystems are: the wing, landing gear, fuselage, tail, batteries, and motors.

Wing

The wing box is entirely made from GLARE 3. Its manufacturing processes are comparable to those of sheet metals. Although there are some differences. GLARE 3 has laminates, which induces a risk of delamination of the glass fibre and aluminum. Tools have to be designed specifically for GLARE, as the fibres are highly abrasive resulting in tool wear. Tool geometry shall not be adapted as it is sufficient to only change the tooling material to hard metals or ceramics.

Considering the load carrying wing skin, lay-up can be used as this is a fully composite part. Pre-impregnated (Prepreg) glass fibre is used as well as aluminum sheets. The wing skin is split up in an upper and lower skin panel, which are riveted together. The main advantage of this lay-up technique is that the cross-sectional shape of the skin is easily manufactured. The skin of the wing box has a varying thickness along the span, for which manufacturing need to allow. The manufacturing of this varying thickness can be generated by ply drop-off, where a metal and composite layer is left out to decrease the thickness of the GLARE material as demonstrated in Figure 21.1 [102].

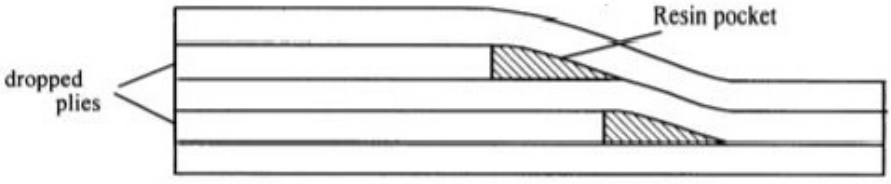

Figure 21.1: Ply drop-off of composite material [103].

In addition to the wing skin, the wing box adopts GLARE stringers. Metal forming is very often used to manufacture those as their thickness is often smaller. However, in case of the E-COmmuter, the L-stringers are relatively thick (large lay-up) resulting in delamination outside the bend zone at corners [102]. Therefore, it is decided that lay-up is used for the stringers as well. Moulds can be made for those as they all have the same geometry and thickness distribution along the span. The varying thickness is achieved with the ply-drop off technique. Exactly the same method is used for the spars to allow for the varying thickness and higher bending radius near the corners.

The high-lift devices need to be shaped aerodynamically to keep the airfoil shape similar. Therefore, the specific shape is obtained using a lay-up technique for the flaps and ailerons similarly as for the wing skin.

Landing Gear
A subcontractor manufactures the landing gear, due to the complexity of this system and need for a titanium alloy for this system. Field Aviation[1] could be a top candidate, a company that did manufacturing of the Twin Otter main gear. The Twin Otter is also a high performance aircraft with a considerably large wing loading. However, these landing gears are not retractable, which is a mechanism for which the design is still under consideration.

Fuselage
The fuselage is considered to be made from aluminum alloy as explained in chapter 9. Nominal, readily available manufacturing techniques for aerospace systems can be used. Delamination of GLARE is not present for aluminum, allowing for a higher strain which allows metal forming techniques more easily.

The fuselage skin is manufactured in 4 separated parts with 1 corners each. Using stretch forming (Figure 21.2), the curvature with a radius of 40 cm in the corners is obtained. Fuselage hat-stringers are considered to be of constant thickness, allowing them to be manufactured using the deep drawing technique as illustrated in Figure 21.3. Finally, the fuselage frames are manufactured using the rubber forming technique as this allows double curved parts with thicknesses between 0.5 and 3.0 mm. It is also a cost effective process for batches of up to 2500 parts, as is the case for the frames of the E-COmmuter within the next 5 years.

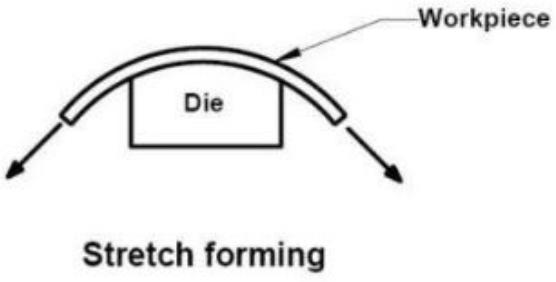

Figure 21.2: Stretchforming fuselage skin manufacturing[2].

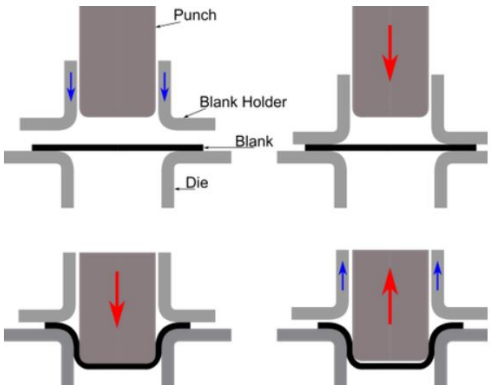

Figure 21.3: Deep drawing fuselage stringer manufacturing[3].

Vertical and Horizontal Tail
No material has been selected for the tail yet. In the upcoming post-DSE design activities, a material selection and a structural design of the tail will be performed. After the load carrying structure is designed, production activities can be planned. However, it is very probable that the tail production process will be very similar to that of the wing/fuselage.

Batteries
Next generation, highly efficient battery cells are supplied by third party Oxis Energy[4]. Their new Lithium-sulfur (Li-S) technology batteries are still in development, but a fireproof casing and thermal control is not provided by them. Therefore, during manufacturing, the battery subsystem will consist of separate parts being the puncture proof casing, fireproof wall, thermal control units and the battery itself. These are to be fitted in the provided wing space.

Motors
The electric motors are supplied by third party Compact Dynamics[5], for the main motors and blown wing motors. The large propellers are provided by Hartzell[6], while the blown wing propellers are custom made. This will be done using CFRP lay-up technique similarly to the wing design for 2 half propeller parts. This process allows the shape of the propeller to be customized to the fullest extent.

The support to connect the motors to the front spars is not designed in detail yet, but will be made from aluminum. Therefore, different metal forming and cutting techniques can be used depending on complexity of the connections and the available tooling.

21.1.2. Assembly

The assembly of the different subsystems is performed after all parts are constructed as mentioned in subsection 21.1.1. Assembly procedures in aircraft manufacturing are commonly performed in parallel for most different parts to be as-

[1]URL: http://www.fieldav.com/ [cited 21 June 2018]
[2]URL: https://www.enggwave.com/sheet-metal-forming [cited 21 June 2018]
[3]URL: http://agmellfem.com/examples/deep%20drawing.html [cited 21 June 2018]
[4]URL: https://oxisenergy.com/ [cited 21 June 2018]
[5]URL: https://www.compact-dynamics.de/unternehmen/ [cited 21 June 2018]
[6]URL: https://hartzellprop.com/ [cited 21 June 2018]

sembled to a subsystem. Doing so, the efficiency of the production is increased.

An example for the assembly of the wing subsystem is displayed in Figure 21.4. First, the parts are manufactured in the yellow boxes using the techniques provided in subsection 21.1.1. Recycled materials, such as aluminum sheets from recycled GLARE can be used in the lay-up of new GLARE reducing waste. After this, the red boxes indicate the assembly of all major wing components to the wing subsystem positioned on an assembly jig. Universal riveting is used as the main assembly technique for the wing as this is a suitable technique for GLARE showing reasonable fatigue characteristics [104].

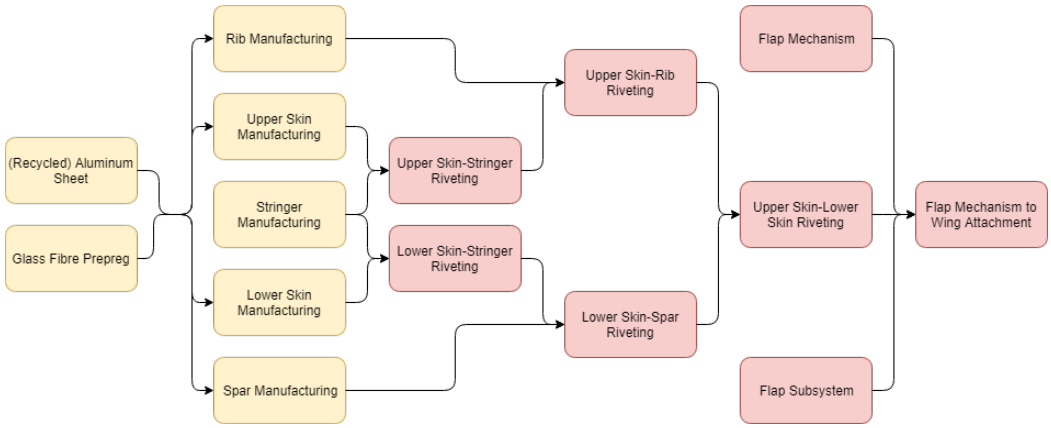

Figure 21.4: Wing subsystem part manufacturing (yellow) and assembly (red) process.

In addition to the wing subsystem, all other subsystems are manufactured in a similar fashion with part manufacturing in parallel. Some subsystems are immediately delivered from third parties as explained in subsection 21.1.1, for reasons of complexity or tooling availability. Once the design of the other subsystems is finished as elaborated upon in chapter 20, it is possible to make a more detailed production plan for the tail, fuselage, landing gear, battery and motor subsystems. The battery is considered as a separate subsystem as it is easily attached to the wing for maintenance reasons. Finally, the vertical and horizontal tail are treated separately and are integrated in the final assembly in Figure 21.1.2.

Integration

During the integration phase of the aircraft production, all different subsystems are integrated into a final aircraft. This process flow is displayed in Figure 21.5. The red boxes indicate subsystems elaborated upon in subsection 21.1.2, while the green box shows the totally integrated aircraft system.

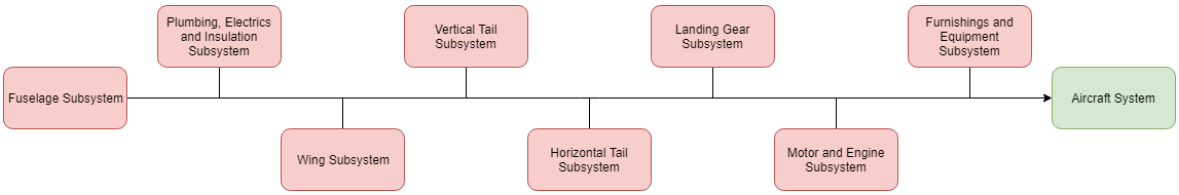

Figure 21.5: Integration of assembled subsystems (red) into the aircraft system (green) process.

After the integration is finished, the aircraft is tested at the end of the integration line for quality. First, the aircraft control surfaces, landing gear retraction mechanism, and avionics are tested at the end of the assembly line. After this, the aircraft is rolled out and a Production Flight Test (PFT) is performed to ensure that the individual aircraft conforms with the type design, thus to earn the Certificate of Airworthiness (CoA). The following tests are performed during PFT to provide quality assurance [105]:

- Operational check of trim, controllability and other flight characteristics.
- Operational check of each crew operated system to establish that instrument readings are in their normal range.
- Check that all flight manuals are installed and instruments are marked accordingly.
- Operational ground handling characteristics.

Once the produced and production flight tested aircraft obtains its Certificates of Waiver or Authorization, the manufacturer hands over the aircraft to the customer and the aircraft becomes operational. Prescribed maintenance techniques discussed in section 17.2 and arising from the type certificate are the responsibility of the operator to keep the aircraft airworthy.

21.2. End-of-Life Strategy

When an aircraft becomes obsolete, meaning that it can be replaced by newer, better alternatives, it becomes an end-of-life aircraft. It enters retirement, either permanently or temporary. Temporary retired aircraft are parked and stored until they become operational again. Permanently retired aircraft are often parked on airplane graveyards [106]. There are several options of what can be done with these aircraft [107]: Reuse, Recycling, Recovery, and Disposal:

Reuse

Four types can be identified:

- Reuse of the entire aircraft: no new resources are required to manufacture a new aircraft.
- Converting the aircraft into a freighter aircraft: the conversion needs to be performed before the aircraft becomes to old to operate.
- Component reuse: parts can be reused in other aircraft after being disassembled. These parts are be for example, engines, aircraft seats, door handles, etc. Some of these components can only be reused on very similar aircraft.
- Alternative reuse: a component is reused without sustaining its original function. An example of this is the 747 Wing House[7]: the wings and tailplanes of an old Boeing 747 are used as roof for this house.

Recycling

The material can be used to create new components. This is discussed later in more detail.

- Primary recycling: scrap material from the production process, such as chips, curls, is recycled. Since this material is of one type of alloy, t can be remelted and used in the same production process.
- Secondary recycling: end-of-life material is recycled. The material needs to be recovered from the aircraft and is often a combination with other materials, making it more challenging to recycle.

Recovery

If the material cannot be recycled, energy can be recovered from the material by for example burning waste.

Disposal

The material that cannot be reused, recycled or recovered is disposed in landfills.

With sustainability in mind, the end-of-life E-COmmuter will be reused as much as possible. When this is no longer an option, the aircraft is recycled. Through its life cycle, from design and manufacturing to operation, the E-COmmuter uses resources. Recycling it when the aircraft becomes obsolete provides an opportunity to return resources, creating an environmental and economical benefit. In order to reuse/recycle, the materials and components need to be harvest from the aircraft: this is done through disassembly and dismantling. Disassembly means that all components that can be reused in other aircraft are removed. This is done under supervision of several aviation authorities, such as the European Aviation Safety Agency (EASA) and the Federal Aviation Administration (FAA). To recycle materials from the aircraft, it needs to be dismantled [107]. This is done after the disassembly.

In the following subsections, the end-of-life process of the E-COmmuter is discussed in more detail. Figure 21.6 shows an overview of the process.

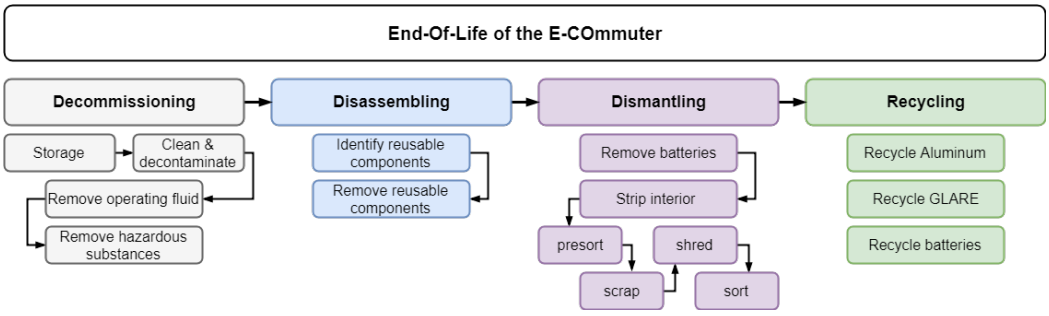

Figure 21.6: End-of-life process of the E-COmmuter.

21.2.1. Decommissioning

The aircraft is taken out of service and put into storage. Then, the aircraft is inspected: valuable parts that can be reused are identified. Next, the aircraft has to be cleaned and decontaminated. This means that all systems, tanks, pipes, pumps, etc. are emptied. Afterwards, any operating fluid that might still be present, such as hydraulic fluids, oil, and fuel are removed. These either be resold and reused or they are disposed under supervision of regulations. Moreover, any potentially dangerous substance should be removed as well [106][108].

[7] URL: `http://www.mro-network.com/maintenance-repair-overhaul/5-surprising-facts-about-aircraft-recycling/gallery?slide=5` [cited 21 June 2018

21.2.2. Disassembly

Disassembling the aircraft starts with deciding which components are valuable and can be removed and reused. The removal of these components is done under supervision of aviation authorities: the most important rule imposed is the safe use of the removed component [107].

During the operation of the aircraft, components can malfunction or be damaged. These are removed from the aircraft and replaced by another working component. The defect part is repaired and stored and eventually used to replace another malfunctioning component. Another replacement option is replacement by end-of-life components. These are not removed from the aircraft because of malfunctioning, but because the aircraft will never fly again.

Before the end-of-life components can be reused, they need to be classified as serviceable. If the aircraft is unserviceable, unregistered, defect or has been involved in an accident/incident when it becomes obsolete, the components automatically becomes unserviceable. Furthermore, if there is no history available on the aircraft, the status of components is unknown and cannot be considered reliable [107]. For the E-COmmuter, parts that could be disassembled and reused in other aircraft are:

- The internal combustion engines
- Propellers
- Electric motors
- Avionics
- Inverters
- Generators
- Furnishing
- Landing gear

21.2.3. Dismantling

There are also parts of the aircraft that cannot be reused, either because they are declared unserviceable, or there is no market for them [107]. The batteries of the E-COmmuter are removed first, and treated in a different way than the rest of the aircraft. Then, the interior of the aircraft is stripped: in the cockpit (avionics, panels, etc) and in the cabin (floor, seats, luggage compartments, etc) [106]. Afterwards, pre-sorting is performed. The aircraft is scrapped and components having similar materials are separated from each other [107]. For the E-COmmuter, this means that the wing (made from GLARE) is sorted from the fuselage and tail (made from an aluminum alloy) and from the landing gear (made from a Titanium alloy). Then, these parts are send to recycling facilities where they are shredded and further sorted.

21.2.4. Recycling

After scrapping and presorting the components, they are send to recycling facilities. For the E-COmmuter, the recycling of the aluminum parts can be discussed, as well as the recycling of GLARE. Moreover, since the E-COmmuter is a hybrid electric aircraft, a look can be taken at the recyclability of the batteries.

Recycling of Aluminum Alloys

The aluminum components are entered in a shredder and are chopped in smaller pieces. The scrap or fluff is sucked away and the aluminum pieces are passed by a magnet, to separate the ferrous from the nonferrous ones. The nonferrous parts are sorted further using more sophisticated techniques, based on the difference in physical properties. For example, an Eddy current device can sort the aluminum parts based on their electric conductivity, a sink floating device can sort them based on their density. This way, different alloys can be sorted [107]. Aluminum can be separated into their 2xxx and 7xxx series: the 2xxx aluminum can then be recycled into a Al2024-like alloy, while the 7xxx can be recycled into a Al7075-like alloy [109]. Afterwards, the shredded pieces are decoated and molten. This can then be used to manufacture new parts. Since, the quality of recycled aluminum is questionable, it are destined for downcycling. It can be used to manufacture non-critical aircraft components such as stringers, flaps, low to moderately stressed components. The recycled material cannot be used in fracture-critical parts: clean aluminum allays should be used for this. Furthermore, the recycled metal can also be used in other applications, such as the car/truck industry [107]. Aluminum alloys have a recycling rate of approximately 90% [110].

Recycling of GLARE

The wing is made from GLARE. GLARE is a laminated material consisting of thin layers of aluminum metal sheets and a prepeg, glass fiber embedded in an epoxy resin [38]. To recycle GLARE, the metal sheets should be separated from the glass fibers. These can then be recycled separately. The recycling of GLARE is still under investigation. Two major techniques are considered: cryogenic delamination and thermal delamination [38].

In cryogenic delamination, only the aluminum sheets are recovered. First, the GLARE scrap is reduced to small pieces of 10 mm size in the presence of liquid nitrogen at -192°. A low temperature cryogenic liberation is started to separate the aluminum sheets from the glass fibers and epoxy resin, using their large differences in thermal expansion coefficients. The mixture of separated aluminum parts, glass fibers, resin and unseparated GLARE is passed by an Eddy current separated, to isolate the aluminum [38]. The aluminum can then be processed again. This technique has a high cost compared to the market value of recovered aluminum scrap and the glass fibres are not recycled making this technique less sustainable.

A second method is thermal delamination. GLARE can be delaminated at a temperature of 500°. This results in clean glass fibres and aluminum parts. The glass fibres can then be reused in lower level applications, while the aluminum

can just be remelted and reused with its original quality to make new GLARE [38].

In order to recycle the entire wing of the E-COmmuter, the latter technique is used, so that both the aluminum and glass fibres can be recycled.

Since GLARE is a novel material in the aerospace industry and no actually end-of-life recycling has been applied yet, the recycling methods proposed here are still under investigation. Consequently, no recycling rate is determined. However, when using thermal delamination, both the fibers and aluminum can be recycled. Therefore, it is save to assume that by 2030, the method will be further developed, resulting in a recycling rate equal/higher than 85%.

Recycling of Batteries

The batteries used in the E-COmmuter are Li-S batteries. Recycling batteries is a complicated process and is not well-developed for Li-S batteries since this is a novel battery. Therefore, recycling methods for Li-Ion batteries are refined to fit Li-S batteries.

The recycling of batteries mainly focuses on retrieving of the metal, the process consists of multiple steps [111]:

1. The battery is discharged.
2. The container and plastics are separated and recycled [112].
3. Mechanical crushing/shredding: the electrode and electrolyte go to the next step.
4. Electrolyte extraction: the electrolyte is liquid and is dispersed in the electrodes. If this as a whole is immersed in a suitable solvent, the electrodes can be extracted. After the separation, the solvent is evaporated and pure electrolyte is left. This can be reused in other batteries [111][113].
5. Electrode dissolution: electrodes are cast on a binder and need to be separated. By immersing this in a suitable solvent and stirring it at a suitable temperature, the binder dissolves and the electrode particles are separated. These particles are then sieved and filtered to recover valuable materials. The metals can be filtrated out of the solution [111][113].
6. The metals can directly be reused to make new batteries.

Recycling Rate of the Aircraft

An overall recycling rate of the aircraft can be defined. The recycling rate of an aircraft is obtained by applying Equation 21.1 [107].

$$R_{cyc} = \frac{M_{uses} + M_{cyc}}{M_v} \tag{21.1}$$

Here, M_{uses} represents the total mass of the components that can be reused in other aircraft or applications. M_{cyc} represents the mass of all he components that can be recycled and M_v is the total vehicle mass, which is in the case of the E-COmmuter equal to the empty weight.

Component	Mass	Component	Mass
Reused mass			
ICE	364.4 kg	Propellers	81 kg
Electric motors	83.4 kg	Inverters	80.2 kg
Generators	65.9 kg	Avionics	267.6 kg
Furnishing	310.1 kg	Landing gear	283.0 kg
Recycled mass			
Wing structure	596.3 kg	Fuselage structure	669.3 kg
Tail structure	99.4 kg	Batteries	587 kg

Table 21.1: Reusable and recyclable component masses of the E-COmmuter.

To evaluate the recycling rate of the aircraft, the masses shown in Table 21.1 cannot be directly implemented in Equation 21.1. The total reusable component mass is 1535 kg, which is around 45% of the total aircraft empty weight of 4080 kg. However, it cannot be assumed that all of these components are always able to be reused. A factor needs to be applied to account for scenarios where the aircraft components become unserviceable (for example when the E-COmmuter has been involved in an accident/incident or is unserviceable when it enters end-of-life) or when there is no market for the components. A factor of 0.85 is applied, assuming that 15% of the reusable components cannot be reused due to unforeseen circumstances. Furthermore, to account for the material recycling rates, the masses of the recyclable components are multiplied by there respective recycling rate. For the batteries, since the recycling process is not well-defined yet for Li-S batteries, it is assumed that it only has a recycling rate of 60%. So, a reusable mass of 1305 kg and a recyclable mass of 1550 kg. Resulting in a total aircraft recycling rate of 70%.

22

Cost Analysis

With the E-COmmuter manufacturing approach developed the feasibility of further developing and producing the aircraft a preliminary cost estimation is performed. Performing a cost analysis provides insight in the affordability of the aircraft, both on purchase costs and costs during operations. As it directly relates to affordability of the aircraft, it is of major importance for the sustainability of the project.

The cost analysis is divided into two parts, the production and development costs (initial fixed costs) and the direct operating costs. They both are broken down in smaller categories, all calculated in the models described in the following sections. The cost breakdown structure is shown in Figure 22.1. The total life cycle cost breakdown as seen in the figure is calculated per aircraft.

The main focus of this chapter is on the costs for an operator. This is chosen rater than focusing on the manufacturing side as the operator side provides insight in the unit costs and the operating costs of the aircraft, two values having large impact on the choice of an airline to buy and operate an aircraft type.

The equations provided in this chapter are mostly found from statistical values or from reference values. During the chapter most parameters used in the equations are provided with their assumed values. However, some come directly from the design of the aircraft as discussed in previous chapters. Most notable of these are the airframe weight (W_{airframe}) and the maximum level flight velocity (V_H), equalling 1630 kg and 97 m s^{-1}, respectively.

Firstly the production and development cost analysis is performed in section 22.1 to find the cost of development and the minimum sales price of a single aircraft. This analysis then is used in the calculations on direct operating costs (DOC), in section 22.2, which show if the aircraft is affordable when operating. A complete overview of the results of the two analyses is elaborated upon in section 22.3.

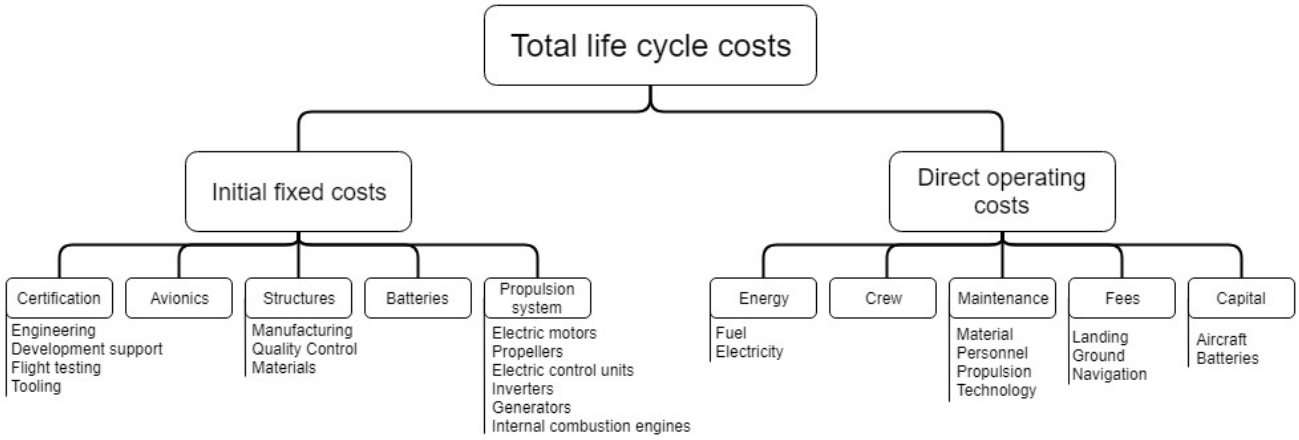

Figure 22.1: Cost breakdown structure of the cost analysis. The subcategories are according to the models in Sections 22.1 and 22.2.

22.1. Production & Development Cost Analysis

The production and development cost analysis is based on the 1987 Rand Corporation method Development and Procurement Cost of Aircraft, version IV (DAPCA IV). Although this method is relatively old, most current cost analyses are either shortened versions of DAPCA IV (eg. Raymer [31]) or they are applied to recent years' cost and economy (eg. Gudmundsson [25]). Therefore, the DAPCA IV method, applied to general aviation aircraft by Gudmundsson, is used in the cost analysis. The analysis is however performed keeping in mind the novelty of the aircraft, as well as the expected high costs of batteries and hybrid propulsion system.

The aircraft price analysis is performed by calculating certification costs (engineering, flight tests, development and tooling), structures costs (manufacturing, quality control and materials), propulsion system costs (motors, internal combustion engines and propellers), avionics- and battery costs. This cost analysis thus covers the basic parts of an aircraft driving the unit price. Interior and control surfaces are assumed to be included in the structures cost.

The adapted DAPCA IV cost analysis is described by Gudmundsson. As DAPCA IV is an old method, the costs are converted to 2012 dollar values by Gudmundsson using the consumer price index (CPI). The conversion to current costs is then performed using the CPI of 2018 relative to 2012, $CPI_{2012} = 1.0958$[1]. Assumed is that worldwide inflation is approximately the same, thus CPI factors for European currencies are comparable to American Dollar CPIs. Furthermore, all costs are calculated in Euros, converting Dollars to Euros with a factor 0.87[2].

The cost analysis first calculates the man hours required for engineering, tooling, manufacturing and quality control, the latter being a function of manufacturing. By multiplying these with the hourly rates of the personnel involved in the respective departments, the total cost is calculated. Note that the author made an error in the model, as the CPI from 1986 to 2012 is used in the calculations. Hourly rates are already provided in 2012 currency values. Moreover, the novelty of the aircraft is assumed to be very high with respect to the model calculations. The model thus has to be adapted to this novelty, which is done by using a factor of 1.5 for engineering, tooling, manufacturing, and quality control hours required.

Engineering

The engineering hours and costs then are calculated with Equations 22.1 and 22.2. In the Equation 22.1 the airframe weight (W_{airframe}, lbf), maximum level flight velocity (V_H, KTAS), number of aircraft built in 5 years of production (N) and the fraction of the airframe made of composites (f_{comp}) are required. The cost equation furthermore requires the hourly rate of an engineer (R_{eng}), assumed to be \$92 h^{-1} in 2012 [25].

$$H_{\text{eng}} = 0.0396 \cdot W_{\text{airframe}}^{0.791} \cdot V_H^{1.526} \cdot N^{0.183} \cdot (1 + f_{comp}) \quad (22.1)$$

$$C_{\text{eng}} = 1.5 \cdot H_{\text{eng}} \cdot R_{\text{eng}} \cdot CPI_{2012} \quad (22.2)$$

Tooling

All man hours and costs for building tools, molds, etc. required to produce aircraft are included in the tooling cost calculation given in Equation 22.4. Apart from some parameters used in engineering cost calculations, the production rate per month ($Q_m = \frac{N}{60}$) and the tooling hourly rate (R_{tool}) are required (see Equation 22.3). The latter is assumed \$61 h^{-1} in 2012 [25].

$$H_{\text{tool}} = 1.0032 \cdot W_{\text{airframe}}^{0.764} \cdot V_H^{0.899} \cdot N^{0.178} \cdot Q_m^{0.066} \cdot (1 + f_{\text{comp}}) \quad (22.3)$$

$$C_{\text{tool}} = 1.5 \cdot H_{\text{tool}} \cdot R_{\text{tool}} \cdot CPI_{2012} \quad (22.4)$$

Manufacturing, Material and Quality Control

Using the same parameters, manufacturing hours and costs are determined. Manufacturing labor rate (R_{mfg}) of \$53 h^{-1} in 2012 is used. Using the cost of manufacturing in Equation 22.6, the quality control expenses (C_{QC}) are calculated in Equation 22.8. Furthermore, the raw material costs (C_{mat}) are to be calculated for production of the aircraft.

$$H_{\text{mfg}} = 9.6613 \cdot W_{\text{airframe}}^{0.74} \cdot V_H^{0.543} \cdot N^{0.524} \cdot (1 + 0.25 \cdot f_{\text{comp}}) \quad (22.5)$$

$$C_{\text{mfg}} = 1.5 \cdot H_{\text{mfg}} \cdot R_{\text{mfg}} \cdot CPI_{2012} \quad (22.6)$$

$$C_{\text{mat}} = 24.896 \cdot W_{\text{airframe}}^{0.689} \cdot V_H^{0.624} \cdot N^{0.792} \cdot CPI_{2012} \quad (22.7)$$

$$C_{\text{QC}} = 0.13 \cdot C_{\text{mfg}} \cdot (1 + 0.5 \cdot f_{\text{comp}}) \quad (22.8)$$

Development Support and Flight Tests

The cost for development support (C_{dev}) of the aircraft (administration, human resources, facility personnel etc.) are calculated with a statistical relation, including the number of prototype aircraft built (N_p). This parameter is again used in the cost of flight test operations (C_{ft}).

$$C_{\text{dev}} = 0.06458 \cdot W_{\text{airframe}}^{0.873} \cdot V_H^{1.89} \cdot N_p^{0.346} \cdot (1 + 0.5 \cdot f_{\text{comp}}) \cdot CPI_{2012} \quad (22.9)$$

$$C_{\text{ft}} = 0.009646 \cdot W_{\text{airframe}}^{1.16} \cdot V_H^{1.3718} \cdot N_p^{1.281} \cdot CPI_{2012} \quad (22.10)$$

Propulsion System

Propulsion system costs are calculated from the propulsion architecture, using the input power and the assumed cost per kW or a reference cost, in case of the internal combustion engines (ICE). These are expected to cost \$50.000 each[3]. The cost of the novel Lithium-sulfur batteries is estimated based on the raw materials cost. The cell materials have a cost of \$100 kW^{-1} [51]. It is expected that in the coming five years, a total battery cost of \$250 kW^{-1} can be achieved [61]. Consequently, a value of \$200 kW^{-1} is assumed for 2035.

[1] URL: https://www.officialdata.org/2012-dollars-in-2018 [cited 15 June 2018]

[2] URL: https://ecb.europa.eu/stats/policy_and_exchange_rates/euro_reference_exchange_rates/html/eurofxref-graph-usd.en.html [cited 19 June 2018]

[3] URL: http://airpowerinc.com/productcart/pc/TCEngineDetail.asp?catID=69&prodID=24252 [cited 14 June 2018]

Total costs then are calculated using the number of each part in the aircraft and, if required, converted to Euros. Table 22.1 provides the assumed costs per kW for propulsion system components other than the ICE and the batteries. References in which the assumptions are based are provided in the table. For expected the costs of electric motors, engineers of Pipistrel were contacted.

Table 22.1: Assumed costs for propulsion system components and batteries.

	Electric motor	**Electronic control unit**	**Inverter**	**Generator**
Assumed cost per kW	\$100	\$100	\$75	\$200

Costs for propellers are calculated from statistical cost relations [25]. The small blown wing propellers are fixed pitch, the costs calculated in Equation 22.11. Large propellers are constant speed propellers, for which Equation 22.12 holds. In the equations the number of propellers (N_{pp}), the diameter of the propellers (D_p) and the shaft power (P_{shp}) are required. The number of propellers is assumed to be the number of blades per propeller multiplied by the number of motors.

$$C_{\text{fixprop}} = 3145 \cdot N_{\text{pp}} \cdot CPI_{2012} \tag{22.11}$$

$$C_{\text{cstprop}} = 209.69 \cdot N_{\text{pp}} \cdot CPI_{2012} \cdot D_p^2 \cdot \left(\frac{P_{\text{shp}}}{D_p}\right)^{0.12} \tag{22.12}$$

Miscellaneous
In the calculations, the cost of retractable landing gear is already included [25]. Avionics are estimated to cost \$60.000 per aircraft [114]. Lastly, liability costs are added to the aircraft cost. These are to account for any possible incidents happening, and are estimated at 17% of the total cost [25].

22.2. Direct Operating Costs

With the sales price of the aircraft, the cost analysis is far from complete. It is of high importance to know the direct operating costs (DOC) of the aircraft, as they are a major part of aircraft life cycle cost (LCC), up to 94% [115]. It thus is of importance for the operator to know the expected DOC in advance in order to make a considered decision on which aircraft to purchase. This section will elaborate on the method used in the analysis, then provide an initial estimation of DOC.

The method used in this analysis is based on a DOC model by Bardenhagen and Gobbin [116], which is altered to be used for hybrid-electric aircraft by Hoelzen et al. [117]. The DOC is divided into different categories, each to be calculated, and the sum of all categories provides an estimate for annual operating costs. The categories to be analyzed are energy consumption (both fuel and electricity), crew, maintenance, capital costs and fees.

First, the number of flight cycles per year have to be determined, as these are used regularly in the model. From section 17.3 can be seen that the hourly calculated availability of the aircraft is 93.7%. This includes however nightly hours, in which flying is not considered possible. Using the days per overhaul cycle in which the aircraft is available (2000 days in 2046 days' cycle, scheduled availability), the availability is 97.7%. Thus, on a yearly basis the aircraft is available for approximately 356 days. At six flights per day, derived in section 17.3 and Hoelzen et al. [117], the total flights per year equal 2136. Taking into account a margin for unscheduled maintenance and repairs, as well as delays and scheduling lowering daily flights, the annual flight cycles are estimated 2100.

Energy
Energy DOC are found by finding the average fuel burn (FB) and electrical energy (E_{Bat}) consumption per flight, and multiplying them with their expected prices. Then multiplying with the annual flight cycles yields the annual energy DOC. The price for fuel (p_{Fuel}) is expected to be \$0.934 kg^{-1} [117], which is converted to Euros with the previously provided exchange rate of 0.87 to €0.813. Electric energy price (p_{Elec}) forecasts for industrial purposes are approximately €0.11 kW^{-1} h^{-1} [118]. The energy DOC equation is provided in Equation 22.13.

$$\text{DOC}_{\text{Energy}} = \text{FC} \cdot (\text{FB} \cdot p_{\text{Fuel}} + E_{\text{Bat}} \cdot p_{\text{Elec}}) \tag{22.13}$$

Crew
Crew costs are calculated using the yearly salary of the pilots (s_{Pilot}) and the number of pilots required to fly throughout the week. Median pilot salaries in the USA are approximately \$100.000[4], or €87.000. Two pilots (n_{Pilot}) are required to fly the aircraft. The crew complement (CC), the number of crews required to fly the aircraft during the week, is estimated 3. The CC is determined assuming two crew shifts (morning and afternoon/evening) are required each day, the three crews rotating between days off, morning- and afternoon shifts. Equation 22.14 provides the final expression of crew DOC.

$$\text{DOC}_{\text{Crew}} = s_{\text{Pilot}} \cdot n_{\text{Pilot}} \cdot \text{CC} \tag{22.14}$$

[4] URL: `https://payscale.com/research/US/Job=Airline_Pilot%2c_Copilot%2c_or_Flight_Engineer/Salary` [cited 20 June 2018]

Maintenance

Maintenance DOC (DOC_{Ma}) is divided in material- (DOC_{AFmat}), personnel- (DOC_{AFper}), engine- (DOC_{Eng}) and overhead technology costs (DOC_{Tech}). Of these DOC, the technology costs are set directly in annual costs, the rest is determined per FC. In the maintenance equations, the airframe weight ($W_{airframe}$) is required in kg, but otherwise is the same as defined before. Total time (t_{Total}) is the average total block time per flight in hours, determined from the time analysis. Maintenance labor rate (R_{maint}) is estimated at €50 h^{-1} [117]. The total propulsion efficiency ($\eta_{prop,TO}$), takeoff propulsion power ($P_{Total,\,max}$), wing span (b) and fuselage length ($l_{fuselage}$) are all inputs from the design phase, set in SI units. The respective parts of maintenance DOC as well as the total are calculated with the following equations:

$$DOC_{AFmat} = W_{airframe} \cdot (0.0010136 \cdot t_{Total} + 0.0012632) \tag{22.15}$$

$$DOC_{AFper} = R_{maint} \cdot \left(\left(W_{airframe} \cdot 10^{-4} + 0.5 \right) \cdot t_{Total} + \left(W_{airframe} \cdot 10^{-4} + 0.25 \right) \right) \tag{22.16}$$

$$DOC_{Eng} = 7.621 \cdot 10^{-4} \cdot \frac{\eta_{prop,TO} \cdot P_{Total,max}}{V_1} + 30.5 \cdot t_{Total} + 10.6 \tag{22.17}$$

$$DOC_{Tech} = 5000 \cdot (b \cdot l_{fus})^{0.75} \tag{22.18}$$

$$DOC_{Ma} = FC \cdot (DOC_{AFmat} + DOC_{AFper} + DOC_{Eng}) + DOC_{Tech} \tag{22.19}$$

Capital

Capital costs (DOC_{Cap}) are determined to include the purchase costs of the aircraft, as well as the depreciation costs in the DOC model. These are split in two parts, the aircraft capital costs (DOC_{CapAC}) and the battery capital costs (DOC_{CapBat}). The sum of the two provides the annual DOC for capital cost, Equation 22.20.

To find the yearly annuity rate (a) of the aircraft, the depreciation per year, Equation 22.21 is used. Here, the interest rate (IR), residual value at end of life (f_{RV}) and the depreciation rate (DP) are used. Furthermore, aircraft commonly are insured, the insurance rate (f_{ins}) for capital DOC is estimated 0.5% [117], which is to be used in both capital cost calculations.

$$DOC_{Cap} = DOC_{CapAC} + DOC_{CapBat} \tag{22.20}$$

$$a = IR \cdot \frac{1 - f_{RV} \cdot (1 + IR)^{-DP}}{1 - (1 + IR)^{-DP}} \tag{22.21}$$

The capital aircraft DOC are calculated in Equation 22.22 using the previously discussed annuity (a_{AC} for the aircraft) and insurance rates. Included in the aircraft capital costs are the purchase costs of airframe (C_{af}), internal combustion engines (C_{ice}), electric motors (C_{em}), inverters (C_{inv}), controllers (C_{contr}) and generators (C_{gen}), all determined in section 22.1. The interest rate for aircraft annuity is estimated at 5%, the residual value at 10% [117] and the depreciation rate is 20 years.

Apart from the aircraft itself, the capital costs also include spare parts in stock. The number of spare parts per subsystem considered are all derived from Hoelzen et al. [117], given as a fraction of total parts. The spare part fractions are 0.1 for airframe, 0.3 for the ICE, 0.2 for electric motors and 0.2 for inverters, controllers and generators together. Moreover, the electric motor efficiency (η_{em}) and the power electronics efficiency (η_{elec}).

$$DOC_{CapAC} = \left(C_{af} \cdot 1.1 + C_{ice} \cdot 1.3 + C_{em} \cdot 1.2 + (C_{inv} + C_{gen} + C_{contr}) \cdot \left((\eta_{em} \cdot \eta_{elec})^{-1} + (\eta_{em} \cdot \eta_{elec}^2)^{-1} \right) \right) \cdot (a_{AC} + f_{ins}) \tag{22.22}$$

Battery capital DOC use the same insurance- and interest rates, but residual value is estimated at 40% [117]. The depreciation rate is determined using the battery lifetime cycles ($N_{Bat,cycles}$). In section 12.6, it is explained that the life cycle is estimated at 1500 cycles.

Dividing them with the yearly flight cycles FC, the depreciation rate is found, assuming the batteries are fully reloaded each flight cycle. The following equations then describe the battery capital DOC:

$$DP_{Bat} = \frac{N_{Bat,cycles}}{FC} \tag{22.23}$$

$$DOC_{CapBat} = C_{Bat} \cdot (a_{Bat} + f_{ins}) \tag{22.24}$$

Fees

All annual fees are grouped in the fees DOC (DOC_{Fees}). These include landing- (DOC_{Ldg}), ground- (DOC_{Ground}) and navigation fees (DOC_{Nav}). All three are dependent on the number of flight cycles per year, as is to be expected, as they are mainly charged when flying or landing the aircraft. The three fees are furthermore determined by the maximum takeoff and payload weight (MTOW, PL), t_{Total}, range and a navigation fee factor (k_{Nav}). The navigation fee factor is estimated €850 km^{-1} [117]. The following equations then determine the fees, the sum of them being DOC_{Fees}:

$$DOC_{Ldg} = \left(9.5 \cdot 10^{-3} - 10^{-3} \cdot \ln(t_{Total}) \right) \cdot MTOW \cdot FC \tag{22.25}$$

$$DOC_{Ground} = \left(0.11 \cdot PL - 5 \cdot 10^{-7} \cdot PL^2 \right) \cdot FC \tag{22.26}$$

$$DOC_{Nav} = \left(k_{Nav} \cdot \frac{Range}{1000} \cdot \sqrt{\frac{MTOW}{50000}} \right) \cdot FC \tag{22.27}$$

$$DOC_{Fees} = DOC_{Ldg} + DOC_{Ground} + DOC_{Nav} \tag{22.28}$$

Total DOC

With all DOC categories determined, the total DOC is estimated as the sum of all categories, as seen in Equation 22.29. Using the preliminary cost analysis, the costs for operating the aircraft per flight cycle, per block hour or other possible desirable analyses can be performed. Results of the total analysis, with parameters from the E-COmmuter, can be found in the following section.

$$DOC = DOC_{Energy} + DOC_{Crew} + DOC_{Ma} + DOC_{Cap} + DOC_{Fees} \tag{22.29}$$

22.3. Cost Analysis Results

With the analyses discussed in sections 22.1 and 22.2, calculations are done to have an initial estimate of aircraft purchase costs, fixed project costs and direct operating costs. With these estimates, further calculations and analyses can be performed to find, for instance, return on investment. subsection 22.3.1 shows the results of the production and development cost analysis, subsection 22.3.2 then provides insight in the annual DOC. Finally, the return on investment and ticket pricing is discussed.

22.3.1. Production & Development Costs

With the whole model built, the total production and development costs can be calculated. By then analyzing the minimum sales price and setting a first price estimate the return of investment can be calculated, which is discussed in the last part of this subsection.

The production and development costs highly depend on the design parameters from the design chapters 8 to 15. However, there are still some parameters to be set, which are not related to the actual design. Firstly the number of aircraft built in five years highly influences the cost. With more aircraft built, the cost per aircraft will drop, as fixed costs such as design hours do not linearly go up with number to be built. For the sake of cost, the production rate thus should be as high as possible. However, the operators are not expected to immediately order the E-COmmuter at very large numbers, as the small feeder concept is not applied broadly within Europe. Moreover, the extra investments on airports and airfields are expected to further decrease the interest of operators. Considering these influences, estimated is 100 aircraft in the first five years.

The second number to be determined is the number of prototype and test aircraft, required for the flight tests, as well as the structural integrity tests. In the development of civil (commercial) aircraft, this number can be estimated between two and eight aircraft [31][119]. As the aircraft is expected to require significant flight testing due to the novelties involved, the number of prototypes is set at six.

With all required parameters either calculated in the design phase or determined otherwise, a preliminary cost analysis result can be determined. Table 22.2 shows the results of the analysis discussed before. The table shows in its first column all cost categories. All italic categories are summed into the next bold entry of the table, gray entries are not calculated.

Within the analysis some categories are grouped. The certification costs are all fixed costs of the development in order to begin production. Structures cost includes all manufacturing, materials and quality control required to produce the airframe. As both structures and certification costs' categories are not to be seen separately, since they are highly related to each other, the costs per aircraft are only provided in the grouped cost categories.

Propulsion system consists of all propulsion components as found in the propulsion architecture, except the batteries and the fuel tanks, the latter is assumed to be included in the structures cost. All costs in the table are converted to cost per aircraft, such that the unit price of the aircraft can be calculated.

As seen in Table 22.2 the minimum sales price of the aircraft is approximately €3.1 million. Taking the certification cost as the investment costs and all other as variable, the break even cost can be calculated. With the minimum sales price, the break even point of the aircraft is at 100 aircraft built, thus after 5 years of production. If the price were to be increased, the number of aircraft built until break-even point is reached will lower. Return on investment per aircraft in this case is 1%.

If a profit margin is to be included in the sales price, the return of investment grows and the break-even point goes down. Profit margins within aviation are ranging from 4% to 10%[5] [120]. Taking a profit margin of 5%, thus being on the lower side, the aircraft sales price is approximately €3.3 million. Break-even point then is reached after 83 aircraft sold. The return on investment per aircraft is 1.2%.

Although the return on investment per aircraft is low, the expectation is that this sales price will provide a good position within the market. Based on the budgeting researched discussed in chapter 8, the price of the aircraft is budgeted as high as €3.9 million. As the current sales price thus is lower than the budget, further research into sales prices and

[5] URL: `https://www.textron.com/assets/FB/2017/aviation.html` [cited 20 June 2018]

cost can take margins to account for research and development delays. This is expected to be required, since the novelty of the aircraft can result in rising costs due to unforeseen errors.

Table 22.2: Production & development cost breakdown.

Cost category	Total cost (million)	Cost per aircraft (thousand)
Engineering	€46.8	
Development support	€4.4	
Flight testing	€1.9	
Tooling	€23.8	
Certification	€76.9	€768.6
Manufacturing	€75.3	
Quality control	€14.7	
Materials	€6.8	
Structures	€96.8	€967.7
Propulsion system		€779.0
Batteries		€75.0
Avionics		€57.2
Subtotal		**€2647.5**
Liability (17%)		€450.0
Aircraft minimum sales price		**€3097.6**

Table 22.3: Direct operating cost per aircraft per year.

DOC category	Cost (thousand)
Fuel	€343.5
Electricity	€100.0
Energy	€443.0
Crew	€547.2
Material	€12.4
Personnel	€204.0
Propulsion	€169.2
Technology	€361.2
Maintenance	€765.0
Aircraft	€187.7
Batteries	€67.6
Capital	€255.3
Landing	€112.1
Ground	€326.8
Navigation	€236.6
Fees	€675.6
Total	€2686.3

22.3.2. Direct Operating Costs

With the model completely described in section 22.2, the results are calculated by implementing all required design parameters. Then the DOC can be further analyzed to find the operating cost per passenger per flight or per flight hour, to determine preliminary ticket pricing. Results of the analysis are found in Table 22.3. In the table all categories (bold) are provided, along with the subcategories (italic) of each entry, if present.

What directly becomes clear is the large costs for maintenance, crew and fees. Of these costs, the most influential DOC is maintenance. The other two are more or less fixed costs, as the crew salaries are not expected to be cut significantly, and the fees are determined by external parties. The landing fees, however, can become lower, as the model does not distinguish between airports and airfields. As airfields have fewer facilities and they are less busy, the landing fees are expected to be significantly lower.

Concerning the maintenance DOC, the propulsion system costs are significantly higher than other parts. Although the propulsion system consists of electric motors, generally considered more reliable than engines [117], the system consists of many more parts. Therefore, the intensity of maintenance on the propulsion system can be expected to be equal to conventional propulsion. Maintenance costs are expected to stay the same during the aircraft life time. Although it is expected that failure occur more when the aircraft ages, the maintenance learning curve might counter the extra time required.

The total DOC of €2.69 million can be divided by the total annual flight cycles and the amount of passengers to find the operating cost per passenger per flight. This is a rough indication of the passenger ticket price, if an extra margin is taken into account for, for instance, profit, taxes and airport facilities. The DOC per passenger per flight is €91. Within this cost, the main contributors such as fuel, crew and aircraft maintenance and depreciation are included. Therefore, the ticket price of a flight is not considered to be much larger than the DOC. It is furthermore of importance, taking sustainability into account, that the ticket is as affordable as possible, while still covering the costs.

The aforementioned DOC per passenger per flight of €91 is calculated assuming full flights, it is however common that flights are not fully booked. In the United Kingdom, for instance, the average occupancy of flights ranges between 50% and 95%[6]. It is to be expected that the average is lower than 95% however, as these averages are found most in the low cost airliners. British airways, one of the airliners fitting the operator's profile described in chapter 2, has an occupancy rate of approximately 80%. Therefore, this rate is estimated as the average occupancy rate of the E-COmmuter. With this percentage taken into account, the DOC per passenger is €114.

The average profit per passenger in the United States was $7.54 in 2017. Converting to Euros, this is approximately €6.55, using the aforementioned exchange rate of 0.87. The total ticket price, including occupancy rate and profit added to DOC, the ticket price is estimated at €120. This corresponds to a cost of €0.32 km^{-1}.

[6] URL: https://statista.com/statistics/304117/uk-airline-passenger-seat-occupancy/ [cited 25 June 2018]

Now, this price is compared to the price of the travel by car to check whether it is competitive. In section 2.5, an average price is calculated. However, this price does not take into account a travel back. In order to include this, the parking cost is halved and a new price per kilometer is calculated. This results in a cost of €0.28 km^{-1}, €0.25 km^{-1} and €0.20 km^{-1} are found for the cases of France, Spain and Poland, respectively. This corresponds to an average price of €0.24 km^{-1}. The Netherlands is not covered here, as it is not one of the target areas. This means the E-COmmuter is on average 33% more expensive than ground transportation. This is indeed a significant difference, implying **HEF-PAX-01** is not met. However, for the case of France, the E-COmmuter is only 14% more expensive, so here the E-COmmuter is cost competitive. Furthermore, car depreciation cost and purchase cost are not taken into account yet, which can significantly influence the comparison. Also, with the large reduction in travel time (see section 16.2), the difference of 33% is still considered competitive. Possibly, families and holiday travellers may be less likely to use the E-COmmuter service, as cost is of greater importance for them than time. Nevertheless, for business people the opposite is usually true. This is as was expected during the market analysis in chapter 2.

23

Project Revision

This chapter discusses the requirements which are not met and gives and update of the budget breakdown.

23.1. Requirement Revision

As explained in the compliance matrix in chapter 4 there is one stakeholder requirement and seven subsystem requirements which cannot be check at this stage of the project. Respectively: **HEF-REG-01**, **HEF-STR-01**, **HEF-STR-02**, **HEF-STR-04**, **HEF-STR-07**, **HEF-STR-09**, **HEF-SC-01**, **HEF-SC-07**, and **HEF-OPS-03**. A brief overview of the post DSE activities is given in chapter 20 in which these requirements are designed for. Further recommendations for the project are given in chapter 24

The requirement that are not met are: **HEF-OPR-05**, **HEF-PAX-01**, and **HEF-SC-16**. The first two requirements are cost related. **HEF-OPR-05** considers the direct operating costs (DOC), which are exceeded by €95h^{-1} compared to the requirement. The fact that it is higher has to do with the fact that the batteries make the E-COmmuter just a bit more expensive in terms of operations. It is expected that the prices of batteries will decrease together with the handling of batteries in aviation industry. As for now, the requirement is not met but in the coming years this might change, depending on the economy. **HEF-PAX-01** concerns the passengers, ticket prices are estimated to be 133% of the ground transportation and parking costs. This is 8% higher compared to the requirement, but the pricing is still competitive with ground transportation which is also desired. Still further research has to be done in order to bring down the costs.

HEF-SC-16 states the allowed nose landing gear loads. As discussed in subsection 14.2.1, due to the c.g. range the nose landing gear could not be attached to the fuselage by applying the the initial allowed nose lading gear loads. The maximum allowed load is therefore increased to 17%, as discussed in subsection 14.2.1. This is still within realistic values given by Raymer [31]. The nose landing gear is also structurally designed to withstand the increased loads.

23.2. Budget Breakdown Update

With the aircraft designed in more detail, the budget breakdown of section 8.2 is revised in this section. Reviewing the budget breakdown shows if the expected subsystem budgets are met within their set contingencies (see Table 8.4). If this is not the case, it either has to be argued why the budget is considered valid or the design has to be revised in order to meet the set budgets.

Table 23.1 shows the current budgets of the design next to the previously estimated budgets from the preliminary estimations and the Class II weight estimations.

Table 23.1: Updated budget breakdown showing the current status of the design.

Resource parameter	**Preliminary estimation**	**After Class II**	**Current budget**
Required power	1000 kW	780 kW	776 kW
Total energy consumption	1000 kW h	1350 kW h	769 kW h
Operating empty weight	3600 kg	4800 kg	4300 kg
Propulsion system mass	1000 kg	2000 kg	860 kg
Development & production cost	€3870000	€3870000	€3123000

From the table directly becomes clear that required power approximately stayed the same between the conceptual design and the preliminary design. However, the propulsion mass decreased significantly, and it is not within the specified budget set after conceptual design. Reason for the large difference is the inclusion of hybridization in the performance analysis. Conceptual design on the propulsion did not take these parameters into account, thus propulsion subsystems were designed separately to provide the required power. By including the hybridization, the power of ICEs and batteries can be combined, reducing the required power per subsystem. Therefore, the deviation is considered valid and major revision of the propulsion system with respect to mass contingencies is not required.

Together with the decrease in power, the operating empty weight is decreased. This is expected to be the result of a reverse snowball effect from the decrease in propulsion system mass. Furthermore, the increase in battery specific energy reduced the battery mass, again initiating a reverse snowball effect.

Lastly the cost of the aircraft has decreased significantly, although it is still within contingency margins. The major factor decreasing the cost is the more detailed analysis on costs. As discussed in subsection 8.2.5, the preliminary cost budget is a very rough estimation, thus large contingency was added. With the finer analysis performed in chapter 22, the contingency now is lower. It can be expected, however, that the cost per aircraft increases towards the end of the development, as novelty of the aircraft subsystems can cause delays.

24
Recommendations

As stated in the beginning of this report, the objective of the project was to design a short range hybrid electric aircraft capable of carrying 14 passengers from local (grass) airfields to major/commercial airports, by 10 students in 10 weeks time. Hence, it is logical to expect that the outcome of this project will not be an aircraft that is ready to produce. There is a reason that aircraft design can take up to 8 years in total and this project serves as a demonstration of the possibilities of hybrid aircraft. Of course, while designing the E-COmmuter, many questions came to mind that were either outside the scope of the project or the team simply lacked the expertise to answer them. These questions are stated in this chapter as recommendations in the hope that they will benefit future designs of aircraft similar to the E-COmmuter.

24.1. Structures

In this design, the wing is the only structural component that has been designed in detail. Nevertheless, the design could have been improved if more time was provided: flutter could be considered, twist and bending deflection could be elaborated upon. In next processes of the wing design, the wing should be modeled in a Finite Element Method program, to verify its strength and stiffness. Doing so, cutouts can be added for the battery replacement accessibility.

Furthermore, the fuselage and tail can be designed in more detail. Their design now is preliminary and mainly based on reference aircraft. Initially, the plan was to perform a stress analysis on the fuselage as well, but due to time constraints the design is limited. In the future, the structural fuselage design is thus an important activity. This also includes a load analysis of the fuselage, including wing lift, empennage, landing gear loads and payload. The fuselage-wing and fuselage-landing gear interaction can also be further investigated. This will then result in a design process such as performed for the wing. Finally, the wing-propeller interaction can be modeled more accurately. It is a very complex interaction that requires a lot more investigation to model accurately.

24.2. Performance

The blown wing concept is still a novel concept. There is not a lot of information available. Further research and testing have to be done to get a more accurate analysis of the aircraft performance. The behaviour and application of the distributed propulsion system during flight phases like landing needs to be further investigated. For range, extracting data from current hybrid aircraft and analyzing this data can improve the design further. Together with an additional analysis of endurance of the aircraft to truly analyze all the possible mission the E-COmmuter can perform.

24.3. Propulsion

As the propulsion system of the E-COmmuter is probably its most unique aspect, there is much that can be improved in its design. First and foremost, the E-COmmuter features different divisions of energy between its power sources for every one of its flight phases. A very crucial part of this division which has not been designed in this project, is the design of a control system that would be responsible for communicating how much power the aircraft has left and that decides which power system is active at what moment. Due to the large amount of propellers and the two energy sources, this control system will need to be very complex to use the right amount of propellers and energy sources to fly the aircraft optimally while also having additional functions like maintaining the stability of the aircraft using the control surfaces and supported by using the yaw moment of the blown wing. These kind of novel applications are possible but sadly were outside the scope of the project.

Secondly, it became quite clear during the project that a detailed analysis on the propellers of the E-COmmuter was very difficult to perform due to a lack of expertise in the field of propeller design. Such an analysis is especially important considering that the blown wing propellers are experimental high-lift propellers, which deviate from the theory as taught in many aircraft design literature. This detailed analysis becomes even more important when considering that the E-COmmuter has folding propellers, of which the mechanism will also impose constraints on the propeller design. It is therefore strongly recommended that future studies include a detailed propeller design to obtain an accurate picture of the performance of the E-COmmuter.

It is also recommended to further analyze the feasibility of using Lithium-sulfur batteries. For example, the specific energy of 750 $W\,h\,kg^{-1}$ is very large compared to existing batteries. Although some research claims that this value is attainable, extra analysis should be performed. Moreover, the charging time of 20 min should be investigated, as limitations in charging facilities can increase this value.

24.4. Operations

A more detailed market analysis should be performed. The airport accessibility can be quantified using the LogSum method [9] and the market size can be determined more accurately if more data is available. Alternative applications can be looked into as well, for example, implementation in other continents or the E-COmmuter as in island hopper in the Caribbean. Moreover, target areas, airfields and customers can be specified more accurately. Consequently, a more exact time analysis can be carried out as well. If it turns out that the target customers are mainly business people, it can be of interest to consider alternative, more luxurious cabin layouts. An analysis of the required initial investments for the infrastructure at the airfields can be performed as well as these costs are expected to be rather large.

Furthermore, a more detailed maintenance plan should be set up. It has to extensively explain how every maintenance activity has to be performed. This manual should then be certified by regulatory institutions.

Regarding the security level of the airfields, a detailed analysis can be performed to check its feasibility. If this cannot be ensured, measures should be taken to increase this level as much as possible. This can also influence the ground operations: extra checks upon arrival at the airport may be required.

24.5. Cost Analysis

The cost analysis performed is based on statistical data from an adapted DAPCA IV method. This method is however outdated, as the first data were published in 1986. Therefore, a better cost analysis based on more recent data, if present, is recommended to be performed. Furthermore, cost data on batteries, electric motors and other parts of the propulsion system are to be researched for more accurate data.

In the case of direct operating costs (DOC), it is recommended to implement the maintenance schedule and more accurate reliability and unscheduled maintenance. It should also be analyzed how the DOC can be lowered in order to be more competitive with ground transportation. Alternative solutions to be more competitive can also be investigated.

24.6. Stability & Control

Sizing the vertical tail is currently based on tail volume coefficient methods. Since this is based on data from reference aircraft, the method is not specifically based on the aircraft design. The accuracy is questionable especially since the deviation of tail volume coefficients for similar aircraft varies significantly. Also, the dorsal fin is currently not taken into account as a vertical tail area. Currently, the sole purpose for it, is to postpone the stall angle of the vertical tail. It is recommended for the next design phase to apply more accurate tail sizing method which is based on directional stability and takes the dorsal fin area into account as well.

For landing gear, the current methods to define the position are mainly dependant on locations of center of gravity. For determining the c.g. locations several assumptions are applied since part of the geometry are not defined yet. Especially exact c.g. locations of structural sections are difficult to determine at this point of the design. By increasing the accuracy of the geometry, the accuracy of the location of the landing gear will increase as well. Furthermore this will increase the moment of inertia evaluation on its turn as well, which improves the stability assessment.

Furthermore, one of the most difficult parts during the design of the stability & control subsystem turned out to be the estimation of the stability derivatives of the aircraft. As described in this report, Digital DATCOM was used to find the derivatives via input of aircraft geometry. This is by far the most reliable method publicly available today. Only, there are some drawbacks to this method. First, it is significantly outdated. This is not immediately a bad method, but it is effortful to use at least. The program is not user friendly and mistakes are easily made. Also, the input of geometry of the aircraft is ambiguous. One could easily make a large erroneous geometry input without realizing the effect. Next to this, virtually no reliable ways of verification are available. This can have some quite negative consequences as a large number of stability and control calculations depend on the stability derivatives found by DATCOM. A large improvement to the design of the stability & control subsystem would be the availability of a robust CFD method that also supports the input of fuselages in combination with lifting surfaces.

In the extension of this, for a large number of stability & control components, the sizing is based on literature with idealized equations and simple programs such as XFoil. Not only is this prone to errors, it also decreases the accuracy of the output. Moreover, the starting point for the sizing are often the derivatives of DATCOM, which decrease the reliability of the sizing even more. Verifying takes place using XFLR5, which again does not support some geometries, also decreasing the reliability of the verification by an unknown extent. Again, here a strong and robust CFD software that can estimate stability derivatives and control surface effects would greatly increase the quality of the stability & control subsystem.

25
Conclusion

The goal of this project was to design an innovative mini-feeder aircraft, that is competitive to private road transportation to/from commercial airports, in terms of travel time, cost and exhaust emissions. The E-COmmuter is a hybrid electric commuter aircraft that is able to carry 14 passengers from local airfields to commercial airports. The travel time is approximately 35% less compared to driving to the airport by car. 5% less exhaust emissions are expelled compared to private road transportation, but the ticket price is 33% higher with respect to the total cost associated with driving, refueling, and parking a car.

The design is tackled in a structured way. First, a market analysis is performed to familiarize with the problem and the market. The range is determined and four case studies are performed to analyze the current situation. Then, a functional analysis is done: the functions that the aircraft needs to full fill are investigated. Based on this and the market analysis, stakeholders are identified and requirements the aircraft has to comply with are set up. Afterwards, the mission profile is defined: takeoff and landing are fully electric, climb is hybrid electric, and cruise has two parts conventional and eclectic. The E-COmmuter can be refueled/recharged at both the airport and airfield. Using the requirements and the mission profile, different design options can be explored. These options are traded-off against each other to end up with a final concept. Two trade-offs are performed: an aircraft configuration trade-off and a propulsion system trade-off. The results is a high-wing T-tail configuration with hybrid electric distributed propulsion system along the wing.

The technical design starts with a Class I and Class II estimation. Different subsystems are designed: a preliminary fuselage design is done. The fuselage has a rectangular cross-section to optimally use all the space available. Two Continental IO-550 internal combustion engines together with two generators are located in the tailcone. The wing is designed to sustain all the loads acting on it: a wing box is designed, accommodating the Lithium-sulfur batteries and fuel tanks. The wing is made out of GLARE to provide fire safety. A wing span of 20.92 m and a wing surface of 36.48 m^2 is obtained. Then, a performance analysis is performed. The flight phases are analyzed to meet the requirements and to size the propulsion system. A payload range diagram is constructed to identify alternative missions and an aerodynamic analysis of the aircraft is done: it becomes clear that the distributed electric propulsion system provides advantages in terms of lift generation. Then, the propulsion system can be designed: 14 small propellers are distributed along the wing and two larger propellers are located at the root. Engines, propellers, and batteries are chosen to match the mission. Afterwards, a look is taken at the stability and control of the E-COmmuter: the wing location is determined, as well as the horizontal tail size and the landing gear position. From this, the entire tail and main and nose landing gear are designed. Furthermore, possible blown wing applications are considered: the propellers can be used as "control surfaces". After iterating, a full aircraft configuration is obtained, having a maximum takeoff weight of 5835 kg and a range of 389 km. The operations of the E-COmmuter are investigated: the novel design requires additional infrastructure on the airstrips it lands on, such as charging facilities. This concludes the design of E-COmmuter mission.

Sustainability is taken into account for every design choices: propellers are chosen to minimize the noise, recyclable material is used, takeoff and landing are zero emissions flight phases. A sustainability strategy is made based on accessibility, safety, ecosystem health, resource use, noise and affordability of the E-COmmuter.

Further design stages are considered, and based on this a production and end-of-life plan are constructed. The E-COmmuter is 70% recyclable/reusable. A cost analysis is performed and finally, the requirements are checked to be met: all stakeholder requirements are met, with the exception of those relating to the cost of the E-COmmuter. Even though, the cost are higher than the corresponding ground transportation, it still stays competitive.

Bibliography

[1] P.A.R. Brill et al. *Project Plan Design Synthesis Excercise*. Technical report. TU Delft, 2018.

[2] M. Voskuijl, J. van Bogaert, and A.G. Rao. *Analysis and Design of Hybrid Electric Regional Turboprop Aircraft*. 2017.

[3] E.K.A. Gill. *Verification and Validation*. Lecture 6 of AE3211-I Systems Engineering & Aerospace Design. Apr. 2018.

[4] P.A.R. Brill et al. *Midterm Report Design Synthesis Excercise*. Technical report. TU Delft, 2018.

[5] D.G. Simons and M. Snellen. *Airframe Noise Modelling ANOPP method*. Lecture of AE4463 Advanced Aircraft Noise Modelling and Measurement. June 2018.

[6] P.A.R. Brill et al. *Baseline Report Design Synthesis Excercise*. Technical report. TU Delft, 2018.

[7] P. Trzepacz. *Airport Accessibility and Characteristics of the Catchment Area – the Case of Poland*. 2014, pp. 97–118.

[8] X. Kong, Z. Xu, and G. Shen. "Urban Traffic Congestion Estimation and Prediction Based on Floating Car Trajectory Data". In: *Future Generation Computer System* 61 (2015), pp. 97–107.

[9] M. Kouwenhoven. "The Role of Accessibility in Passengers Choice of Airports". In: (2008).

[10] J. Reichmuth et al. *Topical Report: Airline Business Models*. Dec. 2008.

[11] J.P. Heimlich. *Status of Air Travel In The USA*. Apr. 2016.

[12] A.R.C. De Haan. "Aircraft technology's: Contribution to sustainable development". PhD thesis. Delft: Technische Universiteit Delft, June 2007.

[13] B. Owen, D.S. Lee, and L. Lim. "Flying Into the Future: Aviation Emissions Scenarios to 2050". In: *Environmental Science and Technology* 44 (2010), pp. 2255–2260.

[14] DG Environment European Commission. *Assessment of Resource Efficiency Indicators and Targets*. Technical report. European Union.

[15] S.A. Stansfeld et al. "Aircraft and Road Traffic Noise and Children's Cognition and Health: a Cross-National Study". In: *The Lancet* 365 (2005), pp. 1942–1949.

[16] A. Huss et al. *Aircraft Noise, Air Pollution, and Mortality From Myocardial Infarction*. 2010.

[17] K.T. Chau and Y.S. Wong. "Overview of Power Management in Hybrid Electric Vehicles". In: *Energy Conversion and Management* 43.15 (2002), pp. 1953–1968.

[18] F. Oliviero. *Project Guide DSE: Hybrid Electric "mini-feeder" case*. Reader & Assignment for DSE. Apr. 2018.

[19] Siemens. *Hypstair: WP4 Hybrid System Components*. Project Meeting Presentation. Mar. 2014.

[20] S.O.L. Zijp. "Development of a Life Cycle Cost Model for Conventional and Unconventional Aircraft". MA thesis. Technische Universiteit Delft, June 2014.

[21] W. Verhagen. *Concurrent Engineering & Design for Life Cycle*. Lecture 9 of AE3211-I. 2018.

[22] W. Verhagen. *Risk Management & Reliability Engineering*. Lecture 8 of AE3211-I Systems Engineering & Aerospace Design. 2018.

[23] E. Torenbeek. *Synthesis of Subsonic Airplane Design*. 1st ed. Delft University Press, Kluwer Academic Publishers, 1982.

[24] European Aviation Safety Agency. *CS-23*. 2015.

[25] S. Gudmundsson. *General Aviation Aircraft Design: Applied Methods and Procedures*. 1st ed. Elsevier Inc., 2014.

[26] B. Ganesh, B.V. Kumar, and D. Muppala. "Design and Structural Analysis of Aircraft Floor Panel". In: *International Journal of Advanced Engineering and Global Technology* 3.12 (2015), p. 1451.

[27] J. Roskam. *Part II: Preliminary Configuration Design and Integration of the Propulsion System*. 1st ed. University of Kansas, 1989.

[28] P. Rambabu, N. Esawara Prasad, and V.V. Kutumbarao. *Aluminium Alloys for Aerospace Applications*. Indian Institute of Metal Series, 2017.

[29] I. Martinez. *Aircraft Environmental Control*. Escuela Tecnica Superior de Ingenieros Aeronauticos, 2018.

[30] J. McGhee and D. Beasley. *Low speed aerodynamic characteristics of a 17 percent thick airfoil section designed for general aviation applications*. Jan. 1974.

[31] D.P. Raymer. *Aircraft Design: a Conceptual Approach*. 2nd ed. American Institute of Aeronautics and Astronautics, Inc., 1992.

[32] J.A. Mulder et al. *Flight Dynamics Lecture Notes*. TU Delft, Mar. 2013.

[33] R. de Vries, M.T.H. Brown, and R. Vos. "A Preliminary Sizing Method for Hybrid-Electric Aircraft Including Aero-Propulsive Interaction Effects". In: *18th AIAA Aviation Technology, Integration, and Operations Conference* (2018), pp. 16–19.

[34] M.D. Patterson. *Conceptual Design of High-Lift Propeller Systems for Small Electric Aircraft*. American Institute of Aeronautics and Astronautics, Inc., 2016.

[35] L.L.M. Veldhuis. *Propeller Wing Aerodynamic Interference*. TU Delft, 2005.

[36] A. Mathai, A.P. Kurian, and B. Jacob. "Ply Orientation of Carbon Fiber Reinforced Aircraft Wing - A Parametric Study". In: *International Journal of Engineering Research and Applications* 4.5 (2014), p. 53.

[37] C. Soutis. "Carbon Fiber Reinforced Plastics in Aircraft Construction". In: *Materials Science and Engineering* (2005), pp. 171–175.

[38] G. Zhu. "Recycling of Glass Fibre Reinforced Aluminum Laminates and Silicon Removal from Aerospace Al Alloy". MA thesis. TU Delft, Oct. 2012.

[39] M.S. Wilk and R.E. Sliwa. "The Influence of Features of Aluminium Alloys 2024, 6061, 7075 on the Properties of GLARE-type Composites". In: *Archives of Metallurgy and Materials* 60.4 (2015), pp. 3102–3105.

[40] B. Müller, S. Teixeira De Freitas, and J. Sinke. "Thermal Cycling Fiber Metal Laminates: Considerations, Test Setup and Results". In: *20th International Conference on Composite Materials* 60.4 (2015), pp. 3102–3105.

[41] G.H.J.J. Roebroeks. "Fibre-metal laminates: Recent developments and applications". In: *Fatigue* 16.1 (1994), pp. 33–37.

[42] P.A. Hooijmeijer and A. Vlot. *Fibre Metal Laminates Exposed to High Temperatures*. TU Delft, 2017.

[43] A. Asundi and A.Y.N. Choi. "Fiber Metal Laminates: an Advanced Material for Future Aircraft". In: *Journals of Materials Processing Technology* 63 (1997), pp. 384–394.

[44] P. Chiozzotto. "Wing Weight Estimation in Conceptual Design: a Method for Strut-Braced Wings Considering Static Aeroelastic Effects". In: *CEAS Aeronautical Journal* 7 (Sept. 2016).

[45] R. Alderliesten. *Fatigue and Fracture of Fibre Metal Laminates*. Springer International Publishing, 2017.

[46] T.H.G. Megson. *Aircraft Structures for Engineering Students*. Elsevier Science, 2007.

[47] R. Hibbeler. *Mechanics of Materials*. Oct. 2013.

[48] C. Niu and M.C.Y. Niu. *Airframe Stress Analysis and Sizing*. Conmilit Press, 1999.

[49] G. Wu and J. Yang. "The Mechanical Behavior of GLARE Laminates for Aircraft Structures". In: *JOM - Journal of the Minerals, Metals and Materials Society* (Jan. 2005).

[50] Anonymous. *Wing Bending Calculations: Lab 10 lecture notes*. MIT, 2017.

[51] A. Fotouhi et al. "Lithium-Sulfur Battery Technology Readiness and Applications - a Review". In: *Energies* 10 (Nov. 2017).

[52] A. Elham. *Aircraft Aerodynamic Analysis - Drag*. Lecture 3 of AE2111-II Aerospace Design and Systems Engineering Elements II. Sept. 2016.

[53] G.J.J. Ruijgrok. *Elements of Airplane Performance*. 2nd ed. Delft Academic Press, 2009.

[54] A. Viré. *Aerodynamic Theory*. Lecture 2 of AE3W02TU - Introduction to Wind Turbines. Sept. 2016.

[55] C. Lenfers et al. "Experimental Investigation of the Propeller Design for Future QESTOL Aircraft in the BNF Project". In: *AIAA SciTech, 52nd Aerospace Sciences Meeting*. 2014.

[56] B.L. Litherland et al. *A Method for Designing Conforming Folding Propellers*. Technical report. National Aeronautics and Space Administration, 2017.

[57] AA Portable Power Corp. *Specification of Li-ion Polymer Battery 3.7V 10000 mAh*. 2nd ed. Battery Space.

[58] G. Girishkumar et al. "Lithium-air Battery: Promise and Challenges". In: *The Journal of Physical Chemistry Letters* 1 (July 2010), pp. 2193–2203.

[59] P. Tan et al. "Advances and Challenges in Lithium-air Batteries". In: *Applied Energy* 204 (Oct. 2017), pp. 780–806.

[60] L. Grande et al. “The Lithium/Air Battery: Still an Emerging System or a Practical Reality”. In: *Advanced Materials* 27 (Dec. 2014), pp. 784–800.

[61] K. Patel. “Lithium-Sulfur Battery: Chemistry, Challenges, Cost, and Future”. In: *Journal of Undergraduate Research* 9 (2016), pp. 39–42.

[62] H. Yang et al. “Lithium Sulfur Batteries With Compatible Electrolyte Both for Stable Cathode and Dendrite-free Anode”. In: *Energy Storage Materials* 15 (May 2018), pp. 299–307.

[63] OXIS Energy. *Long Life Lithium Sulfur Pouch Cell*. Online brochure. Oxfordshire, United Kingdom, July 2017.

[64] D.C. Giancoli. *Physics for Scientists & Engineers With Modern Physics*. 4th ed. London, United Kingdom: Pearson Education Limited, July 2009.

[65] A. Harish et al. *Economics of Advanced Thin-Haul Concepts and Operations*. June 2017.

[66] F. Oliviero. *Weight & Balance Estimation in Aircraft Design*. Lecture 3 of AE3211-I Systems Engineering & Aerospace Design. Apr. 2018.

[67] F. Oliviero. *Requirement Analysis and Design Principles for A/C Stability and Control (Part I)*. Lecture 4 of AE3211-I Systems Engineering & Aerospace Design. Apr. 2018.

[68] F. Oliviero. *Requirement Analysis and Design Principles for A/C Stability and Control (Part II)*. Lecture 5 of AE3211-I Systems Engineering & Aerospace Design. Apr. 2018.

[69] R.D. Finck. *USAF Stability and Control DATCOM*. Technical Report. McDonnell Douglas Corporation, 1978.

[70] J.E. Williams and S.R. Vulkelich. *USAF Stability and Control Digital DATCOM. Volume I, User Manual*. Technical Report. McDonnell Douglas Astronautics Company, 1979.

[71] M. Sadraey. *Aircraft Design: s Systems Engineering Approach*. Wiley Publications, 2012.

[72] J. Roskam. *Part III: Layout Design of Cockpit, Fuselage, Wing and Empennage: Cutaways and Inboard Profiles*. 1st ed. University of Kansas, 1989.

[73] F. Nicolosi et al. *Aerodynamic Design Guidelines of an Aircraft Dorsal Fin Throughout Numerical and Experimental Analyses*. University of Naples Federico II. June 2016.

[74] V. Jeevanantham, Vadivelu P., and Manigandan P. “Material Based Structural Analysis of a Typical Landing Gear”. In: *International Journal of Innovative Science, Engineering & Technology* 4.4 (2017), pp. 295–300.

[75] N.S. Currey. *Aircraft Landing Gear Design: Principles and Practices*. Aiaa, 1988.

[76] A. Schwaninger. “Increasing Efficiency in Airport Security Screening”. In: *WIT Transactions on the Built Environment* 84 (Jan. 2005), pp. 405–416.

[77] S. Jafer and W. Mi. “Comparative Study of Aircraft Boarding Strategies Using Cellular Discrete Event Simulation”. In: *Aerospace* 4 (Nov. 2017).

[78] M.K. Song, Y. Zhang, and E.J. Caims. “A Long-Life High-Rate Lithium/Sulfur Cell: a Multifaceted Approach to Enhancing Cell Performance”. In: *Nano Letters* 13 (Nov. 2013), pp. 5891–5899.

[79] Environment Canada, Emergencies Science and Technology Division. *Aviation Gasoline 100LL*. 1998.

[80] A. De Nicola, S. Gitto, and P. Mancuso. “Airport Quality and Productivity Changes: a Malmquist Index Decomposition Assessment”. In: *Transportation Research Part E: Logistics and Transportation Review* (May 2013).

[81] The Institute of Electrical and Electronics Engineers. *IEEE Standard Computer Dictionary*. 1990.

[82] G.J.W. van Bussel. *Maintenance Concepts & Maintenance Strategies*. Lecture 4 of AE3512 Asset Management. 2016.

[83] National Transportation Safety Board. *NTSB Aviation Coding Manual*. Dec. 1998.

[84] European Aviation Safety Agency. *Maintenance Organisation Approvals Part-145 Detailed Course*. Oct. 2008.

[85] European Aviation Safety Agency. *Annual Safety Review 2016*. Review report. EASA, 2016.

[86] T. Cowan, E. Acar, and E. Fancolin. *Analysis of Causes and Statistics of Commercial Jet Plane Accidents between 1983 and 2003*. Technical report. University of Florida.

[87] Federal Aviation Administration. *Causal Factors for General Aviation Accidents/Incidents Between January 1984 and October 2004*. Technical report.

[88] De Havilland Aircraft. *Maintenance Manual Twin Otter DHC-6*. 1st ed. Downsview, Ontario, Canada, Mar. 1968.

[89] Diamond Aircraft Industries. *Aircraft Maintenance Manual*. 22nd ed. London, Ontario, Canada, May 2014.

[90] Aircraft Commerce. “Owner’s & Operator’s Guide: ERJ-135/-140/-145”. In: *Aircraft Commerce Magazine* 61 (Dec. 2008), pp. 5–28.

[91] Aircraft Commerce. “Owner’s & Operator’s Guide: E-jet Family”. In: *Aircraft Commerce Magazine* 64 (July 2009), pp. 5–28.

[92] S.J. Cowan et al. *Airplane Hard Landing Indication System*. Patent. Jan. 2004.

[93] Federal Aviation Administration. *Advisory Circular: Nickel-Cadmium Battery Operational, Maintenance, and Overhaul Practices*. 1st ed. U.S. Department of Transportation. Washington D.C., Feb. 1973.

[94] M.J. Behbahani-Pour and G. Radice. “Fuel Leak Detection on Large Transport Airplanes”. In: *Journal of Aeronautics and Aerospace Engineering* 5 (2016).

[95] Federal Aviation Administration. *Advisory Circular: Aircraft Propeller Maintenance*. 1st ed. U.S. Department of Transportation. Washington D.C., Sept. 2005.

[96] International Air Transport Association. *Aircraft Operational Availability*. Montreal: IATA, 2018.

[97] C. Andela. *Improvements of Aircraft Availability Within the Royal Netherlands Air Force*. Emmeloord: National Aerospace Laboratory NLR.

[98] D. Casalino et al. “Aircraft Noise Reduction Technologies: a Bibliographic Review”. In: *Aerospace Science and Technology* 12 (2008), pp. 1–17.

[99] J.E. Marte and D.W. Kurtz. *A Review of Aerodynamic Noise From Propellers, Rotors, and Lift Fans*. Technical report. National Aeronautics and Space Administration, 1970.

[100] J.E. Made and D.W. Kurtz. *A Review of Aerodynamic Noise From Propellers, Rotors, and Lift Fans*. 1970.

[101] International Civil Aviation Organisation. *Environmental Protection: Volume I, Aircraft Noise*. 5th ed. International Civil Aviation Organisation, 2008.

[102] J. Sinke. “Manufacturing of GLARE parts and Structures”. In: 10 (July 2003), pp. 293–305.

[103] A. Mukherjee and B. Varughese. “Design Guidelines for Ply Drop-off in Laminated Composite Structures”. In: *Composites Part B: Engineering* (2001).

[104] C. Rans, P. Straznicky, and R. Alderliesten. “Riveting Process Induced Residual Stresses Around Solid Rivets in Mechanical Joints”. In: (Jan. 2007).

[105] Australian Government. *Production Flight Testing: Information for Manufacturers*. Civil Aviation Safety Authority, 2012.

[106] S. Suomalainen and A. Celikel. *Aircraft Metals Recycling: Process, Challenges and Opportunities*. ENVISA.

[107] D. van Heerden and R. Curran. *Value Extraction from End-of-life Aircraft*. TU Delft.

[108] J.S Ribeiro and J. de Oliviera Gomes. “Proposed Framework for End-of-Life Aircraft Recycling”. In: *12th Global Conference on Sustainable Manufacturing* (2015), pp. 312–314.

[109] S.K. Das and J.G. Kaufman. “Recycling Aluminum Aerospace Alloys”. In: *Light Metals 2007* (2007), pp. 1161–1163.

[110] S. Kelly and D. Apelian. *Automotive aluminum recycling at end of life:a grave-to-grave analysis*.

[111] H. Zou. “Development of a Recycling Process for Li-Ion Batteries”. MA thesis. Worcester Polytechnic Institute, 2012.

[112] J. Xu and H.R. Thomas. “A Review of Processes and Technologies for the Recycling of Lithium Ion Secondary Batteries”. In: *Journal of Power Sources* (2008), pp. 514–516.

[113] O.E. Bankole. “Battery Recycling Technologies: Recycling Waste Lithium Ion Batteries with the Impact on the Environment In-View”. In: *Journal of Environment and Ecology* (2013), pp. 19–21.

[114] A.M. Stoll. *Design Studies of Thin-Haul Commuter Aircraft with Distributed Electric Propulsion*. June 2016.

[115] K.O. Ploetner et al. *Operating Cost Estimation for Electric-Powered Transport Aircraft*. Conference paper from Aviation Technology, Integration and Operations Conference. Aug. 2013.

[116] A. Bardenhagen and A. Gobbin. *Flugzeugentwurf II*. University of Stuttgart, 2017.

[117] J. Hoelzen et al. “Conceptual Design of Operation Strategies for Hybrid Electric Aircraft”. In: *MDPI - Energies* 11 (Jan. 2018).

[118] P. Capros et al. *EU Reference Scenario 2016: Energy, Transport and GHG Emissions Trends to 2050*. July 2016.

[119] J. Roskam. *Part VIII: Airplane Cost Estimation: Design, Development, Manufacturing and Operating*. 1st ed. University of Kansas, 1990.

[120] A.K. Kundu. *Aircraft Design*. Cambridge University Press, 2010.

[121] Continental Motors. *Maintenance and Overhaul Manual*. 2nd ed. Mobile, Alabama, U.S.A., Feb. 2015.

[122] Hartzell Propeller. *Propeller Owner’s Manual and Logbook*. 19th ed. Piqua, Ohio, U.S.A., Nov. 2013.

A

Functional Flow Diagram and Functional Breakdown Structure

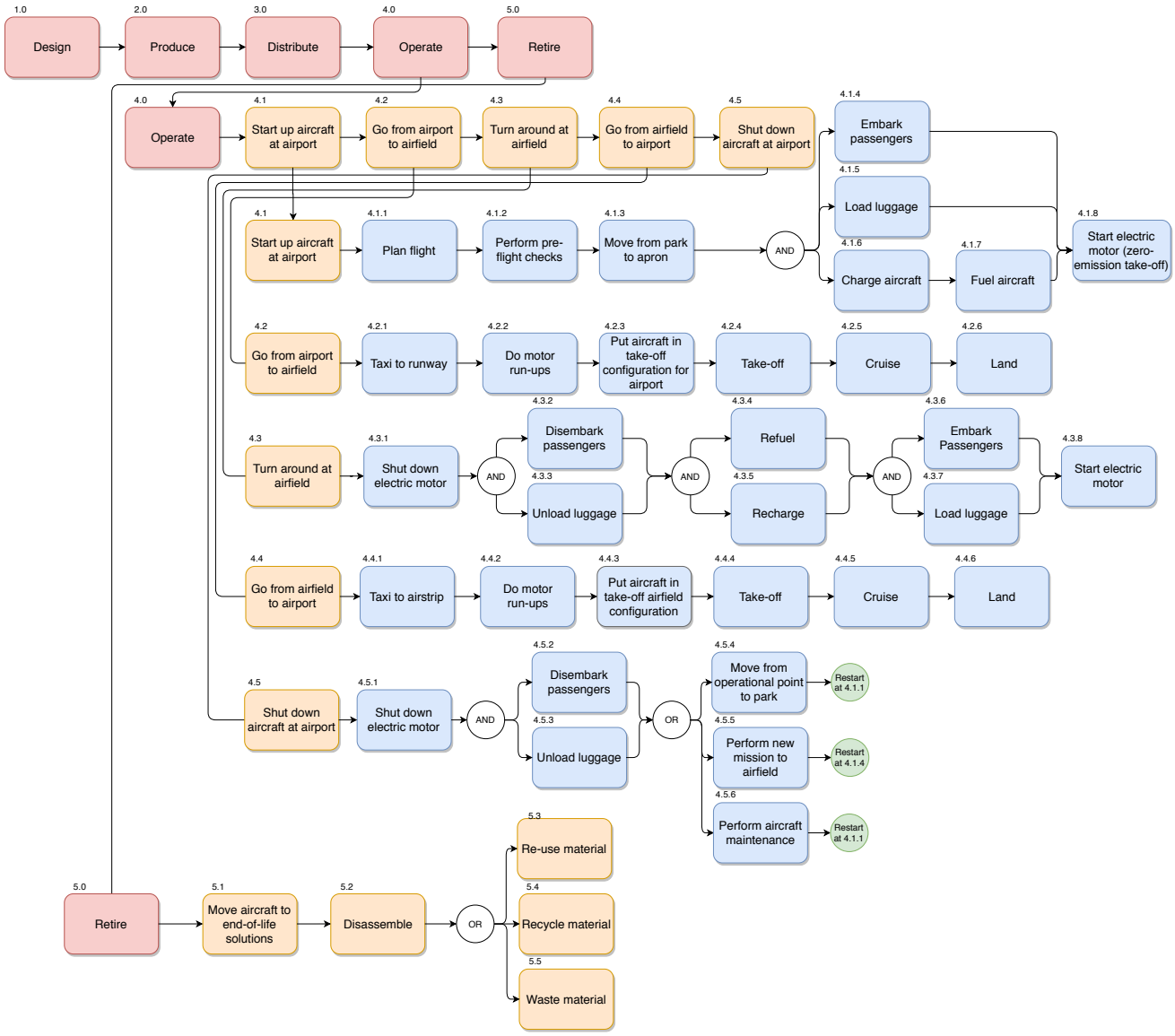

Figure A.1: Functional flow diagram of the aircraft system focusing on the operational and retirement phase.

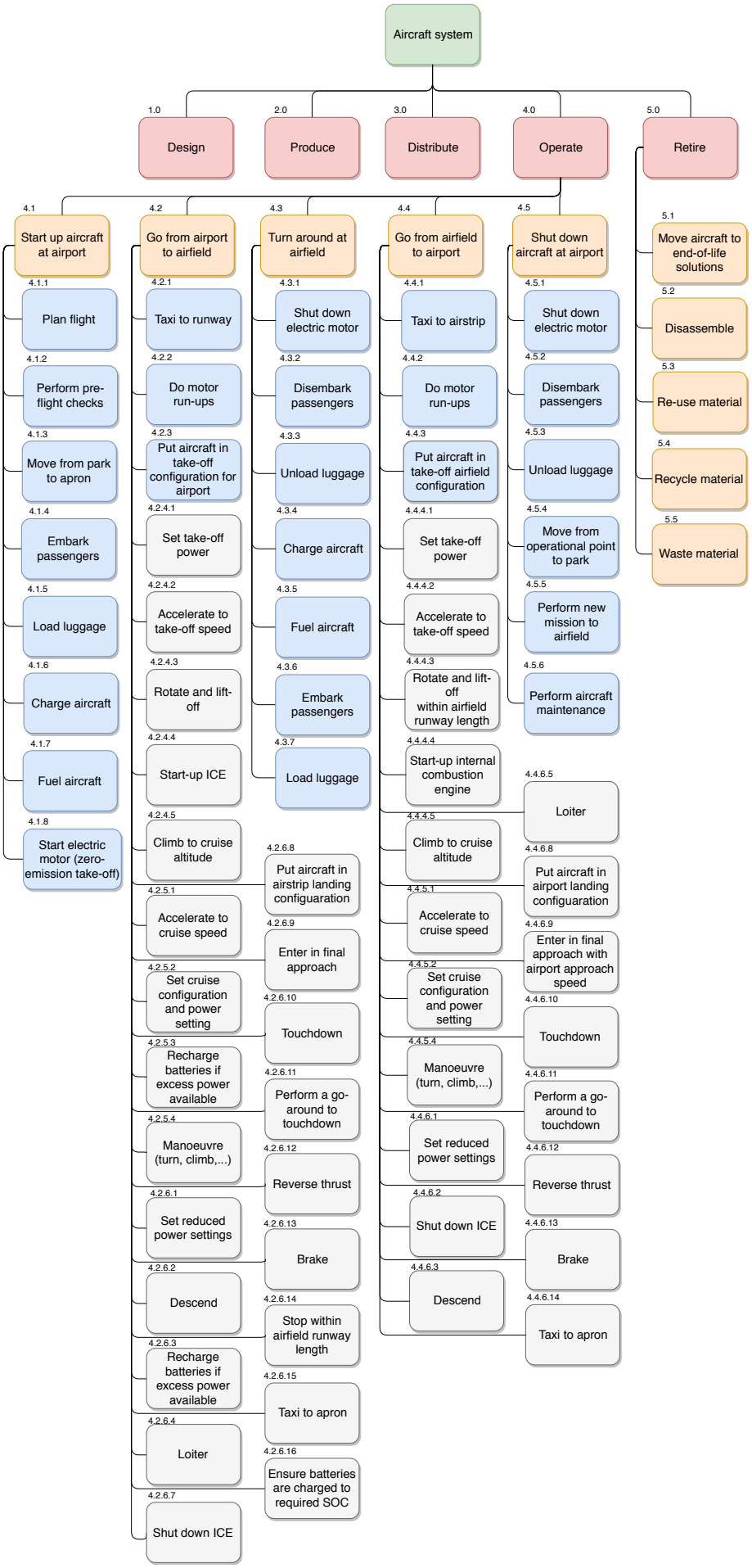

Figure A.2: Functional breakdown structure of the aircraft system.

B

Preliminary Maintenance Manual

Table B.1: Scheduled maintenance plan for the E-COmmuter [88][89].

	Service	Line	Type A	Type B	Type C	Type D
Cockpit						
Test pedals and indicators (fuel quantity, battery level, speed, rudder, etc.)	x	x	x	x	x	x
Test internal and external lights	x	x	x	x	x	x
Examine attachments of control sticks and pedals			x	x	x	x
Examine instruments and their wiring (remove instrument panel)				x	x	x
Visually inspect and test pilot's and copilot's seat for damage and functioning				x	x	x
Cabin						
Visually inspect cabin for loose items and state of the seats		x	x	x	x	x
Examine the fire extinguisher, check the expiry date		x	x	x	x	x
Perform a cabin heat check				x	x	x
Landing gear						
Visually inspect tires for cuts, cracks, wear-out and inflation pressure	x	x	x	x	x	x
Visually inspect landing gear for leaks and damage	x	x	x	x	x	x
Visually inspect landing gear for cracks, deformation, strut distortion, corrosion and paint condition	x	x	x	x	x	x
Test brakes (landing and parking)			x	x	x	x
Check wheel fairings for cracks and loose components (dismount fairing)			x	x	x	x
Check struts for cracks and lubricate			x	x	x	x
Visually inspect damper for damage			x	x	x	x
Clean and lubricate bearings (dismount wheels)			x	x	x	x
Extensively inspect and test complete landing gear for stresses, damage and functioning (e.g. shock absorption) (dismount landing gear)				x	x	x
Wing						
Examine surfaces for damage (dents, cracks, holes, delamination, buckling) and paint condition		x	x	x	x	x
Repaint wing, extensively inspect and test for buckling, stresses, dents, cracks, wear-out and test support structure (dismount wing)						x
Tail						
Examine surfaces for damage (dents, cracks, holes, delamination, buckling) and paint condition		x	x	x	x	x
Repaint tail, extensively inspect and test for buckling, stresses, dents, cracks, wear-out and test support structure (dismount horizontal tail)					x	x
Control surfaces						

Examine surfaces for damage (dents, cracks, holes, delamination, buckling) and paint condition		x	x	x	x	x
Lubricate, visually inspect for damage, check hinges			x	x	x	x
Inspect support and connections with wing or tail			x	x	x	x
Repaint control surfaces, extensively inspect and test for buckling, stresses, dents, cracks, wear-out and test support structure (dismount control surfaces)					x	x
Airframe structure						
Examine external surfaces for leakages, damage (dents, cracks, holes, delamination, buckling) and paint condition	x	x	x	x	x	x
Extensively inspect and test frame for fatigue, cracks and stresses (dismount furniture, floors, paint)						x
Engines						
Upon every maintenance activity, consult engine manufacturer manual for more detail: [121]						
Examine engine for oil and fuel leaks (open cowling)	x	x	x	x	x	x
Check oil level and fill if required	x	x	x	x	x	x
Visually inspect for cracks and temperature damage			x	x	x	x
Examine and clean exhaust system for cracks and heat damage			x	x	x	x
Examine engine mount and casing for cracks, corrosion, assembly and condition of fasteners				x	x	x
Extensively inspect and test functioning and for damage (dismount engines)				x	x	x
Fuel system						
Visually inspect exterior of wing for fuel leakage	x	x	x	x	x	x
Examine fuel tanks and pipes for cracks, corrosion, leakages and proper assembly				x	x	x
Extensively inspect for damage, corrosion, cracks (dismount system)					x	x
Motors						
Upon every maintenance activity, consult motor manufacturer manual for more detail						
Visually inspect for cracks and temperature damage		x	x	x	x	x
Examine motor mount and casing for cracks, corrosion, assembly and condition of fasteners					x	x
Extensively inspect and test functioning and for damage (dismount motors)						x
Propellers						
Upon every maintenance activity, consult propeller manufacturer manual for more detail: [122]						
Visually inspect blades and spinners, check for oil leakage	x	x	x	x	x	x
Visually inspect attachments to motor and retraction mechanism		x	x	x	x	x
Clean and extensively examine propellers for cracks and functioning (dismount propellers)				x	x	x
Battery						
Upon every maintenance activity, consult battery manufacturer manual for more detail						
Visually inspect for leakage and damage due to temperature or impact	x	x	x	x	x	x
Test current and voltage output (connect ammeter and voltmeter)			x	x	x	x
Clean and extensively inspect casing (incl. firewall) and battery (dismount batteries)			x	x	x	x
Extensively inspect and externally test battery (dismount batteries)			x	x	x	x